# MODELLING THE IMPACT OF URBANISATION ON THE REGIONAL CLIMATE OF THE GREATER LONDON AREA

by
HEATHER L. THOMPSON

A thesis submitted to
The University of Birmingham
for the degree of
DOCTOR OF PHILOSOPHY

School of Geography
The University of Birmingham
September 2008

# Abstract

Urban areas have well documented effects on climate, such as the urban heat island effect, reduction of wind speeds, enhanced turbulence and boundary layer heights, and changes in cloud cover and precipitation. This PhD examines the impact of the urban surface on the major agglomeration of London on local and regional climate by means of the numerical mesoscale model METRAS (Schlünzen 1988) coupled for the first time with the sophisticated urban canopy scheme BEP, developed by Martilli et al. (2002).

The robustness of the new model is demonstrated through a series of simulations and sensitivity studies for an idealised urban domain. The model is then configured for the London region, and evaluated using data from a range of meteorological monitoring sites. Implementation of the urban canopy scheme results in a marked improvement in model performance. Under ideal meteorological conditions, peak urban heat island intensities of up to 2.5 K are found during night time hours, with the timing and magnitude of the peak showing good agreement with previous experimental studies for London.

The new model is then used to investigate how growth of the Greater London urban area affects the urban heat island intensity. The results show that the relative fractions of urban land cover and of vegetation within the urban area have important implications for the near surface temperature, diurnal temperature range, wind speed and urban heat island intensity.

The results also suggest that extensive future growth of the London urban area has the potential to increase temperatures, with significant increases for both daytime and night time. The specific forms of urban development, such as densification and spatial expansion, have an impact on these fields. These results have important implications for the design of cities and the management of urban climate.

# Acknowledgments

This thesis could not have been researched and written without the help of many people and organisations. Firstly, I would like to thank my supervisor, Dr. Jenny Salmond, for inspiring me to come to Birmingham to study urban climate and for her support and encouragement over the past four years; and my supervisor, Dr. Xiaoming Cai, for his assistance and guidance throughout this project. There is one person at Birmingham without whose help this project would not have got beyond the starting blocks – I want to thank Dr. David Grawe for his invaluable patience and many long hours spent drinking strong coffee and deciphering the model code. I would also like to thank Dr Sue Grimmond for her help during this project.

This PhD has been sponsored by the National Environmental Research Council. I would also like to acknowledge Dr. Heinke Schlünzen, for allowing me to use the METRAS model, and Dr. Alberto Martilli, for permitting me to use his urban canopy scheme.

Thanks must also go to my fellow PhD students in Room 425 for many fun times over the course of my time in Birmingham; to my colleagues at Severn Trent, and especially Kar Yee, Di and Tim, for their encouragement over the past year; and to Hannah for her friendship throughout all my years as a student.

I am immensely grateful to my family for their continued love and encouragement throughout my life, and especially my sister Jennine, my grandmothers, and my parents, who have given me so much support and set me such a wonderful example.

Finally this thesis is dedicated to Andrew, for his unfailing love, support and encouragement, and his patience during the past year of writing this thesis.

# Abbreviations

| | |
|---|---|
| aLMo | Meteo Swiss operational model |
| BADC | British Atmospheric Data Centre |
| BBP | Beaufort Bracknell Park |
| BEP | Building Energy Parameterization |
| BUBBLE | Basel Urban Boundary Layer Experiment |
| CFD | Computational Fluid Dynamics |
| COMEAP | Committee on Medical Effects of Air Pollutants |
| DETR | Department of Environment, Transport and Regions |
| DJF | December, January, February |
| DMI-HIRLAM | Danish Meteorological Institute High Resolution Limited Area Model |
| DTR | Diurnal Temperature Range |
| GLA | Greater London Authority |
| JJA | June, July, August |
| LCCP | London Climate Change Partnership |
| LCM 2000 | CEH Land Cover Map 2000 |
| LHR | London Heathrow |
| LUMPS | Local-scale urban meteorological Parameterization scheme |
| LWC | London Weather Centre |
| MC2 | Mesoscale Compressible Community model |
| METRAS | Mesoskalige Transport und Stromungsmodell |
| MM5 | PSU/NCAR mesoscale model |
| MOST | Monin-Obukhov Similarity Theory |
| NWP | Numerical Weather Prediction |
| OHM | Objective Hysteresis Model |
| PBL | Planetary Boundary Layer |
| REI | Regional Effect Index |
| RSL | Roughness Sub-Layer |
| SJP | St James' Park |
| TEB | Town Energy Balance |
| TKE | Turbulent Kinetic Energy |
| TVM | Topographic Vorticity mode mesoscale Model |
| UBL | Urban Boundary Layer |
| UCL | Urban Canopy Layer |
| UHI | Urban Heat Island |
| UKMO | UK Met Office |
| WRF | Weather Research and Forecasting (model) |
| WMO | World Meteorological Organization |

# Table of Contents


Chapter 1: Introduction ..... 1
1.1 Aims and Objectives ..... 4
1.2 Structure of this thesis ..... 6

Chapter 2: Literature review ..... 8
2.1 Urban climate modification ..... 9
2.1.1 Mechanical effects ..... 9
2.1.2 Thermal effects ..... 10
2.1.3 Scale and the urban effect ..... 12
2.1.4 The Urban Heat Island ..... 16
2.1.5 Other effects of the urban surface ..... 20
2.1.6 Mitigation of excessive urban temperatures and UHIs ..... 21
2.2 The impact of urbanisation on local and regional climate ..... 24
2.3 Justification of modelling approach ..... 27
2.3.1 Representation of the urban area in mesoscale models ..... 29
2.4 Urbanisation of the South East of England ..... 38
2.4.1 Expansion of London and urban forms ..... 40
2.4.2 The climate of London ..... 46
2.4.3 The London urban heat island ..... 47
2.4.4 London Warming? Trends in the UHI intensity ..... 49
2.5 Summary ..... 52

Chapter 3: Methods ..... 54
3.1 METRAS ..... 54
3.1.1 Model overview ..... 54
3.1.2 Model equations ..... 57
3.1.3 Model boundary conditions ..... 62
3.1.4 Model initialisation ..... 64
3.2 BEP ..... 66
3.2.1 Calculation of dynamical effects ..... 69
3.2.2 Calculation of thermodynamic effects ..... 70
3.3 Implementation of BEP in METRAS ..... 73
3.4 Computational demand ..... 75
3.5 Data sources ..... 76
3.5.1 Land cover data ..... 76
3.5.2 Orography data ..... 79
3.5.3 Data used for the model initialisation ..... 79
3.5.4 BEP urban data ..... 79
3.5.5 Meteorological data for model validation ..... 82
3.6 Summary ..... 85

Chapter 4: Results from the implementation of BEP in METRAS for an idealised domain ..... 86
4.1 Set up of the idealised test cases ..... 86
4.2 Results for an idealised domain ..... 88
4.2.1 Horizontal cross sections of potential temperature and horizontal wind speed ..... 93

4.2.2 Impact of the urban area on the mesoscale flow ..... 95
4.2.3 Diurnal cycle of the UHI intensity ..... 103
4.3 Sensitivity tests ..... 106
4.3.1 Sensitivity to the building height distribution ..... 106
4.3.2 Sensitivity to the temperature inside the buildings ..... 110
4.3.3 Sensitivity to the surface albedo ..... 111
4.3.4 Sensitivity to the vegetation fraction ..... 115
4.3.5 Sensitivity to the size of the urban area ..... 120
4.3.6 Sensitivity to the surrounding rural land cover class ..... 122
4.3.7 Sensitivity to the geostrophic wind speed ..... 125
4.4 Summary ..... 130

Chapter 5: Evaluation of the urbanised METRAS model for the London region ..... 133
5.1 Set up of the model for London simulation ..... 134
5.1.1 Urban parameters ..... 139
5.2 Model evaluation ..... 140
5.2.1 Air temperature evaluation ..... 143
5.2.2 Wind speed and direction evaluation ..... 151
5.2.3 Discussion of other simulation cases ..... 157
5.3 Summary and discussion of the evaluation ..... 158

Chapter 6: The effects of urban land cover modifications on near surface temperature and wind speed ..... 161
6.1 Description of model runs ..... 163
6.1.1 Urban BASE CASE ..... 163
6.1.2 NOURB CASE ..... 164
6.1.3 COMBINED series ..... 164
6.1.4 RADIUS SERIES and DENSITY SERIES ..... 166
6.1.5 Model configuration for the scenarios ..... 168
6.2 Effects of the current state of urban land cover on near surface temperature and wind speed ..... 169
6.2.1 Spatially averaged near surface potential temperature ..... 169
6.2.2 Diurnal temperature range (DTR) ..... 172
6.2.3 Diurnal cycle of the urban heat island intensity ..... 174
6.2.4 Wind speed and direction ..... 179
6.2.5 Spatial expansion of urban climate anomalies ..... 181
6.3 Effects of the past radial expansion and densification of the city on near surface temperature and wind speed ..... 184
6.3.1 Effect of urban growth on the spatially average near surface potential temperature ..... 186
6.3.2 Effect of urban growth on the REI and effective radius ..... 190
6.3.3 Effect of urban growth on the DTR ..... 194
6.3.4 Effect of urban growth on the UHI intensity ..... 196
6.3.5 Effect of urban growth on the wind speed ..... 201
6.4 Summary and discussion ..... 204

Chapter 7: The effects of future urban expansion and possible mitigation strategies ..... 208
7.1 Description of model runs ..... 210

7.1.1 EXPANSION series ..... 211
7.1.2 DENSIFICATION series ..... 212
7.1.3 Model configuration for the scenarios ..... 214
7.2 Effects of urbanisation for the EXPANSION series ..... 215
7.2.1 Spatially averaged near surface temperature ..... 215
7.2.2 Diurnal temperature range (DTR) ..... 220
7.2.3 Wind speed ..... 223
7.3 Effects of urbanisation for the DENSIFICATION series ..... 225
7.3.1 Spatially averaged near surface temperature ..... 226
7.3.2 Wind speed ..... 229
7.4 Summary and discussion ..... 230

Chapter 8: Conclusions and recommendations for future work ..... 234
8.1 Conclusions ..... 236
8.2 Improvements and recommendations for future work ..... 240

**References** ..... 243

# List of figures

Figure 2.1: Scales of interest when studying urban areas (Inspired by Harman (2003)) ..... 13
Figure 2.2: A schematic representation of the vertical layers of the urban boundary layer at the local scale and the representative flow (from Britter and Hanna, 2003)..... 14
Figure 2.3: A schematic representation of the regional influence of the urban surface on the boundary layer. 'PBL' stands for the planetary boundary layer, and 'UBL' for the urban boundary layer. Modified from a figure in Oke (1997). ..... 16
Figure 2.4: Fraction of urban land cover in the London region. ..... 39
Figure 2.5(a-f): Built-up area of London in 1800 (a), 1850 (b), 1880 (c), 1914 (d), 1939 (e) and 1958 (f). From Mogridge et al. (1997). ..... 43
Figure 2.6: Built up area for London in 1981, from Mogridge et al. (1997). The red box shows the domain used in Chapters 6 and 7 for the scenarios representing past and future urbanisation. ..... 44
Figure 2.7: Urban classes taken from Chandler (1965) ..... 46
Figure 3.1: Three dimensional representation of the METRAS ARAKAWA C grid. Taken from Schlünzen et al. (1996) ..... 56
Figure 3.2: A diagram showing how the METRAS mesoscale grid interacts with the BEP urban grid. ..... 67
Figure 3.3: A schematic representation of the urban grid, in which W is the street width, B is the building width, IU is the centre of a vertical model level, $F_{iu}^{H}$ represents the flux of a quantity through the horizontal surfaces with the area $S_{iu}^{H}$, and $F_{IU}^{V}$ represents the flux of a quantity through the vertical surfaces with the area of $S_{IU}^{V}$. (Taken from Martilli et al. 2002, page 267)..... 68
Figure 3.4: Percentage of the "Meadows" land cover class (left) and the "Mixed forest" land cover class (right) for each grid cell in the domain ..... 78
Figure 3.5: Percentage of the "Continuous urban" land cover class (left) and the "Suburban-rural developed" land cover class (right) for each grid cell in the domain ..... 78
Figure 3.6: Locations of Met Office weather stations in the South-East of England (taken from www.metoffice.gov.uk) ..... 84
Figure 4.1: Vertical profiles of potential temperature (K) at x=0, y=0 as computed by the *Rural* (yellow), *Orig* (green) and *urban_BEP* (black) simulations at 04:00 for the second day of simulation. ..... 89
Figure 4.2: Vertical profile of wind speed ($ms^{-1}$) at x=0, y=0 as computed by the *Rural* (yellow), *Orig* (green) and *urban_BEP* (black) simulations at 04:00 for the second day of simulation. ..... 91
Figure 4.3: Vertical profile of turbulent kinetic energy (TKE) ($m^2s^{-2}$) at x=0, y=0 as computed by the rural (yellow), *Orig* (green) and *urban_BEP* (black) simulations at 04:00 for the second day of simulation. ..... 92
Figure 4.4: Horizontal cross section at z=10 m (a) and z=30 m (b) of potential temperature (K) as computed by the *urban_BEP* simulation at 04:00 for the second day of simulation. ..... 93
Figure 4.5: Horizontal cross section at z=10 m (a) and 30 m (b) of wind speed ($ms^{-1}$) and direction as computed by the *urban_BEP* simulation at 04:00 for the second day of simulation. The arrows represent the magnitude and direction of the horizontal wind and the shaded plot represents the magnitude of the horizontal wind speed ($ms^{-1}$). .... 94

Figure 4.6: Vertical section at y=0 of potential temperature (K) as computed by the *urban_BEP* simulation at 12:00 noon of the second day of the simulation. ..... 96
Figure 4.7: Vertical section at y=0 of the horizontal speed ($ms^{-1}$) as computed by the *urban_BEP* simulation at 12:00 noon of the second day of simulation. ..... 97
Figure 4.8: Vertical sections at y=0 of (a) potential temperature (K) and (b) horizontal wind speed ($ms^{-1}$) (b) as computed by the *Orig* simulation at 12:00 noon of the second day of simulation. ..... 98
Figure 4.9: Vertical section at y=0 of the TKE ($m^2s^{-2}$) as computed by (a) the *urban_BEP* simulation and (b) the *Orig* simulation at 12:00 noon of the second day of simulation. 99
Figure 4.10: Vertical section at y=0 of potential temperature (K) as computed by the *urban_BEP* simulation at 04:00 of the second day of simulation. ..... 101
Figure 4.11: Vertical section at y=0 of horizontal wind speed ($ms^{-1}$) as computed by the *urban_BEP* simulation at 04:00 of second day of simulation. ..... 102
Figure 4.12: Vertical sections at y=0 of (a) the potential temperature (K) and (b) the horizontal wind speed ($ms^{-1}$) as computed by the *Orig* simulation at 04:00 of the second day of simulation. ..... 102
Figure 4.13: Diurnal variation of the UHI intensity (K) for the second day of simulation, calculated as the maximum difference in potential temperature at the first grid level between the urban area and a rural point upwind of the city. The pink line represents the *urban_BEP* simulation, and the blue line the *Orig* simulation. Sunrise and sunset are around 04:00 and 20:00 respectively. ..... 103
Figure 4.14: Potential temperature (K) along the line y=0, z=10m as computed by the three simulations *bh2* (black line), *a01* (green) and *bh3* (yellow) at 04:00 on the second day of simulation. The simulations represent a mean building height of 7 m (*bh2*), 15 m (*a01*) and 29.5 m (*bh3*) respectively. ..... 108
Figure 4.15: Vertical profiles of (a) wind speed ($ms^{-1}$) and (b) TKE ($m^2s^{-2}$) at x=0, y=0 as computed by the three simulations *bh2* (black line), *a01* (green) and *bh3* (yellow) at 04:00 of the second day of simulations. The simulations represent a mean building height of 7 m (*bh2*), 15 m (*a01*) and 29.5 m (*bh3*) respectively. ..... 109
Figure 4.16: Potential temperature (K) along the line y=0, z=10 m, as computed by the three simulations with the internal temperatures behind urban walls and roofs ('twini' and 'trini') both set to 293 K (black line), 295 K (green) and 297 K (yellow) at 04:00 for the second day of simulation. ..... 111
Figure 4.17: Diurnal variation of the difference in potential temperature (K) between the simulations *alb1* and the control simulation *a01* (blue line) and between the simulations *alb2* and *a01* (pink line) at x=0, y=0, z=10 m for the second day of simulation. The *alb1* simulation represents an urban albedo of 0.30 and the *alb2* simulation represents an urban albedo of 0.15. ..... 115
Figure 4.18: Diurnal variation of the difference in potential temperature (K) between the control simulation *a01* and the vegetated simulations *veg1* (blue) and *veg2* (pink) at x=0, y=0, z=10 m for the second day of simulation. The *veg1* simulation represents an urban area with 10% vegetated fraction, and the *veg2* simulation represents an urban area with 30% vegetated fraction. ..... 118
Figure 4.19: Correlation between the fraction of vegetation in the urban area and the potential temperature (K) at x=y=0, z=10, at 12:00 noon for the second day of simulations .. 119
Figure 4.20: Potential temperature (K) along the line y=0, z=10 m as computed by the three simulations with the urban area measuring 6 km, 10 km and 20 km respectively (yellow, green and black), at 04:00 for the second day of simulation ..... 122

Figure 4.21: Diurnal variation of the UHI intensity (K) as computed by the simulations representing different examples of rural land cover surrounding the urban area for the second day of simulation. ..... 124
Figure 4.22: Vertical profiles of (a) potential temperature (K), (b) wind speed ($ms^{-1}$) and (c) TKE ($m^2s^{-2}$) at x=0, y=0 as computed by the three simulations with geostrophic wind speed of 2 $ms^{-1}$, 4 $ms^{-1}$ and 8 $ms^{-1}$ (black, green and yellow respectively), at 04:00 of the second day of simulation. ..... 127
Figure 4.23: Vertical cross section at y=0 of the horizontal wind speed ($ms^{-1}$) as computed by the simulation with the low wind speed of 2 $ms^{-1}$ (a), and that with strong wind speed of 8 $ms^{-1}$ (b) at 12:00 noon of the second day of simulation. ..... 128
Figure 4.24: Vertical cross section at y=0 of the potential temperature (K) as computed by the simulation with the low wind speed of 2 $ms^{-1}$ (a), and that with strong wind speed of 8 $ms^{-1}$ (b) at 12:00 noon of the second day of simulation. ..... 128
Figure 4.25: Vertical cross section at y=0 of the TKE ($m^2s$-$^2$) as computed by the simulation with the low wind speed of 2 $ms^{-1}$ (a), and that with strong wind speed of 8 $ms^{-1}$ (b) at 12:00 noon of the second day of simulation. ..... 129
Figure 5.1: Orography for the domain of the simulations (US Geological Survey). ..... 134
Figure 5.2: Percentage of urban land use in the domain (taken from the CEH Land Cover 2000 data). ..... 135
Figure 5.3: Count of the number of hottest days represented by each weather type. Data was taken for the London Heathrow weather station for the summers 1995-2000, and the 10$^{th}$ percentile hottest days were taken into account in this summary. ..... 137
Figure 5.4: Diurnal cycle of air temperature (ºC) at the LWC site from August 6$^{th}$ to August 7$^{th}$ 1998 according to the measurements at LWC (blue), the METRAS traditional simulation (pink) and the simulation with BEP (yellow). ..... 144
Figure 5.5: Diurnal cycle of air temperature (ºC) at the LWC site from July 30$^{th}$ to July 31$^{st}$ 1999 according to the measurements at LWC (blue), the METRAS traditional simulation (pink) and the simulation with BEP (yellow). ..... 146
Figure 5.6: Diurnal cycle of air temperature (ºC) at the LHR site from August 6$^{th}$ to August 7$^{th}$ 1998 according to the measurements at LHR (blue), the traditional simulation (pink) and the simulation with BEP (yellow). ..... 147
Figure 5.7: Diurnal cycle of air temperature (ºC) at the LHR site from July 30$^{th}$ to July 31$^{st}$ 1999 according to the LHR measurements (blue), the traditional METRAS simulation (pink) and the simulation with BEP (yellow). ..... 149
Figure 5.8: Diurnal cycle of air temperature (ºC) at the SJP site from August 6$^{th}$ to August 7$^{th}$ 1998 according to the SJP measurements (blue), the traditional simulation (pink) and the simulation with BEP (yellow). ..... 150
Figure 5.9: Diurnal cycle of air temperature (ºC) at the BBP site from August 6$^{th}$ to August 7$^{th}$ 1998 according to the BBP measurements (blue), the traditional METRAS simulation (pink) and the simulation with BEP (yellow). ..... 151
Figure 5.10: Diurnal cycle of the wind speed ($ms^{-1}$) (the upper panel) and wind direction (the lower panel) at the LWC station from August 6$^{th}$ to August 7$^{th}$ 1998 according to LWC measurements (blue), the traditional METRAS simulation (pink) and the simulation with BEP (yellow). ..... 153
Figure 5.11: Diurnal cycle of the wind speed ($ms^{-1}$) at the LWC station from 30$^{th}$ to the 31$^{st}$ July 1999 according to LWC measurements (blue), the traditional METRAS simulation (pink) and the simulation with BEP (yellow). ..... 154

Figure 5.12: Diurnal cycle of the wind speed ($ms^{-1}$) (the upper panel) and wind direction (the lower panel) at the LHR station from August 6th to August 7th 1998 according to LHR measurements (blue), the traditional METRAS simulation (pink) and the simulation with BEP (yellow). ..... 155
Figure 5.13: Diurnal cycle of the wind speed ($ms^{-1}$) at the LHR station from 30th-31st July 1999 according to LHR measurements (blue), the traditional METRAS simulation (pink) and the simulation with BEP (yellow). ..... 156
Figure 6.1: Potential temperature difference (K) between the base case of current urbanised land use (URB_BASE) and a rural case (NOURB) at z = 10 m at 04:00 (left) and 12:00 (right) of the second day of simulation. ..... 170
Figure 6.2: Diurnal cycle of the maximum UHI intensity (K) for the second day of simulation for the URB_BASE case. The UHI intensity is calculated for the current urban land cover case with respect to the rural domain (NOURB). ..... 176
Figure 6.3: Diurnal variation of the London UHI with respect to Bracknell for six days in July and August 1999/2000. Taken from Wilby (2003). ..... 178
Figure 6.4: Horizontal wind speed difference ($ms^{-1}$) between the base case of current urbanised land cover (URB_BASE) and rural domain (NOURB) at z = 10 m at 04:00 (left) and 12:00 noon (right) of the second day of simulation. ..... 180
Figure 6.5: Horizontal wind speed and direction ($ms^{-1}$) for the base case of current urbanised land cover (URB_BASE) (left) and rural domain (NOURB) (right) at z = 10 m at 04:00 of the second day of simulation. ..... 181
Figure 6.6: Mean potential temperature (K) as a function of the mean urban land cover fraction for the COMBINED, RADIUS and DENSITY series, at 04:00 of the second day of simulation. ..... 188
Figure 6.7: Mean potential temperature (K) as a function of the mean urban land cover fraction for the COMBINED, RADIUS and DENSITY series, at 12:00 of the second day of simulation. ..... 189
Figure 6.8: Mean DTR (K) as a function of the mean urban land cover fraction for the COMBINED, RADIUS and DENSITY series, for the second day of simulation. ..... 194
Figure 6.9: Spatially averaged maximum diurnal temperature (K) as a function of the mean urban land cover fraction for the COMBINED, RADIUS and DENSITY series, for the second day of simulation. ..... 195
Figure 6.10: Spatially averaged minimum diurnal temperature (K) as a function of the mean urban land cover fraction for the COMBINED, RADIUS and DENSITY series, for the second day of simulation. ..... 196
Figure 6.11: Diurnal cycle of the maximum UHI intensity (K) for the second day of simulation for the RADIUS series ..... 197
Figure 6.12: Diurnal cycle of the maximum UHI intensity (K) for the second day of simulation for the DENSITY series ..... 198
Figure 6.13: Diurnal cycle of the maximum UHI intensity (K) for the second day of simulation for the COMBINED series ..... 198
Figure 6.14: Maximum UHI intensity (K) as a function of mean urban land cover fraction for the RADIUS, DENSITY and COMBINED series of model runs, at 02:00 of the second day of simulation. ..... 199
Figure 6.15: Mean horizontal wind speed at z = 10 m as a function of the mean urban land cover fraction for the RADIUS, DENSITY and COMBINED series of model runs, at 12:00 of the second day of simulation. ..... 201

Figure 6.16: Mean horizontal wind speed at z = 10 m as a function of the mean urban land cover fraction for the RADIUS, DENSITY and COMBINED series of model runs, at 04:00 of the second day of simulation..... 202
Figure 7.1: Mean potential temperature (K) as a function of the mean urban land cover fraction as computed by the simulations of the EXPANSION series at 04:00 of the second day of simulation ..... 216
Figure 7.2: Mean potential temperature (K) as a function of the mean urban land cover fraction as computed by the simulations of the EXPANSION series at 12:00 of the second day of simulation ..... 217
Figure 7.3: Diurnal cycle of the maximum UHI intensity (K) as computed by the simulations of the EXPANSION series for the second day of simulation..... 219
Figure 7.4: Maximum UHI intensity (K) as a function of mean urban land cover fraction as computed by the simulations in the EXPANSION series at 02:00 of the second day of simulation..... 220
Figure 7.5: Mean DTR (K) as a function of the mean urban land cover fraction as computed by the simulations in the EXPANSION series for the second day of simulation..... 222
Figure 7.6: Mean horizontal wind speed ($ms^{-1}$) at z = 10 m as a function of the mean urban land cover fraction as computed by the simulations in the EXPANSION series at 04:00 (blue) and 12:00 (pink) for the second day of simulation..... 223
Figure 7.7: Change in urban land cover for the model simulation '30F' expressed as a percentage change..... 226
Figure 7.8: Change in the near surface potential temperature [K] at 12:00 noon for the '30F' simulation compared to the base case of current urban land use for London..... 228

# List of tables

Table 2.1: SWOT analysis for the BEP urban scheme ..... 36
Table 2.2: SWOT analysis for the METRAS mesoscale model ..... 37
Table 3.1: Surface characteristics for the land-use classes (Schlünzen et al. 2003) ..... 57
Table 3.2: Summary of the boundary conditions used for all METRAS model runs ..... 63
Table 3.3: Description of how the 27 land cover classes in the CEH Land Cover Map 2000 are summarised into the 10 METRAS land cover classes ..... 77
Table 3.4: Definition of the BEP urban classes based on the CEH Land Cover map 2000 classification ..... 80
Table 3.5: Distribution of building heights for the two urban classes defined for the simulations representing London ..... 81
Table 3.6: Parameters for the city for the urban simulation. $\varkappa_s$ is the thermal diffusivity of the material, $C_s$ is the specific heat of the material, $T_{int}$ is the initial temperature of the material (equal to the temperature of the deepest layer), $\varepsilon$ is the surface emissivity, $\alpha$ is the albedo and $z_0$ is the roughness length of the surface. ..... 81
Table 3.7: Summary of available data for the MIDAS weather stations used in the model evaluation in Chapter 5 ..... 83
Table 4.1: Summary of the idealised test cases ..... 87
Table 4.2: Building height distribution for the three sensitivity simulations. ..... 107
Table 4.3: Typical albedo values for rural and urban surfaces, taken from Oke (1987) and Taha (1997) ..... 112
Table 4.4: Details of the simulations with different land cover classes surrounding the central urban area ..... 123
Table 5.1: Summary of the Lamb classification ..... 136
Table 5.2: Selected periods of simulation for the evaluation of METRAS+BEP ..... 139
Table 6.1: Summary of simulations which form the COMBINED series of runs ..... 165
Table 6.2: Comparison of model simulations and the approximate year of urban development 166
Table 6.3: Summary of simulations which form the RADIUS series of model runs ..... 167
Table 6.4: Summary of simulations which form the DENSITY series of model runs ..... 168
Table 6.5: REI for the URB_BASE-NOURB model comparison, calculated for the second day of simulation. ..... 183
Table 6.6: Comparison of the maximum variation in near surface potential temperature (%) for daytime and night time for each series of model runs. ..... 186
Table 6.7: Effective radius (km) and the ratio of the effective radius $R_{eff}$ to the actual radius of the urban area $R_{urb}$ for the RADIUS and COMBINED series of model runs. The effective radius is calculated for the second day of simulation at 04:00 ..... 191
Table 6.8: REI for the RADIUS, DENSITY and COMBINED model series, for night time (04:00) and daytime (12:00), for the second day of simulation. ..... 193
Table 7.1: Summary of simulations which form the EXPANSION series of model runs, which represents the urban expansion over all grid cells, independently of whether they are already urbanised or not. ..... 211
Table 7.2: Summary of simulations which form the DENSIFICATION series of model runs, which represents the urban expansion for existing urban cells (where the urban fraction exceeds a threshold percentage) only ..... 213

# Chapter 1: Introduction

Urban areas are one of the most obvious examples of human modification of the Earth's surface. Despite covering only 1.2% of the Earth's surface (Lamptey et al. 2005; Shepherd 2005), it is estimated that in 2003 about 48% of the World's population resided in urban settlements (UN 2004). By 2030 it is expected that 61% of the World's population will be living in urban areas (UN 2004). Urbanisation is an extreme example of human land use modification, since it radically alters the physical properties of the Earth's surface and may also affect the thermal, radiative and aerodynamic character of the surface (Oke 1987). Since such a high proportion of the World's population reside in urban areas it is important to understand the processes determining urban climates, and how both past and future urbanisation patterns might affect climate at the local and regional scale.

Urban areas have well documented effects on the environment, such as changes to the local winds and turbulence (Roth 2000), changes in cloud cover and precipitation (Changnon 1992) and the urban heat island phenomenon, i.e. the increased temperature of the urban surface compared to its rural surroundings (Oke 1981). All these effects result from mechanical and thermal modifications induced by the urban surface. The most important modifications to the surface energy balance in urban areas consist in the moisture availability controlling the partitioning into sensible and latent heat fluxes, the street geometry and surface radiative properties affecting the radiation balance and the thermal properties of the building materials causing the heat storage in the city to be significantly larger than in surrounding areas (Oke 1982).

Human activities in urban areas are also large sources of atmospheric pollutants (e.g. from traffic and industry) and anthropogenic heat (e.g. from heating and air conditioning of buildings). All these effects of the urban surface can have economic consequences, as well as those on human health, as seen for example during the summer heat wave in Europe in 2003 (Johnson et al. 2005). Collier (2006) estimated that changes to weather due to the urban surface may approach the magnitude of those induced locally by climate change.

Many studies focus on the effects of the urban surface at the microscale, however it is both interesting and necessary to understand how both past and future urbanisation and suburbanisation might have affected weather and climate, and in particular to understand how these effects can extend beyond the city, affecting the climate at the regional scale. Urban heat island perturbations have been observed 10-20 km outside the urban area, and a warm urban plume aloft may extend up to 100 km downwind of the city (Britter et al. 2003).

Estimating the effects of urbanisation at a regional scale is far from easy, since for most areas a comprehensive set of representative pre-urban measurements is not available, or is not appropriate for a current comparison. Often it is possible to compare data from an urban station with that from a rural one in the surrounding area. However it is also necessary to account for the effects of topography and other natural features, which might, in some cases, exceed urban effects (Schultz et al. 1982), and to be certain that the rural station is not influenced by the urban area (for example if it is downwind of the city) and has not been excessively modified over time by human activity, such as farming or drainage. Results can often be dependent on the methods used to classify urban and rural areas. Kalnay et al. (2003) estimated the urban effect by comparing trends in observed surface temperatures (which are sensitive to changes in land use)

with trends derived from a statistical reanalysis of global weather. The reanalysis trends should be insensitive to urbanisation and land use changes, but will be susceptible to climatic changes which affect observations above the surface since the reanalysis uses atmospheric vertical soundings to estimate surface values). Other studies (Ichinose 2001; Klaic et al. 2002) attempt to estimate the urban effect at a city or regional scale using a modelling approach, but in order to do this it is necessary to parameterise the effects of the urban surface in the model (Ichinose 2001; Trusilova 2006; Lee et al. 2008), so that the urban boundary layer and surface energy budget are correctly simulated.

.

## 1.1 Aims and Objectives

The aim of this PhD study is to quantify the effects of the major agglomeration of London on the local and regional climate by means of a numerical mesoscale model which has been coupled with an urban canopy scheme.

The objectives through which this aim will be achieved are:

- To couple the mesoscale model METRAS with an urban canopy scheme (BEP).
- To investigate the underlying processes which determine the urban impact on local and regional climate through detailed sensitivity tests.
- To ascertain the impact of London on regional climate using simulations with and without the urban area.
- To investigate the historical impact of London on regional climate due to past urbanisation characteristics.
- To investigate the effects of future urbanisation on the nocturnal urban heat island and on urban daytime temperatures.

There are a number of different ways of parameterising the urban surface in a mesoscale model, ranging from the simple roughness length approach to more sophisticated multi-layer urban canopy schemes (Kusaka et al. 2001; Martilli et al. 2002). When this PhD study was started it was not possible to run an existing mesoscale model that already had a sophisticated urban

scheme, and therefore it was necessary to implement one into a mesoscale model. The urban canopy scheme BEP, developed by Martilli et al. (2002) was chosen, since it has the advantage of being a validated multi-layer canopy scheme which incorporates the influence of surface morphology and spreads the influence of the urban surface in the vertical.

METRAS (Schlünzen 1988) is a mesoscale model which has been used to study the effects of the urban surface on air quality. Although this model has been used to simulate the dominant effects of the urban surface, it has a simple parameterisation of the urban surface based on the roughness length approach. The urban surface is simulated in the same way as other land use types by using appropriate values of surface parameters such as the albedo, roughness length. This method neglects many of the urban canopy layer and boundary layer effects which are parameterised by more sophisticated multi-layer urban canopy schemes. The implementation of the BEP urban canopy scheme into METRAS provides a tool to address important research questions on the effect of urban land use changes at the regional scale.

In order to investigate the problem of thermal modifications due to urbanisation it was also necessary to select a study area to model. London was chosen for this study, since it is a major world urban centre, which has grown considerably in time, and for which key environmental, social and economic impacts associated with climate change have been identified (LCCP 2002). There is very limited numerical modelling work on the London area and the possible effects of the urban structure on climate.

This work is important because it explores whether the climate in the London region has been influenced by the urban structure, as well as ascertaining which properties of the city which are most important in terms of modifying climate. By running the model with different land use

types, building heights, and different amounts of vegetation coverage, it is possible to consider how urban planners can design cities which maximise comfort and sustainable energy use. There are also important links between this work and climate change, since London could be particularly vulnerable to future changes in its climate, such as increased flooding events and exacerbated summer heat waves.

## 1.2 Structure of this thesis

A review of the current literature is presented in Chapter 2. Chapter 3 describes the mesoscale model METRAS which is used for this study, the urban scheme BEP chosen to be implemented in the model, as well as the methods used in the implementation and the data sources required to configure the modelling system for the London domain and to evaluate the model.

The results from the implementation of the urban scheme in METRAS are presented in Chapter 4. The model is initially run for an idealised domain, and sensitivity tests are carried out to enable a full understanding of the model performance and the underlying processes which determine the urban impact on the model results. The model is then run for London, and the results are evaluated against meteorological data from London weather stations (Chapter 5).

In Chapter 6 the effects of past urbanisation scenarios are investigated for a particular meteorological case for which the model was evaluated and for which a significant urban effect was identified. The effects of urbanisation on the regional climate are isolated from other effects by comparing simulations performed with a land cover map representing urban land use in 2000 and hypothetical land cover maps based on a literature survey.

The effects of future urban expansion scenarios are investigated for London in Chapter 7. Conclusions and recommendations for future work are made in Chapter 8.

# Chapter 2: Literature review

This thesis investigates the problem of thermal modifications due to an urban area at the regional scale. In order to understand the background to this problem, the main effects of the urban surface on weather and climate, and the scales at which they operate, are reviewed in Section 2.1. The most pronounced, and particularly well documented, example of the urban effect on climate is the urban heat island phenomenon, which is reviewed in Section 2.1.4. The relative abundance of information and records on this topic justifies the selection of thermal modifications and the UHI as the focus of this PhD study.

Having reviewed some of the more specific effects of the urban surface, land use change through time as a result of urbanisation is reviewed in Section 2.2. The effects of urbanisation are not easy to quantify and the advantages of a modelling approach over a comparison of observations are reviewed in Section 2.3. Having justified the adoption of a modelling approach to investigate the problem of thermal modifications due to the urban area at a regional scale, the representation of the urban surface in models is reviewed in Section 2.3.1, and the selection of the mesoscale model METRAS and the urban canopy scheme BEP for this work is explained. The climate of London and key investigations of urban effects in this region are reviewed in Section 2.4.

## 2.1 Urban climate modification

Urban areas have well documented effects on air quality and weather, such as the urban heat island (e.g. Landsberg 1981; Oke 1982), reduced winds (Lee 1979) and increased atmospheric turbulence (e.g. Roth et al. 1993). There might also be less obvious effects such as changes in cloud cover (Changnon et al. 1971; Rabin et al. 1996; Inoue et al. 2004), enhancement of storms and changes in precipitation (Palumbo et al. 1980; Oke 1987; Jauregui et al. 1996; Bornstein et al. 2000; Shepherd et al. 2002; Shepherd 2005), and changes in humidity and atmospheric electricity (Changnon et al. 1971). All these effects result from mechanical and thermal modifications induced by the urban surface.

### *2.1.1 Mechanical effects*

Urban areas mechanically affect air flow in the following ways: increased drag force due to the presence of buildings; the enhancement of the transformation of mean kinetic energy into turbulent kinetic energy in the shear layer at the top of the canopy; turbulent wakes generated by roughness elements which serve to mix pollutants, momentum, heat and moisture; and enhanced drag force by thermal plumes from street canyons at night time and roof tops in the day time (Roth 2000). These factors have the effect of increasing turbulent mixing, and modifying boundary layer wind fields. There are also changes in wind speed and direction induced when air blows across the boundary between two surfaces of different roughness (Klaic et al. 2002), and a thermal circulation with the convergence of horizontal wind into the city, and vertical motions over the city, caused by the urban heat island phenomenon (Britter et al. 2003). Most urban areas have a warm urban plume aloft which can extend to 100 km downwind of the city (Britter et al. 2003).

*2.1.2 Thermal effects*

In urban areas there is a distinct modification of the heat fluxes due to shadowing effects, which cause differential heating/cooling of surfaces and radiative trapping in the urban canyon (Masson 2006). The main impact of urbanisation is to favour the partitioning of energy into sensible rather than latent heat, whilst the greater thermal heat capacity and conductivity of the building materials increase the heat storage in the urban area compared to the rural surroundings (Oke 1982). During daytime heat is stored in the urban surface, and during night time heat is released, maintaining warmer urban temperatures compared to the surrounding countryside and becoming one of the primary reasons for the complex urban heat island (UHI) effect and the weakly convective nocturnal boundary layer. The UHI is examined in more detail in Section 2.1.4.

It is important to understand the surface energy balance for urban areas because the modified partitioning into the component fluxes will have an effect on the stability and thermodynamic properties of the boundary layer, as well as the mixing layer height (Christen et al. 2004). The equation for surface energy balance is as follows:

$$Q^* + Q_F = Q_H + Q_E + \Delta Q_S$$

where $Q^* = (K_\downarrow - K_\uparrow) + (L_\downarrow - L_\uparrow)$ **(Equation 2.1)**

Q* represents the net radiation at the surface and its component terms are the shortwave (denoted by K) and longwave (denoted by L) radiation fluxes. The arrows denote the direction of the flux densities. The differences in Q* between rural and central city areas are small in absence of snow cover (Arnfield 2003), but there are urban induced differences in the component flux terms of the radiation budget. The incoming solar irradiance, $K_\downarrow$, can be attenuated by the pollutants in the urban boundary layer (Oke 1987; Arnfield 2003) and its spectral composition can be altered. The albedo of typical urban surfaces is typically low compared to their rural surroundings in mid

latitudes (Taha 1997), and this is expected to offset the reduction in $K_{\downarrow}$. In general therefore urban-rural differences in net shortwave radiation are not expected to be large (Oke 1987). Urban-rural differences in net longwave radiation are also expected to be small overall. The incoming longwave radiation $L_{\downarrow}$ is generally expected to be increased in urban areas, both due to the urban heat island effect and the enhanced atmospheric emissivity (Arnfield 2003). More longwave radiation is however emitted into the atmosphere since the urban area is usually warmer at night than its surroundings (Oke 1987).

$Q_H$ and $Q_E$ represent the sensible and latent heat fluxes respectively. Compared to rural areas there are distinct differences in the partitioning of energy between sensible and latent heat (Masson 2006). For example Grimmond and Oke (2002) observe extremely small latent heat fluxes for urban measurement sites representing source areas with little vegetation, and Martilli et al. (2003) neglect these in the validation of their urban parameterisation scheme for Athens. This however is dependent on the city and the characteristics of the surrounding rural area.

$\Delta Q_S$ is the stored heat flux term. This represents the storage of energy in the urban built up materials, or in the ground and roads. During daytime the storage term in the urban area is usually positive and higher than surrounding rural areas due to the thermal properties of the urban building materials, and the urban surface geometry. At night time it is negative, i.e. it becomes a source of energy as energy partitioned into storage during the daytime is released (Masson 2006).

In urban areas an additional term, $Q_F$, is added to represent the anthropogenic heat flux, since compared to rural areas there are sources of energy due to human activities such as car traffic and industry, domestic heating and cooling and electricity use (Fan et al. 2005; Masson 2006).

Evaluating the magnitude of the anthropogenic heat flux term is an interesting problem (Myrup 1969). In general this term can either be specified arbitrarily, or it can be parameterised based on energy consumption data (Bornstein et al. 2001). However it is not clear whether this term should be added to the surface energy balance equation, or to the surface layer via the thermodynamic equation, or both. The anthropogenic heat flux is also a problematic term to evaluate in a measurement campaign, since it is not possible to distinguish between $Q_H$ and $Q_F$ with a heat flux instrument. Klysik et al. (1999) find a distinct annual cycle for the anthropogenic heat emission for Lodz, Poland, with values reaching 70-90 $Wm^{-2}$ in the city centre in winter, and 20-25 $Wm^{-2}$ in summer. In particular in January (in the Northern Hemisphere) it becomes a dominant climate-influencing factor since it is larger than the absorbed solar energy (Taha 1997; Ichinose et al. 1999). As the anthropogenic heat flux is often hard to determine, model simulations usually take place in the summer months when it is not the dominant term. There have however also been a number of modelling studies investigating the impact of anthropogenic heat on urban climate (e.g. Ichinose et al. 1999; Fan et al. 2005).

### *2.1.3 Scale and the urban effect*

The urban effects described in Sections 2.1.1 and 2.1.2 can be observed on a variety of scales. The aim of this thesis is to address the problem of thermal modifications due to an urban area at the regional scale. In order to do so it is necessary to understand the spatial scales on which the elements of the urban surface interact with the atmospheric layers (Arnfield 2003) and to comprehend which processes need to be parameterised in a regional scale model. Britter and Hanna (2003) define four scales of interest when studying urban areas and their characteristic flow structures, as shown in Figure 2.1 below.

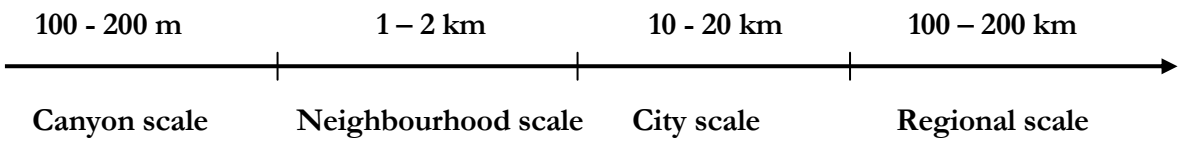


**Figure 2.1: Scales of interest when studying urban areas (Inspired by Harman (2003))**

The canyon, microscale or street scale (10-100 m) is highly relevant since people spend most of their time within the urban canopy layer (UCL), which extends roughly from the ground to roof level (see Figure 2.2 overleaf). The airflow in the UCL is complicated, and thermal and dynamic processes are controlled by microscale, site specific effects (Arnfield 2003). It is possible to study the flow and dispersion of within street canyons, around individual buildings, and at street intersections; however the details of the flow are hard to measure representatively or model accurately without using highly detailed computational fluid dynamics (CFD) modelling techniques. This scale is important for the understanding of the dispersion of pollutants which have direct human impacts and is therefore highly relevant to pollution monitoring. However CFD models are highly detailed and computationally expensive, and therefore are confined to a small area of a city (e.g. Hunter et al. 1991).

At the neighbourhood (or local) scale (1-2 km) the flow within the urban canopy is still significant, although it is also possible to treat the buildings statistically. At this scale the inertial sub-layer and the roughness sub-layer (RSL) (see Figure 2.2 overleaf) are significant phenomena and need to be parameterised (Rotach 1999) and for this reason sophisticated urban canopy parameterisation schemes have been developed (Masson 2000; Martilli et al. 2002). The RSL is a non equilibrium transition layer located close to the roughness elements, and typically extends to a height that is 2.5 times the mean building height, although this can depend on the homogeneity of the surface (e.g. Feigenwinter et al. 1999). The flow in the RSL is three dimensional and

consists of interacting wakes and plumes of heat, humidity and pollutants influenced both mechanically and thermally by the roughness elements (Arnfield 2003). Due to local scale advection the flow and turbulence fields are horizontally heterogeneous and controlled by factors such as the height of the roughness elements, building shape and separation (Roth 2000). Field measurements in the roughness sub-layer have shown the Monin-Obukhov similarity theory (MOST) to have limited value (e.g. Rotach, 1993).

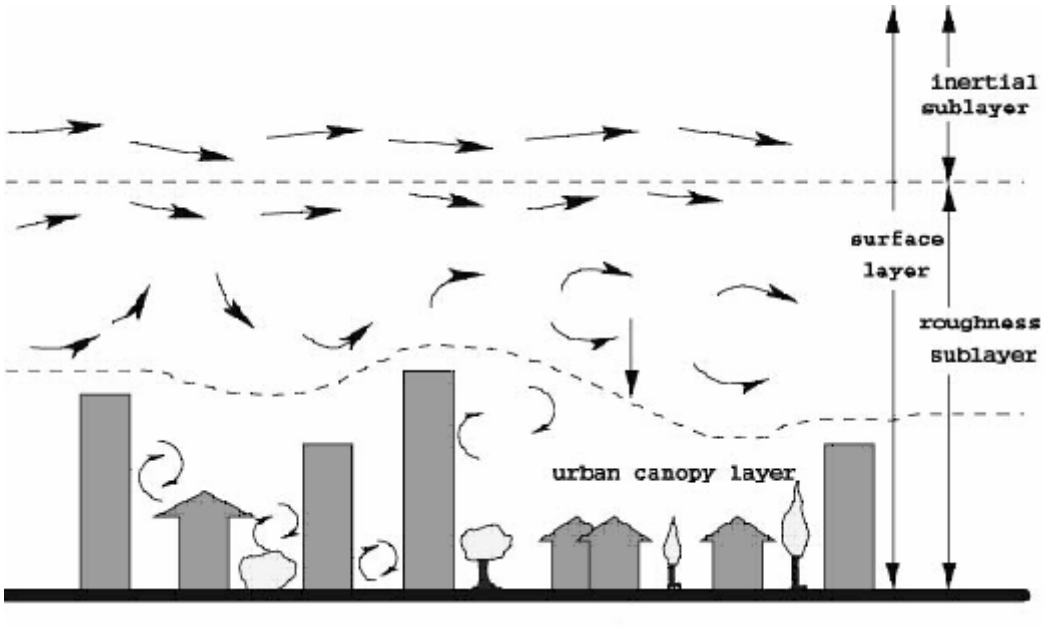


**Figure 2.2: A schematic representation of the vertical layers of the urban boundary layer at the local scale and the representative flow (from Britter and Hanna, 2003)**

In the inertial sub-layer the urban form of MOST may be applicable in order to one-dimensionally describe the turbulent fluxes, and to calculate the exchange of momentum, heat and mass. MOST is a first order approximation in which turbulent fluxes are assumed to be constant with height. This will occur if the turbulent mixing at this height above the canopy has cancelled out the significance of the individual roughness elements (Arnfield 2003). In order to

representatively sample the underlying surface measurement towers should be located in the inertial sub-layer.

Both the city scale (represented by the average city diameter) and the regional scale take into account the modification of the atmospheric boundary layer by the urban surface, i.e. the urban boundary layer (UBL) (see Figure 2.3 overleaf). Stull (1988) defines the atmospheric boundary layer as "that part of the atmosphere that is directly influenced by the presence of the Earth's surface, and responds to surface forcing with a time scale of about an hour or less". Surface forcing are for example pollutant emission, heat transfer, frictional drag and terrain induced flow modifications. Turbulence is the main process which defines the boundary layer, and is responsible for the vertical transport of quantities such as heat, moisture, momentum and pollutants. The kinetic energy of the flow can be partitioned into that associated with the mean wind, and that associated with the turbulence. This defines the turbulent kinetic energy (TKE), which is one of the most important quantities used to study the turbulent boundary layer. The horizontal transport in the boundary layer (advection) is on the other hand dominated by the mean wind.

At the city and regional scale (see Figure 2.3 overleaf), variations in flow and dispersion around individual buildings are averaged out and the urban surface represents a perturbation to the mean flow. Urban climate effects such as the urban heat island and urban pollution plume are apparent. As cities grow it is possible that regional wind and temperature circulations will be influenced, especially if general wind patterns are weak, although it is unlikely that these will be significant on the global scale. In terms of pollutant emission, large amounts of pollutants are emitted at the

city scale, although their dispersion and the formation of secondary pollutants also affect the larger regional scale (Martilli et al. 2002).

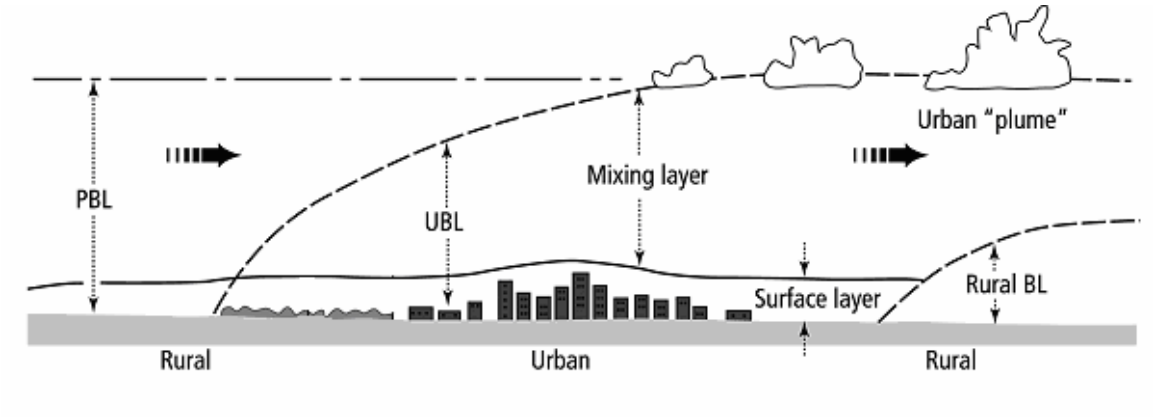


**Figure 2.3: A schematic representation of the regional influence of the urban surface on the boundary layer. 'PBL' stands for the planetary boundary layer, and 'UBL' for the urban boundary layer. Modified from a figure in Oke (1997).**

*2.1.4 The Urban Heat Island*

The urban heat island (UHI) is a particularly important example of how the urban area can influence climate and the most obvious climate manifestation of urbanisation (e.g. Oke 1987; Arnfield 2003; Fan et al. 2005). It is caused by a variety of factors which contribute to higher temperatures in the urban centre, either of the surface or the atmosphere, compared to the surrounding rural areas. The UHI can be particularly significant in exacerbating the effects of summer heat-waves, with consequent problems such as increased mortality (Johnson et al. 2005) and marked air pollution events (Stedman 2004). A UHI can also affect the regional scale flow by means of a thermodynamically driven circulation pattern (e.g. Oke 1995; Bornstein et al. 2000; Collier 2006) caused by the UHI modifying the local pressure field and the stability. If the synoptic winds are weak, and the temperature gradients are strong, then there can be a closed circulation pattern associated with the UHI, which is characterised by a strong updraft motion

over the city centre, convergent flow near the surface and divergent flow aloft (e.g. Lemonsu et al. 2002; Collier 2006). In the case of a strong synoptic flow the existence of a warm urban plume aloft extending up to 100 km downwind of the city has been established (Shea et al. 1978; Pujadas et al. 2000; Britter et al. 2003).

The existence of an urban heat island was first measured for London by Luke Howard in 1818 (Howard 1833), when a significant difference between urban and rural temperatures was observed. Modern investigations have subsequently been performed for many other cities and although the heat island climatology is dependent on the particular city structure and surroundings, the existence of the UHI has been confirmed beyond all doubt (Oke 1982).

Many factors are responsible for the UHI, including the following (e.g. Tumanov et al. 1999):

- Anthropogenic heat emission (industrial activities, residential heating etc…).
- Modification of heat fluxes due to shadowing effects.
- Differences in the albedo of urban and rural surfaces.
- Differences in the heat storage capacity of urban building materials compared to rural ones resulting in greater energy uptake during the day and release at night
- Compared to a rural environment less surface area is exposed to evapo-transpiration (though this is not the case for some specific cities).
- Differences in heat exchange due to turbulence induced by buildings.

A single, distinct type of UHI does not exist, and it is possible to define many different types, each with its own spatial and temporal characteristics (Oke 1982). Examples are the urban boundary layer heat island (increased temperatures in the atmosphere above the city), the canopy layer heat island (increased temperatures of the atmosphere between the ground and the mean building height) and the surface heat island (this refers to the difference in surface temperature between the urban and rural surface).

The intensity of the UHI is defined as the maximum difference in temperature between an urban and rural location within a defined time period, for example a diurnal cycle. The intensity of the canopy layer UHI depends strongly on the weather conditions and synoptic wind (e.g. Shea et al. 1978; Wong et al. 1978; Tumanov et al. 1999). It is highest during anti-cyclonic conditions, with clear skies and light winds (Klysik et al. 1999; Pinho et al. 2000; Morris et al. 2001; Gedzelman et al. 2003). Atmospheric fronts (whether warm, cold or occluded) act to enhance air mixing, with the effect of equalling urban and rural temperatures and weakening the UHI intensity (Tumanov et al. 1999). Strong winds will also significantly weaken or cancel out the UHI (Morris et al. 2001).

A distinct diurnal and seasonal course has been documented for the UHI intensity (e.g. Klysik et al. 1999; Gedzelman et al. 2003; Shepherd 2005). During daytime the UHI is less intense and can even vanish, whereas during the night it reaches its greatest intensity. This is due to the release of heat absorbed during the day by building materials. For many mid latitude cities the UHI intensity is greatest in summer months. During winter months, although the anthropogenic heat flux tends to be greater, there is also much less daytime solar energy to be absorbed and subsequently released by the buildings. This tends to weaken the UHI intensity.

Cold islands can also occur in urban areas, particularly during daytime when the UHI is less intense and can become negative. This is due to increased energy being partitioned into storage, which can be especially high due to the urban building vertical surfaces and heat capacities of the construction materials.

For many cities in the world an increasing trend in the UHI intensity has been identified (e.g. Lee 1992; Velazquez-Lozada et al. 2006; He et al. 2007) and this is expected to be due to an increase in population and the city area. However, it is not easy (or indeed possible) to establish a definite, linear relationship between the population (as a surrogate indicator of city size) and the UHI intensity. Although population was originally linked to the UHI development and its intensity, Oke (1987) found that any relationship would differ in North American and European cities. Also, cities located at tropical latitudes do not appear to fit into either range, probably due to different urban-rural contrasts in soil moisture. The geographic location of a city (and the corresponding regional climate, characteristics of the rural surroundings and the influences of local topography) is clearly a controlling factor in determining the UHI intensity (e.g. Nitis et al. 2005). It can also be seen that characteristics such as city structure, population density, building compactness, sky view factor, the percentage of artificial surfaces and vegetation fraction in the city are important factors in controlling the UHI development (Oke 1987). Other factors such as the frequency of suitable synoptic conditions and regional climatic fluctuations might also affect long term trends (Chandler 1965). Nonetheless population growth could be an important factor in the UHI development, since it is accompanied by increases in urban surface area, housing, roads, public transport and other services, all of which affect the surface energy balance. In recent years some major cities (for example London) have seen a decrease in population in the centre, with a migratory flux towards the suburbs. However the decrease in population is not necessarily

accompanied by a reduction in city size, or a change in the surface energy balance. In this case relationships previously established in the case of city growth can no longer be expected to apply and population change alone is not capable of explaining observed trends in the London UHI intensity (Lee 1992).

### *2.1.5 Other effects of the urban surface*

Other effects of the urban areas include increased air pollution, and effects on the hydrological cycle.

Air pollution is a serious health problem in many cities even under the current climate (Anderson et al. 1996; COMEAP 1998). Human activities in urban and industrial areas are major sources of pollutants (Fenger 1999) and carbon dioxide emissions (Svirejeva-Hopkins et al. 2004), and their distribution and evolution is driven by the thermal and dynamic processes above the city (Sarrat et al. 2006). Therefore the accurate representation of meteorological models is becoming increasingly important in air pollution studies (Seaman 2000; Sarrat et al. 2006; Muller 2007; Baklanov et al. 2008).

Increased air pollution in urban areas can also affect radiation transfer and the hydrological cycle (Givati et al. 2004) and the amount of radiation received and lost at the surface (e.g. Oke 1988; Stanhill et al. 1995; Jauregui et al. 1999). Climate change and urban expansion is expected to cause further deterioration in air quality in large urban areas (Romero et al. 1999), and future local and regional scale meteorology will have a major influence on the production, transport and dispersal of pollutants. Any increase in the frequency of hot, anticyclonic weather in summer will favour the creation of more temperature inversions trapping pollutants in the near-surface layer

of the atmosphere. For example, it has been estimated that a 1ºC rise in summer air temperature is associated with a 14% increase in surface ozone concentrations in London (Lee 1993).

The urban surface also has extensively documented impacts on precipitation and cloud cover (e.g. Changnon et al. 1971; Palumbo et al. 1980; Oke 1987; Rabin et al. 1996; Bornstein et al. 2000; Shepherd et al. 2002; Inoue et al. 2004; Shepherd 2005). These were not however considered in this PhD study since the METRAS+BEP model was not felt to be a suitable tool for analysing the impact of the urban surface on rainfall, since BEP neglects the urban latent heat flux.

*2.1.6 Mitigation of excessive urban temperatures and UHIs*

A number of studies have examined ways of mitigating the UHI, as well as excessive daytime urban temperatures, by adopting strategies such as green roofs, tree planting and modifying the albedo of buildings and road surfaces (e.g. Rosenfeld et al. 1995; Sailor 1995; Avissar 1996; Taha 1997; Taha 1997). Other ways of mitigating the effect of rising temperatures in urban areas include the reduction of building densities; changing building height, spacing and street orientation to increase shade and reduce the receipt of solar radiation; enhancing natural ventilation through a variation of building height and density; the use of high-albedo (reflective) building materials; and improved building and cooling system design (Oke, 1987).

It has been shown that the presence of large green spaces and vegetation can have an effect on local air temperatures in a city (e.g. Rosenfeld et al. 1995; Eliasson 1996; Ca et al. 1998; Rosenfeld et al. 1998; Spronken-Smith et al. 2000). A large park area would be expected to reduce the air temperature in and downwind of the park (Jauregui 1990; Ca et al. 1998), however

smaller green areas can also influence urban temperatures and have a noticeable effect (Shashua-Bar et al. 2000).

The effect of vegetation on urban climate is due to that fact that moisture availability is one of the key variables controlling the partitioning between latent and sensible heat fluxes (Oke 1982). Vegetated surfaces within cities are likely to be irrigated, and have the same water storage capacities as rural areas, and this could explain the faster cooling rates observed in parks compared to urban areas (Upmanis et al. 1998). Changes in surface albedo, and shading due to trees, also have a mitigating effect on daytime temperatures (Upmanis et al. 1998). Graves et al. (2001) find the air temperature in the Primrose Hill park area in London to be 0.6 °C cooler on average than the air temperature outside the park. This effect was shown to extend 200-400 m around the park. Best et al. (2002) find that the fraction of vegetation in the London urban area can influence the intensity of the UHI, in a non linear way which depends on the size of the urban area.

The BEP urban canopy scheme which is used in this PhD study neglects the urban latent heat flux. Since London is a highly vegetated urban area this might not be considered ideal. However the vegetated surfaces, as identified by the CEH Land Cover data, are represented by the METRAS rural land classes at the sub-grid scale. This method has also been previously used (Hamdi 2005) to represent urban areas with high vegetated fractions.

Changes in surface albedo, for example the use of solar reflective alternatives to traditional absorptive urban surface, also have the potential to mitigate urban temperatures and lower boundary layer heights (Sailor 1995; Taha 1997). Adopting high albedo, solar reflective materials helps maintain low building surface temperatures during sunlit hours by reducing the

amount of solar radiation absorbed in the building material, and therefore the convective transport of heat to the air will also be lower. The adoption of high albedo material could have a positive impact on cooling demand and ozone concentrations (Taha 1997).

## 2.2 The impact of urbanisation on local and regional climate

As seen in Section 2.1, the different effects of the urban surface are well documented. However, less is known about the impact of urbanisation on climate at a regional scale (Shepherd et al. 2006; Trusilova 2006). It is necessary to develop a metric to quantify how urbanisation affects regional and global climate, since neglecting this effect will lead to an inaccurate quantification of climate change (Pielke et al. 2002).

The emission of greenhouse gases and changes in land-use practices are two most important anthropogenic influences on climate (Kalnay et al. 2003). However the separation of these effects will often be difficult. Land-use and land cover change affects the surface albedo, roughness and Bowen ratio and therefore can be expected to have a significant impact on climate through changes in temperature, precipitation, humidity and wind speed. Land use change on the present scale may contribute significantly to changing the local and regional climate (IPCC 2001), can be expected to dominate over climate change effects due to changes in anthropogenic greenhouse gases (Stohlgren et al. 1998; Pielke et al. 2002) and could cause continental-scale changes in climate (Pitman 2003). Many studies on the effect of land-use change on climate consider modern vegetation compared to natural vegetation (Bonan 1997), desertification (e.g. Charney et al. 1977; Laval et al. 1986; Xue et al. 1993), tropical deforestation (in particular the Amazonian deforestation) (e.g. Henderson-Sellers et al. 1993) but urbanisation is also an extreme form of land-use change, since it radically alters the physical properties of the Earth's surface and may also affect its thermal, radiative and aerodynamic character (Oke 1987).

The current increase in urbanisation began with the Industrial Revolution, 200 years ago, and has lead to significant microscale and mesoscale changes in the climate and weather in urban areas

(Peterson 1969; Changnon 1992; Collier 2006). These changes are often comparable to those projected by future global and regional climate change (Baker et al. 2002). Despite covering only 1.2% of the Earth's surface (Shepherd 2005), the UN estimated that in 2003 48% of the World's population resided in urban settlements (UN 2004). By 2030 it is expected that 61% of the World's population will be living in urban areas (UN 2004). It is therefore important to understand how these increasing urbanisation patterns might be affecting local and regional climate, both from the point of view of human wellbeing (Jin et al. 2005), their support systems (Baker et al. 2002), and the effect on long term temperature records. In particular controversy exists over the influence of urban warming on large scale surface-air temperature trends (Kalnay et al. 2003) and there are indications that some long term stations might have been affected by urbanisation (Karl et al. 1988; Philandras et al. 1999).

Estimating the urban effect and the UHI in particular is far from easy. As seen in Section 2.1.3 urban effects manifest themselves at different scales. Obtaining representative measurements at the city scale is not easy. One possibility is to compare data from an urban station with that from a rural one in the surrounding area (Karaca et al. 1995; Tayanc et al. 1997; Figueroa et al. 1998; Brazdil et al. 1999; Philandras et al. 1999; Baker et al. 2002; Jauregui 2005). However it is also necessary to account for the effects of topography and other natural features, and to be certain that the rural station is not influenced by the urban area (for example if it is downwind of the city). Another possibility is to analyse the urban effect through historical analysis of the temperature time series of stations that are considered urban due to city growth (Jones et al. 1990; Yague et al. 1996; Philandras et al. 1999), however for most areas a comprehensive set of pre-urban measurements is not available for comparison and it is necessary to stratify station-by-station differences before and after urbanisation according to weather type (Lowry 1998). Other

experimental methods to investigate the urban effect are the method of transects through the city (Moreno 1994; Klysik et al. 1999; Tumanov et al. 1999; Unger et al. 2001) and the analysis of satellite data (e.g. Roth et al. 1984; Lee 1988).

The analysis of the urban effect can also be dependent on the methods used to classify urban and rural areas, for example in the US two methods are used, based on population data (Easterling et al. 1997) and satellite night-light measurements (Gallo et al. 1999) and different estimates for the impact of urbanisation are obtained for each method (Gallo et al. 1999). Kalnay et al. (2003) estimated the urban effect by comparing trends in observed surface temperatures (sensitive to changes in land use) with trends derived from a reanalysis of global weather which should be insensitive to these surface effects. They estimated a mean surface warming of 0.27 °C per century due to both urban and agricultural land use changes, and commented that the comparison of urban and rural measurements, without taking into account agricultural effects, could lead to the underestimation of the total impact of land use changes. Zhou et al. (2004) used the same method to estimate a mean surface temperature warming of 0.05 °C per decade in southeast China due to urbanisation. Satellite imagery is another tool that can be used to define a normalised vegetation index to estimate land use changes, which can then be related to meteorological data and satellite thermal data (Romero et al. 1999).

All these factors make it difficult to measure the urban impact on temperature and wind fields using a comparison of observations. As described in Section 2.3, a modelling approach is another possible way of investigating the effects of urbanisation.

## 2.3 Justification of modelling approach

In Section 2.2 the difficulties in measuring the urban impact on temperature by the comparison of observations have been discussed. Due to these difficulties modelling may be a valuable tool for investigating the effects of land use change, and urbanisation in particular, on weather and climate at a regional scale (Lamptey et al. 2005). An advantage of the modelling approach is that it is possible to eliminate the effect of climate variability and non stationarity.

For example, although their focus was primarily on vegetation, Stohlgren et al. (1998) performed simulations for different land use scenarios representing the natural pre-European settlement state of vegetation, current land use and an increase in irrigated land and concluded that the effects of land use practices on regional climate could overshadow larger scale effects such as those due to greenhouse gases.

Many modelling studies focusing on the expansion of the urban area have not fully represented the effects of the urban area on the mesoscale flow. For example a modelling study by Ichinose (2001) on the regional warming due to land use change during the past 135 years in Japan has shown that the effect of urbanisation through time has produced a change in mesoscale flows, through the weakening of the daytime penetration of the sea breezes, and a regional warming. However this study did not consider the effects of the urban canopy structure and the shadowing and trapping of radiation therein are not accounted for in the mesoscale model used in this work, which could be the cause of the disagreement between the simulated daily minimum temperatures and those estimated from observed data (Ichinose 2001). Likewise, Klaić et al. (2002) investigated the impact of two scenarios of hypothetical urbanisation in the Zagreb area on the local winds but in this study the urban surface was represented as a land class

characterised by appropriate values of the roughness length, albedo, evaporation, heat capacity and thermal conductivity. It was found that the hypothetical urbanisation scenarios (increase in densely urbanised area of 12.5% and 37.5%) did not cause a significant modification of the local winds over the Greater Zagreb area. In the urbanised areas and their vicinity reductions in the average wind speed were found, but no significant change in wind direction was documented. Mölders and Olsen (2004) performed simulations to investigate the impact of urban growth (the town area is enlarged by 20%) on precipitation for a high latitude city, but as in previous studies the city was represented by appropriate values of the albedo, emissivity, roughness length and stomatal resistance, and by a change in the empirical values used to calculate transpiration.

All the above literature examples consisted of short term simulations, generally 48-72 hours long, for typical summertime conditions and investigated physical processes involved in the UHI formation and related effects. This is the approach that will be followed in this PhD study as well. A small number of other studies have conducted longer simulations, for example Lamptey et al. (2005) performed 5 year simulations for the North-Eastern United States to examine the presence of the urban areas on climate. However, the focus of Lamptey et al. was on the long term climate and therefore the results were averaged monthly or seasonally in order to smooth out differences in urban effects for different days, for example the increase in intensity of the urban heat island for calm, clear nights. Also the large spatial resolution (36 km) adopted means that different land use zones within cities were ignored, which might have influenced the results. Lamptey et al. found an increase in near surface temperatures of more than 1 K over urban sites, in both summer and winter, as a result of urbanisation, and a decrease in the diurnal temperature range of 0.4 K due to the same cause.

Trusilova (2006) carried out a study to examine the effects of urbanisation with a mesoscale model with a more detailed representation of the urban surface. In this case a version of the single layer Town Energy Balance (TEB) scheme (Masson 2000) was implemented into the model MM5, and simulations were performed for two months (January and July, since the strongest urban heat island effect occurs in summer and winter) for six years (2000 to 2005) for a domain representing most of Europe. A six year period was considered sufficient to investigate urbanisation driven climate changes rather than feedbacks between urban environments and the global climate. A base line case scenario was simulated in which the urban surface was removed, and further simulations representing current urbanisation and an increase in city area and mean building height. A regional effect index was introduced in order to characterise the spatial extent of the urban climate anomalies. Trusilova (2006) found that the conversion from rural to urban land resulted in significant changes to the near surface temperature and in particular to the diurnal temperature range. The main differences between the work of Trusilova (2006) and this PhD study include the large horizontal resolution (10 km, compared to 1 km used in this PhD thesis) and the focus on a domain representing the whole of Western Europe. The focus in this thesis is on a large number of simulations representing many states of urban land cover for one city (London), rather than longer simulations focusing on average climatic effects.

### *2.3.1 Representation of the urban area in mesoscale models*

Models can be used at a variety of scales to understand the effects of the urban area. For example meteorological models at a variety of scales can be used to assess the effects of urban areas on phenomena such as the urban heat island (e.g. Tapper et al. 1981; Atkinson 2003), wind flow patterns (e.g. Klaic et al. 2002), boundary layer structure and growth (e.g. Seaman et al. 1989;

Pino et al. 2004), convective activity and precipitation (e.g. Bornstein et al. 2000; Thielen et al. 2000), and air quality (e.g. Sarrat et al. 2006).

The correct representation of the thermal and dynamic effects of the urban surface on the atmospheric boundary layer in mesoscale models has important implications for understanding the urban effect, as well as studying pollutant dispersion and for simulating urban air quality. In urban areas human activities are large sources of atmospheric pollutants, and their spatial distribution, concentration and residence time in the atmosphere is driven largely by thermal and dynamic processes over the city. In order to understand pollutant dispersion and assess urban air quality and human exposure, dispersion models rely on atmospheric mesoscale models to provide accurate meteorological fields representing the urban boundary layer (Seaman 2000; Collier 2006; Sarrat et al. 2006).

At the microscale, the energy balance of the urban surface can be studied with building resolved models, but due to computational costs and the need to provide highly detailed input data, these are limited to analysing local urban meteorological and climatic conditions, or highly specific studies such as the dispersion of pollutants from a specific source. In a mesoscale model with typical spatial resolution of the order of a kilometre, it is impossible to resolve the effects of single buildings due to computational cost, and it becomes more efficient, and indeed necessary, to adopt a building averaged approach (Martilli et al. 2002).

In mesoscale models (i.e. models with a grid size that ranges from 100 m for research models to 10 km for operational mesoscale models) the interaction between the ground surface and the atmosphere has typically been based on MOST, a first order approximation which assumes a

constant flux surface layer in the lowest tenths of meters of the atmosphere. Field measurements in the RSL have shown MOST to have limited value, for urban areas (Rotach 1993).

Given the extremely heterogeneous and complex nature of the urban surface, the parameterisation of urban effects in models is not easy. According to Piringer et al. (2002) the main aspects of the urban surface that need to be taken into account are: the influence of the urban canopy on airflow, thermal properties including radiation trapping and shadowing effects, and the reduction in albedo due to radiative trapping between the canyon walls. The model should be able to simulate the UHI effect, the near neutral nocturnal boundary layer and the surface heat fluxes.

The urban surface can be parameterised in mesoscale models in a number of different ways (Masson 2006). The first attempt to urbanise a mesoscale model was that of Myrup (1969) who constructed a 1-D diagnostic urban heat island model which specified the urban surface by its roughness length, albedo, soil heat capacity and relative humidity. Subsequently a number of different techniques were used to extend this work in 1-D, 2-D and 3-D models, which are reviewed in Bornstein et al. (2001) and Craig et al. (2002). Schultz and Warner (1982), despite finding that the urban effects on air circulation were smaller than those due to sea breezes and local topography, stated the need to include the correct characteristics of the urban surface in order to represent the urban heat island effect. Arnfield (1998) also considered the need to represent the effects of land surface heterogeneity at the sub-grid scale on surface fluxes, in both regional and global climate models. All the early first generation of models however used a simple zero building height approach to simulate urban effects, which presents numerous limitations.

More recent efforts to parameterise urban effects on the thermodynamic and momentum fields are reviewed in Craig et al. (2002), Masson (2006) and Martilli (2007). The nature of the parameterisation used should depend on the aim of the simulation and the CPU power available. Recent efforts have focused on the dynamic or the thermodynamic properties of the urban surface (Masson 2006). The dynamics of the urban surface can be parameterised by a change in roughness length based on the characteristics of the urban area (e.g. Bottema 1997), or by introducing a drag term (e.g. Uno et al. 1989; Brown 2000; Ca et al. 2002; Martilli et al. 2002; Dupont et al. 2004) to the momentum and turbulent kinetic energy (TKE) equations in order to represent the drag induced by the presence of buildings (this approach is derived from that used for vegetation canopies).

The thermodynamic effects of the surface can be parameterised by modifying the urban surface energy balance in a number of ways, aimed at either finding a relationship between heat storage and net radiation, or solving the physics of the problem (Martilli 2007). A simple approach is based on the semi-empirical objective hysteresis model (OHM), an empirical formulation for heat storage, of Grimmond et al. (1991) together with the LUMPS scheme (Grimmond et al. 2002) to estimate the turbulent fluxes. However this approach is limited by the availability of field data. Another simple approach to represent one of the urban effects consists in incorporating an anthropogenic heat term (Fan et al. 2005), although the success of this will also be dependent on the availability of extensive data on energy consumption and traffic. More sophisticated physical approaches consist in parameterising the shadowing and trapping of radiation in the canyon (Masson 2000) as well as the advanced SM2-U approach of Dupont et al. (2004) which uses a modified soil module which computes the heat fluxes and surface temperatures following

the vertical distribution of vegetation and buildings in the canyon, as well as the drag force approach to represent dynamic and turbulent effects.

Urban canopy models aim to solve the surface energy budget for a three dimensional urban canopy with simplified geometry, by computing separate energy budgets for roofs, roads and walls and treating the radiative interactions between roads and walls (Masson 2006). Canopy models can be either single layer models (Masson 2000; Kusaka et al. 2001) in which the canyon air is parameterised and the base of the atmospheric model is at roof level, or multi-layer models (Ca et al. 1999; Martilli et al. 2002) in which several atmospheric levels are influenced by the buildings. The coupling between atmospheric mesoscale models and multi layer canopy models is complicated due to the direct interaction between the canopy scheme and the mesoscale model equations; however these canopy models are able to represent the turbulent profiles in the canopy and roughness sub layers. Urban canopy models have been developed for, and implemented into a large number of mesoscale models in recent times (e.g. Otte et al. 2004; Sarrat et al. 2006) with the aim of improving the representation of the urban surface.

Operational or Numerical Weather Prediction (NWP) mesoscale models typically have grid cells of an order of magnitude higher than those models used to study the impact of the urban surface on air flow. The requirements of accuracy and timeliness for weather forecasting mean high computational resources, and for this reason the methods used to represent the urban surface are different. Best (2006) reviewed progress made in implementing urban surface schemes into operational mesoscale models (resolution of the order of 10 km, which is not sufficient for a detailed representation of the city), global models and climate change models. The easiest scheme to implement in an operational mesoscale model is the general canopy scheme of Best

(2005), which uses a simple energy balance similar to that of vegetation, without distinguishing between different urban surfaces or incorporating the anthropogenic heat. This scheme has already been implemented into the UK Met Office Mesoscale model and evaluation has shown that the complexity of the scheme probably needs to be increased to improve model performance (Best et al. 2006). Complex schemes such as those devised for non operational models can also be implemented, although the computational cost is a limiting factor. Work is however ongoing to implement the scheme of Masson (2000) into the Meteo France and Environment Canada operational mesoscale models (Mailhot et al. 2007), and to implement that of Martilli et al. (2002) into the Meteo Swiss mesoscale model (Clappier et al. 2005; Muller 2007).

For this PhD study the urban canopy parameterisation scheme BEP (Martilli et al. 2002) was chosen to be implemented in the mesoscale model METRAS. BEP is a sophisticated multi-layer urban canopy scheme which combines the drag force approach for the momentum and TKE, with the treatment of urban thermodynamics (including the shadowing and trapping of radiation in the urban canyon) developed by Masson (2000)). The urban scheme represents the impact of the horizontal and vertical building surfaces in the momentum, TKE and heat equations, and is described in more detail in Chapter 3. The urbanised model will then be used to simulate the effects of urbanisation and changes in urban form on regional climate in the London area. The set up of this model for London is important as urbanised mesoscale models could be of increasing practical application in managing London's air quality and response to climate variability.

The choice of BEP has the advantage that it is one of the most complex schemes used to represent the urban surface (Best 2006), which enables a process based study to be undertaken. It has the advantage over the Masson scheme of allowing different urban classes to be represented

using different building parameters. The performance of BEP has been validated for the city of Athens (Martilli 2003), for Basel with measurements from the BUBBLE campaign (Hamdi et al. 2005; Roulet et al. 2005) and for Marseilles with measurements from the ESCOMPTE campaign (Hamdi et al. 2005). In general the validations find the largest differences between simulations with and without BEP occur for downtown and suburban areas during night time, with rural sites showing similar results. Following the implementation of the BEP scheme better agreement is found with measurements for both daytime and night time conditions.

Since this work began, BEP has been chosen as the urban scheme to be implemented in a number of mesoscale research and operational models, such as MC2 (Krayenhoff et al. 2005), TVM (Hamdi et al. 2005), WRF (Martilli et al. 2007), DMI-HIRLAM (Baklanov et al. 2005) and the Meteo Swiss operational Forecasting model aLMo (Clappier et al. 2005; Muller 2007). However, it has the disadvantage of being more computationally expensive compared to a simpler scheme, as well as the difficulty in obtaining all the required input information for an extensive domain. Another disadvantage of the BEP scheme is that it does not include latent heat fluxes. This means it does not take into account the contributions of urban parks and gardens to the surface energy budget. This is overcome in this PhD study by using the relevant METRAS land surface schemes to treat the urban vegetation.

A SWOT (Strengths, Weaknesses, Opportunities and Threats) analysis was carried out to summarise the choice of the BEP and METRAS models (see Table 2.1 and Table 2.2).

**Table 2.1: SWOT analysis for the BEP urban scheme**

| BEP urban canopy scheme | |
|---|---|
| **Strengths** | **Weaknesses** |
| Sophisticated multi-layer urban canopy scheme which is well respected in research field | No explicit latent heat treatment |
| Validated in a number of research studies for detailed urban campaigns | Simplistic anthropogenic heat treatment |
| Expanding implementation into a number of research and operational models | |
| Availability of model code from author and permission to use in this PhD research | |
| **Opportunities** | **Threats** |
| Use of a number of urban classes allows best fit to CEH Land Use data and resolves some of the complexity of the urban surface | Sophisticated scheme has the effect of being computationally expensive compared to more simple urban schemes |
| Interpolation of results from the BEP grid back to the METRAS grid allows a higher vertical resolution over urban area | Extensive data requirements |
| Opportunity to compare model results and validation with literature | Latent heat fluxes must be incorporated for use for London domain since this city differs widely in the vegetated fraction from Mediterranean cities where first implemented |

**Table 2.2: SWOT analysis for the METRAS mesoscale model**

| METRAS mesoscale model | |
|---|---|
| **Strengths** | **Weaknesses** |
| Used for meteorological simulations in urban areas and impact of urban surface on air quality | Very simple treatment of urban surface |
| Part of a unique modelling system consisting of a microscale and mesoscale model using the same code | Relatively small number of land use classes compared to more advanced models, especially for vegetation |
| Good agreement of simulated and meteorological data for an urban agglomeration | Complex routines to assimilate land cover data and meteorological data for initialization |
| Possibility to prescribe sub grid scale land cover classes | |
| Established use in department | |
| **Opportunities** | **Threats** |
| Opportunity to develop more advanced urban surface representation | Computationally expensive for long and complex simulations |
| Opportunity to contribute towards the METRAS model development | Complex code structure and differences between BEP and METRAS structures |
| Opportunity for integration with the microscale model and urban air quality studies | Simple shortwave and long wave radiation treatment are not compatible directly with BEP code structure |
| Ongoing development into parallelisation and speeding up model code | |

## 2.4 Urbanisation of the South East of England

There is much interest in the social and economic consequences, both positive and negative, of climate change in London, since it is not only the capital of the UK but a major world city. Changes to the World's climate will affect all parts of our globe. This will fundamentally affect the environmental, economic, social and political drivers that influence London. The UHI effect exacerbates many impacts of climate change in London, and as an example this may result in increased summer heat stress and mortality.

London, with 6.7 million inhabitants (12% of the population of Great Britain) and an area of 1942 $km^2$, is one of the largest cities in the European Community. It is as large as Paris and twice as large as Berlin. London is a World city, on a similar scale to New York, Tokyo, Los Angeles or indeed Mexico City or Bombay. It is also an old city, founded in Roman times (AD43) and the average age of its infrastructure (e.g. the housing stock) is high compared to the rest Great Britain. London is politically divided into by 33 local authorities, 32 boroughs and the Corporation of London. The nuclei of London are the areas known of the City (an area of 3 $km^2$ in the centre of London) and Westminster, and it is bordered by the Chilterns in the NW, and the North Downs in the South. The main features of London's surface morphology are the North Downs escarpments (rising to 268.8 m), the Thames floodplain; the area of North London rising up to 122 m, and the commons and parks of South London with rise 30-45 m above surrounding low lying districts.

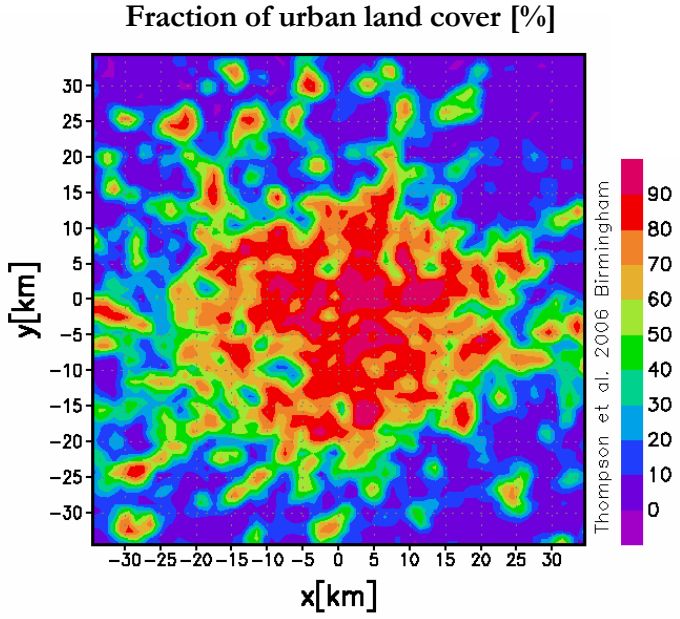


**Figure 2.4: Fraction of urban land cover in the London region.**

Figure 2.4 shows the fraction of urban land cover in the London region. Urban parks such as Richmond Park are visible as areas of very low urban fractions. The land cover for the model domain is analysed further in Chapter 3 and maps of the major rural land cover types are presented.

Key environmental impacts that have been noted for London in a number of different studies (LCCP 2002; Hunt 2005; West et al. 2005; Wilby et al. 2006, London Climate Change Adaptation 2008) are:

- Flood risk (London is vulnerable to 3 types of flooding, the inundation of floodplains by river water, local flooding when the drainage network is overwhelmed by intense rainfall, and by tidal surges in the Thames. Climate change could adversely affect all three with the latter leading to more frequent operation of the Thames Barrier).

- Heat waves

- Water resources (reduction in summer soil moisture, lower summer and higher winter flows in rivers).

- Air Quality

- Biodiversity

A study called "London's Warming: The impacts of climate change on London" was launched in Oct 2002 by London Climate Change Partnership (LCCP 2002), with the overall objective of outlining the 'threats and opportunities presented by climate change, and starting to address the responses needed'. A further study in 2008 entitled "The London Climate Change Adaptation Strategy – Draft Report" aims to "protect and enhance the quality of life of Londoners and to promote and facilitate sustainable development of London by helping London and Londoners prepare for the impact of climate change and extreme weather" (GLA 2008). This will identify the climate impacts that are likely for London and provide guidance and policies for precaution and adaptation.

### *2.4.1 Expansion of London and urban forms*

London has been expanding since the Roman times, although different periods in history have been characterised by different rates, and forms, of physical expansion (Mogridge et al. 1997). The population of 6.7 million quoted above is that of Greater London, which represents the continuously built-up area. If the outer metropolitan area is included in the estimate, the population rises to around 13.2 million, and for the South East region to around 17 million (Parker 1995). Population growth will not however be the focus of this review, since land use change is the predominant driver of urban effects on climate.

The built up area of London can currently be identified with some precision, thanks to the Green Belt policy of the post war period. The Metropolitan Green Belt describes the open land which extends for between 25-40 km in width around the city of London (Longley et al. 1992). The Green Belt was implemented in the 1944 Greater London Plan (Abercrombie 1945) with the aim of containing the growth of the urban area, preventing urban sprawl, preserving open land for agriculture and recreation, as well as preventing the coalescence of the small and medium sized towns located within it. Longley et al. (1992) argue that the Green Belt is likely to have significantly affected the geometry of the urban form, and the continuous built-up area of London has not extended much beyond that of 1939, although the Green Belt policy has caused the densification of the suburbs and infilling.

Two types of growth have been apparent in the London region: the peripheral expansion of the metropolis, and expansion clearly related to London but occurring beyond the boundary of the continuous built-up area (Hall 1974). The former dominated from around 1870 to 1930, the latter form of expansion has dominated since 1930, although both have been present at all times. In latter years the continuous built-up area has increased very slowly, while there have been higher rates of growth, both in urban coverage and population beyond the Green Belt.

From the maps presented in Figure 2.5 and Figure 2.6 (page 43 and 44) it is possible to analyse the expansion of London at given times in the past 200 years. These maps are taken from Sinclair (1964) and Mogridge et al. (1997). In 1800 the city consisted of a compact urban area with a small number of outlying centres. By 1850 some expansion had taken place in both the centre and the outlying areas, with the central built-up area still remaining relatively compact. A map for 1880 shows both substantial suburban development as well as the growth of the centres

beyond the boundaries of the continuous built-up area. By 1914 the metropolis had substantially enlarged, as had the urban areas distant from the metropolis itself. By the outbreak of the First World War London occupied a circular area of radius between 6-8 miles (Thomas 1970), with settlements growing rapidly outside the built-up area. The area of London had doubled by 1939 although the density of the inter-war development was very low. By 1939 Thomas (1970) estimated that London occupied a circle of 12 miles. The map for 1939 shows the last major expansion of the metropolis, and the growth of the surrounding urban areas. The map for 1958 indicates infilling caused by the adoption of the Metropolitan Green Belt, and the establishment of new towns (indicated by the letter N) within or beyond the Green Belt. Post Second World War development has been a lot denser than in the inter war period, with land being used intensively and older war damaged buildings replaced by taller, more compact structures (Thomas 1970). By 1981 further expansion of the surrounding urban areas had taken place, with second generation new towns such as Milton Keynes (indicated by the letter M and located about 75 km North-West of London) having been established. Clearly in the past 50 years there has been an evident growth of London as a region, rather than of the metropolis itself (Mogridge et al. 1997). The population of Inner and Outer London peaked in 1939 (Thomas 1970), and has slowly decreased ever since, whilst the surrounding settlements have gained in population. The domain used for the scenarios representing past and future urbanisation is shown in Figure 2.6.

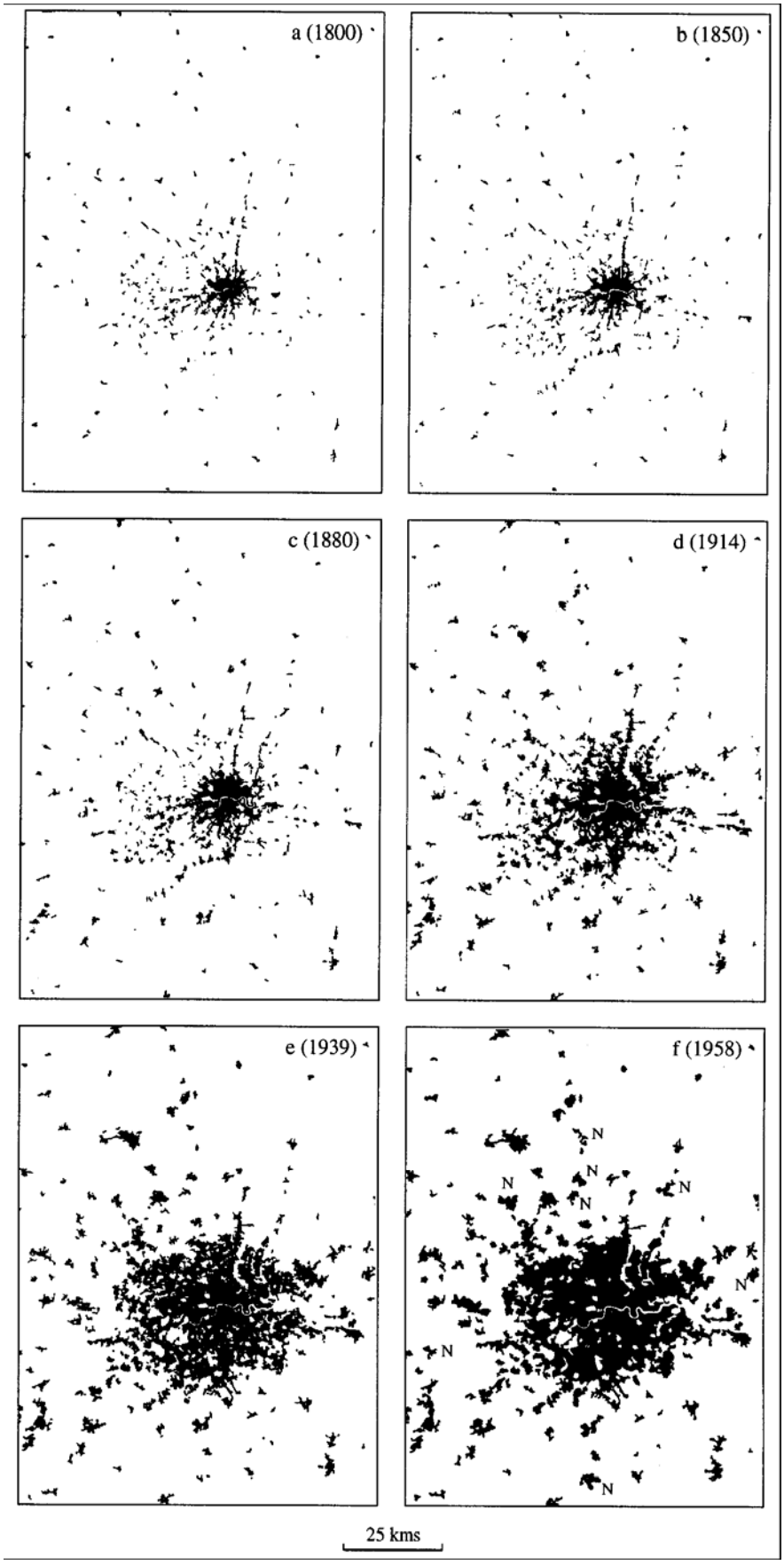


**Figure 2.5(a-f): Built-up area of London in 1800 (a), 1850 (b), 1880 (c), 1914 (d), 1939 (e) and 1958 (f). From Mogridge et al. (1997).**

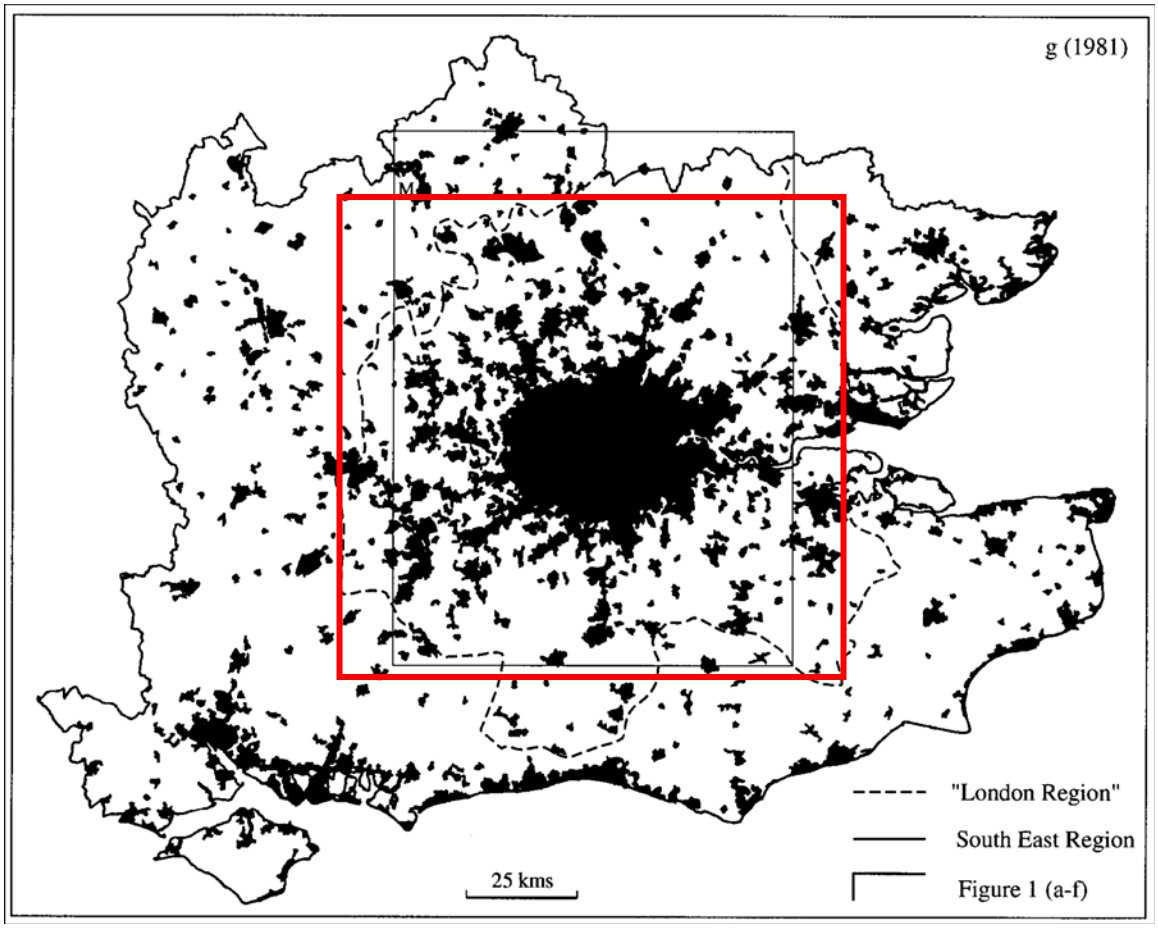


**Figure 2.6: Built up area for London in 1981, from Mogridge et al. (1997). The red box shows the domain used in Chapters 6 and 7 for the scenarios representing past and future urbanisation.**

In terms of the urban form of the city, Chandler (1965) identified a roughly concentric pattern of urban forms, from the outward growth from the two nuclei (see Figure 2.7).

- Central London: central high density commercial district; characterised by modern buildings of steel, concrete and glass, and lower but equally massive and closely spaced Victorian (and older) buildings. Open spaces in Central London: St James's Park (93 acres), Green Park (53 acres). Kensington Gardens (275 acres) and Hyde Park (360 acres).

- Mainly high density development (residential, industrial and dockside in the east) with a large number of open spaces from the years 1750-1914.

- Mainly low density development from post 1914. Characterised by smaller, 2 storey, semi-detached and detached houses with gardens, on fairly wide roads, frequent open spaces such as playing fields and allotments, and some one of two storey factories.

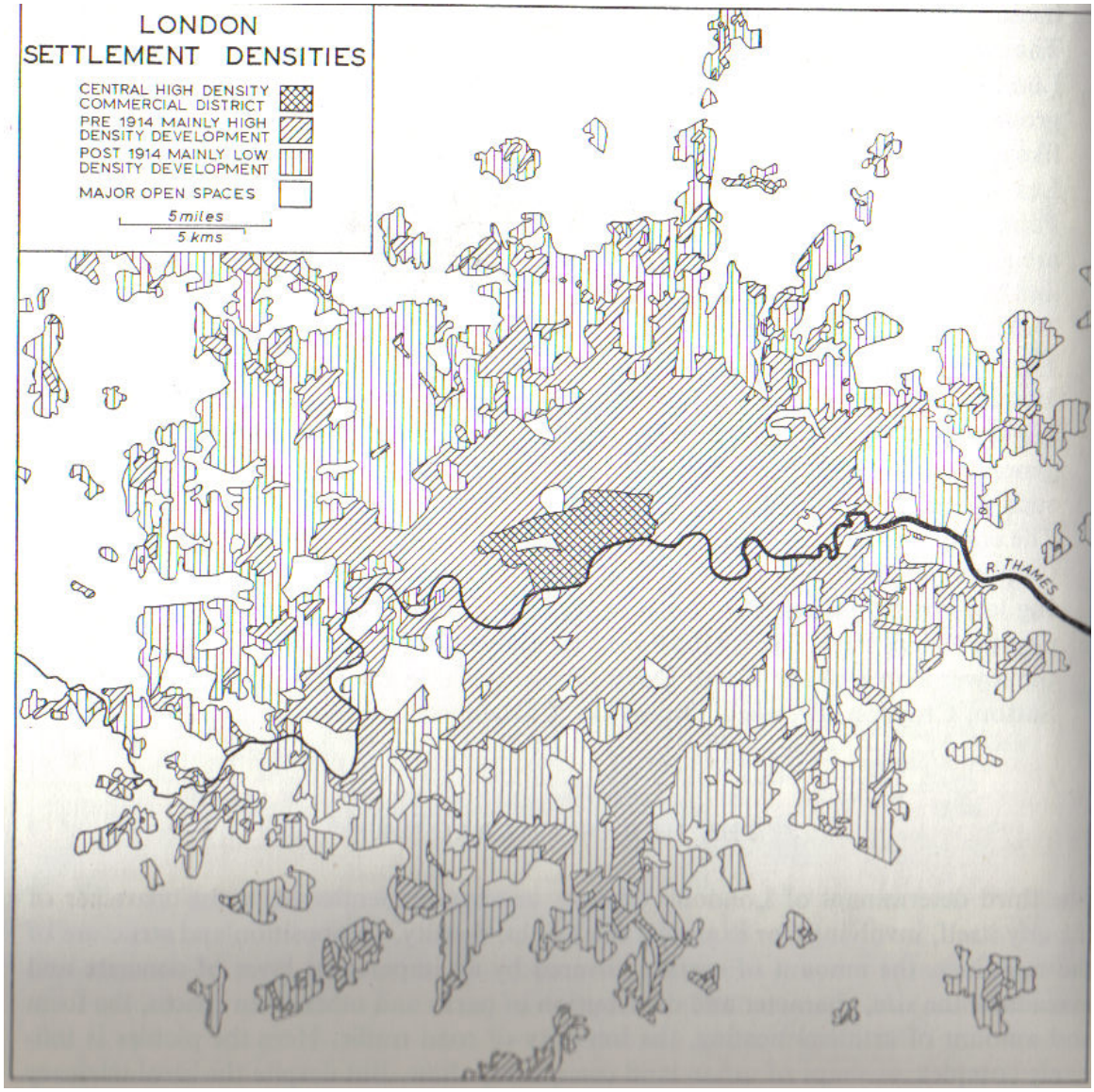


**Figure 2.7: Urban classes taken from Chandler (1965)**

*2.4.2 The climate of London*

The London regional climate is temperate, with average temperatures of 5.5 °C (January) and 18.1 °C (July), and prevailing South-Westerly winds. In 1964 there were 18 climate and synoptic stations within or very near London. This represents substantial coverage for the built up area, though more readings are needed for a detailed spatial study of the

climate of London, and currently only one of the UK Met Office MIDAS network of weather stations (the London Weather Centre) is truly located in the London urban area.

Chandler (1965) identified three factors which determine the climate of a city. These are the general regional climate, modifications due to local geomorphology and those due to the urban development (e.g. the character of the city, for example the height, density, composition and structure of the buildings, amount of surface covered by concrete, size, character and distribution of parks and open spaces, intensity of road traffic and amount of artificial heating). Relatively few references on the climatic implications of urban sprawl were available, which is surprising considering the radical and easily perceptible differences between the climates inside and outside towns. It is hard however to isolate the effects of the urban area on regional climate from other influences such as those due to drainage and topography (Chandler 1962).

### *2.4.3 The London urban heat island*

London displays a variety of urban forms and densities which complicate the measurement of the UHI intensity. There is also the problem of identifying a rural site that has not been influenced by the development of the city.

The UHI of London was first measured by Luke Howard at the start of the 19$^{th}$ century. He found that Central London could be several degrees warmer than surrounding rural areas, and attributed this to anthropogenic heat emissions due to increased fuel burning in urban areas. Bilham (1938) found that the over London mean wind speeds, as well as the number of calms, were reduced.

In 1965 Chandler observed that the London climate was profoundly modified by human activities and found a mean difference of 4-6 °C between the nocturnal temperature in the centre of London, and that of its surrounding rural areas (Chandler, 1965). An early survey of London's heat island indicated that the peak usually lied North-East of central London in Hackney and Islington, reflecting the density of urban development, and the displacement of the heat-island by prevailing South-Westerly winds (Chandler, 1965). The highest intensity heat islands were typically recorded one or two hours before dawn, and the weakest mid-afternoon (Chandler, 1962). Conditions that appeared to be less favourable for the development of intense heat islands were observed to be high wind speeds, extensive low clouds and high humidity (Chandler 1960). Chandler (1962) also observed the decrease in pollution, and increase in humidity outside central London.

More recently the London UHI has been studied by Lee (1992), Graves et al. (2001), Threlfall (2001), the Greater London Authority (2006) and Hacker et al (2007). Graves et al. (2001) reported the results of a detailed monitoring campaign of hourly air temperatures in London in 1999-2000, designed to investigate whether changes to the building stock, anthropogenic heat releases and air pollution had affected the UHI since Chandler (1965). They reported a mean peak temperature difference between the British Museum and a rural reference station in Langley Country Park (about 30 km west, away from local development) to be 3 ºC over the summer of 1999 (Graves et al. 2001), with maximum UHI intensities of 7 °C recorded. A UHI intensity between 1 and 2 °C was recorded 33% of the time.

For mid-latitude cities, of which London is an example, the UHI typically displays a market seasonal and diurnal pattern, with the strongest UHI intensities recorded on summer nights (due to the release of heat absorbed by buildings during the day), and generally weaker intensities during the winter (despite greater anthropogenic heat flux) due to the reduction in the absorption (and subsequent release) of solar energy. Graves et al. (2001) found that the London UHI is most pronounced at night time (with a near zero intensity observed for the mid afternoon period in summer months), and in calm, clear conditions, that the intensity weakens with increasing wind speed and distance from the centre, and that the location of the maximum UHI intensity shifts with changes in wind direction (typically by several kilometres). The UHI is also highly dependent on weather patterns, and it can vary widely from one day to the next. Wilby (2003) found that the nocturnal UHI was strongest in the summer (peaking at 2.2 °C in August) and weakest in the winter (1.1 °C in January).

Graves et al. (2001) did not observe a weekly cycle in the UHI intensity in summer months. This suggests that there is no weekly cycle in the heat released from buildings and traffic. In winter months it is expected that the anthropogenic heat flux will play a more significant role, as an increase in UHI intensity from late afternoon to mid morning is observed (Threlfall 2001).

### *2.4.4 London Warming? Trends in the UHI intensity*

Lee (1992) analysed recent trends in London's heat island over a period characterised by a decline in population due to counter-urbanisation. It is difficult to establish whether the observed trends are due to the change in population, or other factors, such as variations in

the seasonal/annual frequency of suitable synoptic conditions (e.g. the frequency of anticyclones). Whereas an increase in population is generally accompanied by an increase in surface area of the city, as well as increases in public transport and other services, the decline in the population of Greater London (in part due to migration from inner city residential areas to the outer suburbs) will not necessarily be accompanied by a decrease in the cities surface area. It is also necessary to take into account the increase in car traffic in London, changes in fuel usage and improved insulation in newer buildings. Lee (1992) took St James's Park to represent central London temperatures (even though temperatures in the park are expected to differ from those of surrounding streets), and Wisley was selected as the rural site. When performing an urban-rural comparison between these two sites it is not possible to accurately calculate the absolute magnitude and spatial variation of the London UHI; however it will still be possible to identify trends.

Graves et al (2001) found an increase in the number intense nocturnal heat islands (defined as greater than 4 °C), at a rate of 4 nights per decade since the 1950s. On the other hand the number of intense daytime heat islands was found to decline at a rate of 1 day per year since the 1980s.

Wilby (2003) found that since the 1960s the intensity of the nocturnal UHI had increased by approximately 0.12 °C per decade. Lee (1992) suggested that such a trend could be attributed to urban air pollution, changes in population, traffic volume and urban redevelopment. Based on a mid-range emission scenario (Hulme et al. 2002) and not taking into account changes in urban population, energy consumption, building density etc, Wilby (2003) estimated a further increase of 0.26 °C by the 2080s, which equates to an urban

warming of 0.04 °C per decade, in addition to regional warming. The possibility of higher urban temperatures is concerning due to the fact the UHI exacerbates summer heat-waves, leading to increased heat stress and excess mortality. For example, the heat waves in the summers of 1976 and 1995 have been associated with a 15% increase in mortality in Greater London (Rooney et al. 1998; Kovats et al. 2004). On the other hand however, Langford and Bentham (1995) estimated that 9,000 wintertime deaths per year could be avoided by 2025 in England and Wales under a 2.5 ºC increase in average winter temperatures.

## 2.5 Summary

This review has considered the urban modifications to the mechanical, thermal and hydrological properties of the atmosphere. It is difficult to make representative measurements of urban modifications, and to represent all the effects of the urban surface in a model. Modelling studies are however a useful way of investigating effects of the urban surface that can not be easily measured at representative scales and of providing information regarding the impact of past and future examples of urban land cover. Mesoscale modelling studies on the effects of urbanisation to date are limited, and few studies exist which use a sophisticated parameterisation of the urban surface to simulate urban effects.

Possible ways of representing the urban surface in mesoscale models are reviewed. In order to address the aims of this study of understanding how changes in land cover due to urbanisation have affected the London region, a multi-layer urban canopy scheme (BEP) is implemented into the mesoscale model METRAS. This sophisticated treatment of the urban surface, together with that fact that the model is run at a much higher spatial resolution than past studies (1 km compared to for example 10 km for Trusilova et al. (2006)) make it possible to investigate the effect of urbanisation for a single area in much greater detail, with input data specific to the city of London rather than representative of all European cities, and past and future urbanisation scenarios, as well as a base line with no urban areas, specific to London. As for many past studies, the focus will be on representative cases of anti-cyclonic conditions which are favourable to the development of urban effects such as the urban heat island, rather than long term model runs which are computationally very expensive and which, when average monthly or seasonally, smooth

out differences in the urban heat island strength due to favourable meteorological conditions.

# Chapter 3: Methods

In this section the modelling tools used in this study are described. Section 3.1 describes the mesoscale model METRAS which was chosen for the work, and Section 3.2 describes the multi-layer urban canopy scheme BEP (Martilli et al. 2002) which was implemented into the mesoscale model. The methods used to implement the urban scheme are described in Section 3.3. Section 3.5 describes the data sources used in this study, including the topographic data used to configure the model domains, the meteorological data used to initialise the model and the specific urban data needed by the BEP scheme.

## 3.1 METRAS

### *3.1.1 Model overview*

METRAS is a non-hydrostatic, atmospheric model developed by the University of Hamburg (Schlünzen 1990). The model uses time dependent prognostic equations to calculate wind, temperature, turbulent kinetic energy, humidity, and liquid water (cloud and rain) values, and non time dependent diagnostic equations for pressure and density. The anelastic and Boussinesq approximations are made, and the Coriolis parameter is assumed constant in the model area.

The intended typical field applications of the model are, amongst others, wind, temperature, humidity, and precipitation fields at the meso-γ and meso-β range (defined in Stull 1988) over complex terrain and effects of meteorology on air quality. The horizontal resolution

adopted in previous studies ranges from 5 m to 10 km, for a domain size of a minimum 10 km × 10 km to a maximum of 400 km × 400 km.

METRAS is part of the M-SYS model system developed for the assessment of urban air quality (Trukenmüller et al. 2004) at different scales and is unique in being a part of the first model hierarchy that includes both mesoscale and microscale models based on essentially identical equations and code. Trukenmüller et al. (2004) showed a good agreement between simulated and measured meteorological data when the M-SYS system was implemented for the air quality assessment of the Hanover-Brunswick agglomeration.

The model equations are solved on a staggered Arakawa C grid (see Figure 3.1), meaning that the velocity components ($u$,$v$ and $w$) are calculated at the cell interfaces, while all other variables are defined as volumetric cell averages at the cell centre. This type of grid represents gravity waves better than other grids (Mesinger et al. 1976). In the vertical direction, terrain-following coordinates are used, whilst in the horizontal direction, the Cartesian coordinates are used.

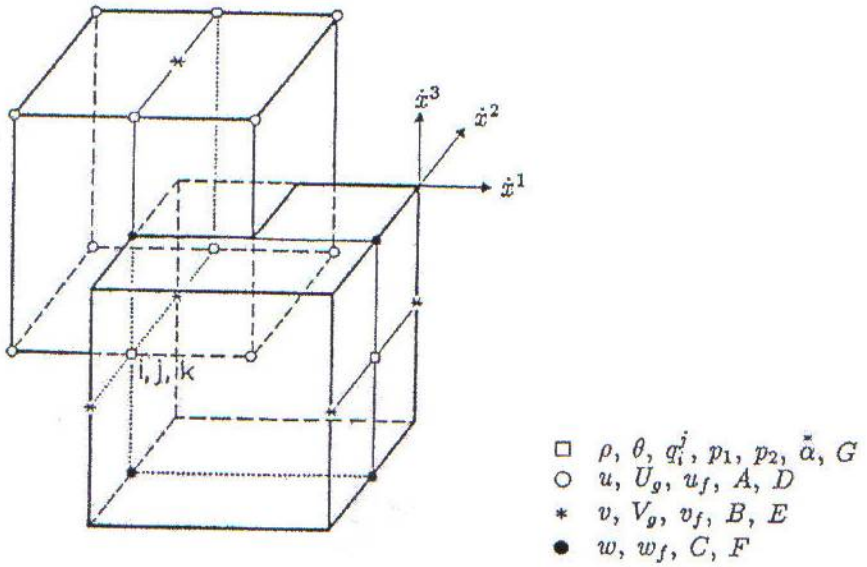


**Figure 3.1: Three dimensional representation of the METRAS ARAKAWA C grid. Taken from Schlünzen et al. (1996)**

On the first vertical model level above the ground, the surface fluxes and vertical exchange coefficients are calculated based on the assumption of surface layer similarity theory. In the atmospheric boundary layer, the sub-grid scale fluxes can be parameterised by first order closure using a local or a non-local scheme. There are six different turbulence schemes, described in Lüpkes et al. (1996), and in the present study, the *k-l* TKE (turbulent kinetic energy) closure formulation is selected, with a dissipation term following Therry et al. (1983), in order to be able to incorporate the urban effect on the TKE equation.

Up to ten different sub-grid scale land use classes can be considered, characterised by appropriate values for the albedo, roughness length, thermal diffusivity and conductivity, soil water availability, and saturation value (see Table 3.1). For the urban class, these coefficients were chosen to be representative of North European cities, with significant vegetated areas. It is expected that the representation of the urban area could be improved

by the implementation of a specific urban canopy scheme, as this simplified approach is not designed specifically to simulate the nocturnal urban island, or parameterise specific urban effects on airflow. The implementation of a specific urban canopy scheme into METRAS will be described in Section 3.3.

**Table 3.1: Surface characteristics for the land-use classes (Schlünzen et al. 2003)**

| Type | Albedo | Thermal diffusivity ($10^{-6}$ $m^2$ $s^{-1}$) | Thermal conductivity (J $K^{-1}$ $s^{-1}$ $m^{-1}$) | Soil water availability | Scaling depth for humidity changes in ground | Roughness length (m) |
|---|---|---|---|---|---|---|
| Water | 0.10 | 0.15 | 100 | 0.98 | 100 | 0.000015 |
| Mudflats | 0.10 | 0.74 | 2.2 | 0.98 | 0.322 | 0.0004 |
| Sand | 0.20 | 0.57 | 1.05 | 0.02 | 0.026 | 0.0012 |
| Mixed land use | 0.20 | 0.52 | 1.33 | 0.05 | 0.138 | 0.04 |
| Meadows | 0.20 | 0.52 | 1.33 | 0.1 | 0.015 | 0.02 |
| Heath | 0.15 | 0.24 | 0.30 | 0.02 | 0.423 | 0.05 |
| Bushes | 0.20 | 0.52 | 1.33 | 0.07 | 0.081 | 0.10 |
| Mixed forest | 0.15 | 0.80 | 2.16 | 0.07 | 0.121 | 1.00 |
| Coniferous forest | 0.10 | 0.80 | 2.16 | 0.07 | 0.161 | 1.20 |
| Urban | 0.15 | 1.40 | 2.93 | 0.01 | 0.968 | 1.0 |

*3.1.2 Model equations*

Every dependent variable is decomposed into an average quantity $\phi$ and a deviation from the average $\phi'$. In the averaged equations the averages for temperature, humidity, concentrations, pressure and density are further decomposed into a mesoscale part $\phi''$ and a large scale part $\phi_0$. The large scale part represents an area, typically the model area, larger

than the mesoscale phenomena being studied. The mesoscale model solves a set of conservation equations for mass, momentum and scalar quantities, described as follows:

*Mass (continuity equation):*

$$\frac{\partial \rho}{\partial t} + \nabla.(\rho \vec{v}) = 0 \qquad \textbf{(Equation 3.1)}$$

where $\vec{v}$ is the 3-dimensional wind vector, t the time and $\rho$ the air density.

*Momentum:*

$$\frac{\partial \vec{v}}{\partial t} + (\vec{v}.\nabla)\vec{v} = -\frac{1}{\rho}\nabla p - 2[\Omega \times \vec{v}] - \nabla\Phi + F \qquad \textbf{(Equation 3.2)}$$

where Ω represents the Earth's angular velocity, Φ the geopotential and F the molecular forces (neglected in the model).

*Scalar quantities:*

$$\frac{\partial \chi}{\partial t} + \vec{v}.\nabla\chi = Q_\chi \qquad \textbf{(Equation 3.3)}$$

where χ represents any scalar quantity, including potential temperature θ, concentration of a pollutant or of atmospheric water vapour. Qχ represents the sources and sinks of the scalar quantity.

These prognostic equations are completed by the diagnostic equations representing the ideal gas law and the definition of potential temperature.

A prognostic equation is used to represent the turbulent transport in the TKE budget equation, with the following source/sink terms being calculated: mechanical production, buoyancy production, pressure correlation and dissipation. The dissipation term follows (Therry et al. 1983). The storage and advection are numerically treated like the other scalar quantities.

A terrain following vertical coordinate is used:

$$\eta = z_t \frac{z - z_s(x,y)}{z_t - z_s(x,y)} \qquad \textbf{(Equation 3.4)}$$

This type of vertical coordinate is used often in mesoscale models (Pielke 1984) since it has the advantage of being invariant in time and in the application of boundary conditions at the lowest η level.

In the surface layer the validity of surface layer similarity theory is assumed since the vertical resolution of the grid does not permit the solution of the conservation equations. Two methods are available to calculate the turbulent fluxes of momentum, heat and water vapour. The first method uses parameter averaging; the second applies the blending height concept. Parameter averaging is a cost efficient approach, in which the turbulent surface scaling values, u* for momentum and χ* for scalars temperature and water vapour, are not calculated separately for each sub-grid-scale land use type, but are derived for each grid cell based on $z_0$, the grid box averaged surface roughness length, using the similarity formulas:

$$u^* = \kappa V(z_{k=1})[\ln(\frac{z_{k=1}}{z_0}) - \Psi_m(\frac{z_{k=1}}{L})]^{-1} \quad \textbf{(Equation 3.5)}$$

$$\chi^* = \kappa[\overline{\chi}(z_{k=1}) - \overline{\chi}(z_0)][\ln(\frac{z_{k=1}}{z_0}) - \Psi_h(\frac{z_{k=1}}{L})]^{-1} \quad \textbf{(Equation 3.6)}$$

where $\kappa$ is the von Karman constant, set equal to 0.4, $z_{k=1}$ is the lowest model level above the ground, $V$ is the horizontal mean wind speed, $\Psi_m$ and $\Psi_h$ are the stability functions for momentum and heat according to Dyer (1974) and $L$ is the Monin-Obukhov length.

When the blending height concept is applied instead, the sub-grid scale fluxes of momentum, heat and moisture are calculated for each surface class based on class specific roughness lengths for momentum, temperature and humidity. The sub-grid-scale fluxes are then averaged over the grid box to get the mean surface fluxes, from which the mean scaling values can be derived. The existence of a blending height, defined as the height at which the flow is horizontally homogeneous in the grid cell, is assumed. The blending height depends on the roughness and sub grid scale heterogeneity. The blending height concept is used throughout the work in this thesis. Although this is a more computationally expensive method, it is recommended for cases in which the surface characteristics are quite distinct (Bohnenstengel et al. 2008).

When model simulations without cloud microphysics are performed, as is the case throughout this PhD study, the long wave and shortwave radiation balance is calculated at the Earth's surface. This calculation takes into account the geographical position, date, time, rotation of the coordinate system, inclination of the surface and shading due to neighbouring hills.

At the surface the temperature is calculated from a surface energy budget equation:

$$(K\downarrow - K\uparrow) + (L\downarrow - L\uparrow) + Q_F = Q_H + Q_E + \Delta Q_S \qquad \textbf{(Equation 3.7)}$$

($K\downarrow$ - K↑) is the net direct and diffusive shortwave radiation term. In the absence of clouds it is calculated from $\mu I_\infty cosZ(t)$, where $\mu$ depends on the albedo α, the amount of clouds, the turbidity of the air and the elevation of the sun. For a cloud free sky it is estimated to be $0.75(1-\alpha)$. $I_\infty$ is the incoming solar radiation and $Z(t)$ is the zenith angle.

The longwave radiation balance for cloud free skies ($L\downarrow$-$L\uparrow$) is calculated taking into account the influence of moisture and a correction term due to the temperature difference between the soil surface and the air above. A mean value of 0.95 is assumed for the longwave emissivity of the soil surface. The calculation follows de Jong (1973).

The sensible and latent heat flux terms $Q_H$ and $Q_E$ are calculated from the friction velocity u*, and the scaling values for temperature θ* and humidity q*.

$\Delta Q_S$ describes the heat flux and exchange with the ground and is calculated as $\Delta Q_S = \upsilon_s (\partial \overline{T} / \partial z)_s$, in which $\upsilon_s$ is the heat conductivity of the ground.

The anthropogenic heat flux $Q_F$ is not explicitly resolved in the METRAS model. For rural areas this is not usually a significant term, however urban areas often have significant anthropogenic heat sources such as traffic and industry. The implementation of the BEP urban scheme allows the parameterization of the anthropogenic heat, even though the treatment in BEP remains simplistic.

A force restore model is used to solve the surface energy budget equation following Tiedke et al. (1975) and Deardroff (1978):

$$\frac{\partial \overline{T}_s}{\partial t} = \frac{2\sqrt{\pi} k_s}{\upsilon_s h}\{\mu I_\infty \cos Z(t) - \varepsilon\sigma \overline{T}_s^4 + c_p \rho_0 \theta * u * + l_{21}\rho_0 q * u * - \sqrt{\pi}\upsilon_s \frac{\overline{T}_s - \overline{T}(-h_\theta)}{h_\theta}\}$$

(**Equation 3.8**)

where $k_s$ is the thermal diffusivity and $\upsilon_s$ is the thermal conductivity of the soil, $h_\theta$ is the depth of the daily temperature wave calculated according to Deardroff (1978) and $T(-h_\theta)$ can be selected to be either the prescribed soil temperature or is calculated according to Deardroff (1978).

*3.1.3 Model boundary conditions*

The METRAS model area is limited in both in the vertical and horizontal directions. Over land the surface height coincides with the lower model boundary, whereas all other boundaries are artificial and therefore the boundary conditions must be formulated such that waves can pass the boundaries without reflections. The boundary conditions used by METRAS are described in this Section. All the boundary conditions are implemented at the model boundary directly – this does not always correspond to a grid point depending on the selected variable. If this is the case the value at the outer grid point is calculated assuming:

$\chi$*(boundary) = 0.5 * (*$\chi$(outer grid point) + $\chi$(next inner grid point))*

The boundary conditions used for this work are described in Table 3.2. These are selected in the m3tras_TAPE5 file before running the model. Only pressure boundary conditions are automatically prescribed, since they are coupled with other boundary conditions.

**Table 3.2: Summary of the boundary conditions used for all METRAS model runs**

| Variable | Lower boundary | Upper boundary | Lateral boundaries |
|---|---|---|---|
| **Wind vector** | Fixed value prescribed | Large scale values are prescribed for wind components normal to the boundary. Zero gradient for wind components parallel to the boundary. | Direct calculation for wind components normal to the boundary. Zero gradient for wind components parallel to the boundary. |
| **Temperature** | Model energy budget equation used | Zero gradient at boundary | Zero gradient at boundary |

The upper boundary of the model has no physical boundary, and therefore the boundary conditions must permit vertically propagating waves to leave the model volume without reflections. Therefore it is assumed that the gradients of horizontal wind components normal to the boundary will be zero and the vertical wind component will vanish. For the temperature field, the boundary conditions results in zero fluxes at the model top.

At the lower boundary the wind velocity vector has a 'no slip' boundary condition at the ground. This means the wind velocity parallel to the surface is zero at the ground, which results in the following conditions at the boundary:

$w(0,j,i) = 0$

$u(0,j,i) = -u(1,j,i)$

$v(0,j,i) = -v(1,j,i)$

For the temperature the surface energy budget is used to calculate surface values (see Equation 1.8). The boundary values (i.e. the lowest grid level) is then calculated from the surface value (i.e. the potential temperature at the ground) and the value at the first grid level with the assumption of constant gradients:

$$\theta(\text{lowest level}) = 2*\theta\ (\text{ground}) - \theta(\text{first level})$$

At the lateral boundaries for the wind vector a zero gradient is assumed for wind components parallel to the boundary. The inflow advection normal to the boundary is calculated using the phase velocity, and the outflow advection is assumed to be constant. For the temperature the zero gradient boundary condition results in zero fluxes at the lateral boundary.

### *3.1.4 Model initialisation*

The METRAS model initialisation has three steps:

1. **Initialisation of orography and land use characteristics**

The first step encompasses the determination of the spatial resolution of model area, the location of the model grid points, and the area weighted interpolation of the characteristic parameters of topography and land use (e.g. orography, roughness, albedo etc…) to those grid points. This uses the GRIGAU or GRITOP pre-processors (Wosik et al. 1994).

2. **Initialisation of the 1-dimensional model**

A 1-dimensional model version (M1TINI) calculates a stationary meteorological profile which is used to initialise the 3-dimensional model. In order to do so the following values

are defined in the file m1tini_TAPE5 files, based on observations, weather charts or analysis:

- Large scale vertical wind
- Large scale pressure at sea level
- Geostrophic wind at sea level, or a profile
- Temperature at sea level and a temperature gradient, or a temperature profile
- Profile of large scale relative humidity
- Profile of liquid water content (cloud and rain water)
- Soil and water temperature

The large scale vertical wind is set to zero, with the assumption of horizontal homogeneity. In the calculation the hydrostatic and geostrophic approximations are made. The 1-dimensional model equations are integrated from the initial profiles, using the same boundary conditions as the 3-dimensional model but without the diurnal cycle. When the wind and temperature profiles are stationary, they can be transferred to the 3-dimensional model for initialisation.

**3. Initialisation of the 3-dimensional model**

Using the assumption of horizontal homogeneity, the data set calculated in the second step is expanded over the model area and used to initialise 3-dimensional model. During the

initialisation phase lasting 2-8 hours the orography grows slowly (diastrophism) until the real heights are established.

## 3.2 BEP

The urban canopy model BEP (Building Energy Parameterisation) developed by Martilli et al. (2002) to parameterise the dynamic and thermodynamic effects of the urban canopy has been implemented into the mesoscale model METRAS. BEP is described and validated in the following papers: Martilli et al. (2002), Martilli (2002) and Roulet et al. (2005). This model has been applied to study air quality for the city of Athens (Martilli 2003; Martilli et al. 2003) and has been subsequently implemented in other mesoscale models in order to improve the representation of the urban surface, for example the MeteoSwiss operational numerical weather prediction model aLMo (Clappier et al. 2005; Muller 2007), the high-resolution version of the operational Danish DMI-HIRLAM model for Copenhagen (Baklanov et al. 2005), and the Topographic Vorticity-Mode Mesoscale model TVM (Hamdi et al. 2005). BEP has also been integrated into the mesoscale model MC2 (Benoit et al. 1997) in order to simulate heat mitigation strategies in Toronto, Canada (Krayenhoff et al. 2005). These validations included comparisons for 2-4 day long episodes, as well as longer periods of up to 14 days within an operational model (Muller 2007), demonstrating that BEP is able to simulated the UHI and momentum fluxes for longer periods.

BEP is a multi-layer model which directly interacts with the atmospheric model, representing the impact of the vertical (walls) and horizontal (canyon floors and roofs) urban surfaces on the momentum, heat and TKE. The impact of the urban surface is vertically distributed in the urban canopy (with the lowest level at the physical ground).

The terms representing the impact of the urban surface are computed on the BEP urban grid (see Figure 3.2.1), which can differ from the mesoscale grid in which BEP is embedded, permitting a higher vertical resolution over the urban area (e.g. a vertical resolution of 5 m). The results are then interpolated back to the METRAS mesoscale grid.

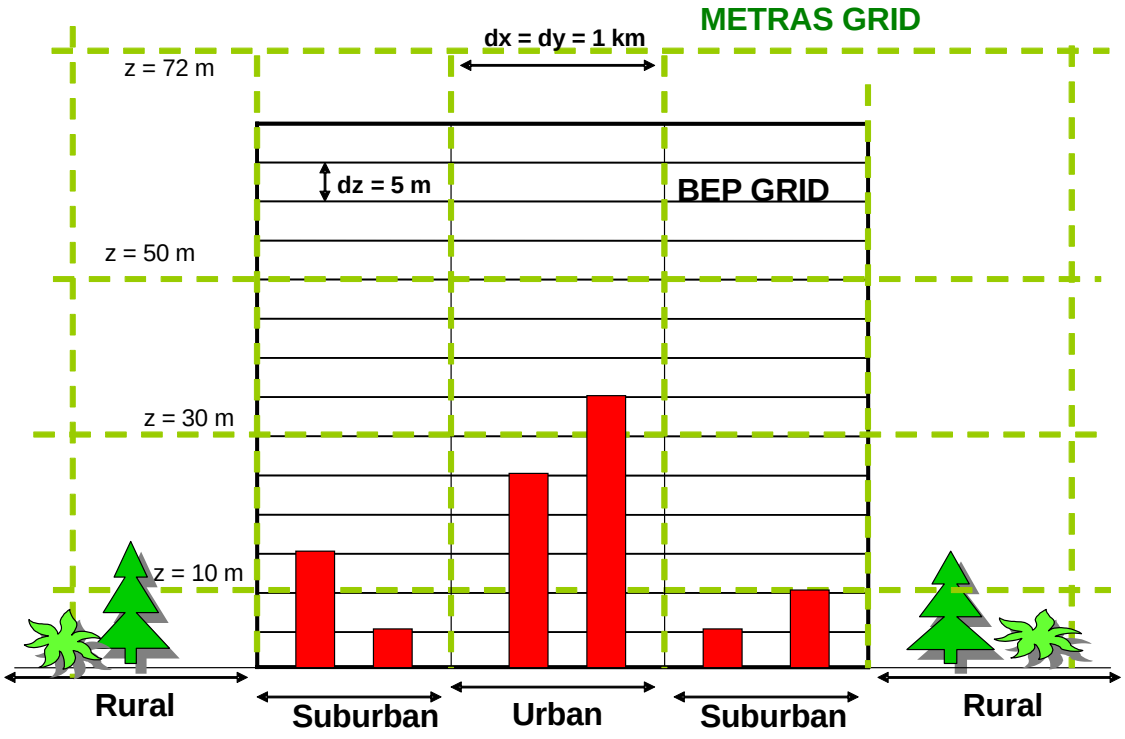


**Figure 3.2: A diagram showing how the METRAS mesoscale grid interacts with the BEP urban grid.**

The urban surface in BEP is represented as an array of parallelepiped buildings of equal width $B$, and separated by a fixed canyon width $W$ (see Figure 3.3). The buildings can however have different heights $h$, and the scheme defines a probability function, $\gamma(h)$, to represent the area density occupied by the buildings of height $h$ in the horizontal grid. These parameters ($W$, $B$, $\gamma(h)$) permit the calculation of the vertical ($S_{IU}^{V}$) and horizontal surfaces ($S_{iu}^{H}$) at each level in the urban grid. The predominant street direction, $\xi$ (º), is also

defined for the horizontal grid in the scheme. Therefore four parameters in total, canyon width, building width, building height distribution and street direction ($W$, $B$, $\gamma(h)$, $\xi$) uniquely define the urban morphology for the BEP scheme. At the mesoscale, a parameter $\lambda_V$ can be defined to represent the percentage of vegetation coverage in the horizontal grid. This represents the land cover percentage of the vegetated land cover classes, such as 'Meadows'.

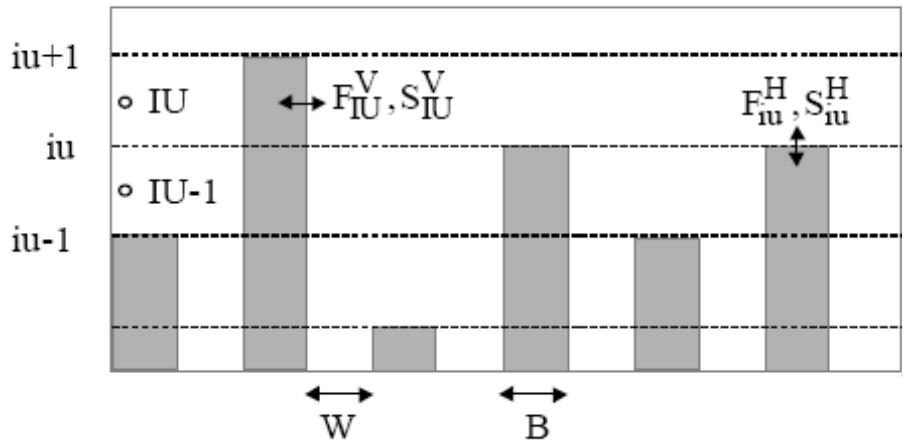


**Figure 3.3: A schematic representation of the urban grid, in which W is the street width, B is the building width, IU is the centre of a vertical model level, $F_{iu}^{H}$ represents the flux of a quantity through the horizontal surfaces with the area $S_{iu}^{H}$, and $F_{IU}^{V}$ represents the flux of a quantity through the vertical surfaces with the area of $S_{IU}^{V}$. (Taken from Martilli et al. 2002, page 267).**

BEP allows the city to be represented by up to ten urban classes, which are characterised by defining the averaged distribution of building heights, the average street direction, length and width and the radiation, roughness and building parameters. Whilst not all this data will be readily available for the London are, this approach allows to resolve some of the complexity of the urban surface, and to study how changes in urban form have affected regional climate. The data sources used for the implementation are described in Section 3.5.

*3.2.1 Calculation of dynamical effects*

The dynamical effects due to buildings calculated by BEP are:

- Loss of momentum due to horizontal surfaces (roofs and canyon floors) inducing a frictional force. For this term the classic surface layer (MOST) formulae of Louis (1979) are used to calculate the momentum flux for the horizontal surfaces. This term is however vertically distributed from ground to the highest building, and is proportional to the fractional area of the horizontal surface in the grid cell $S_{iu}^{H}$. The turbulent momentum flux at level *iu* due to the horizontal surfaces is:

$$\vec{F}u_{iu}^{H} = -\rho \frac{k^2}{[\ln(\frac{\Delta z_{IU}/2}{z_{oiu}})]^2} f_m(\frac{\Delta z_{IU}/2}{z_{oiu}}, Ri_B)\left|U_{IU}^{hor}\right|\vec{U}_{IU} S_{IU}^{H}$$

(**Equation 3.9**)

where $k$ is the von Karmen constant (0.4), $f_m$ comes from Louis (1979), $Ri_B$ is the bulk Richardson number calculated at level IU, and $U_{IU}^{hor}$ is the horizontal wind component.

- Exchange of momentum through the vertical surfaces (walls) due to pressure and viscous drag forces induced by the presence of buildings on the flow. The momentum flux due to the vertical surfaces is:

$$\vec{F}u_{IU}^{V} = -\rho C_d \left|U_{IU}^{ort}\right|\vec{U}_{IU}^{ort} S_{IU}^{V} \qquad \textbf{(Equation 3.10)}$$

where $U_{IU}^{ort}$ is the wind component orthogonal to the street direction at level *IU* and the constant drag coefficient $C_d$ is set to 0.4, as explained in Martilli et al. (2002).

- The impact of the surface is taken into account in the shear and buoyant production terms in the TKE equation. The extra source term for TKE is due to the fact that the presence of buildings increases the conversion of mean kinetic energy into TKE:

$$Fe_{IU}^{V} = C_d \left| \vec{U}_{IU}^{ort} \right|^3 S_{IU}^{V} \qquad \textbf{(Equation 3.11)}$$

- Modification of the turbulent length scales used to calculate the dissipation term in the TKE equation. This modification is needed because the presence of the buildings generated vortices which have the same scale as the buildings. The modification is equivalent to adding a second dissipation terms linked to the scale of the buildings, which has the net effect of increasing the dissipation rate and the cascade of mean kinetic energy to TKE.

*3.2.2 Calculation of thermodynamic effects*

The following thermodynamic effects are calculated:

- The turbulent fluxes of sensible heat from horizontal surfaces (roofs and canyon floors) are calculated, as done for the momentum fluxes, using MOST, where $f_h$ is from Louis (1979):

$$F\theta_{iu}^{H} = -\rho \frac{k^2}{[\ln(\frac{\Delta z_{IU}/2}{z_{oiu}})]^2} \left| U_{IU}^{hor} \right| \Delta\theta \cdot f_h(\frac{\Delta z_{IU}/2}{z_{oiu}}, Ri_B) \cdot S_{iu}^{H} \qquad \textbf{(Equation 3.12)}$$

- The temperature fluxes from the walls are calculated as a function of the temperature difference between air and walls, using the formulation of Clark (1985) which Arnfield et al. (1998) use in their energy budget model:

$$F\theta_{IU}^{V} = \frac{\eta}{C_p}[(\theta_{air} - \theta_{IU}^{westwall}) + (\theta_{air} - \theta_{IU}^{eastwall})]S_{IU}^{V}$$

$$\eta = 5.678[1.09 + 0.23(\frac{U_{IU}^{hor}}{0.3048})] \qquad \textbf{(Equation 3.13)}$$

In this equation (valid for a N-S street direction), $\theta_{IU}^{westwall}$ and $\theta_{IU}^{eastwall}$ are the potential temperatures of the west and east wall, respectively, at level IU.

- An energy budget is calculated for every surface, i.e. roofs, walls and streets in order to calculate the surface temperatures $T_s$. The effects of shadowing and trapping of radiation in the canyon are taken into account in the calculation of longwave and shortwave radiation ($R_s$ and $R_d$), with sky-view factors calculated for each grid level. The energy budget equation is:

$$\frac{\partial T_s}{\partial t} = \frac{1}{\Delta z_s}[\frac{(1-\alpha)R_s + R_d - \varepsilon\sigma T_s^4 + \Delta Q_s}{C_s} - K_s(\frac{\partial T}{\partial z})_s]$$

(**Equation 3.14**)

where $\Delta z_s$ is the vertical grid spacing between the surface and the material, $K_s$ is the thermal conductivity of the material, $\varepsilon$ is the emissivity of the surface, σ the Stefan-Boltzmann constant and $C_s$ the specific heat of the material.

- A heat diffusion equation is solved in several layers in the interior to calculate wall, canyon floor and roof temperatures.

The terms $D_{AI}$ are defined to represent the overall effect of the urban areas on the quantity *'A'* at the vertical level *I*, by adding the horizontal and vertical fluxes due to the presence of buildings ($F_{AI}^{H}$ and $F_{AI}^{V}$ respectively, where *A* represents wind, temperature or TKE) and dividing the result by the volume of air in the cell $V_I^A$, i.e. the grid volume minus the volume of the buildings:

$$D_{AI} = \frac{F_{AI}^{H} + F_{AI}^{V}}{V_I^A}$$

**(Equation 3.15)**

## 3.3 Implementation of BEP in METRAS

The urban scheme BEP was implemented into METRAS by connecting the two codes in the simplest way possible, and therefore BEP was not rewritten. The BEP subroutines are called at each time step in the model code. A series of variables are passed from METRAS to the BEP subroutines (wind components, potential temperature, air density, pressure, grid level heights, solar zenith angle, sun declination, hour angle and short and longwave radiation) and results representing the impact of the urban area of temperature, wind and TKE are passed back to METRAS. In the METRAS routines the total fluxes through the horizontal grid are computed as the area weighted average over the land cover types. This enables the METRAS sub grid scale land classification to be used.

The BEP parameterisation scheme neglects the moisture flux in the urban canyon, which has been shown to be equivalent to neglecting the presence of irrigated parks and gardens (Grimmond et al. 2002). Originally BEP was developed for cities (e.g. Athens) with limited vegetated areas, for which it was possible to neglect these fluxes (Martilli et al. 2003). However some studies (Eliasson 1996) have shown that the air temperature difference observed between a large park and the city centre can be of the same order as the urban-rural air temperature difference. For the city of London, the English Heritage estimates that 30% of the city is covered by parks and gardens (www.english-heritage.org.uk) therefore it would be impossible to neglect the effect of these vegetated surfaces on the city climate. Therefore the effect of vegetation will be taken into account using the method which was devised by Brown and Williams (1998) and used for the BEP scheme by Hamdi (2005). This method consists in dividing the urban grid cells into a vegetated fraction and an urban fraction such that for each grid cell a certain percentage of urban coverage exists. If this is

greater than zero, the model will use the BEP scheme to compute the effect of the urban surface on the relevant equations described above. For the vegetated fraction, the appropriate METRAS land use type (typically 'Meadows' or 'Mixed forest') is used to calculate the surface fluxes of heat and momentum.

A point of complexity in the linking of BEP and METRAS has been the need to implement a third radiation scheme into METRAS since the current schemes (and in particular that without cloud microphysics) do not explicitly calculate the downward shortwave and longwave radiation that are required to force the BEP scheme. For the initial simulations a simple parameterisation has been added, which considers a constant LW↓ equal to 415 $Wm^{-2}$ and a SW↓ term based on the sine expression in Stull (1988). This parameterisation could be subsequently refined, for example by considering some of the ideas in Offerle et al. (2003).

The implementation of BEP in METRAS has also been somewhat complicated by the difference in coding styles and the treatment at the ground surface boundary between the mesoscale model and the BEP scheme. For example in METRAS all non-local variables are stored in modules, whereas in BEP the non-local variables are passed on through the subroutine argument list, thus allowing the same variable to assume different names in different subroutines according to its use in the particular subroutine. While this is an efficient way of using the same subroutine to calculate the effects of 3 different surface types (walls, canyon floors and roofs), it has meant that the BEP code has been quite hard to implement. Another difference is that all 3-dimensional METRAS variables are of the form *s(z,y,x)* while the BEP ones are of the form *s(x,y,z)*. While this has not caused great

difficulties in the linking of the two codes, it will be affecting the CPU time of the simulations using the urban scheme compared to using the original METRAS code. Changing this however would take some time and it is not easy to estimate how much it might improve the CPU time, and therefore was not attempted.

## 3.4 Computational demand

The use of the METRAS TKE scheme, and the implementation of BEP, has slowed down the performance of the model. The performance has been compared for a small domain (40 km x 40 km – 1600 grid cells) with an urban area measuring 20 km across (400 urban grid cells) for the original METRAS model with neither the TKE scheme or BEP, the original model run with the TKE scheme but without BEP, and the new METRAS+BEP model which uses the TKE scheme. This comparison shows that the running time for the METRAS+BEP model was 4.25 times that of the original METRAS model with the TKE scheme, and 5.67 times that of the original model without the TKE scheme.

Computing resources meant that for much of the research time it was only possible to use a maximum of 6-8 CPU split across two different machines. The model runs for a large domain representing the London region in Chapter 6 took up to 1 month to run, although the urban scheme only made this a factor of 10% slower than running METRAS without BEP. The duration of the model runs with the large domain and the limitation of CPU resources obviously had a limiting effect on the selection of cases to simulate.

A possible future development is to recode the BEP scheme to improve the speed, as well as parallelising the METRAS+BEP code.

## 3.5 Data sources

This section describes the data sources which were used for the construction of the model domains, the initialisation of the model runs, and the validation of the model results.

### *3.5.1 Land cover data*

The CEH Land Cover Map 2000 (LCM2000) was used to derive the land cover classification for the model domain. The LCM2000 is a 1 km x 1 km raster dataset covering Great Britain which was created from a 25 m x 25 m pixel resolution dataset within a 1 km x 1 km grid. The dataset is a digital map made by analysis of spectral reflectance data from Earth observation satellites. LMC2000 has two urban land use classes, representing continuous urban land cover and discontinuous suburban land cover. These were used in order to classify the urban land cover into two BEP urban classes with characteristics representing urban and suburban land cover. All large areas of vegetation in LMC2000 (>0.5 ha) are distinguished by the appropriate land cover class, and these will be likewise represented in METRAS by the most appropriate land cover class.

Since LCM2000 has 27 land cover classes, compared to the 10 classes used in the METRAS model, the classes must be summarised into the METRAS classes. A FORTRAN programme was written to convert the LCM2000 data set into the 10 METRAS land cover classes. On the basis of the description of the LCM2000 classes provided, the CEH land cover percentages were aggregated into the 10 METRAS land cover classes using summary in Table 3.3.

**Table 3.3: Description of how the 27 land cover classes in the CEH Land Cover Map 2000 are summarised into the 10 METRAS land cover classes.**

| CEH land class | CEH Description | METRAS land class | METRAS Description |
|---|---|---|---|
| 1 | Sea/Estuary | 0 | Water |
| 2 | Water (inland) | | |
| 5 | Salt marsh | 1 | Mudflats |
| 3 | Littoral rock | 2 | Sand |
| 4 | Littoral sediment | | |
| 6 | Supra-littoral rock | | |
| 7 | Supra-littoral sediment | | |
| 27 | Unclassified | 3 | Mixed land use |
| 14 | Arable cereals | 4 | Meadows |
| 15 | Arable horticulture | | |
| 16 | Non-rotational horticulture | | |
| 17 | Improved grassland | | |
| 18 | Set-aside grass | | |
| 19 | Neutral grass | | |
| 20 | Calcareous grass | | |
| 8 | Bog (deep peat) | 5 | Heath |
| 9 | Dense dwarf shrub heath | | |
| 10 | Open dwarf shrub heath | | |
| 11 | Montane habitats | | |
| 26 | Inland bare ground | | |
| 21 | Acid grass | 6 | Bushes |
| 22 | Bracken | | |
| 23 | Fen, marsh, swamp | | |
| 12 | Broad leaved woodland | 7 | Mixed forest |
| 13 | Coniferous woodland | 8 | Coniferous forest |
| 24 | Suburban, rural developed | 9 | Urban |
| 25 | Continuous urban | | |

Figure 3.4 shows the percentage of the 'Meadows' and of 'Mixed forest' land cover in the domain.

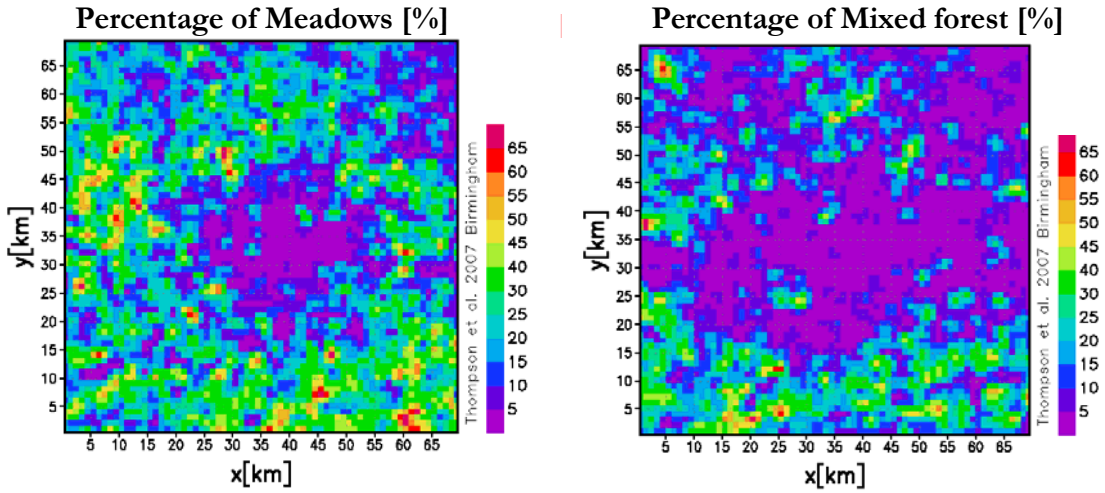


**Figure 3.4: Percentage of the "Meadows" land cover class (left) and the "Mixed forest" land cover class (right) for each grid cell in the domain**

Figure 3.5 shows the percentage of the 'Continuous Urban' and of 'Suburban-rural developed" land cover in the domain. In the METRAS mode these two urban covers form the single Urban land cover which is not distinguished into two separate classes.

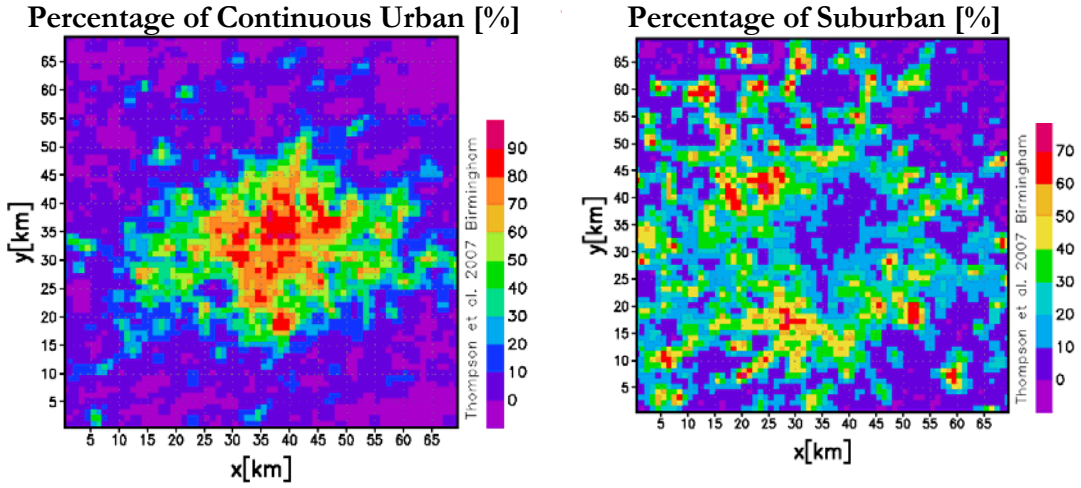


**Figure 3.5: Percentage of the "Continuous urban" land cover class (left) and the "Suburban-rural developed" land cover class (right) for each grid cell in the domain**

### *3.5.2 Orography data*

Orography data was taken from the US Geographical Survey (www.usgs.gov). A FORTRAN programme was written to convert the orography data to the correct format for the METRAS pre-processor GRITOP to read it. The pre-processor GRITOP reads the orography data, creates a model grid and interpolates the land use data and the surface heights to the model grid (Wosik et al. 1994).

For idealised cases presented in Chapter 4, the model was run for a flat terrain, in order to avoid any orographically induced effects. Likewise, all scenario runs to investigate past and future urbanisation in Chapter 6 and 7 were run for a flat terrain to reduce complexity, since the aim was purely to compare results from different simulations where only the land cover had been altered.

### *3.5.3 Data used for the model initialisation*

When the model was used to simulate London, radiosonde measurements taken at the nearest UK Met Office weather stations, Larkhill and Herstmonceux, in the South of England were used to initialise the model. The 1-dimensional model M1TINI was used to calculate a physically balanced profile of wind speed, temperature and humidity above one point (the lowest point in the domain, with the lowest roughness length) from this initialisation data. This result was homogenously used throughout the domain to initialise the 3-dimensional model.

### *3.5.4 BEP urban data*

As explained in Section 3.2 the BEP urban scheme can define a number of urban classes (up to ten), with different distributions of building heights and other building morphology

parameters. As accurate data sources for both urban parameters and the urban land cover in order to define that many urban classes are not available, only two different classes were used for the London simulations, to represent the more highly urbanised city centre area and the suburban areas. These are defined from the CEH Land Cover 2000 data as summarised in Table 3.4 and are mapped in Figure 3.5.

**Table 3.4: Definition of the BEP urban classes based on the CEH Land Cover map 2000 classification**

| BEP class | CEH Land cover class |
|---|---|
| Urban class 1 | Continuous urban |
| Urban class 2 | Suburban/rural developed |

For the idealised test cases presented in Chapter 4 the parameters for the urban area for the idealised test cases were a building height distribution of 10 m (50%) and 20 m (50%), a building width of 30 m and a canyon width 15 m. The mean building height was 15 m, which is typical of European cities (Ratti et al. 2001). Two street directions were defined, and were perpendicular to each other at 45º and 135º (Martilli et al. 2003) – these values were taken from the literature since no information on London street directions was found. The sensitivity to the street directions was tested, and not found to affect the results.

For the simulations representing the London area the building heights were altered based on information from the literature. Two urban classes are defined, with the building height distributions defined in Table 3.5. This takes into account the fact that in the central continuous urban area there are tall buildings over 30 and 40 m. For example for the study area centred on Marylebone Road used in the DAPPLE field study over 70% of the buildings are between 15 m and 35 m, with 4% above 55 m[1]. For the second urban class

[1] Email communication with Tom Lawton, DAPPLE, April 2005

representing suburban development a mean building height of 10 m is considered reasonable, since this represents an average of a typical European city height of 15 m (Ratti et al. 2001) and that for a suburban area such as Guildford, UK (Oestges et al. 1999).

**Table 3.5: Distribution of building heights for the two urban classes defined for the simulations representing London**

| | Percentage of buildings | |
|---|---|---|
| **Building height (m)** | **Urban class 1** | **Urban class 2** |
| 5 | | 20 |
| 10 | 10 | 60 |
| 15 | 25 | 20 |
| 20 | 35 | |
| 25 | 25 | |
| 30 | 10 | |
| 35 | | |
| 40 | 10 | |
| 45 | | |
| 50 | 5 | |
| **Average height (m)** | 23 | 10 |

The values used for the thermal characteristics of the buildings for both the idealised simulations and the London simulations were taken from the literature (Martilli et al. 2002) and are summarised in Table 3.6.

**Table 3.6: Parameters for the city for the urban simulation. $\kappa_s$ is the thermal diffusivity of the material, $C_s$ is the specific heat of the material, $T_{int}$ is the initial temperature of the material (equal to the temperature of the deepest layer), $\varepsilon$ is the surface emissivity, $\alpha$ is the albedo and $z_0$ is the roughness length of the surface.**

| Surface | $\kappa_s$ ($m^2s^{-1}$) | $C_s$ (J $m^{-3}$ $K^{-1}$) | $T_{int}$ (K) | $\varepsilon$ | $\alpha$ | $z_0$ (m) |
|---|---|---|---|---|---|---|
| Wall (urban) | $0.57 * 10^{-6}$ | $1.54 * 10^{6}$ | 293 | 0.9 | 0.2 | n/a |
| Roof (urban) | $0.62 * 10^{-6}$ | $1.5 * 10^{6}$ | 293 | 0.95 | 0.2 | 0.01 |
| Floor (urban) | $0.47 * 10^{-6}$ | $1.74 * 10^{6}$ | 290 | 0.9 | 0.2 | 0.01 |

*3.5.5 Meteorological data for model validation*

Limited meteorological data was available for the model validation. Temperature, wind speed and wind direction data were obtained from the British Atmospheric Data Centre (BADC) for the MIDAS (UK Met Office land surface weather stations) network in and around London.

The MIDAS network (http://badc.nerc.ac.uk/data/ukmo-midas) comprises of daily and hourly rain measurements, soil temperature, daily temperature, mean wind measurements and hourly weather which form a long term record of UK weather conditions. The hourly weather data includes measurements of wind speed and direction, air temperature, as well as information on cloud types and amounts, and visibility. Each MIDAS network station is identified via a unique source identifier. General guidelines exist for the location of sites and measurement methods and heights[2]. Not all sites however meet these requirements, for example sites located in city centres may be located on roof tops, or close to large obstacles and this may compromise the validity of the measurements.

The MIDAS stations used were the London Weather Centre (LWC), which is classified as an urban station; the Heathrow airport station (classified as peri-urban) and St James's Park (classified as an urban green space station) (see Figure 3.6). These three stations were chosen because they provide the most comprehensive data sets and are located in the London area. All three have hourly measurements of air temperature, wind speed and direction for at least the last ten years, although data can be missing for some periods.

[2] Met Office Surface Data Users Guide (UK Met Office document, taken from MIDAS Data User Guide), available at http://badc.nerc.ac.uk/data/ukmo-midas/

Table 3.7 shows a summary of the MIDAS weather stations used in the model evaluation in Chapter 5.

**Table 3.7: Summary of available data for the MIDAS weather stations used in the model evaluation in Chapter 5**

| | London weather centre | London Heathrow | St James' Park | Bracknell Beaufort Park |
|---|---|---|---|---|
| **BADC Station ID** | 19144 | 708 | 697 | 838 |
| **Site elevation** | 43 m | 25 m | 5 m | 74 m |
| **Location characteristics** | Roof top | Airport | Urban park | Rural |
| **Latitude** | 51.521 | 51.479 | 51.504 | 51.39 |
| **Longitude** | -0.11 | -0.449 | -0.129 | -0.784 |
| **Hourly temperature data** | Yes - for all detailed evaluation cases | Yes - for all detailed evaluation cases | Partial - missing data | Partial - missing data |
| **Hourly wind speed data** | Yes - for all detailed evaluation cases | Yes - for all detailed evaluation cases | Partial - missing data | Partial - missing data |
| **Station start date** | 1929 | 1947 | 1903 | 1965 |
| **Station end date** | Current | Current | Current | 2003 |

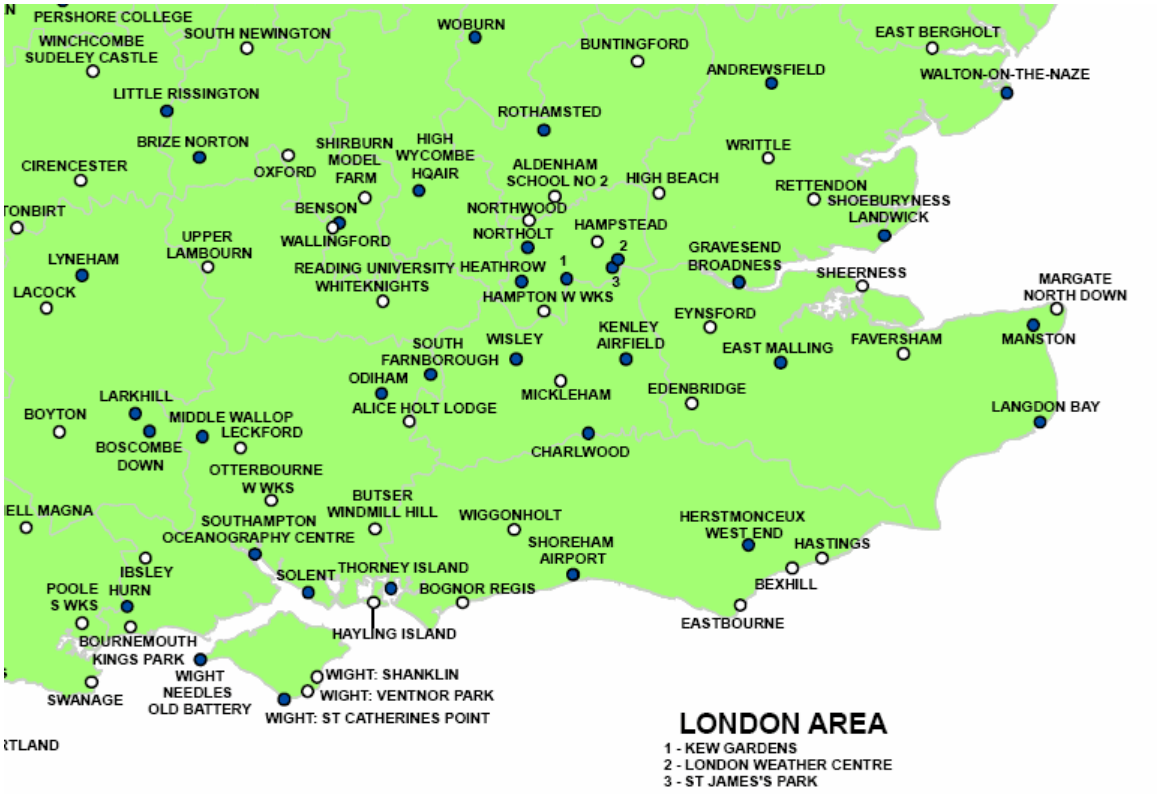


**Figure 3.6: Locations of Met Office weather stations in the South-East of England (taken from www.metoffice.gov.uk)**

No data on the energy balance was found to use to validate the model results.

Data from the Heathrow MIDAS station was also analysed in order to select the case studies during summer i.e. June-July-August (JJA) and winter i.e. December-January-February (DJF) to be simulated for the model evaluation (see Chapter 5).

## 3.6 Summary

In this PhD study the mesoscale model METRAS is used together with the urban canopy parameterisation scheme (BEP) developed by Martilli et al. (2002) in order to simulate the effects of urban land cover for the city of London. This Chapter presents an overview of the mesoscale model METRAS. The model equations are described, and the boundary conditions used in this study are presented. The initialisation process for setting up model simulations is also explained.

The Martilli urban scheme (BEP) computes both the dynamic and thermodynamic effects of the urban surface. The scheme and its implementation are described in this Chapter, together with an analysis of the computational demand of the new METRAS+BEP modelling system.

A number of different data sources were used to set up the domains for simulation and to initialise and run the model. Land cover data from the CEH Land Cover Map 2000, and orography data from the US Geological Survey, were used to set up model domains for the simulations. UK Met Office meteorological data from radiosondes and weather stations was used to initialise the model and to validate model results respectively. Urban parameters derived from the literature were used as an input to the BEP urban canopy scheme.

Any additional information which is specific to the simulations presented in each of the Results Chapters is contained therein for reasons of clarity.

# Chapter 4: Results from the implementation of BEP in METRAS for an idealised domain

BEP has been coupled with METRAS by the addition of the urban terms in the horizontal momentum equations, the temperature equation and the turbulent kinetic energy equation, as well as the modification of the turbulent length scale, as described in Chapter 3. In this chapter the new version of METRAS+BEP has been used to investigate the impact of an idealised urban area on the air flow, temperature and other atmospheric parameters. A comparison between the model results with and without the urban scheme is made in Section 4.3, and in Section 4.4 a sensitivity study was carried out to further investigate and understand the model performance. The model was then applied to city of London, and evaluated against data from the UK Met Office MIDAS weather stations in Chapter 5.

## 4.1 Set up of the idealised test cases

To test the effect of BEP on METRAS, the combined model was run for an idealised flat 3D domain (40 km x 40 km), with 1 km horizontal resolution. A 3D simulation means the interactions between urban and rural regions can be adequately modelled (e.g. Sailor 1998). The mesoscale vertical resolution was 20 m in the first 60 m, and was then stretched with a grid increasing factor of 1.175 to a maximum of 1,350 m at the top of the domain (11,627 m). The BEP urban subroutines were used on a distinct urban grid with a uniform 5 m vertical resolution and 14 vertical levels, and the results were interpolated back to the mesoscale grid. BEP was forced with profiles of the horizontal wind and potential

temperature, air pressure and air density, as well as the solar declination, hour angle, azimuthal angle, shortwave and downward long wave radiation calculated by METRAS. The model boundary conditions are described in Chapter 3.

For the idealised urban runs, the urban area was in the centre of the domain, and was represented by a square which measures 20 km across. The topography was assumed to be flat. The urban area was surrounded on all sides by an area of rural (METRAS land cover class 4 – 'Meadows') land cover. The simulation with the combined METRAS+BEP model was named *urban_BEP*. For comparison the model was also run for the same domain, with a central urban area, using the original representation of the urban surface in METRAS (*Orig*), and for a domain covered completely by the rural surface class (*Rural*). See Table 4.1 for a summary of the test cases.

**Table 4.1: Summary of the idealised test cases**

| Simulation | Model | Land cover |
|---|---|---|
| *Urban_BEP* | METRAS+BEP | Urban and Meadows |
| *Orig* | METRAS | Urban and Meadows |
| *Rural* | METRAS | Meadows only |

The meteorological initial conditions were set to a geostrophic wind from the west of 4.0 $ms^{-1}$ and an initial stable atmospheric thermal stratification equivalent to 3.5 K $km^{-1}$ in potential temperature in the bottom 1,000 m and 4 K $km^{-1}$ above 1,000 m. The vertical wind is equal to 0 $ms^{-1}$. These conditions were chosen to replicate those in Martilli et al. (2002) since the first aim of this Chapter was to establish that the BEP scheme has been accurately implemented into METRAS and that the new model gave consistent results with those validated in Martilli et al. (2002). The simulation was performed for 3 days, starting

on the 1st July at 00:00. The centre of the domain was at 51.3° N, 0° E. To ease the interpretation of the results all simulations took place on cloud free days, and the rain and cloud METRAS routines were not used.

The parameters for the urban area for the idealised *urban_BEP* test case have been defined in Section 3.5.4. The parameters for the METRAS 'Urban' class (used in the *Orig* simulation) and 'Meadows' land cover class (used in the all simulations) have been defined in Table 3.1 on page 57 in Chapter 3. The *urban_BEP* idealised test case was used as the control simulation in the sensitivity study.

## 4.2 Results for an idealised domain

In the following sections the results for the implementation of BEP within METRAS for an idealised domain are presented. The focus is on reproducing results documented in the literature in order to establish that BEP has been correctly implemented, and to demonstrate the robustness of the new METRAS+BEP model.

As the simulations started at midnight the first day was considered to be part of the spin up phase, and therefore all the results presented were taken from the second day of simulation.

Vertical profiles of potential temperature, wind speed and turbulent kinetic energy

Figure 4.1 shows the vertical profile of potential temperature at the centre of the domain for the Rural simulation, the Orig simulation and the urban_BEP simulation at 04:00 of the second day of simulation.

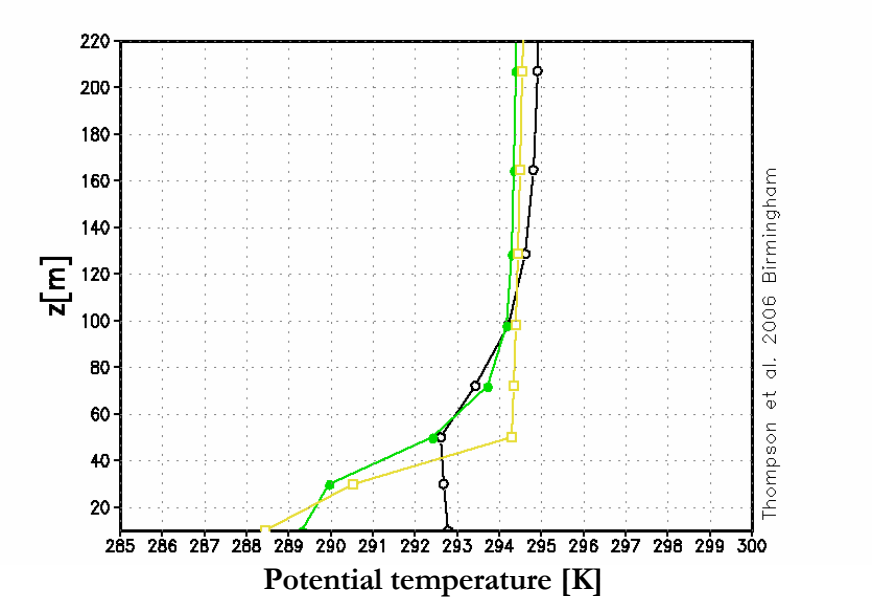


**Figure 4.1: Vertical profiles of potential temperature (K) at x=0, y=0 as computed by the *Rural* (yellow), *Orig* (green) and *urban_BEP* (black) simulations at 04:00 for the second day of simulation.**

Whilst in the *Orig* and *Rural* simulations the vertical profiles of potential temperature are very similar and present a stable layer close to the ground, the simulation with the BEP urban scheme shows a more neutral profile above the city, up to 50 m above the ground, which is due to the heat stored in the urban area. This was higher than the average building height in the simulation which is 15 m. The presence of a neutral layer above the city is well documented (e.g. Oke 1995; Rotach 1995) and is consistent with the observation of reduced atmospheric stability near the urban surface (Roth 2000). These results can be compared to those presented by Martilli et al. (2002) who found a near neutral profile which extended to 150 m above ground and Oke (1995), who found the depth of the neutral layer to be 100-300 m. Martilli (2003) found a near neutral layer with a depth of 40-50 m for simulations of an urban area in a coastal environment. The results above are also in agreement with those presented by Dupont et al. (2004) for the implementation of an urban canopy scheme in the model MM5 and by Hamdi (2005) who finds a neutral layer of 60 m

for the implementation of BEP in the TVM model. There is a large variety in the depth of the neutral layer for different studies using urban canopy models, and the results in this study, as well as that of Hamdi (2005) and Martilli (2003) are at the lower end of the scale, with a depth of around 40-60 m. The height of the neutral layer will depend on the rural conditions surrounding the urban area, as well as the specific urban conditions such as building heights and wind speed. The height of the neutral layer will also typically decrease during the night.

There is a difference of more than 3 K in the potential temperature at the lowest grid level, between the *urban_BEP* and *Orig* simulations. This illustrates the nocturnal urban heat island (UHI) which is not simulated by the *Orig* simulation, due to the fact that it does not fully take into account the shadowing and trapping of radiation in the street canyon, as well as the partitioning and storage of the daytime solar radiation in the urban building materials.

Figure 4.2 shows the vertical profile of the wind speed at the centre of the rural domain (yellow), the *Orig* urban domain (green) and the *urban_BEP* domain (black) at 04:00 of the second day of simulation.

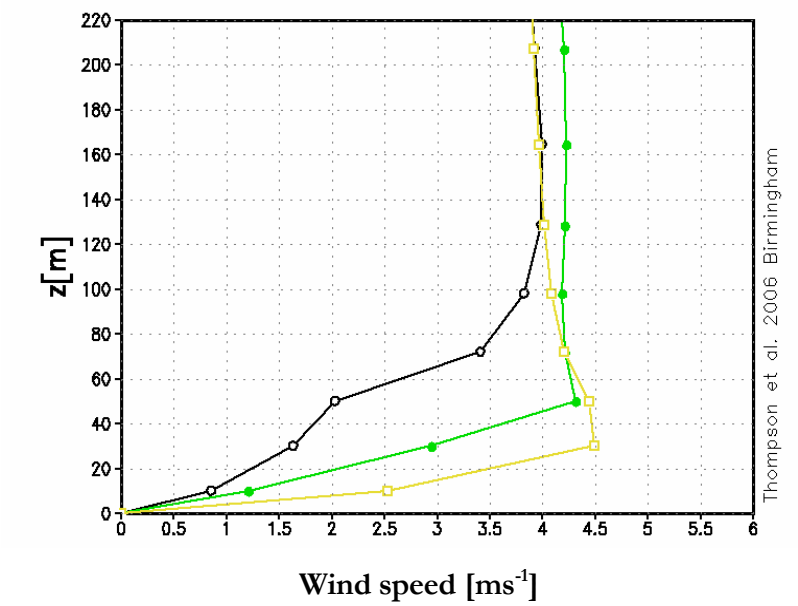


**Figure 4.2: Vertical profile of wind speed ($ms^{-1}$) at x=0, y=0 as computed by the *Rural* (yellow), *Orig* (green) and *urban_BEP* (black) simulations at 04:00 for the second day of simulation.**

The wind vertical profile of wind speed shows a reduction over the urban area up to a height of 100 m, compared to the profile over the rural land cover domain and the *Orig* simulation. This is due to the drag effect of the building surfaces, which in the BEP urban scheme is distributed in the vertical. Reduced wind speeds are expected over the urban area since the large buildings increase surface drag and wake turbulence (Roth 2000). Above 120 m the wind speed is the same as that in the rural simulation, and is very close to that in the *Orig* simulation. The initial geostrophic wind speed was the same (4 $ms^{-1}$) for all three simulations.

Figure 4.3 shows the vertical profile of the turbulent kinetic energy (TKE) at the centre of the rural domain (yellow), the *Orig* urban domain (green) and the *urban_BEP* urban domain (black) at 04:00 for the second day of simulation.

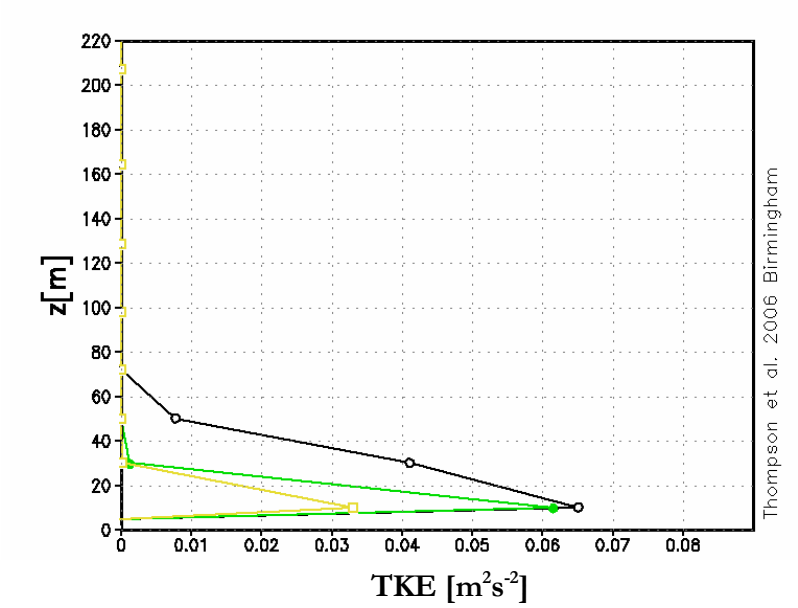


**Figure 4.3: Vertical profile of turbulent kinetic energy (TKE) ($m^2s^{-2}$) at x=0, y=0 as computed by the rural (yellow), *Orig* (green) and *urban_BEP* (black) simulations at 04:00 for the second day of simulation.**

The TKE for the rural and *Orig* simulations has virtually decayed to zero by the second vertical level (30 m), whereas in the *urban_BEP* simulation the region of influence extends up to around 70 m. The TKE in the *urban_BEP* simulation peaks at the first grid level (20 m) which is close to the mean building height. This is in agreement with the modelling results presented in Martilli (2002), Otte et al. (2004) and Hamdi (2005). The maximum TKE in the rural simulation is less than half that in the urban simulations. Although the maximum TKE in the *Orig* simulation is close to that in the *urban_BEP* simulation, the latter demonstrates the vertical distribution of the TKE, compared to the *Orig* simulation where the source is at the ground only. The urban canopy parameterisation enhances TKE in the urban canopy, especially at roof level, which results in additional mixing in the roughness sub layer and a deeper PBL than with the roughness approach.

*4.2.1 Horizontal cross sections of potential temperature and horizontal wind speed*

Figure 4.4 shows the horizontal cross section at the first and second vertical grid levels of the potential temperature for night time (04:00 of the second day of simulation), and demonstrates the presence of a surface layer urban heat island. At this time the intensity of the near surface urban heat island (calculated as the difference in temperature between the urban surface and the rural surface upwind of the city at the first and second vertical grid levels, respectively) is positive and peaks at 4.7 K, and the area of maximum urban heat island intensity is shifted downwind from the city centre. At the second grid level the location of the highest potential temperature is advected further in the downwind direction compared with the first grid level, as expected due to the higher wind speed at the higher level (see Figure 4.2).

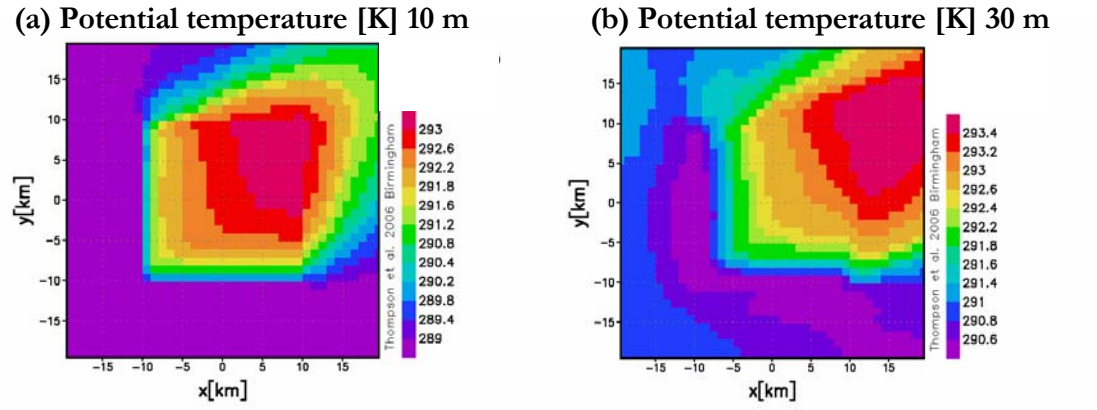


**Figure 4.4: Horizontal cross section at z=10 m (a) and z=30 m (b) of potential temperature (K) as computed by the *urban_BEP* simulation at 04:00 for the second day of simulation.**

It is apparent from Figure 4.4 that there is a large displacement and distortion in the area of maximum urban heat island intensity at 30 m when compared to the near surface results at 10 m. This has been observed in previous observational studies, for example Zhang et al.

(2006) find a spatial displacement of the urban heat island core with height with a shift of up to 6 km at 50 m.

Figure 4.5 shows the horizontal cross section at the first and second grid levels of the horizontal wind speed and wind vectors. The wind speed over the city at the first vertical level of 10 m is reduced by more than 50% compared to the surrounding upwind rural area. There is also a noted deflection of the wind vectors around the urban boundaries. The same results are replicated at the second grid level (30 m above the surface) although the area showing the reduction in wind speed is smaller, and is shifted down wind of the centre of the domain.

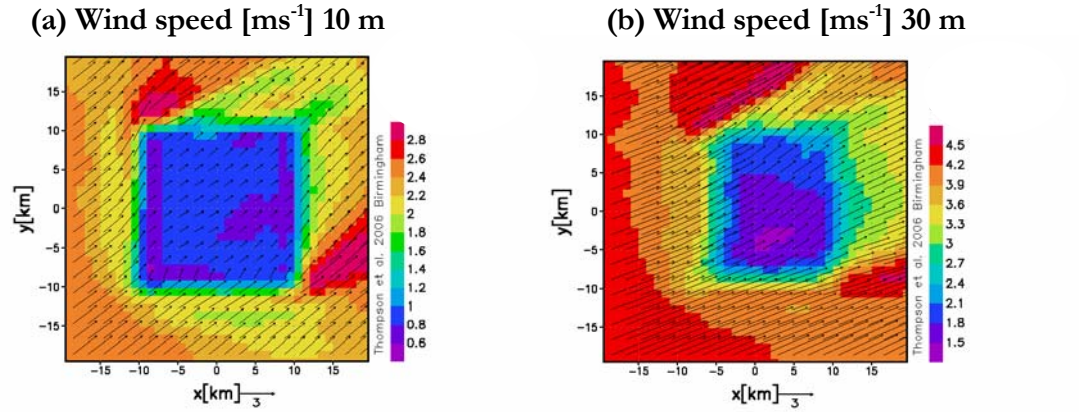


**Figure 4.5: Horizontal cross section at z=10 m (a) and 30 m (b) of wind speed ($ms^{-1}$) and direction as computed by the *urban_BEP* simulation at 04:00 for the second day of simulation. The arrows represent the magnitude and direction of the horizontal wind and the shaded plot represents the magnitude of the horizontal wind speed ($ms^{-1}$).**

Wind speeds over urban areas are expected to be slower due to the drag effect of the buildings (Roth 2000) and increased roughness of the surface. It has been observed for example that above approximately 4 $ms^{-1}$ wind speeds near the centre of New York are lower than those outside the city (Bornstein et al. 1977). Wind directions can also be

affected, as the flow bends around and over the urban area (Britter et al. 2003). As in Otte et al. (2004) some convergence over the urban area is observed, caused by the concentrated heat over the city. Both these effects are observed in the results presented in Figure 4.5.

### *4.2.2 Impact of the urban area on the mesoscale flow*

The vertical profiles of potential temperature and wind speed show how the urbanised model reproduces features of observations made close to the urban surface. This section analyses the impact of the urban surface on the mesoscale flow and the atmospheric boundary layer, during both daytime and night time, and shows that the results are in agreement with observations and other numerical studies.

Daytime

Figure 4.6 represents a vertical section of the potential temperature in the middle of the urban domain at 12:00 noon of the second day of the simulation. This shows the formation of a plume of hot air above the city, which is displaced downwind by the geostrophic wind, thus transporting the urban heat towards the surrounding rural areas. The plume is due to the higher turbulent activity over the urban area caused by the greater roughness of the city and greater sensible heat fluxes compared to rural areas where the energy released is partitioned between the sensible and latent heat fluxes. The urban heat island is visible both below 300 m, and, at much smaller intensities, up to around 2 km. This compares well with the results for the daytime UHI simulated by Martilli et al. (2002), Martilli (2003), Atkinson (2003), Kusaka et al. (2004) and Hamdi (2005). The thermal circulation and

presence of the dome of warmer air above the city have been documented in a number of experimental and numerical studies (e.g. Bornstein et al. 2000; Lin et al. 2008).

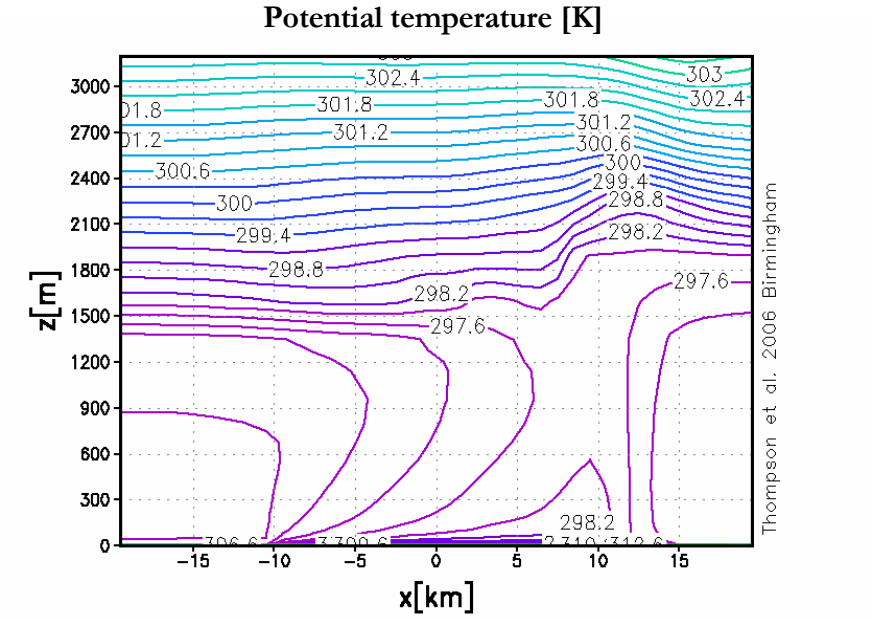


**Figure 4.6: Vertical section at y=0 of potential temperature (K) as computed by the *urban_BEP* simulation at 12:00 noon of the second day of the simulation.**

Figure 4.7 represents a vertical section of the horizontal wind speed at the centre of the urban domain at 12:00 noon. This shows the convergence of low level winds over the city, and divergence aloft. The convergence zone is displaced to the east by the geostrophic wind, as seen in Martilli et al. (2002) and Martilli (2003). This behaviour can be explained in terms of the three competing forces over the urban area: the drag induced by the urban surface, the pressure gradient due to higher urban temperatures, and advection due to the general synoptic flow. As seen in Figure 4.5 low winds are observed near the urban surface due to the dominance of the drag effects. Aloft (at about 400 m above the ground) however the pressure gradient and the advection have the same sign, causing a maximum.

Downwind of the city on the other hand the pressure gradient and advection have opposite signs, causing the observed minimum.

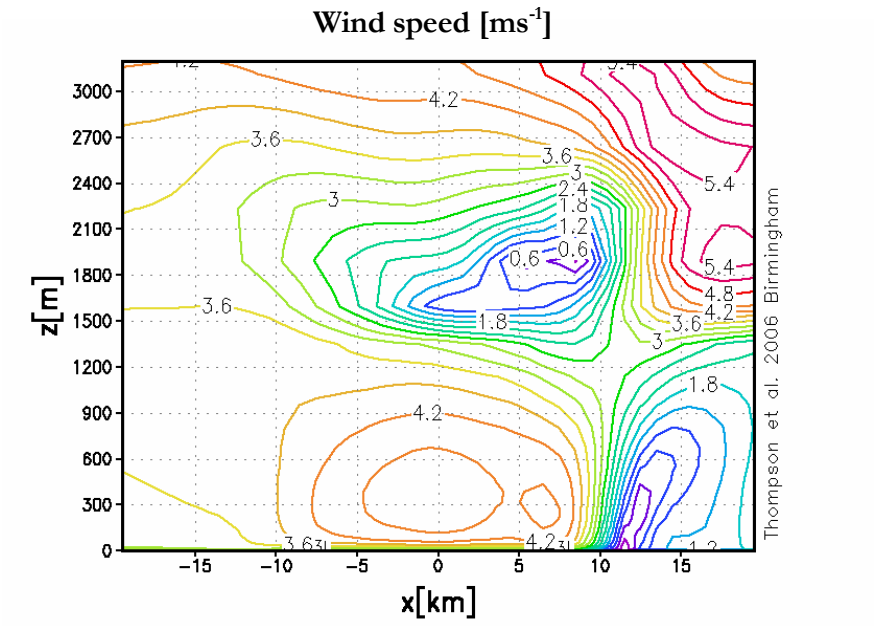


**Figure 4.7: Vertical section at y=0 of the horizontal speed (ms$^{-1}$) as computed by the *urban_BEP* simulation at 12:00 noon of the second day of simulation.**

These results can be compared to those obtained for the potential temperature and wind speed vertical sections for the *Orig* simulation, as seen in Figure 4.8. The *Orig* simulation shows very different results from those obtained in the *urban_BEP* simulation. The *Orig* simulation does not reproduce the plume of hot air above the city at noon, nor does it reproduce the circulation pattern above the city seen at this time.

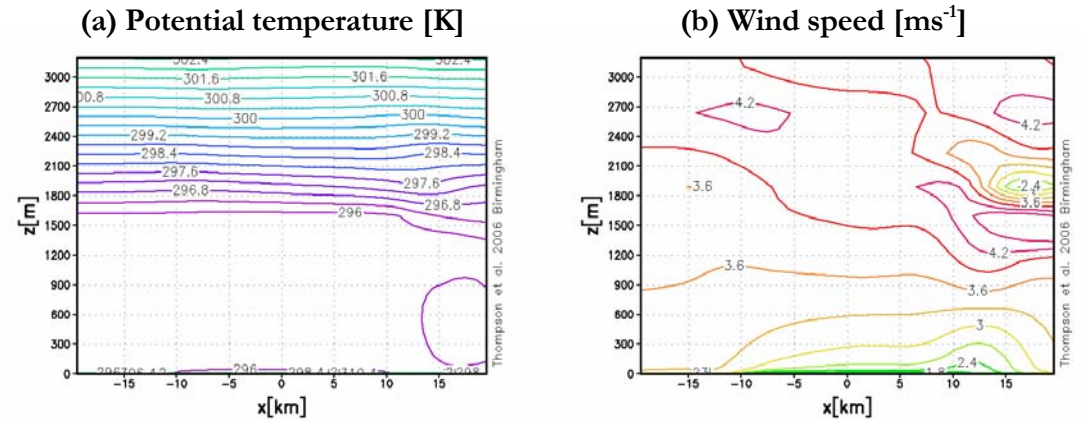


**Figure 4.8: Vertical sections at y=0 of (a) potential temperature (K) and (b) horizontal wind speed ($ms^{-1}$) (b) as computed by the *Orig* simulation at 12:00 noon of the second day of simulation.**

During day time, even though the urban plume of hot air above the city is observed, the dynamic processes may dominate over the thermal and radiative effects (Sarrat et al. 2006). The geostrophic wind speed chosen for this case study is relatively strong and therefore mechanical effects are expected to be dominant. The development and increased height of the planetary boundary layer (PBL) above the city is caused by the mechanical generation of turbulence, due to the higher roughness of the buildings and urban surface, and the buoyant production due to the thermal properties of the urban surface, e.g. heat storage in the urban fabric (e.g. Rigby et al. 2008). Both these effects enhance the daytime production of TKE. The PBL height is defined by Martilli (2002) as the lowest height at which the TKE falls below 0.01 $m^2s^{-2}$ and is a crucial parameter for air pollution dispersion.

As seen in Figure 4.9, the *urban_BEP* simulation reproduces the increase in planetary boundary layer (PBL) height over the urban area, compared to over the rural surroundings and that for the *Orig* simulation. The increased PBL heights are also advected downwind of

the city, which is expected since the wind speed in this simulation is quite strong. Increased PBL heights over the urban area have been observed in several field campaigns. For example Spangler and Dirks (1974) found a thermally induced dome over St. Louis, and the height of the inversion layer to be a few hundred meters higher than over rural areas. A similar behaviour has been observed by Spanton et al. (1988) for the London boundary layer and by Dupont et al. (1999) during the ECLAP campaign. In general a large variation is height difference in noted, with a standard deviation of approximately 300 m (Angevine et al. 2003).

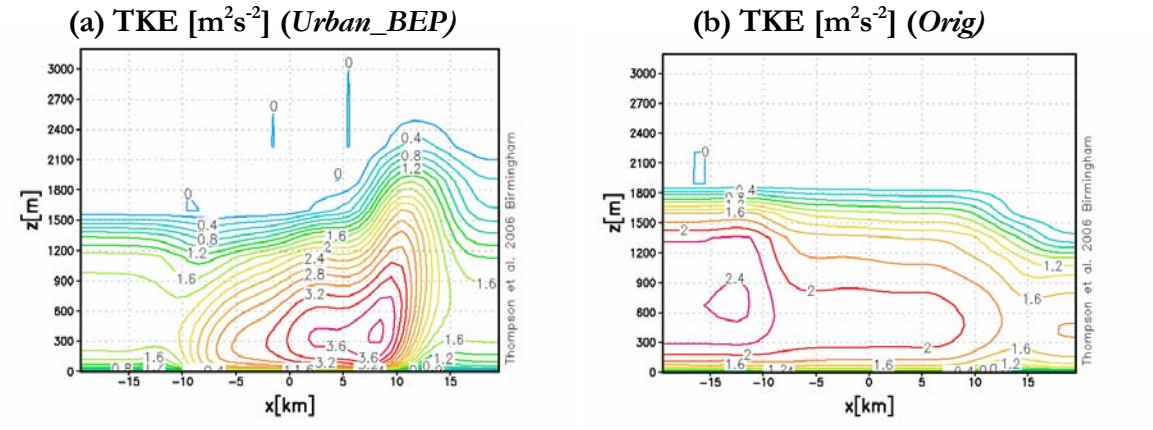


**Figure 4.9: Vertical section at y=0 of the TKE ($m^2s^{-2}$) as computed by (a) the *urban_BEP* simulation and (b) the *Orig* simulation at 12:00 noon of the second day of simulation.**

These results are also confirmed by with numerical modelling results. For example whilst simulating the summer urban breeze over Paris, Lemonsu et al. (2002) found that the depth of the PBL reached 2,500 m over the city during the daytime (at 15:00 hours), and 1,800 m over the surrounding non urban area. Martilli et al. (2002) found a difference of 400 m between the boundary layer height over the urban area and that over the rural area and Otte et al. (2004) found PBL heights of up to 2,000 m over, and advected downwind of, the

urban core, with differences of 300-500 m between simulations with and without an urban canopy scheme. Sarrat et al. (2006) found a maximum difference of 300 m between the top of the PBL for a simulation with an urban canopy scheme (that of Masson 2000) and one without.

Night time

During night time the urban processes are primarily of a thermal origin. Figure 4.10 shows the vertical section of potential temperature for the urban simulation at 04:00 of the second day of simulation. Over the surrounding rural area there is a very stable atmosphere due to the strong cooling, whereas the over the urban area the lower atmosphere becomes unstable due to the increased turbulent fluxes. The night time UHI is much shallower than the daytime UHI, but is visible in the lower part of the atmosphere (up to around 100 m). The higher temperatures above the urban area can also be observed to be shifted downwind of the centre of the urban area. These results compare well with the numerical modelling results (e.g. Uno et al. 1989; Atkinson 2003).

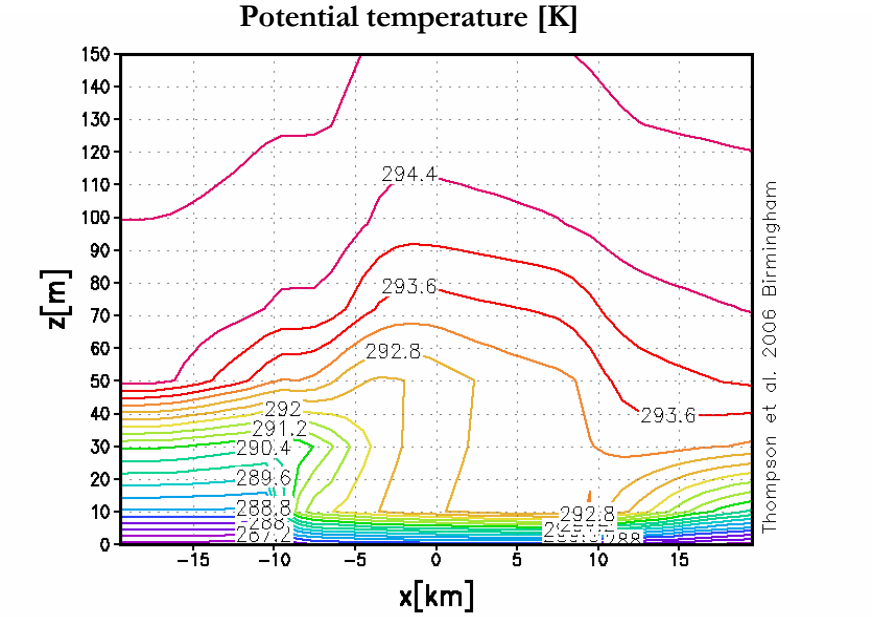


**Figure 4.10: Vertical section at y=0 of potential temperature (K) as computed by the *urban_BEP* simulation at 04:00 of the second day of simulation.**

Figure 4.11 shows the vertical section of the horizontal wind speed at 04:00 of the second day of simulation. This shows the deceleration of the flow over the urban surface, as expected due to the higher roughness of the urban surface and the consequent loss of momentum due to frictional forces. The reduction in the wind speed is observed both directly above the urban area, and also downwind of the urban area, as also observed in Figure 4.5. The difference in wind speed is also found to extend in the vertical above the city, up to at least 120 m. These results compared well with those presented in Hamdi (2005) for the implementation of BEP in a mesoscale model.

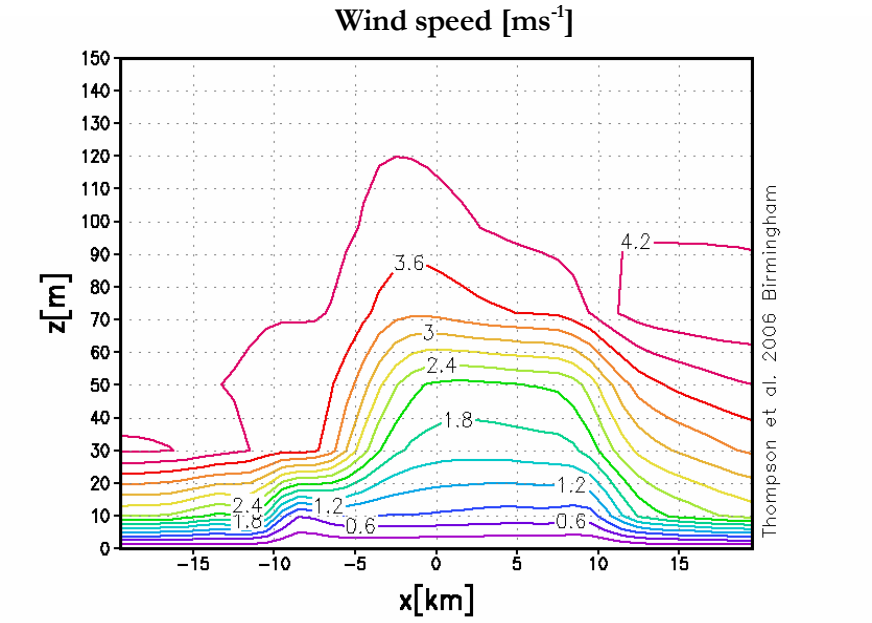


**Figure 4.11: Vertical section at y=0 of horizontal wind speed (ms$^{-1}$) as computed by the *urban_BEP* simulation at 04:00 of second day of simulation.**

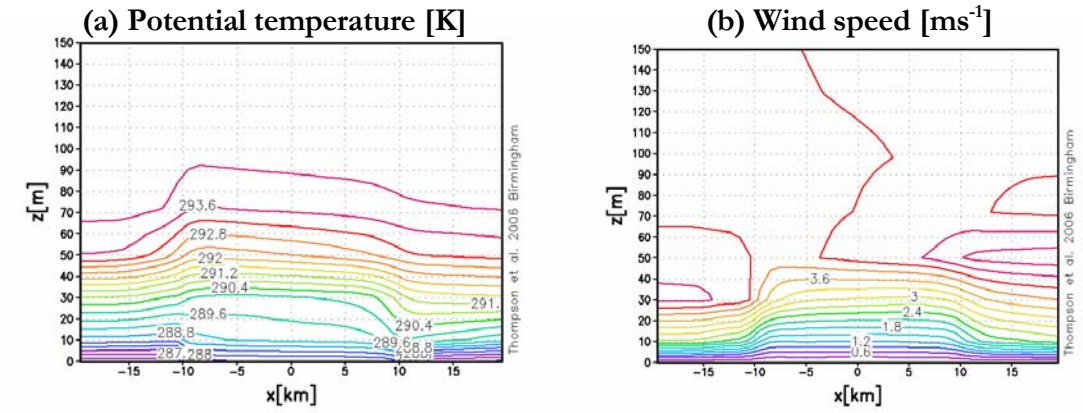


**Figure 4.12: Vertical sections at y=0 of (a) the potential temperature (K) and (b) the horizontal wind speed (ms$^{-1}$) as computed by the *Orig* simulation at 04:00 of the second day of simulation.**

During night time the *Orig* simulation does reproduce a decrease in wind speed above the urban area. However quantitatively this difference is much less than in the *urban_BEP* simulation and is confined to a shallower layer, due to the fact that the drag effect of the urban surface is confined to the lowest level above ground (whereas in the *urban_BEP*

simulation this effect is vertically distributed). The temperature field in the *Orig* simulation does not reproduce the difference in the stability of the layer above the city and that above the surrounding rural area.

### *4.2.3 Diurnal cycle of the UHI intensity*

The presence of a UHI has been established for the *urban_BEP* simulation, in both daytime and night time. In this section the diurnal variation of the UHI phenomenon is investigated.

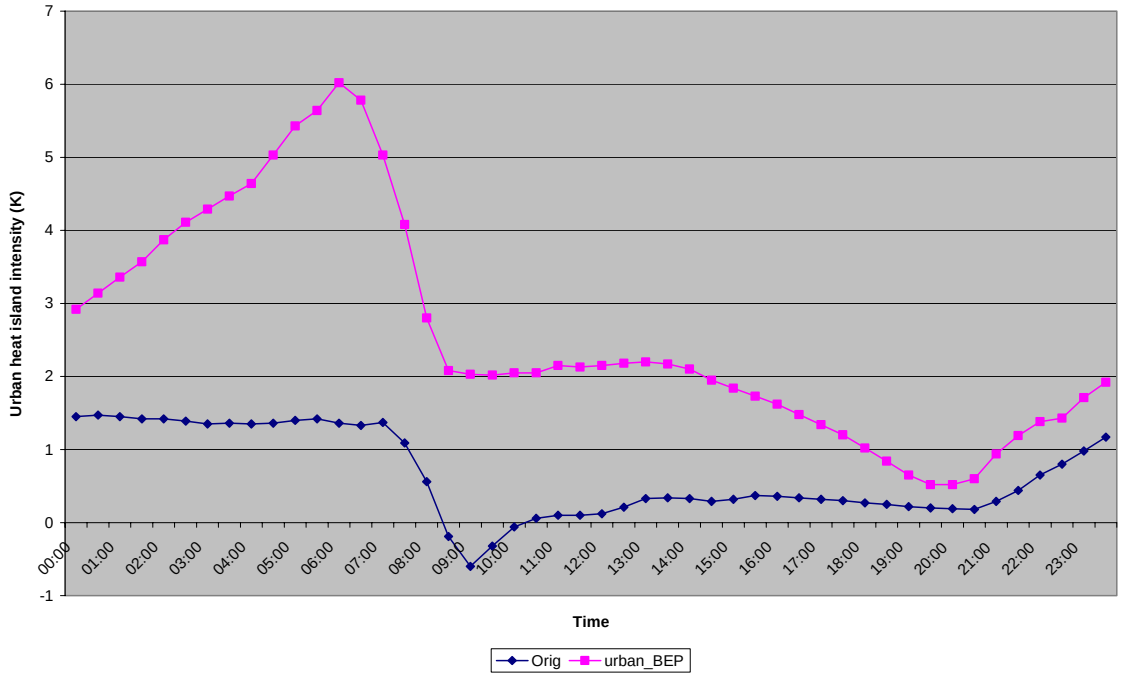


**Figure 4.13: Diurnal variation of the UHI intensity (K) for the second day of simulation, calculated as the maximum difference in potential temperature at the first grid level between the urban area and a rural point upwind of the city. The pink line represents the *urban_BEP* simulation, and the blue line the *Orig* simulation. Sunrise and sunset are around 04:00 and 20:00 respectively.**

Figure 4.13 shows the diurnal variation of the maximum UHI intensity, for the second day of the simulation. For the *Orig* simulation the maximum UHI intensity is 1.5 K, which occurs during the night time. Between midnight and 06:00, a couple of hours after dawn,

the UHI intensity is constant, it then decreases rapidly reaching a minimum at 08:00 when the air above the urban area is cooler than that above the rural area. The UHI intensity then increases and during the greater parts of the daytime it is between 0 and 0.5 K. After sunset the UHI increases. Although the *Orig* simulation does reproduce a UHI, the intensity is, for all times, lower than those found for example in Sarrat et al. (2006).

For the *urban_BEP* simulation the UHI intensity continues to increase between 00:00 and 06:00, reaching a peak of 6 K at 06:00. This well developed UHI is expected as conditions favourable to the formation of well developed heat islands were chosen for the test case, e.g. clear skies and anticyclonic conditions. Then, like the *Orig* simulation, the UHI intensity drops off rapidly until 08:00. This occurs because after sunrise (around 04:00) the temperature above the rural surroundings increases more rapidly compared to that over the urban area. The timing of the peak UHI intensity is found to depend on local conditions (Oleson et al. 2008), for example some studies find the peak occurs a few hours after sunset (e.g. Oke et al. 1975), whereas others (e.g. Jauregui 1997) observe an increase throughout the night, reaching a peak around sunrise.

During the day time the UHI is much less intense and shows little variation in the morning hours. As simulated by Atkinson (2003), after midday there is a further decrease in its strength, as solar radiation is decreased, until after sunset, when it increases, more rapidly than the *Orig* simulation. The increase in the UHI intensity after sunset is due to the release of heat stored in the urban area during the daytime. For the *urban_BEP* simulation the UHI intensity is always positive, in agreement with the simulations by Atkinson (2003) for a similar geographical location and domain size. The smaller urban-rural temperature

differences are expected during daytime, as the solar heating prevails over the difference in thermal properties between the urban and rural areas. The diurnal cycle of the UHI presented above is also in good agreement with Lemonsu et al. (2002), Hamdi (2005) and the timing of the UHI peak in particular is in agreement with experimental results presented for the city of London in Wilby (2003). The UHI for London with its current land cover configuration will be further examined and discussed in Chapter 6.

## 4.3 Sensitivity tests

In Section 4.3 it was established that the METRAS+BEP model works and is a reliable model. In the current section the characteristics of the urban area are modified in a controlled way and the effects on meteorological variables are analysed. If the model is working correctly then it is expected that the results will be important for understanding the sensitivity of the climate system to changes in the urban surface.

In this sensitivity study the influence of the city characteristics (e.g. building morphology, albedo and temperature inside the buildings), the rural surroundings (in particular the different land cover classes in the METRAS model) and synoptic conditions (e.g. the wind speed and relative humidity) on the local meteorology, UHI and the mesoscale circulation were investigated.

The sensitivity study was also designed to be a further examination of the implementation of the BEP urban scheme, and therefore some of the tests carried out are the same as those performed in Martilli (2002) and Hamdi (2005). Other tests were also performed in order to investigate how the urban scheme reacts to key METRAS parameters and characteristics, such as the surface land cover classes that may surround the urban area.

### *4.3.1 Sensitivity to the building height distribution*

The sensitivity of the model to the building height distribution is analysed in this section. The building height distribution is one of the characteristics of the urban area which can be specified for each urban class within the BEP scheme. Building height can have a significant effect on surface temperatures, since tall buildings, with their large shadows,

tend to cool the surface, but can also increase the trapping of radiative heat (Kusaka et al. 2001).

Two more simulations were carried out, which can be compared to the control simulation a01, which has been analysed in the previous section. The information of building heights of the three simulations can be seen in Table 4.2. These simulations differed only in the building height distributions and all other parameters and initial conditions were the same. The mean building height for each simulation was chosen to be characteristic of a particular urban land cover type, for example a mean building height of 7 m (simulation bh2) could characterise suburban areas, such as Guildford, UK (Oestges et al. 1999), or light industrial estates (Burian et al. 2002), whereas a mean building height of 15 m (control simulation a01) would be typical of a densely urbanised area, such as Soho, London, UK (Oestges et al. 1999) and other European cities (Ratti et al. 2001), and a mean building height of 30 m would be typical of downtown areas in American cities (Burian et al. 2002).

**Table 4.2: Building height distribution for the three sensitivity simulations.**

| | **bh2** | **a01 (control)** | **bh3** |
|---|---|---|---|
| 5 m | 60% | | |
| 10 m | 40% | 50% | |
| 20 m | | 50% | 20% |
| 25 m | | | 10% |
| 30 m | | | 50% |
| 40 m | | | 20% |
| **Mean building height** | 7 m | 15 m | 29.5 m |

The building height distribution, as explained in Martilli (2002), is expected to have both mechanical and thermal effects. The different height-to-width (H/W) ratios caused by the

different building heights will affect the cooling rates by modifying the sky view factors (thermal effect), whilst the difference in the vertical distribution will affect both the drag term and the TKE production (dynamic effects).

Figure 4.14 represents the horizontal cross section at y = 0 m of potential temperature at the first grid level (10 m) at 04:00 of the second day of simulation for the three simulations described above. This shows that the UHI intensity increases as the mean building height increases, due to reduced nocturnal cooling (caused by the higher H/W ratio) and reduced advection of cold air from the rural area (Martilli 2002). In each case the relatively high wind speed causes the UHI peak to be shifted downwind of the city centre, and for this reason the potential temperature downwind of the urban area is higher than that upwind of the urban area.

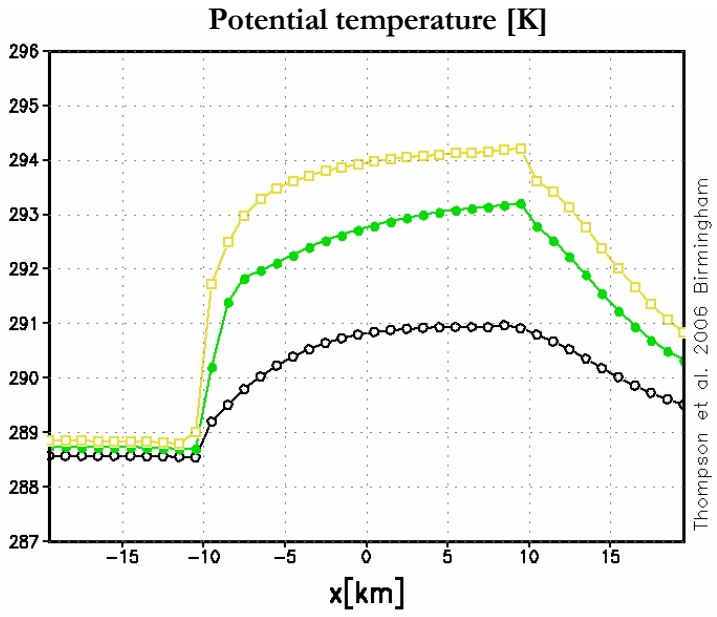


**Figure 4.14: Potential temperature (K) along the line y=0, z=10m as computed by the three simulations *bh2* (black line), *a01* (green) and *bh3* (yellow) at 04:00 on the second day of simulation. The simulations represent a mean building height of 7 m (*bh2*), 15 m (*a01*) and 29.5 m (*bh3*) respectively.**

Figure 4.15 shows the vertical profiles of wind speed and TKE at the centre of the domain for the three simulations at 04:00 for the second day of simulation. The wind speed near the ground above the urban area decreases, as the building height increases. This is expected due to the fact that increasing the height of the buildings will increase the drag force, as well as affecting its vertical distribution. It has been observed that the construction of taller buildings will result in lower wind speeds being experienced near the ground (Gaffin et al. 2008).

The two simulations with mean building heights of 7 m and 15 m show a TKE peak at the first grid level (10 m), whereas the simulation with the mean building height of 29.5 m peaks at the second grid level. For each simulation the maximum TKE occurs near the mean building height, as expected since the shear generation of TKE peaks at the top of the buildings. With increasing building height distribution the mechanical TKE production increases, and the region of influence of the TKE increases, i.e. the boundary layer height increases with building height (Martilli 2002).

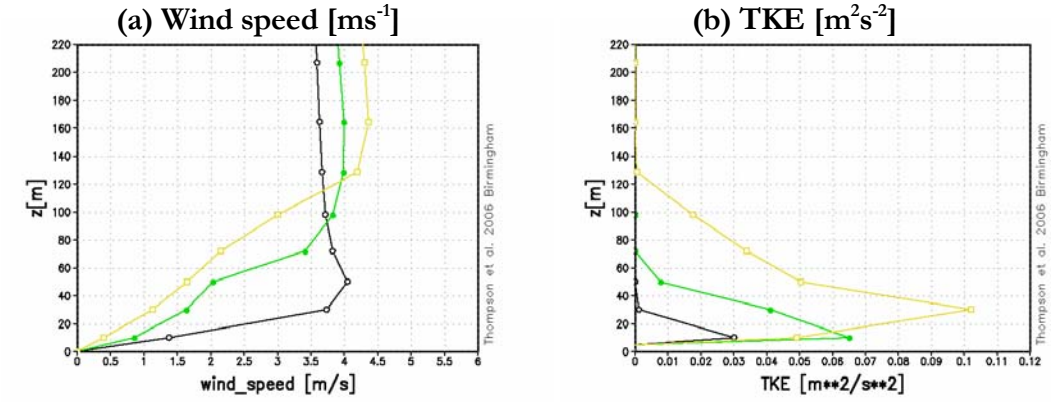


**Figure 4.15: Vertical profiles of (a) wind speed ($ms^{-1}$) and (b) TKE ($m^2s^{-2}$) at x=0, y=0 as computed by the three simulations *bh2* (black line), *a01* (green) and *bh3* (yellow) at 04:00 of the second day of simulations. The simulations represent a mean building height of 7 m (*bh2*), 15 m (*a01*) and 29.5 m (*bh3*) respectively.**

### *4.3.2 Sensitivity to the temperature inside the buildings*

The sensitivity of the model to the BEP urban scheme parameters 'twini' and 'trini' is analysed in this section. These parameters represent the initial temperature inside the buildings, behind the walls and roofs respectively. This is the only way in which the BEP scheme accounts for any change in anthropogenic heat flux for the urban area. This is obviously a very simplistic treatment of the anthropogenic heat flux; however this is a source which is hard to estimate and a great deal of detailed data would be needed for an accurate treatment (Sailor et al. 2004).

In the control simulation, both parameters were set to 295 K, as this was the value suggested in the original BEP model code. Two additional simulations were carried out, in which both parameters were set to 293 K and 297 K. In particular 293 K was chosen as the value used in both Martilli et al. (2002), Martilli (2003), Roulet et al. (2005) and Hamdi (2005). It is interesting to analyse the sensitivity of the UHI to this parameter, as well as other building characteristics, as research by Oke et al. (1991) suggested that these factors could be important in determining the UHI strength. This variable in particular was not investigated in the sensitivity work of Martilli (2002) or Hamdi (2005).

Figure 4.16 shows the horizontal cross section along the line at y = 0 m of the potential temperature at the first model grid level for the three simulations. Increasing the internal temperature by 2 K causes a less than 1 K increase in the potential temperature at 04:00 am. There is less than a 2 K difference in the maximum heat island intensity between the three simulations, and as could be expected the UHI increases as the parameters describing the temperature inside the buildings behind roofs and walls increase. Selecting the most

appropriate value for these parameters to use in future work on the city of London is not easy, and there is little available literature to assist in the choice.

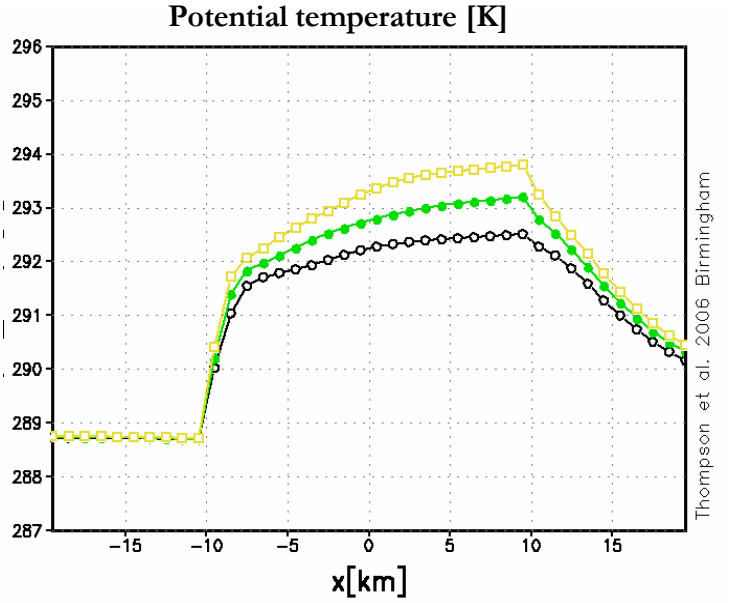


**Figure 4.16: Potential temperature (K) along the line y=0, z=10 m, as computed by the three simulations with the internal temperatures behind urban walls and roofs ('twini' and 'trini') both set to 293 K (black line), 295 K (green) and 297 K (yellow) at 04:00 for the second day of simulation.**

*4.3.3 Sensitivity to the surface albedo*

The sensitivity of the model to the albedo values of the urban surfaces was investigated. The albedo of a surface is defined as its hemispherically and wavelength integrated reflectivity (Taha 1997).

The difference in albedo between rural and urban surfaces is one of the factors which can affect the surface energy balance in urban areas. The albedo for the urban area is typically lower than that of the rural surroundings, and therefore less radiation is reflected back from the urban area, which can lead to a higher heat content, thus contributing to the UHI phenomenon (Oke 1987; Taha 1997; Atkinson 2003). A decrease in the UHI intensity is

expected if the difference between the urban and rural albedo is removed by increasing the albedo of the urban surface (Atkinson 2003).

A summary of albedo values for typical urban and rural surfaces is shown in Table 4.3. For most surfaces a range is presented, as precise albedo values are not certain.

**Table 4.3: Typical albedo values for rural and urban surfaces, taken from Oke (1987) and Taha (1997)**

| Surface type | Albedo |
|---|---|
| Grass | 0.16 - 0.28 |
| Crops | 0.15 - 0.24 |
| Forests | 0.10 - 0.18 |
| Gravel | 0.09 |
| Tile roof | 0.10 - 0.35 |
| Asphalt | 0.05 - 0.20 |
| Concrete walls | 0.10 - 0.35 |
| Brick | 0.20 - 0.40 |
| Stone | 0.20 - 0.35 |
| Average urban areas (Oke 1987) | 0.15 |
| European and US cities (Taha 1997) | 0.20 |
| White paint | 0.50 - 0.90 |

Simple modifications of the albedo in urban areas, for example by using high reflective building materials, white surface coatings for roofs and walls, and lighter street surfaces, could be part of a mitigation strategy in attempting to counter the effects of rising urban temperatures, reduce cooling energy use and improve air quality (Oke 1987; Sailor 1995; Bretz et al. 1998; LCCP 2002). Increasing the albedo will affect the surface energy balance by increasing the percentage of incoming solar radiation which is reflected back to space. The use of solar reflective, or high albedo, materials maintains low surface temperatures in sunlight, and thus reduces the convective heat transfer from the surface to the ambient air, and helps create cooler communities (Taha 1997; Bretz et al. 1998). For example Taha et al. (1992) found a difference of 25 K between the temperature of a white surface (albedo of

0.61) and that of conventional gravel (with an albedo of 0.09), compared to the ambient temperature. For this reason in warm climates buildings are often painted white.

A number of modelling studies have shown reductions in temperature over urban areas by decreasing the surface albedo. For example Taha et al. (1988) showed, using one-dimensional meteorological simulations, that for a typical mid latitude city in summer it is possible to reduce local air afternoon temperatures by as much as 4 K by increasing the surface albedo from 0.25 to 0.40. Seaman et al. (1989) showed that by increasing the urban-rural albedo difference from 0.025 to 0.05 the UHI is weakened by 0.3 K. Sailor (1995) used a 3-D meteorological simulation of Los Angeles, USA to show decreased peak summertime temperatures of up to 1.5 K by increasing the surface albedo by 0.14 downtown, and 0.08 over the entire basin. Atkinson (2003) found a reduction in temperature over the urban area of 0.3 K by increasing the urban albedo from 0.15 to that of the rural surroundings (0.18).

Lower ambient air temperatures, achievable through an increase in albedo, also have implications on air quality (Sailor 1995; Taha 1997) and can effect substantial energy savings in areas where air conditioning is prevalent (Rosenfeld et al. 1998) since the direct heat transfer from the building surface into the building is also reduced.

In the control simulation of the present study the albedo for all urban surfaces, i.e. roofs, walls and roads, was set to 0.20 as suggested in the original BEP scheme code. This is a typical urban albedo value (Taha (1997) suggested a range of 0.15 to 0.20 for US and European cities). However, this value of 0.20 is equal to the albedo of the rural surface, which is also set to 0.20 for the METRAS 'Meadows' urban class. For this reason a

simulation was carried out in which the urban albedo is either reduced to 0.15, a value at the lower end of the range suggested by Taha (1997), or increased to 0.30. It is expected that the decrease in the albedo to a value 0.5 lower than the rural surroundings would enhance the temperature over the urban area, and vice versa.

The two simulations were therefore carried out with the following parameters:

- *alb1*: Albedo for all three surface types increased to 0.30
- *alb2*: Albedo reduced to 0.15, the urban value used by Sailor (1998) and Atkinson (2003)

In Figure 4.17 it is apparent that if the albedo of the urban surfaces is reduced to 0.15 then temperatures over the city increase by up 0.2 K. On the other hand increasing the albedo of all three urban surface types (roofs, roads and walls) determines a net reduction in the temperature near to the urban surface which is observed during the daytime, whereas night time temperatures are very similar. Around 06:00 the results, especially for the high albedo situation, appear to show an uncertain behaviour; however this is likely to be due to the fact this time corresponds to sunrise and the fact these are point measurements, not averaged over the urban surface. The maximum reduction observed is 0.4 K, and it peaks around midday when the solar radiation is highest. These results compare well with those in the literature discussed above.

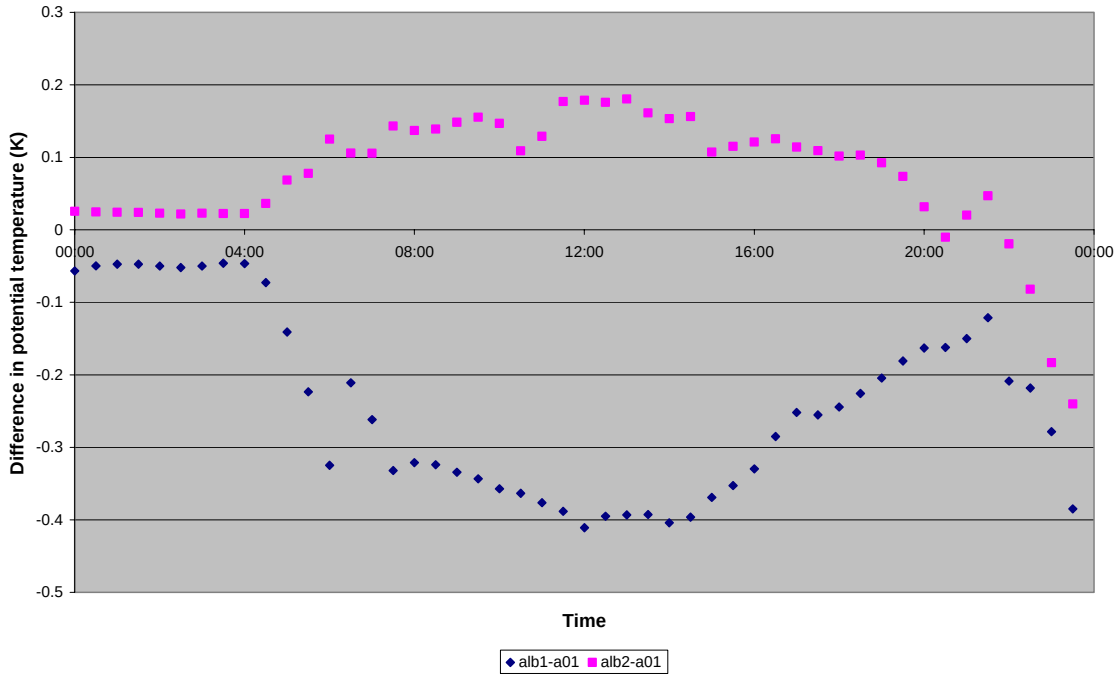


**Figure 4.17: Diurnal variation of the difference in potential temperature (K) between the simulations *alb1* and the control simulation *a01* (blue line) and between the simulations *alb2* and *a01* (pink line) at x=0, y=0, z=10 m for the second day of simulation. The *alb1* simulation represents an urban albedo of 0.30 and the *alb2* simulation represents an urban albedo of 0.15.**

It is clear that changing the albedo could be a relatively economical and achievable way of influencing the urban daytime temperatures, and this could be investigated further at the city scale for London, UK. The potential for increasing urban albedo has been investigated for some others cities, for example Bretz et al. (1998) estimated the potential to modify the albedo of Sacramento, California by 18%.

### *4.3.4 Sensitivity to the vegetation fraction*

Like the surface albedo, the vegetative cover in the urban area also affects the surface energy balance, and is another city characteristic which could be used as part of an adaptation strategy to reduce urban temperatures (Sailor 1995, 1998; LCCP 2002). For an urban area, the vegetation density and the land cover are crucial in determining the urban

climate (Jonsson 2004). Increasing the vegetated fraction in an urban area, for example by planting trees, will affect the amount of the incident radiation which is converted into latent heat through evapo-transpiration, as well as, in the case of trees, increasing shading in the street canyon.

There is significant evidence of reduced temperatures in large city parks and vegetated areas, especially during clear and calm nights (Chandler 1965; Oke 1987). Upmanis et al. (1998) presented data from various cities throughout the world and found differences ranging from 1 K to 6.8 K between the parks and their surroundings. Jonsson (2004) found temperature differences of 2-4 K across the city of Gabarone, Botswana which were attributed to the vegetation, and Gomez (1998) observed a drop of 2.5 K in green areas in Valencia, Spain with respect to the cities maximum temperature. These temperature differences between park and surrounding urban area are influenced by many variables, such as the wind speed and size of the park area. Larger parks also influence their surroundings at larger distances outside the park (Ca et al. 1998; Upmanis et al. 1998; Dimoudi et al. 2003).

There are also a significant number of modelling studies which show the effects of urban vegetation cover on meteorological parameters. Sailor (1995) showed the potential to reduce peak summertime temperatures in Los Angeles by more than 1.3 K with a 0.14 increase in the vegetated surface fraction. Sailor (1998) simulated an indirect regional cooling associated with increased vegetative cover in the urban area. Civerolo et al. (2000) found that the reclassification of 40% of the New York City metropolitan area as deciduous forest, the dominant vegetation type of the domain, instead of urban land cover, led to

reduced near surface temperatures of more than 1 K. Moreover these temperature changes were not always confined to the grid cells for which the land cover classification had been modified. Dhakal et al. (2002) found the maximum reduction in average noon temperatures due to greening the area surrounding the buildings to be 0.47 K. Another benefit of urban vegetation, and especially of trees, is the effect on air quality. For example Nowak et al. (2000) showed that increased tree cover can help reduce high ozone concentrations and those of other pollutants. Simulations in Taha (1996) indicated that the net effect of increased urban vegetation was a decrease in ozone concentrations, if the trees are low emitters.

In the control simulation the urban area had no vegetated fraction at all. This is obviously not a very realistic situation, although some Mediterranean cities have a very low fraction of vegetation, but the choice was made in order to ease the interpretation of the model results for the test case. Two further simulations were carried out:

- *veg1*: 10% vegetation evenly distributed within the urban area
- *veg2*: 30% vegetation evenly distributed within the urban area

In particular, 30% is a realistic assumption for the vegetated fraction and is a good approximation for the city of London, where the vegetation coverage is estimated at 20-30% (www.english-heritage.org.uk). The vegetated area was treated as the METRAS land cover class of 'Meadows', the rest of the urban area was treated with the BEP urban scheme.

Figure 4.18 shows the diurnal variation of the UHI difference between the vegetated simulations and the control simulation for the second day of the simulation. This shows peak reductions of up to 0.7 K at noon for the simulation with 30% vegetated fraction (*veg2*), and of over 0.3 K for the simulation with 10% vegetated fraction (*veg1*). There is also a smaller peak around 06:00 am. The timing of the peak agrees with Civerolo et al. (2000) who also find the largest differences occur at noon.

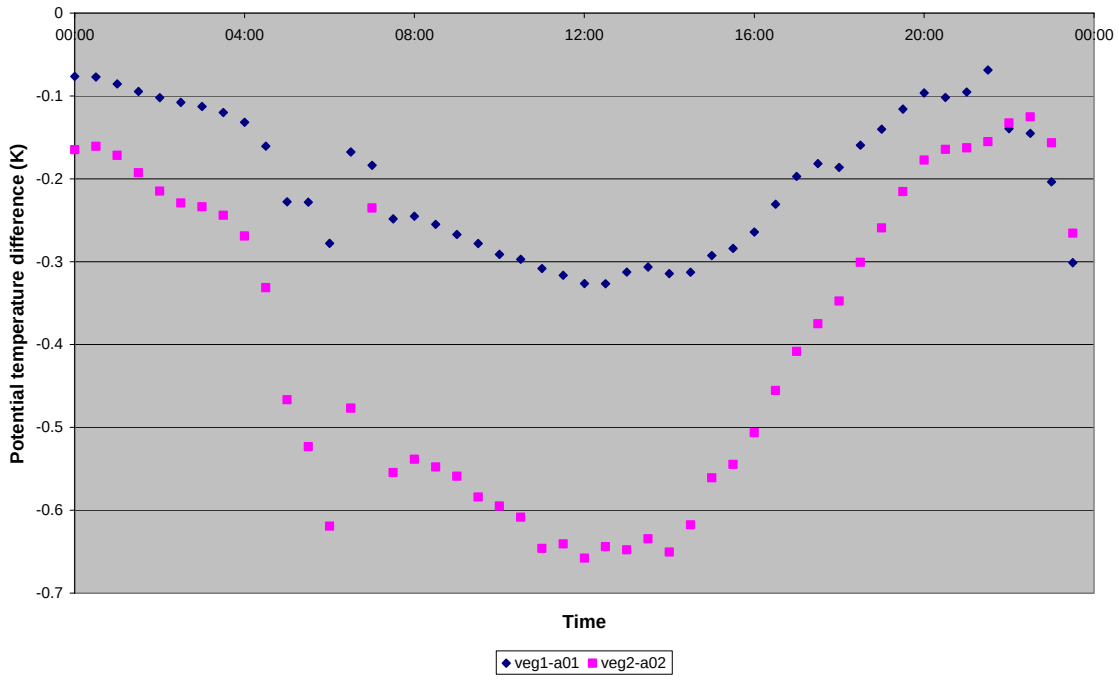


**Figure 4.18: Diurnal variation of the difference in potential temperature (K) between the control simulation *a01* and the vegetated simulations *veg1* (blue) and *veg2* (pink) at x=0, y=0, z=10 m for the second day of simulation. The *veg1* simulation represents an urban area with 10% vegetated fraction, and the *veg2* simulation represents an urban area with 30% vegetated fraction.**

In order to investigate the existence of a correlation between the fraction of vegetated land cover and temperature, a further set of simulations was carried out, in which the vegetated

fraction was increased in steps of 10% from 0% to 40%. Figure 4.19 shows the correlation between the fraction of vegetation and the temperature at the centre of the urban area at noon, the time of day at which the results in Figure 4.18 showed that the peak differences occur. It can be seen that there is a linear correlation between the vegetation fraction and the potential temperature for the range covered by these model simulations. The effect of increasing the vegetation from non-existent to 40% is to reduce the potential temperature by almost 1.5 K. Clearly the amount of vegetation within an urban area could have important consequences for daytime temperatures and human comfort levels.

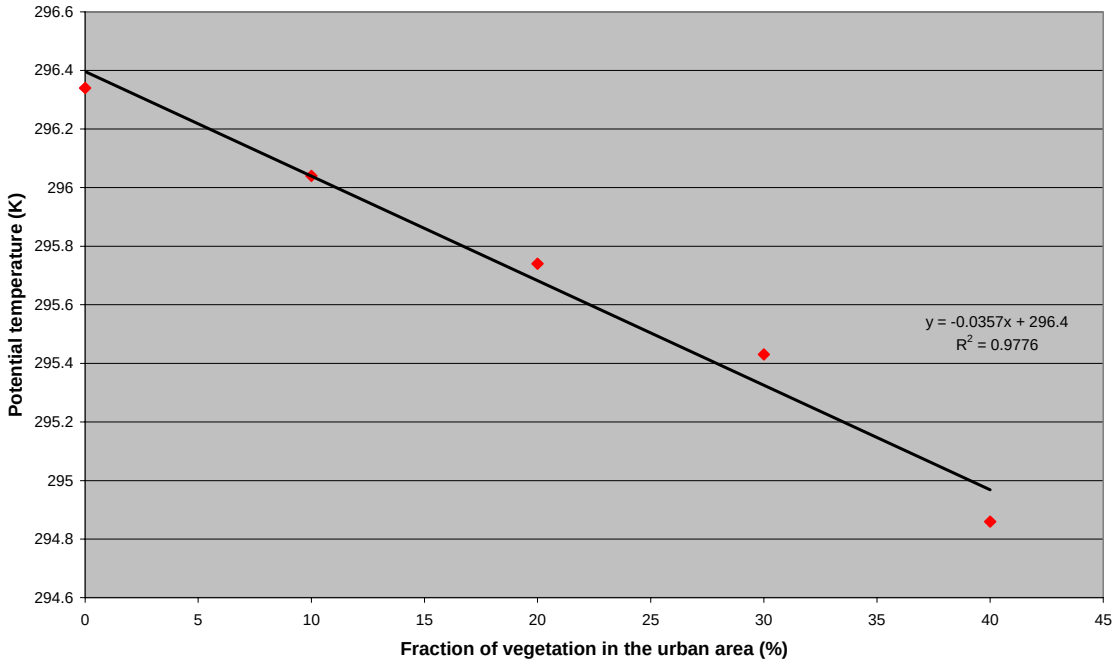


**Figure 4.19: Correlation between the fraction of vegetation in the urban area and the potential temperature (K) at x=y=0, z=10, at 12:00 noon for the second day of simulations**

It order to estimate whether increasing the vegetated fraction could be used as part of a mitigation strategy for urban temperatures it is necessary to consider what the realistic potential for changing this parameter in the city is. For example Sailor (1998)

conservatively estimated the potential for the increase in vegetated fraction to be 0.065 for a hypothetical city, although Bretz et al. (1992) found increases of more than twice this can be attained in some cities. It is likely that the majority of the vegetation increase would have to take place in residential areas (Sailor 1998).

### *4.3.5 Sensitivity to the size of the urban area*

The existence of a relationship between the size of an urban area and the intensity of the heat island has been debated for some time. Some studies, such as Oke et al. (1991), strongly suggest that the size of the urban area has little effect on the UHI intensity, and that other factors such as the urban fabric and geometry might be more important in determining the difference in temperature between an urban area and its rural surroundings. Chandler (1964) compared the heat island intensity of London and Leicester and found no significant effect which could be attributed to the disparity in size between these two cities. Seaman et al. (1989) only found an increase of 0.1 K in the UHI intensity when simulating an increase in city size by a factor of three. Atkinson (2003) performed a series of simulations in which the horizontal dimension of the city was increased from 6 km to 10 km, in steps of 2 km, and found that the maximum UHI intensity for the largest urban area was only 0.2 K greater than for the smallest urban area. However other studies have also indicated that trends in the temperature and UHI are correlated with regional land cover and its change pattern (e.g. Shudo et al. 1997; He et al. 2007).

Since part of the aim of this work was to establish whether urbanisation in the London area has affected regional climate, it is important to investigate the sensitivity of the model results to the size of an idealised urban area and understand how the urban climate system

works. In the control simulation the central square urban area measured 20 km x 20 km. Two further simulations were carried out, in which the urban area was reduced to a 10 km x 10 km region, and a 6 km x 6 km region. Since regional climate effects were central to the aim of this work, the control simulation was repeated for a larger domain, measuring 50 km x 50 km, in which the city was displaced towards the left hand boundary of the domain. For both simulations with smaller urban areas, the city was also displaced towards the left hand boundary. This was to enable a full appreciation of the downwind effect of the urban area.

Figure 4.20 shows the horizontal cross section of the potential temperature at the first grid level for the three simulations with increasing urban area. It is shown that the temperature patterns for the three cases match each other quite well for the corresponding fetches upstream to the urban fringe. The temperature increases significantly within a fetch of less than 10 km from the upstream urban fringe, and gradually reaches a saturated value when the fetch is greater than 15 km, indicating a small dependence of UHI on urban size.

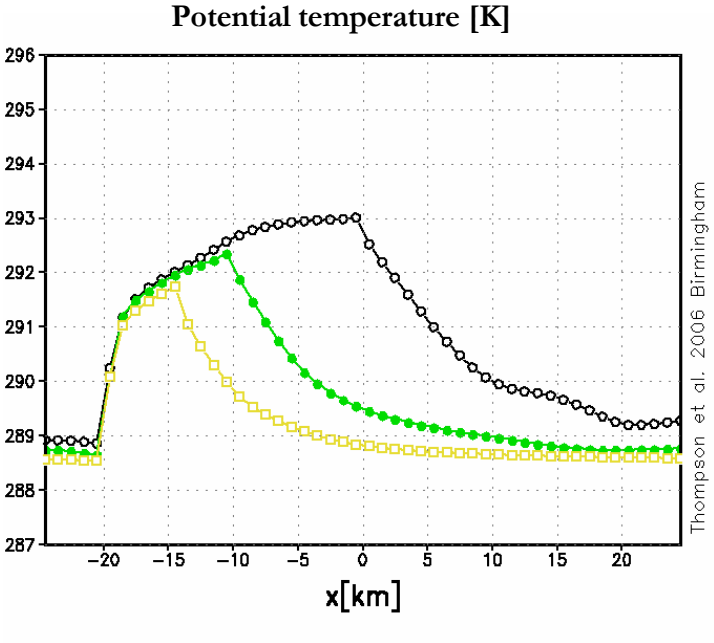


**Figure 4.20: Potential temperature (K) along the line y=0, z=10 m as computed by the three simulations with the urban area measuring 6 km, 10 km and 20 km respectively (yellow, green and black), at 04:00 for the second day of simulation**

There is a difference of more than 1 K in the maximum UHI intensity between the simulation with the largest urban area, and that with the smallest. This is clearly more than that found by Seaman et al. (1989) and Atkinson (2003). However a fundamental difference between the latter two papers and this work is that this work has been performed by a model with a sophisticated urban canopy scheme. This relationship between city size and the UHI intensity will be investigated further for the city of London.

### *4.3.6 Sensitivity to the surrounding rural land cover class*

The idealised results presented in Section 4.2 assume that the urban area is surrounded by the 'Meadows' land cover class. In order to analyse the sensitivity of the model results over the urban area to the land cover class which surrounds the city, six simulations where performed as well as the control simulation (see Table 4.4). The land cover classes are

characterised by the albedo, thermal diffusivity and conductivity, soil water availability, saturation value for water content and roughness length. The values for each class are presented in Table 3.1 on page 57.

**Table 4.4: Details of the simulations with different land cover classes surrounding the central urban area**

| | ga2 | ga3 | a01 (control) | ga5 | ga6 | ga7 | ga8 |
|---|---|---|---|---|---|---|---|
| Land cover type | Sand | Mixed | Meadow | Heath | Bushes | Mixed forest | Coniferous forest |

Figure 4.21 shows the diurnal variation in the UHI intensity (calculated as the difference in pot temperature at the first grid level between the location of maximum temperature within the city – as seen this is shifted downwind from the city centre – and a rural location situated upwind of the urban area, and therefore assumed not to be influenced by the presence of the urban area) for each of the six simulations with a different land cover class background, as well as the control simulation (a01).

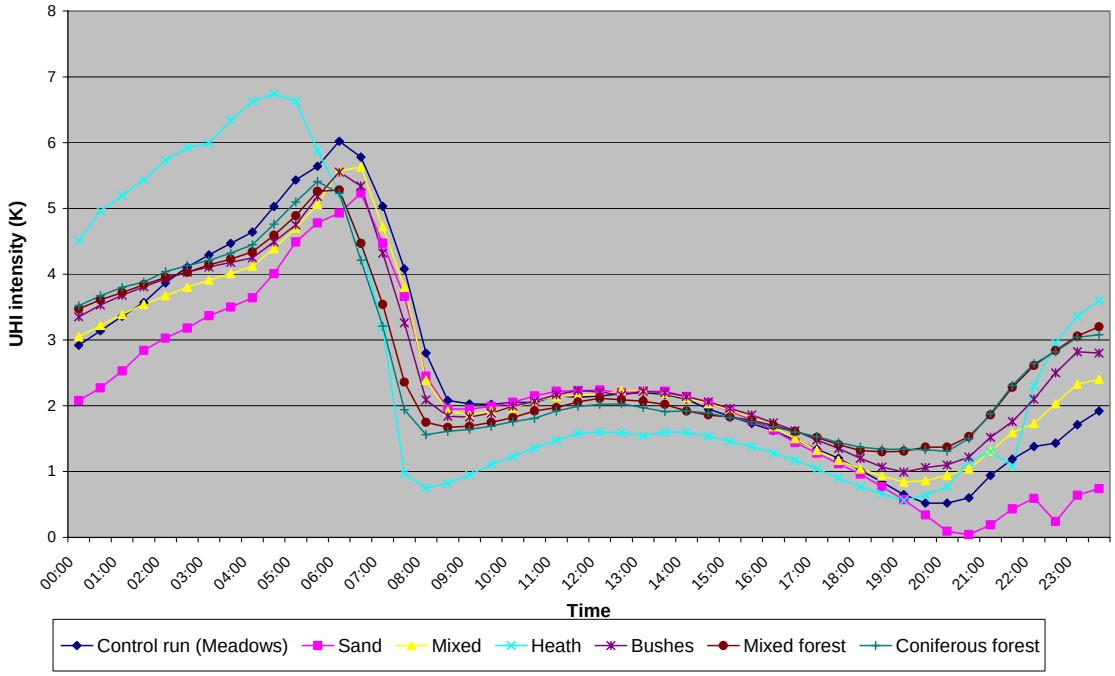


**Figure 4.21: Diurnal variation of the UHI intensity (K) as computed by the simulations representing different examples of rural land cover surrounding the urban area for the second day of simulation.**

The UHI is predominantly a night time phenomena, and in all simulations it is less intense during the day time. The day time peak of 1.5-2.5 K occurs at roughly the same time for all the simulations (13:00). It is observed that the UHI peaks at a maximum value, and at the earliest time (04:30), for the simulation with a 'Heath' background, and is least for the simulation with the 'Sand' background. The two forest simulations (ga7 and ga8) show very similar behaviour as far as the diurnal cycle of the UHI is considered, which is not surprising since their surface characteristics are very similar, and in some cases identical. The 'Heath' land cover class is characterised by a very low thermal conductivity compared to the other classes, which means it will have a smaller ability to conduct heat compared to other classes. It also has a high saturation value for water content. For the city surroundings in the different simulations, the potential temperature over the 'Heath' land cover class at 04:00 is almost 2 K lower than over the mixed land cover class, whereas during daytime it

is higher by a similar amount. The 'Sand' land cover class has a very small roughness length compared to the other classes, and shows the lowest night time UHI intensities.

These results can be compared to those presented in the literature. The UHI intensity has been found to be a function of the characteristics of the rural surface (Hawkins et al. 2004). For example Oleson et al. (2008) found a difference of up to 4 K between a rural surface composed of needle leaf evergreen trees and a grassland surface. The differences found in this PhD study are a lot smaller, with a maximum difference of just over 1.6 K between the two extreme examples of the 'Sand' and the 'Heath' urban class. The difference between the two main rural classes, 'Meadows' and 'Forest' are much smaller, and remain small during night time. For the main simulations presented in Chapter 5, 6 and 7 of this PhD study the rural classification surrounding London will be driven by the CEH Land Cover Map 2000 data, and therefore no assumptions need to be made to define the rural surroundings to the city.

### *4.3.7 Sensitivity to the geostrophic wind speed*

The sensitivity of the model results to different geostrophic wind speed conditions is analysed in this section. A control simulation was run under the conditions described in Section 4.2. A further two simulations were run with very low wind speed (2 $ms^{-1}$) and a very strong wind speed (8 $ms^{-1}$). These wind speeds were chosen in order to span a range from that used by Martilli (2002) to analyse an example in which thermal effects are expected to dominate, up to a maximum of 8 $ms^{-1}$ chosen by Hamdi (2005) as an example of high wind speed for which mechanical effects will be dominant.

Figure 4.22 shows the vertical profiles potential temperature, wind speed and TKE at the centre of the urban area at 04:00 for three simulations with different wind speed. As the wind speed increases there is a marked difference in the potential temperature profile and in the potential temperature at the first grid level. It is apparent that the urban surface temperature is reduced by an increasing geostrophic wind speed. As can be expected the wind speed above the urban area increases with the geostrophic wind speed. In the case with the strongest geostrophic wind speed, the height at which the wind speed becomes nearly constant is greater compared to the other two simulations. The shapes of the TKE profiles are similar, with a maximum at the first grid level in all three simulations. The maximum TKE value increases with the geostrophic wind speed, as does the PBL height. This is due to a higher mechanical production of TKE produced by the buildings and shear generation (Martilli 2002).

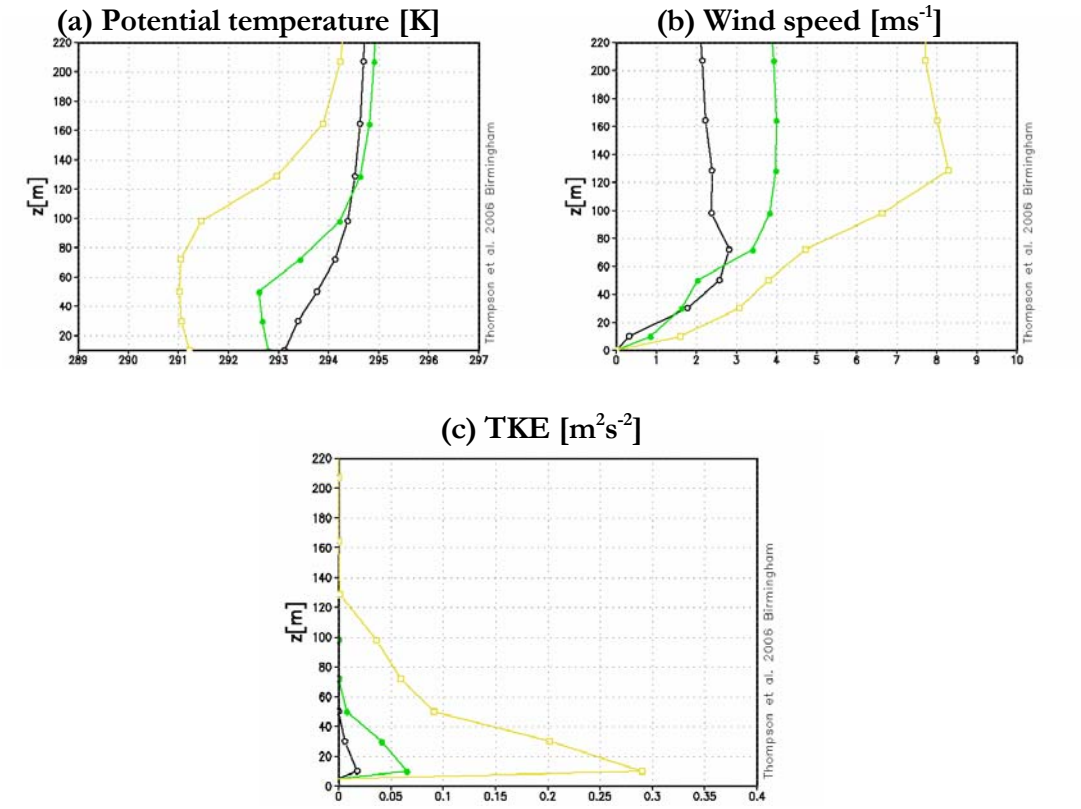


**Figure 4.22: Vertical profiles of (a) potential temperature (K), (b) wind speed ($ms^{-1}$) and (c) TKE ($m^2s^{-2}$) at x=0, y=0 as computed by the three simulations with geostrophic wind speed of 2 $ms^{-1}$, 4 $ms^{-1}$ and 8 $ms^{-1}$ (black, green and yellow respectively), at 04:00 of the second day of simulation.**

Figure 4.23 shows the vertical cross section of the horizontal wind speed for the two simulations with weakest and strongest geostrophic wind speed respectively. These results show that the circulation pattern above the urban area (due to the horizontal temperature gradient between the air above the city and that above the rural area), which has been described for the control simulation and which is strongly recognisable for the simulation with weak geostrophic wind, virtually disappears in the case with the strongest geostrophic wind. The difference in wind speed above the city compared to above the surrounding rural area is also much reduced.

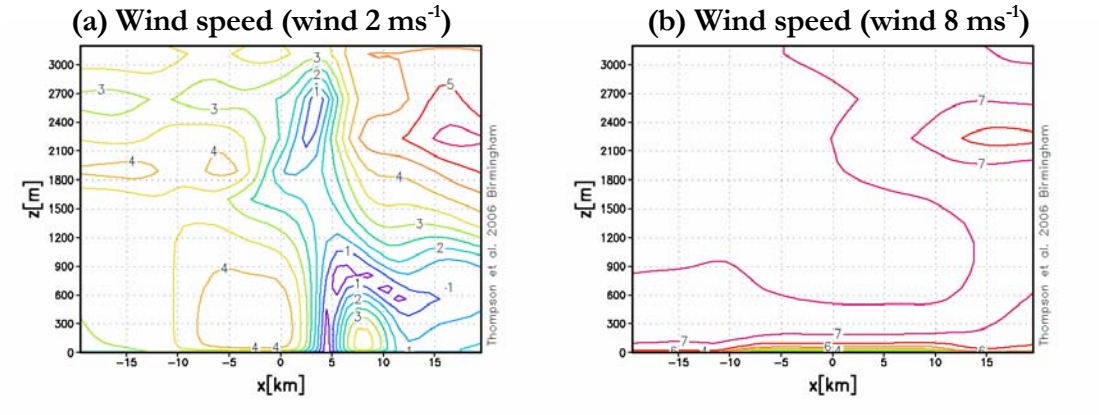


**Figure 4.23: Vertical cross section at y=0 of the horizontal wind speed (ms$^{-1}$) as computed by the simulation with the low wind speed of 2 ms$^{-1}$ (a), and that with strong wind speed of 8 ms$^{-1}$ (b) at 12:00 noon of the second day of simulation.**

Figure 4.24 shows the vertical section of potential temperature for the same two simulations. The pattern for the case with weak geostrophic wind is very similar to the control simulation shown in Figure 4.7. In the simulation with strongest geostrophic wind speed the plume of hot air above the city is displaced even more downwind of the city, so that the region of influence of the urban area is a lot larger.

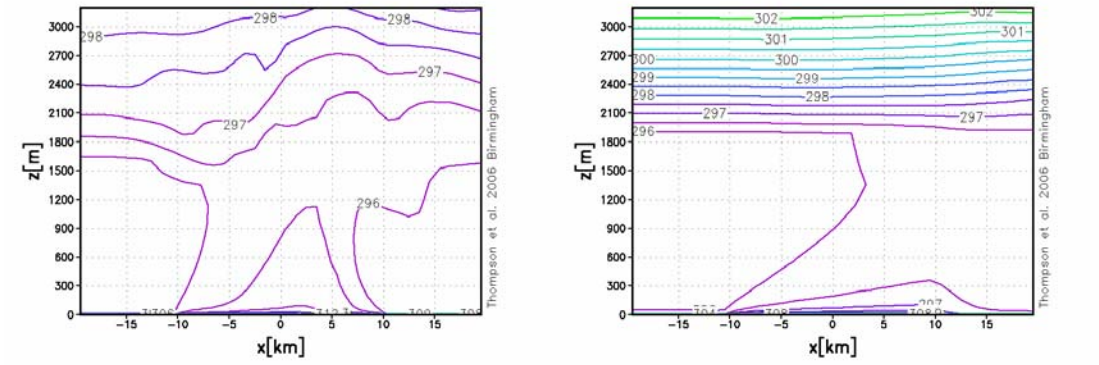


**Figure 4.24: Vertical cross section at y=0 of the potential temperature (K) as computed by the simulation with the low wind speed of 2 ms$^{-1}$ (a), and that with strong wind speed of 8 ms$^{-1}$ (b) at 12:00 noon of the second day of simulation.**

Figure 4.25 shows the vertical section of the TKE for the same two simulations. For the simulation with weakest geostrophic wind there is a strong TKE maximum above the urban area. For the case with strongest geostrophic wind this maximum is both smaller in magnitude, and is significantly displaced downwind of the city. The PBL height is also significantly reduced from around 3,000 m in the case with the weakest wind, to around 2,100 m in the case with the strongest wind.

The PBL height over the city is increased for the simulation with lower wind speed, as is the difference in PBL height over the urban area compared to the rural one. Indeed in the simulation with the strongest wind speed the urban-rural PBL height difference has disappeared. This day time situation is the opposite of what occurs during the night time, when the higher wind speed simulation produces a higher PBL height compared to the simulation with the weaker wind speed (Martilli 2002).

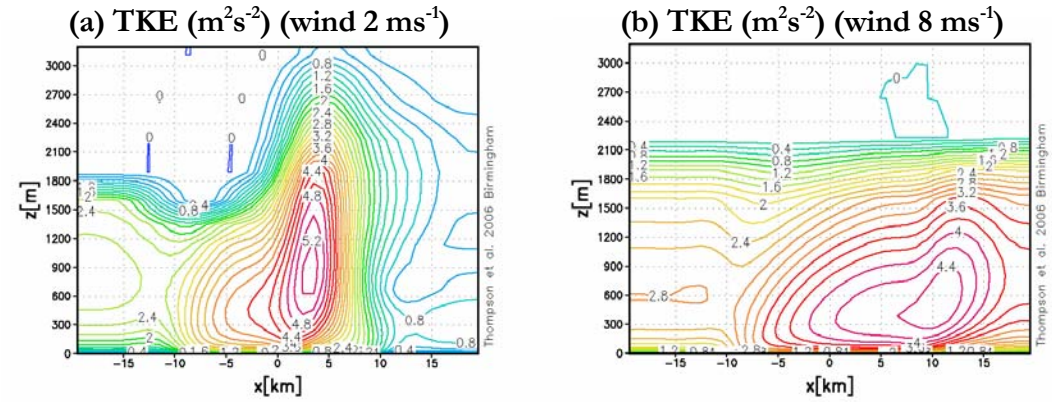


**Figure 4.25: Vertical cross section at y=0 of the TKE ($m^2s^{-2}$) as computed by the simulation with the low wind speed of 2 $ms^{-1}$ (a), and that with strong wind speed of 8 $ms^{-1}$ (b) at 12:00 noon of the second day of simulation.**

## 4.4 Summary

The results presented in Section 4.3 from the implementation of the BEP urban scheme for an idealised domain show that:

- The new modelling system of METRAS+BEP reproduces documented aspects of the air flow over urban areas, such as the circulation patterns over the city, the UHI and the neutral layer above the city, which are better than those produced by the original version of METRAS.

- The results of this implementation are also in excellent qualitative agreement with those presented in Martilli et al. (2002) and in Hamdi (2005), which is an indirect validation of the fact that the scheme has been correctly implemented and the results are correct.

- The results of the implementation are also consistent with a range of field campaigns.

In order to gain a further understanding of how the BEP scheme affects model results under a variety of different conditions, and to further test model results, a sensitivity study was undertaken to examine the robustness of the METRAS+BEP modelling system. The sensitivity study investigated the influence of the city characteristics (e.g. building morphology, albedo and temperature inside the buildings), that of the rural surroundings (in particular the different land cover classes in the METRAS model) and synoptic conditions (e.g. the wind speed) on the local meteorology, UHI and the mesoscale circulation. These

tests also reproduced well documented aspects such as the potential for mitigating urban temperatures by increasing surface albedo and the vegetation fraction, the sensitivity of the model to the building morphology and the influence of the geostrophic wind speed on the mesoscale circulation.

In particular the size of the urban area was found to have an effect on the UHI intensity. Increasing the urban area from 36 $km^2$ to 400 $km^2$ determined an increase of more than 1K in the UHI intensity. This is more than is documented in the literature, but the major contribution of this PhD in this comparison is the implementation of an urban canopy scheme within the mesoscale model METRAS. In Chapter 6 the effect of urban expansion on the UHI intensity will be investigated further for an urban area representing the characteristics of London, rather than an idealised domain.

The fraction of vegetation within each urban grid cell was also found to have a significant effect on the near surface temperature within the urban area, especially during daytime. A 40% increase in the vegetated fraction determined a reduction in the daytime near surface potential temperature of around 1.5 K. The urban land cover and fraction of vegetation within an urban area are crucial factors for determining urban climate (Jonsson 2004). A large number of studies have investigated the sensitivity of the mesoscale atmospheric models to the presence of vegetation in an urban area, and this was found to have a significant impact of simulated near surface temperatures and air quality (Taha 1996, 1997; Civerolo et al. 2000) and the boundary layer structure (Pielke et al. 1998; Seaman 2000). In Chapter 6 and 7 the fraction of vegetation and urban land cover will be varied in order to investigate the impact for the London region.

The mitigating potential of the urban albedo is also examined. It was found that an increase of the albedo of the urban surfaces from 0.20 to 0.30 determined a reduction in daytime near surface temperatures of up to 0.4 K. Small changes in albedo might be used to mitigate daytime urban temperatures and improve comfort levels.

The next step will be the application of the mesoscale model, METRAS+BEP, to a realistic domain representing the city of London. It is important to establish whether the new version of METRAS+BEP model reproduces common features from urban observations and numerical studies, since due to the heterogeneity of the urban surface it is difficult to perform an extensive validation of model results, such as that in Hamdi (2005) without detailed field data. It will then be possible to build on the results of some of the sensitivity tests and analyse the London urban heat island and possible mitigation strategies for urban temperatures, as well as the influence of past and future urbanisation on the urban climate.

# Chapter 5: Evaluation of the urbanised METRAS model for the London region

The model results for an idealised domain have been analyzed in Chapter 4, and sensitivity tests have been performed to investigate how the model responds to the urban area under a variety of different conditions, such as changes to the building morphology and changes to the synoptic conditions.

In this chapter the model was set up for a domain representing the London region, with its current land cover. The aims of the chapter were to evaluate the performance of the model by comparing the results with measurements from London weather stations and discuss the difficulties encountered in model validation and to establish a baseline for current land use for the comparisons in Chapters 6 and 7. Due to the high computational cost of running the model, the runs are performed for single case studies which represent periods for which significant effects of the urban area on the local climate are expected.

The evaluation of the METRAS+BEP model can be compared to the results of other studies in which BEP has been used to represent the urban scheme within a mesoscale model (Martilli 2003; Hamdi et al. 2005; Roulet et al. 2005). In general the implementation of BEP was found to improve model results for all meteorological variables.

## 5.1 Set up of the model for London simulation

The model was set up to study a domain representing the real land cover and topography of London and its immediate surroundings. A domain measuring 70 km x 70 km, with 1 km horizontal resolution was chosen, since this dimension represented a good compromise between the need to have a sufficiently large area surrounding the city centre and computing time. The domain was set up using the US Geographical Survey orography data (see Figure 5.1 overleaf) and the CEH land cover data (see Figure 5.2 overleaf) as described in Chapter 3. The domain was centred on a point with latitude of 51.31 N, and a longitude of 0.0927 W, which represents a central London location. There were 33 vertical levels, with the first level at 10 m above the ground, and a vertical resolution of 20 m in the lowest levels and stretching with a grid increasing factor of 1.175 up to a maximum of 1,348 m resulting in the top of the domain at 11,672 m.

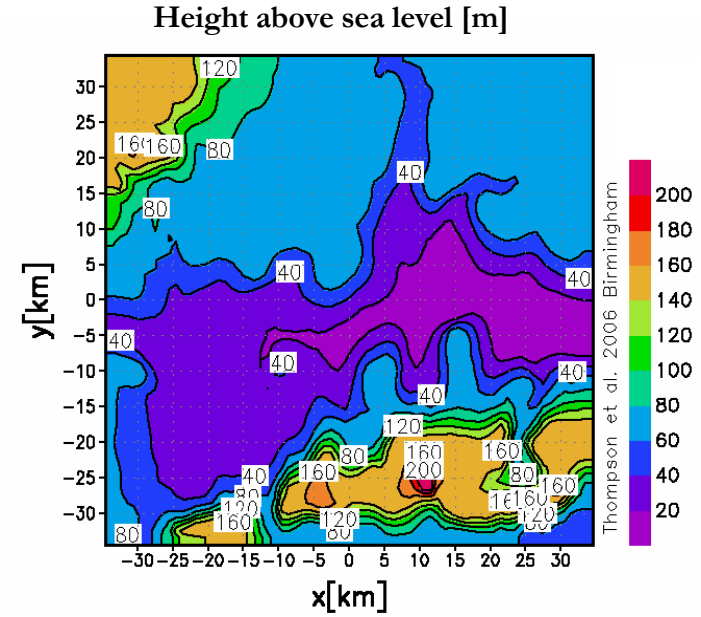


**Figure 5.1: Orography for the domain of the simulations (US Geological Survey).**

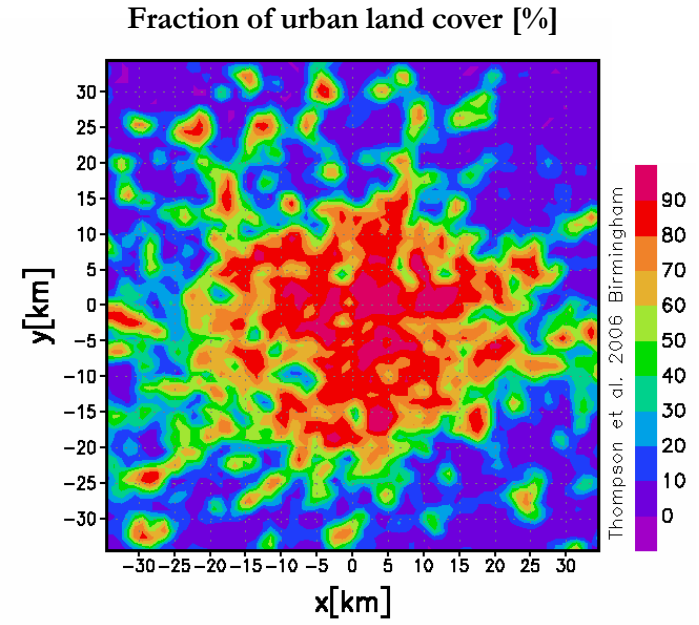


**Figure 5.2: Percentage of urban land use in the domain (taken from the CEH Land Cover 2000 data).**

The simulations were 48-72 hours long, depending on the cases. Periods were chosen with anti-cyclonic meteorological conditions characterised by relatively clear skies and low winds, since these are found to be favourable to the development of a strong UHI (GLA 2006). In particular the heat island is found to be small when cloud cover exceeds 4 oktas, although cloud cover alone cannot be used as a predictor of strong heat island events (GLA 2006). This allows the cloud and rain parameterisation schemes in the METRAS model to be switched off, saving computational time.

In order to select simulation periods characterised by these conditions, the Lamb Weather classification (Hulme et al. 1997) was obtained for each day for the summer (June, July and August - JJA) and winter months (December, January and February - DJF) of years 1995-2000. The Lamb classification is based on surface synoptic charts, which represent the state of the atmospheric circulation close to the ground, and charts at the 500 hPa level. There are three non-directional types, anti-cyclonic (A), cyclonic (C), which are dependent on

whether high or low pressure respectively dominate over the British Isles, and unclassifiable (U). There are also eight directional types which are defined by the general air flow and motion of the synoptic systems embedded in the flow. These can be combined with the non-directional types to categorise more complex circulation systems. Table 5.1 presents a summary of the Lamb classification.

**Table 5.1: Summary of the Lamb classification**

| Number coding | Lamb weather type | Description |
|---|---|---|
| -1 | U | Unclassified (non directional) |
| 0 | A | Anticyclonic (non directional) |
| 1 | ANE | Combined type |
| 2 | AE | |
| 3 | ASE | |
| 4 | AS | |
| 5 | ASW | |
| 6 | AW | |
| 7 | ANW | |
| 8 | AN | |
| | | |
| 11 | NE (North-East) | Directional types |
| 12 | E (East) | |
| 13 | SE (South-East) | |
| 14 | S (South) | |
| 15 | SW (South-West) | |
| 16 | W (West) | |
| 17 | NW (North-West) | |
| 18 | N (North) | |
| | | |
| 20 | C | Cyclonic (non directional) |
| 21 | CNE | Combined type |
| 22 | CE | |
| 23 | CSE | |
| 24 | CS | |
| 25 | CSW | |
| 26 | CW | |
| 27 | CNW | |
| 28 | CN | |

For the summers of 1995-2000 the anti-cyclonic type was the dominant weather type, with the non-directional anti-cyclonic type accounting for 34% of summer (JJA) days in the six years of 1995-2000 (and 41% if the directional anti-cyclonic type is included). When the 10th percentiles of hottest days were considered for the six summers, the non-directional anti-cyclonic type was found to account for 37% of the days (see Figure 5.3).

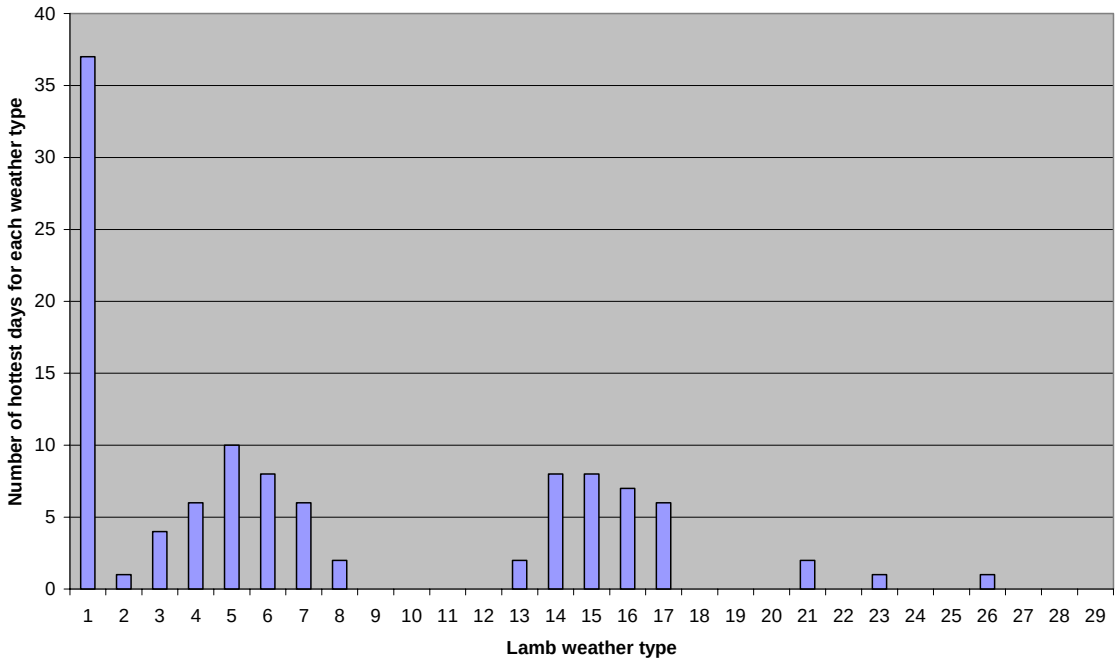


**Figure 5.3: Count of the number of hottest days represented by each weather type. Data was taken for the London Heathrow weather station for the summers 1995-2000, and the 10th percentile hottest days were taken into account in this summary.**

A representative sample of 48-72 hour simulation periods were chosen from the summers of 1995-2000 and are summarised in Table 5.2. The Lamb classification was used to select anti-cyclonic periods. Mean daily temperature, cloud cover and wind speed data from the Met Office MIDAS station at London Heathrow airport (LHR) and the London Weather

Centre (LWC) were used in order to select cases representing both extreme heat events and typical summer conditions.

Since one of the aims of this chapter was to analyse the London urban heat island, some simulations (the 6th-7th August 1998 and 30th-31st July 1999 cases) were performed for periods for which a strong heat island was present and had been referenced in the literature (Best 2005; GLA 2006). For the purposes of selecting the simulations, the heat island was analysed by comparing the central London temperatures from the LWC station with those at the Larkhill station, which is situated sufficiently far from urban land use London so as not to be affected by the city (see Figure 3.6 on page 84). Surface data from this location was also used in the initialization process, together with radiosonde profiles from the UK stations closest to London (Larkhill and Herstmonceux).

**Table 5.2: Selected periods of simulation for the evaluation of METRAS+BEP**

| Simulation period | Description / Weather conditions |
|---|---|
| 28th -30th June 1995 | Non directional anti cyclonic weather type. Low cloud. High average night time temperatures. |
| 18th -20th August 1995 | Non directional anti cyclonic weather type. Low cloud. High average night time temperatures. |
| 15th -16th August 1997 | Anti cyclonic weather type (0/5). High average night time temperatures. Strong UHI. |
| 6th -7th August 1998 | Part of an extended period of strong UHI, clear skies and low winds. Weather type 16/6. |
| 30th -31st July 1999 | Light easterly winds, predominantly clear sky night time conditions. Hotter than average temperatures. Anti cyclonic weather type ¾. |
| 19th -21st July 2000 | Low/few clouds. Non directional anti cyclonic weather type (0). |
| 24th -25th August 2000 | Low cloud. Non directional anti cyclonic weather type (0). |

*5.1.1 Urban parameters*

The methods used to set up the model for the city of London are described in Chapter 3. The urban land use was taken from the CEH Land Cover Map 2000, and the building morphology and thermal parameters characterising the urban area were also described in Chapter 3.

## 5.2 Model evaluation

It was difficult to evaluate the model results due to the lack of detailed field data and the extreme heterogeneity of the urban surface, which cannot be captured by a mesoscale model with 1 km horizontal resolution. Point measurements such as the MIDAS surface stations are influenced by their fetch, which may include high and complicated building structures which are not represented in the mean characteristics in the urban scheme. The surface stations cannot capture the spatial variability within the METRAS grid cells, and ideally a high sampling density of measurements would exist which could be used to calculate spatial averages to evaluate the performance of the model against (Otte et al. 2004). Another way of improving model validation is to run a CFD for a small portion of the urban area and validate it against point measurements; these results once validated could be spatially averaged and used for a comparison with mesoscale model results (Martilli 2007). For this reason the initial focus was on reproducing common features from urban observations for an idealised domain (see Chapter 4).

The diurnal cycle of the air temperature, wind speed and wind direction for the simulations with and without the urban scheme were compared with three MIDAS weather stations within the domain. These were chosen to be the urban station of the London Weather Centre (LWC), the peri-urban station at Heathrow airport (LHR) and the urban park station located at St James' Park (SJP). These are quality-assured UK Met Office sites with hourly observations of air temperature, wind speed and wind direction. In order to evaluate the performance of the model over rural land use, where the implementation of BEP is expected to have little effect, it is necessary to use a rural station which is not influenced by the presence of the city. The station at Wisley, 32 km to the South-West of London, is

commonly used as a rural reference site (Lee 1992; Wilby 2003; Hacker et al. 2007). However, for some of the periods of simulation, hourly weather data was not available for this station and therefore a comparison was made with data from the Bracknell-Beaufort Park station (BBP), which is located outside of the domain.

It is expected that for the rural location the influence of the implementation of the BEP scheme on the meteorological parameters will be small, since the urban fraction is very low. Larger differences are expected for the urban and suburban stations, for which the fractions treated by the BEP scheme are a lot higher.

Specific World Meteorological Organization (WMO) guidelines exist for the siting of measurements for both rural and urban stations. In rural areas temperature and humidity measurements are taken at 2 m, and wind measurements are considered representative if placed 10 m above ground without close obstacles (WMO 1996). Surface energy balance and components are not usually measured at WMO stations. For stations situated in urban areas Piringer et al. (2002) consider it necessary that they be sited so that their data reflect the characteristic meteorological state of the urban terrain zone under consideration, excluding local influences More specific guidelines were published by Oke (WMO 2006). The LWC is an urban station, and it is sited on the roof of a building with measurements taken at an elevation of 43 m (www.badc.nerc.ac.uk). The site has also moved a number of times in the past, for example in 1992 it moved from its old position, where measurements were taken at an elevation of 77 m. At this earlier location wind speed measurements were considered representative of the general air flow above London, rather than influenced by local conditions (Lee 1977). However this is less likely to be the case for the new site

which is considerably lower. The fact the LWC is situated on a roof top means that it can not be considered to meet the UK Met Office guidelines for the location of MIDAS stations or the WMO guidelines published by Oke (WMO 2006), and this might compromise the validity of the measurements. Nevertheless the LWC has in the past been considered representative of the influence of the general urban environment and has been used previously to evaluate model simulations for London (Fragkou et al. 2004).

The SJP station is situated in an urban park, and therefore temperature and humidity measurements could be affected by the vegetated area and be lower than those experienced in surrounding streets (Chandler 1965). It is not possible to capture the urban park character of this measurement site with the METRAS grid, since the closest grid cell to the MIDAS station is highly urbanised (~80% urban fraction) and therefore this will affect the model evaluation for this site.

The Monin-Obukhov similarity theory (MOST) could be used to calculate the temperature at the observation height (2 m) from that at the lowest grid level; however in a rigorous approach MOST is not considered applicable at 2 m for an urban site and therefore it is not used in this PhD study, nor is it used in past validations of urban canopy schemes (Otte et al. 2004; Hamdi 2005; Roulet et al. 2005). The validation also does not consider the effect of differences in elevation across the sites due to the differences within the urban environment of standard lapse rate corrections (Hacker et al. 2007).

The first case study for the evaluation of the model results is the period of the 6$^{th}$-7$^{th}$ August 1998. A second case study representing the period 30$^{th}$-31$^{st}$ July 1999 is also analysed in detail. For both of these case studies two simulations were carried out: the first using the

newly urbanised version of the METRAS+BEP model, and the second using the traditional roughness length approach originally present in METRAS to account for the urban surface. The urban vegetated areas were treated in the same way in both simulations. Having observed the improvements of the newly urbanised version on METRAS relative to the simulations using the traditional approach, both in Chapter 4 and in the evaluation case study here in this chapter, for the remaining meteorological cases detailed in Table 5.2, model simulations were only performed using the newly urbanised version of METRAS.

### *5.2.1 Air temperature evaluation*

London Weather Centre (LWC)

Figure 5.4 shows the comparison for 48 hours ($6^{th}$ – $7^{th}$ August 1998) of the air temperature for the lowest model grid level of the urbanised (METRAS+BEP) simulation and the traditional simulation with measurements from the LWC station. It is reiterated here that the LWC is situated in a highly urbanised grid cell, with an urban fraction of 95%. The model was initialised at 23:00 on the $5^{th}$ August so the first two time steps were ignored in the comparison as they could be affected by model spin up.

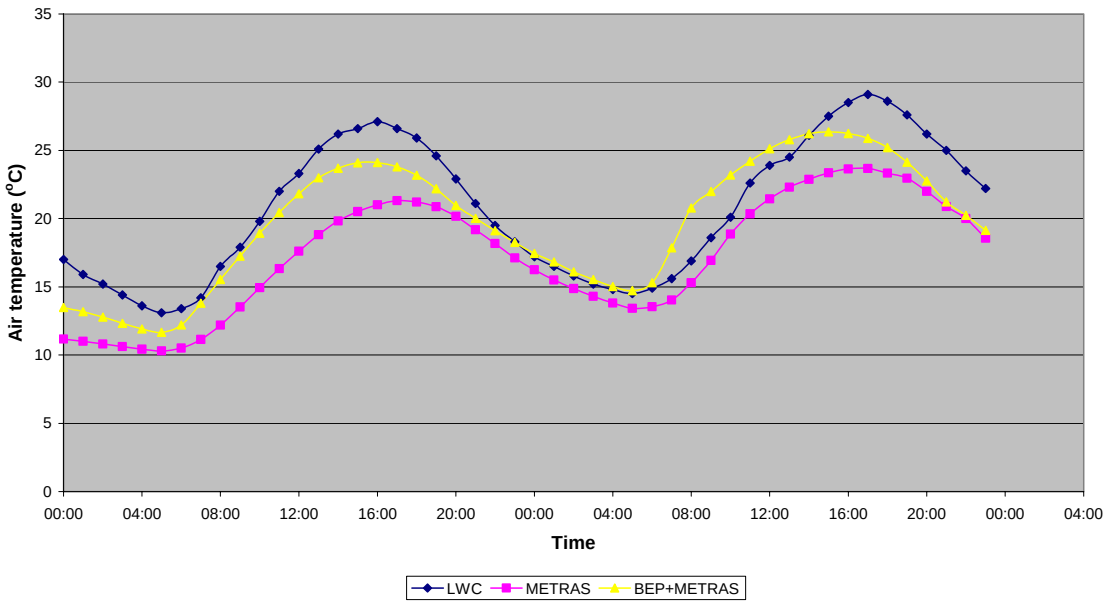


**Figure 5.4: Diurnal cycle of air temperature (ºC) at the LWC site from August 6th to August 7th 1998 according to the measurements at LWC (blue), the METRAS traditional simulation (pink) and the simulation with BEP (yellow).**

The traditional simulation underestimates the maximum daytime temperature by 5.8 ºC, and also underestimates the night time minimum temperature by 1.3 ºC. During daytime the urbanised (METRAS+BEP) simulation shows a better agreement with the measurements, compared to the traditional simulation, but daily maximum temperatures are still underestimated by 3 ºC. This discrepancy may well be due to the fact the LWC measurement is made close to a roof top surface, which is likely to be in direct sunlight and characterised by a different heat capacity and albedo compared to the general city wide characteristics. Therefore in light winds and cloudless skies it is expected to be a much hotter surface during daytime (WMO 2006).

The comparison between the METRAS+BEP simulation and measurements is excellent between the night time hours of 22:00 and 06:00 compared to the traditional simulation due to the fact that during night time the traditional simulation, which does not compute the

radiation trapping in the street canyon, cools more than the BEP simulation. This was also found for the validation of BEP with data from the BUBBLE campaign in Roulet et al. (2005). Trusilova et al. (2008) also found, after implementing an urban canopy scheme into MM5, that the comparison with observations was best during the hours between 21:00 and 06:00.

In the morning hours the METRAS+BEP simulation heats up rather more rapidly than the measurements. This could be due to an increase in cloud cover which occurs at this time (06:00, 7$^{th}$ August), which is seen in the hourly cloud cover data for LWC but is not represented in the model due to the cloud subroutines being turned off.

The comparison for the near surface air temperatures is expected to be improved by the implementation of the BEP scheme, since it takes into account sources of energy in the urban area which the traditional approach neglects, such as the mechanisms of radiation trapping and shadowing in the canyon, and the basic anthropogenic heat treatment.

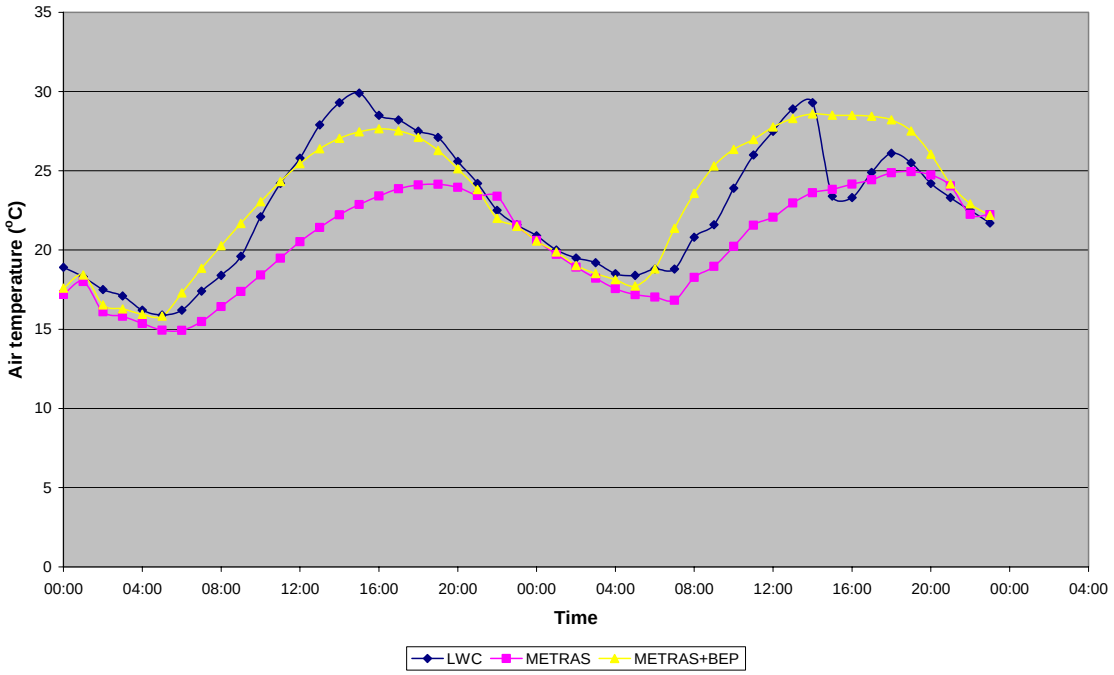


**Figure 5.5: Diurnal cycle of air temperature (°C) at the LWC site from July 30th to July 31st 1999 according to the measurements at LWC (blue), the METRAS traditional simulation (pink) and the simulation with BEP (yellow).**

Figure 5.5 shows the air temperature comparison for the second detailed case study, the period of 30th-31st July 1999. This period was selected because it was used by Best (2005) to test the capability of the UK Met Office operational mesoscale model to reproduce expected urban phenomena. This second case study confirms the improvement in performance of the METRAS+BEP model for a highly urbanised location. The METRAS+BEP simulation shows a better comparison with LWC measurements during both daytime and night time hours. Again a cold bias is found for the day time peak temperature, and the METRAS+BEP model heats up too rapidly on the second day of simulation (31st July 1999). Interestingly for this period of simulation the results for the UK Met Office operational mesoscale model also showed that the air warms too quickly at dawn (Best 2005), giving a warm bias over this period. Neither the METRAS+BEP model, nor the traditional METRAS simulation fully represents the temperature variability during

the second day of simulation (31st July 1999), however this is likely to be due to an increase in cloud cover variability, which is not represented in either simulation.

London Heathrow Airport (LHR)

Figure 5.6 shows the same comparison for air temperature of the two simulations with the LHR station.

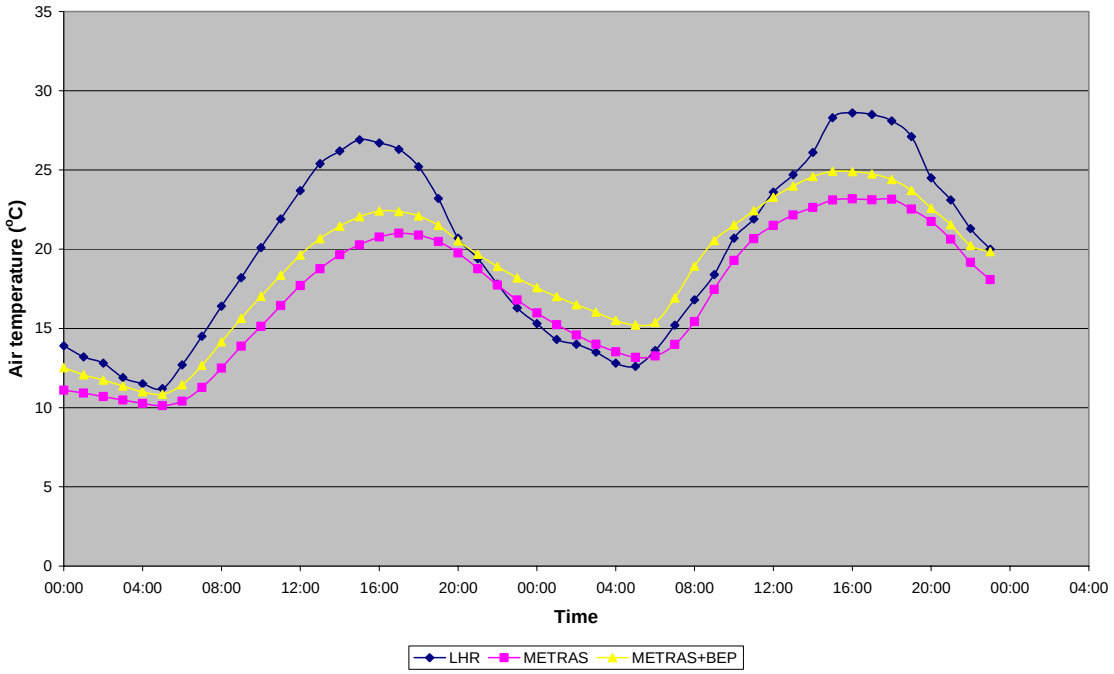


**Figure 5.6: Diurnal cycle of air temperature (ºC) at the LHR site from August 6th to August 7th 1998 according to the measurements at LHR (blue), the traditional simulation (pink) and the simulation with BEP (yellow).**

The LHR station is situated in a suburban model grid cell, with an urban fraction of 56%. The traditional METRAS simulation underestimates the daytime maximum temperature by 5.9 ºC, as well as failing to reproduce the timing of the peak temperature, but shows a good agreement with the measurements during night time. The METRAS+BEP simulation performs better than the traditional one during daytime, although maximum temperatures are still underestimated. During night time the METRAS+BEP simulation overestimates

the minimum temperature by 2.6 ºC. An explanation of the better night time temperature agreement between the measurements and the traditional simulation is that the local characteristics of the airport weather station (an extensive area of open flat concrete and grass with low albedo, and the additional influence of high heat fluxes due to transportation) are better represented by the roughness approach in the original METRAS model, rather than the urban scheme with its vertically distributed impact of the buildings. In this case the LHR surface station would not capture the average characteristics of the whole grid cell, and the comparison would be affected by the local surface characteristics. For the LHR site the METRAS+BEP simulation shows better agreement in terms of the increase in air temperature for the morning of 7$^{th}$ August than the urban LWC station.

Figure 5.7 shows the comparison of the air temperature at LHR for the second case study, the period of 30$^{th}$-31$^{st}$ July 1999. This corroborates the findings for the first case study. Again during daytime the METRAS+BEP simulation performs better than the traditional METRAS simulation, although there is still a cold bias in the peak daytime temperature. The minimum night time temperature is overestimated in both simulations.

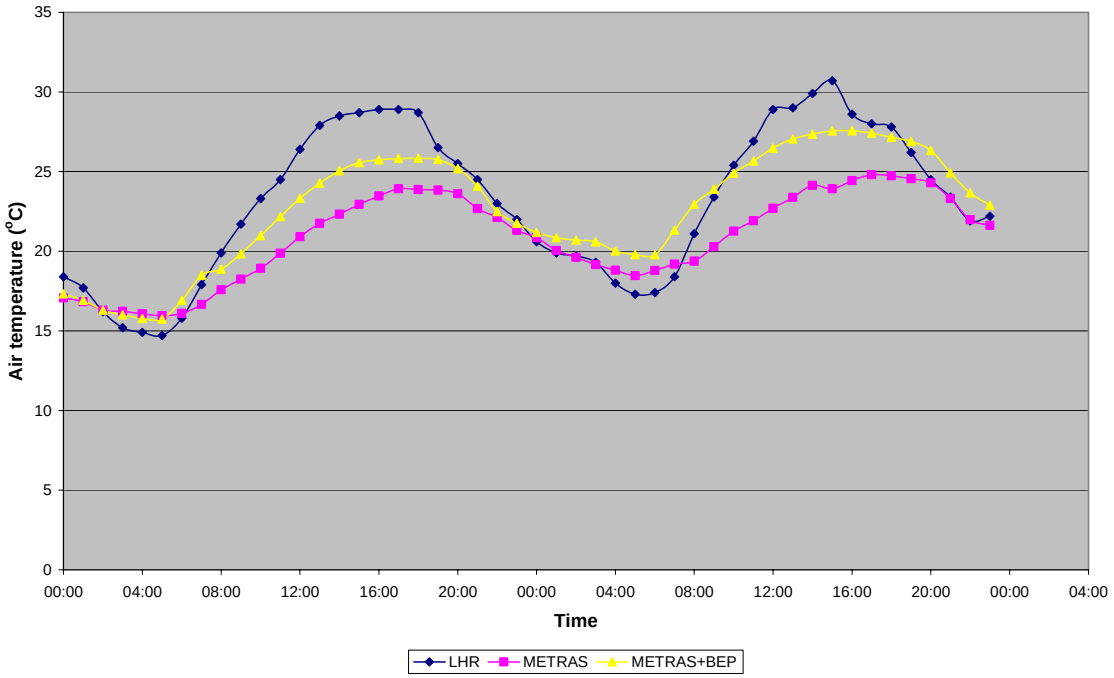


**Figure 5.7: Diurnal cycle of air temperature (°C) at the LHR site from July 30th to July 31st 1999 according to the LHR measurements (blue), the traditional METRAS simulation (pink) and the simulation with BEP (yellow).**

St James' Park (SJP) and Bracknell-Beaufort Park (BBP)

Data at SJP and BBP was only available for comparison for the first case study (6th-7th August 1998). Figure 5.8 shows the air temperature comparison for the SJP urban park site. Again the traditional simulation underestimates daytime maximum temperatures, and fails to capture the timing of the maximum, but represents night time minimum temperatures better than the METRAS+BEP simulation. The METRAS+BEP simulation also underestimates daytime maximum temperatures but does capture the timing of the peak temperature.

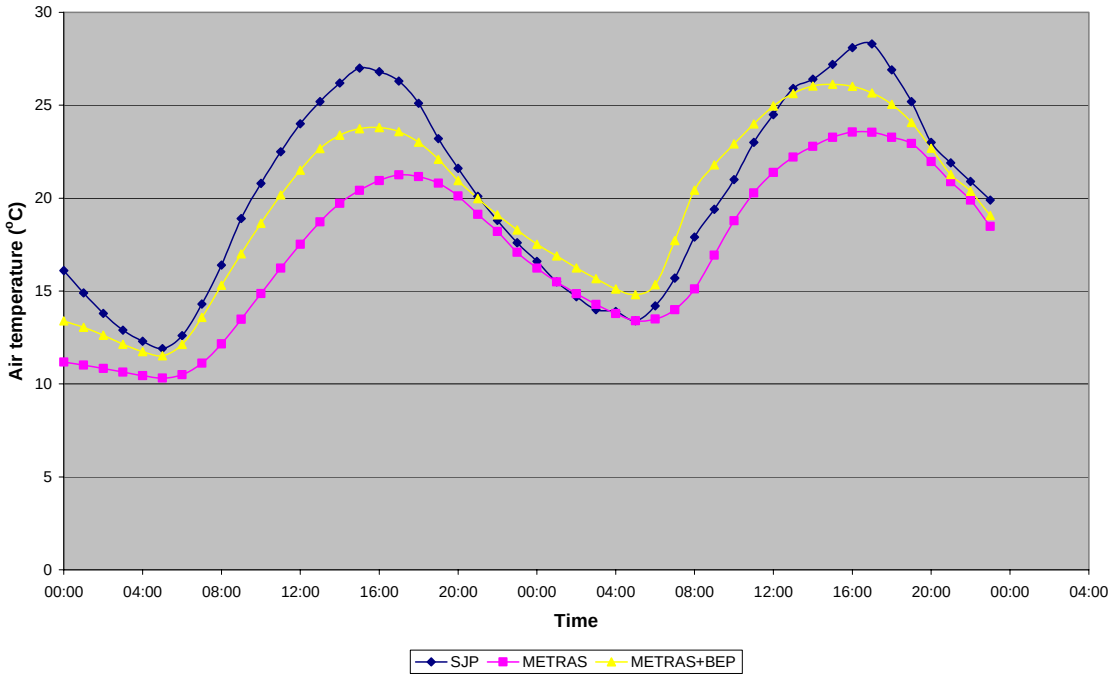


**Figure 5.8: Diurnal cycle of air temperature (°C) at the SJP site from August 6th to August 7th 1998 according to the SJP measurements (blue), the traditional simulation (pink) and the simulation with BEP (yellow).**

Figure 5.9 shows the air temperature comparison for the BBP site. The implementation of the urban canopy scheme should have no direct influence on a completely rural site located upstream of the city (Otte et al. 2004), however as this site is located outside the domain the measurements are compared with the closest grid cell, which has an urban fraction of 20% and is located close to the domain boundary. Differences between the measurements and the model results might also be affected by advection from nearby urban areas. Compared to LWC, LHR and SJP this is the grid cell with lowest urbanised fraction, and for this reason the difference between the traditional and METRAS+BEP air temperatures is much smaller as expected. For both simulations the comparison for the first 6 hours is excellent which probably reflects the fact that out of the four stations used for the validation the BBP station is closest to the Larkhill station whose surface data was used to initialise

the model. The smaller percentage of the urbanised fraction compared to the other locations determines the lack of spread of the results in the initial hours. An overestimation of nocturnal temperatures of up to 2 ºC for rural sites for simulations with and without BEP is also observed by Martilli (2003) for a validation of BEP for the city of Athens.

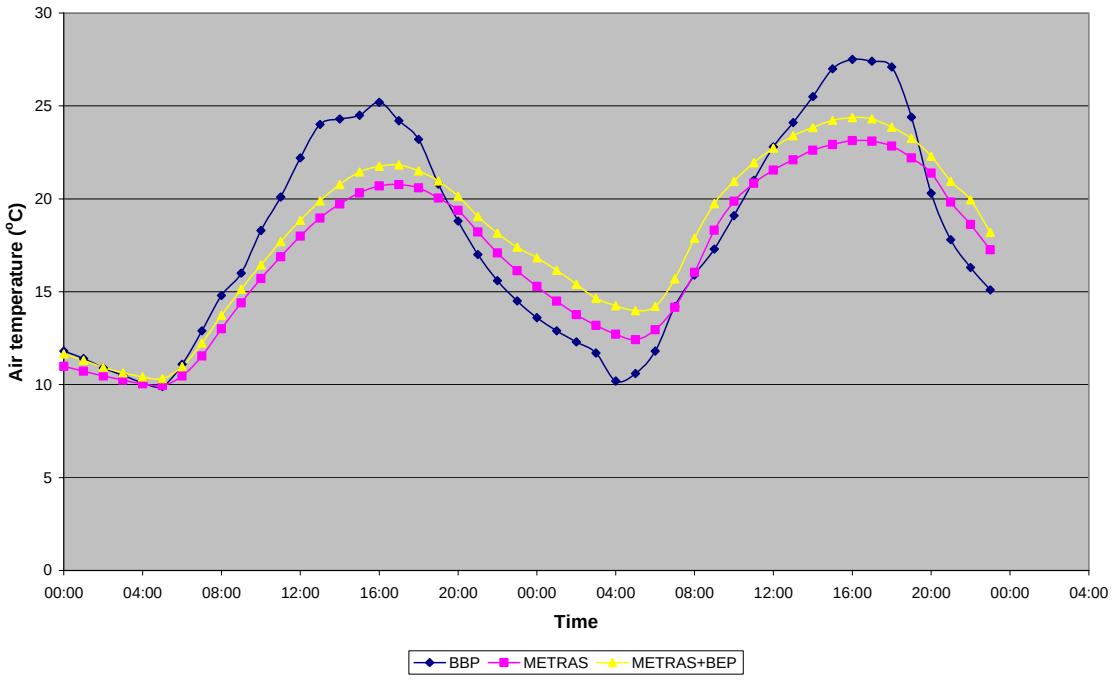


**Figure 5.9: Diurnal cycle of air temperature (ºC) at the BBP site from August 6th to August 7th 1998 according to the BBP measurements (blue), the traditional METRAS simulation (pink) and the simulation with BEP (yellow).**

*5.2.2 Wind speed and direction evaluation*

London Weather Centre (LWC)

Figure 5.10 shows the 10 m wind speed and wind direction comparison for the LWC station with the results of the simulations with and without the urban scheme. Both simulations fail to capture the variability and magnitude of the wind speed; however it is

expected that wind speed will be extremely sensitive to the local scale heterogeneity of roughness elements (Grossman-Clarke et al. 2005). An explanation is that the LWC is situated on the roof of a building, whereas the model output is taken at 10 m which is inside the urban canyon for the METRAS+BEP simulation. When compared to the results for the traditional simulation, the METRAS+BEP simulation represents the deceleration of the wind field caused by the presence of buildings, as also observed in Hamdi (2005) and Roulet et al. (2005). The differences between the two simulations are smaller during daytime. The reason the two simulations produce different results is due to the fact that the traditional simulation only calculates the momentum sink at the ground level by calculating the friction velocity, whereas the BEP simulation computes the dynamical effects of the buildings from ground level up to the highest roof level (Martilli et al. 2002).

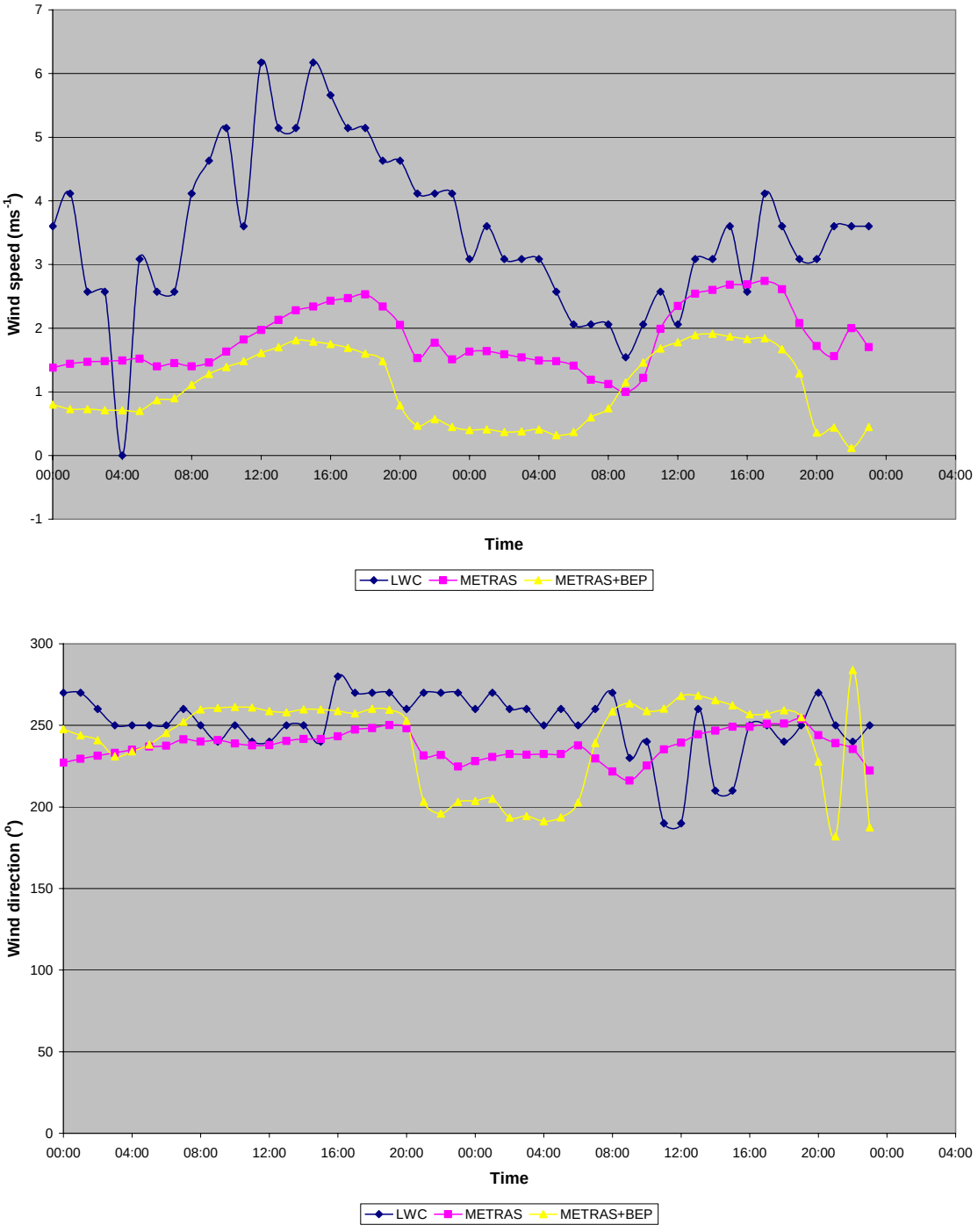


**Figure 5.10: Diurnal cycle of the wind speed ($ms^{-1}$) (the upper panel) and wind direction (the lower panel) at the LWC station from August 6th to August 7th 1998 according to LWC measurements (blue), the traditional METRAS simulation (pink) and the simulation with BEP (yellow).**

It is also interesting to look at the observed and simulated wind direction at 10 m. The variability in the wind direction that is observed in the measurements is very small, especially on the first day of simulation until around 08:00 on the 7th August 1998. The BEP simulation represents a change in wind direction during the night of the 6th –7th August 1998 which is not present in the measurements or in the traditional simulation. A perfect comparison however is not expected, as the model cannot represent the local variability that could affect the measurements at the LWC location.

Figure 5.11 shows the wind speed comparison at LWC for the second case study (30th-31st July 1999). Again both simulations fail to capture the magnitude and variability of the wind speed. This corroborates the results of the first case study, and suggests that the LWC is not a suitably representative site for the measurement of urban wind speeds.

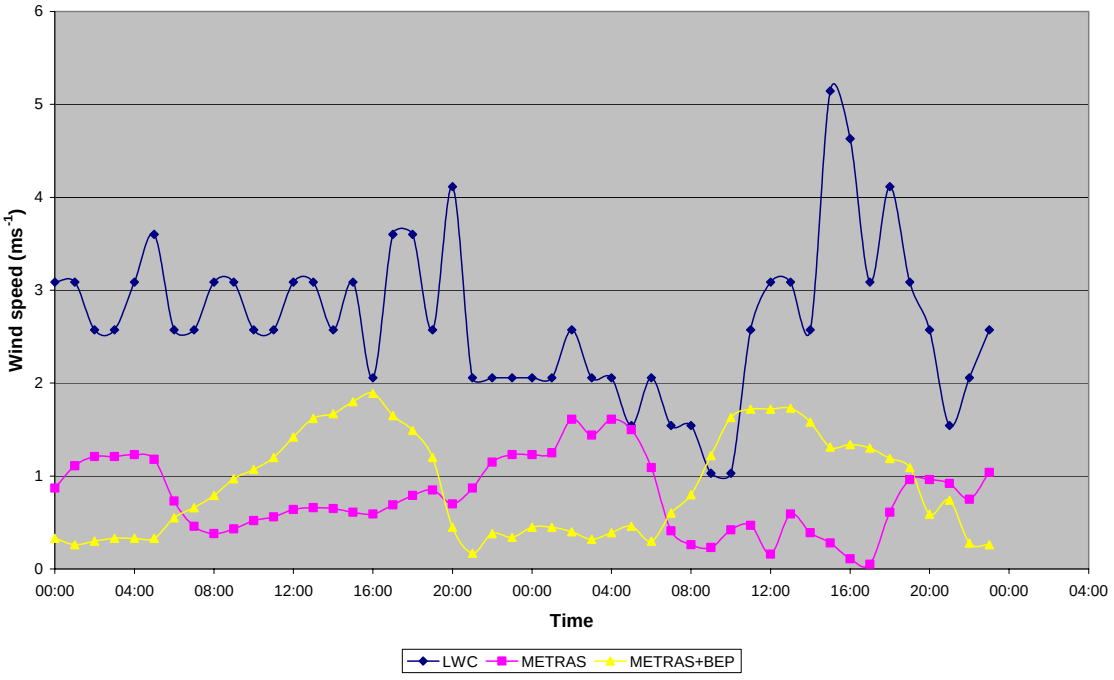


**Figure 5.11: Diurnal cycle of the wind speed ($ms^{-1}$) at the LWC station from 30th to the 31st July 1999 according to LWC measurements (blue), the traditional METRAS simulation (pink) and the simulation with BEP (yellow).**

London Heathrow Airport (LHR)

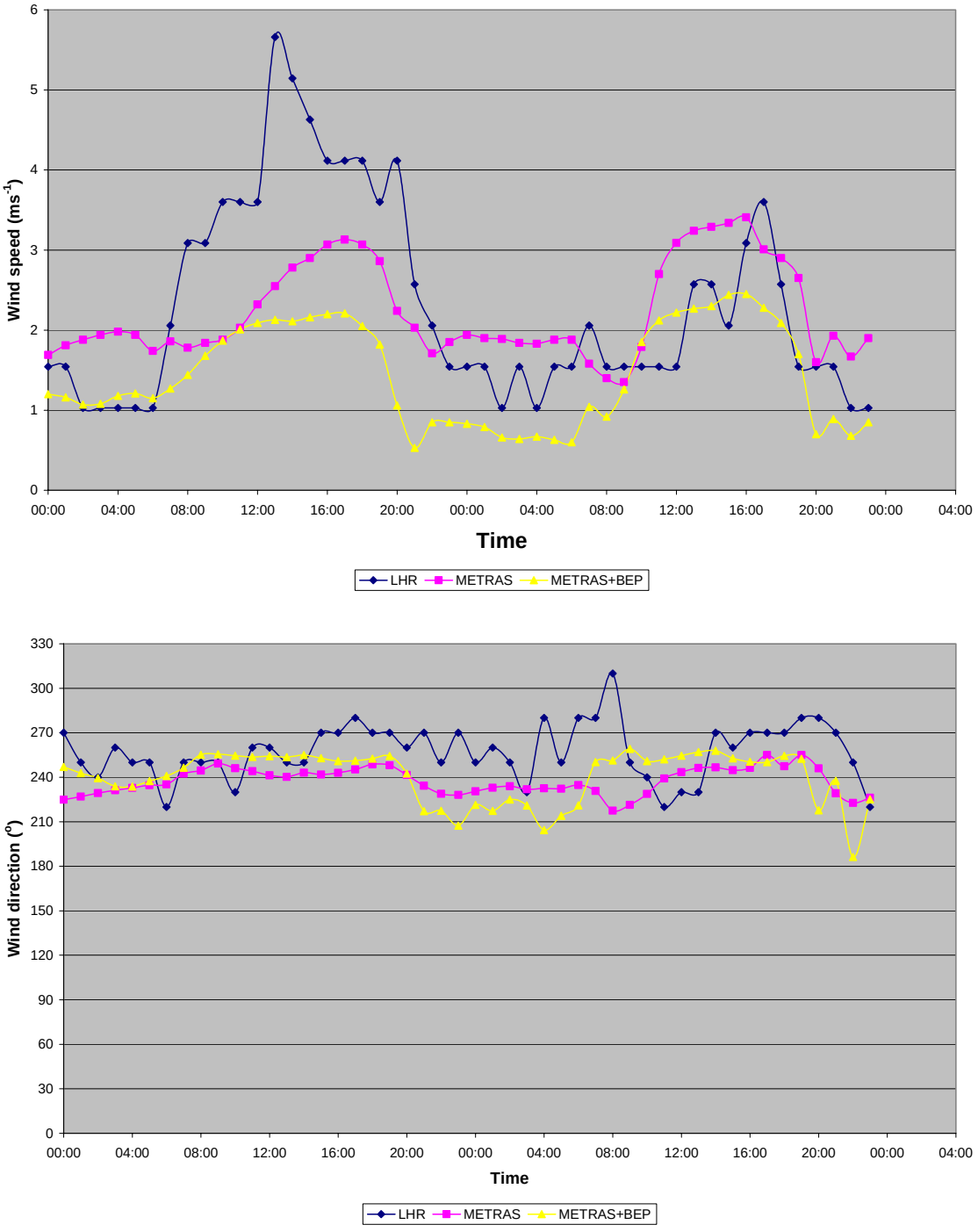


**Figure 5.12: Diurnal cycle of the wind speed ($ms^{-1}$) (the upper panel) and wind direction (the lower panel) at the LHR station from August 6th to August 7th 1998 according to LHR measurements (blue), the traditional METRAS simulation (pink) and the simulation with BEP (yellow).**

Figure 5.12 shows the 10 m wind speed and wind direction for the measurements at the LHR station for both simulations. The METRAS+BEP simulation reproduces the expected deceleration of the flow field caused by the buildings and computes much lower values than the traditional simulation. Neither simulation in Figure 5.12 reproduces the peaks in wind speed that occur in the measurements, although they do reproduce the diurnal trend. The traditional simulation overestimates the night time wind speed as observed by Dupont et al. (2004). The underestimation of the wind speed following the introduction of an urban canopy scheme was also found by Otte et al. (2004). In terms of the wind direction the variability shown in the measurements is very small. The METRAS+BEP simulation shows a change in wind direction during the night of the 6$^{th}$-7$^{th}$ August 1998, although the magnitude of the change is less than that observed for the highly urbanised LWC location. These results are corroborated by the second case study (see Figure 5.13).

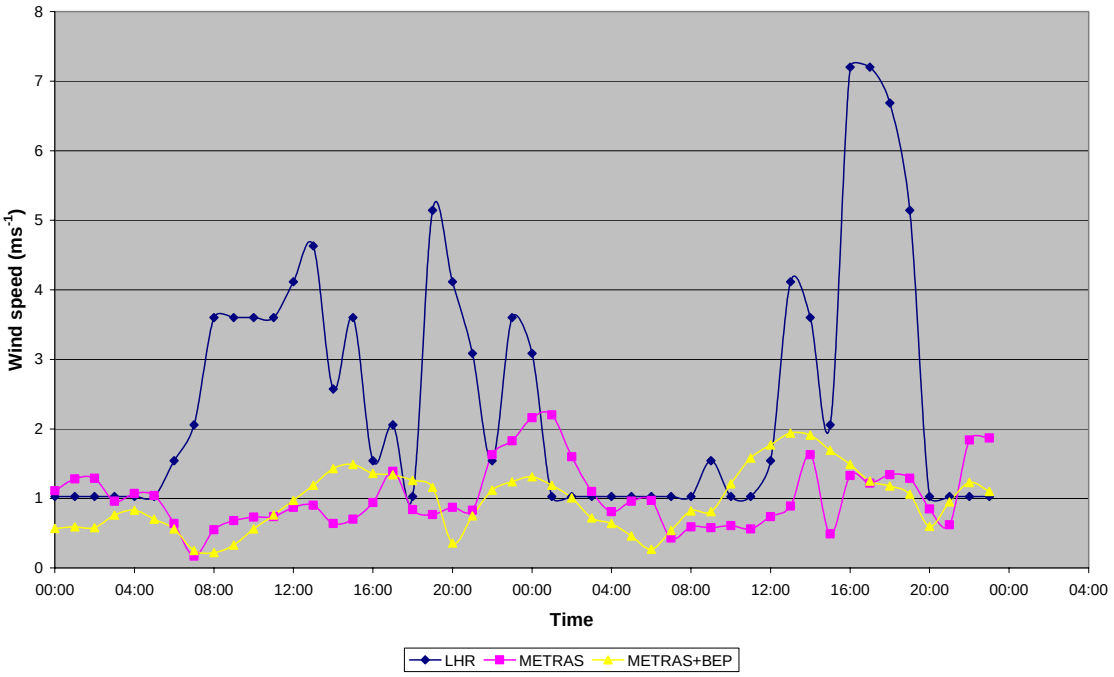


**Figure 5.13: Diurnal cycle of the wind speed (ms$^{-1}$) at the LHR station from 30$^{th}$-31$^{st}$ July 1999 according to LHR measurements (blue), the traditional METRAS simulation (pink) and the simulation with BEP (yellow).**

A full set of hourly wind speed and direction data did not exist for the SJP and BBP stations for this period of simulation.

### *5.2.3 Discussion of other simulation cases*

A detailed discussion has been presented for two evaluation cases, 6th-7th August 1998 and 30th-31st July 1999. A further set of simulations was run, using only the METRAS+BEP model, in order to confirm these results for other case studies. The selected periods were summarised in Table 5.2. All the cases selected were characterised by meteorological conditions considered favourable for the development of UHIs, since the focus of this PhD study was to analyse the effects of the urban surface for meteorological conditions in which these effects are significant. The remaining five case studies showed results which are broadly consistent with those observed for the detailed case studies for the LWC evaluation. Wind speeds remained poorly simulated, and did not fully capture the magnitude of the wind speed at the LWC site. This is not surprising given the reasons identified for the results shown for the detailed cases. The temperature comparison remained better, although some cases underestimated night time temperatures (18th-20th August 1995, 15th-16th August 1997 and 19th-21st July 2000). The comparison with daytime temperatures was however improved for some cases (18th-20th August 1995 and 19th-21st July 2000, and for the 18th-30th June 1995). In general the morning and afternoon comparisons were good, as found for the more detailed cases.

## 5.3 Summary and discussion of the evaluation

To summarise the results of the evaluation of the METRAS+BEP model for London, it is found that there is a cold bias during the daytime for all the air temperature results for the detailed cases; for both the METRAS+BEP model and the METRAS model alone. This affects the comparison for all weather stations and therefore is likely to be caused by a modelling issue rather than the specific local conditions of the stations. The cold bias could be investigated further by refining the simplistic METRAS radiation scheme and analysing the sensitivity to the thermal parameters used to define the METRAS urban land class and the BEP urban materials.

Despite the cold bias the simulation with METRAS+BEP performed better than the traditional simulation. This is due to the treatment of urban radiation sources which are neglected in the traditional simulation. During night time the comparison between METRAS+BEP and the measurements was best for the highly urbanised location (LWC), whereas there is a warm bias for the other locations. This could be due to too much heat storage in the urban area.

Although the additional five case studies only confirmed the difficulties in model evaluation for urban areas, they did prove that the results presented for the more detailed cases were not just specific to those particular dates, but could be replicated for other summertime periods.

It is questionable however whether daytime measurements taken over open spaces exposed to direct sunlight can be used to validate the temperatures computed by an urban canopy scheme, since the model results are aggregated over a heterogeneous area which will

contain both roofs exposed to direct sunlight, as well as shaded and partially shaded canyons and vegetated areas (Trusilova et al. 2008). At night time, in the absence of solar radiation, it is expected that surface temperatures will be distributed more uniformly, and night time measurements taken in stable atmospheric conditions are considered more representative of the urban canopy night time temperature. This would corroborate the fact that a better comparison for the highly urbanised site is found for the night time hours. Roulet et al. (2005) found a good agreement when validating the BEP parameterisation scheme with temperature measurements above roof level for Basel. In this case the observations were taken during the BUBBLE campaign both within the street canyon and near the top of an 18 m tower. These were still point measurements, but many of the specific siting difficulties discussed in this Chapter were avoided as the campaign was designed specifically in part for the validation.

The main problem with the model evaluation is the identification of good observation sites for the comparison. The two sites with the highest urban percentage, LWC and SJP, are not ideal since the first is situated on a rooftop, and the second within an urban park space. Roofs are considered to be poor locations for air temperature, humidity, wind and precipitation measurements unless the instruments are placed on very tall masts (WMO 2006). A station situated within a park is also not representative of urban conditions, since it is in fact monitoring modified rural type conditions (WMO 2006).

The wind speed and direction predictions of the METRAS model, and the METRAS+BEP model are poor. However validating model wind speed predictions against point measurements, and urban point measurements in particular, is not easy due to the

heterogeneity of the surface which cannot be captured in the model. A better comparison could be obtained by using specific urban campaign measurements from masts high above the urban canopy and therefore more representative of average urban conditions.

No observations for London were available at the time of model evaluation in order to validate the components of the turbulent fluxes and surface energy balance. Validating surface temperatures and fluxes at the same time shows the energetic process underlying the thermal estimates are also realistic (Masson et al. 2002), however the heat fluxes over urban areas for the BEP scheme have been extensively validated for two distinct cities in Hamdi (2005) and Roulet et al. (2005) and therefore a further evaluation for the London region was not considered to be essential for this PhD study.

In summary there are significant differences between the modelling results using METRAS+BEP compared to the traditional approach. The comparison with measurements does suggest that the implementation of BEP improved model results for the near surface air temperature over highly urbanised areas, especially during night time. The improvement in the comparison with observations following the implementation of an urban canopy scheme is documented extensively in the literature (Martilli 2003; Otte et al. 2004; Hamdi 2005; Roulet et al. 2005; Sarrat et al. 2006; Trusilova et al. 2008).

# Chapter 6: The effects of urban land cover modifications on near surface temperature and wind speed

The replacement of natural surfaces with roads, buildings and other urban structures alters near surface climate (e.g. Oke 1987; Krayenhoff et al. 2005) through changes in the radiative, aerodynamic and thermodynamic characteristics of the surface.

Many studies exist which analyse temperature records from meteorological observation stations and attempt to define how land cover changes have affected local and regional climate (e.g. Gallo et al. 1996; Kalnay et al. 2006). However there are several limitations in this approach, for example the fact that complete observations do not exist before any urban land cover change took place, the difficulties in finding a representative rural area, especially in regions of complex terrains, and the problem of climate variability in both urban and rural areas. The difficulties in defining 'urban' and 'rural' sites for such observational investigations are described in Stewart (2007). A modelling approach however can overcome some of these limitations. This has been discussed more thoroughly in the literature review in Chapter 2.

Mesoscale models can be used as a tool to investigate urban climate (e.g. Seaman et al. 1989; Taha 1999) since atmospheric processes over urban areas from the regional scale to the local scale are resolved. However it is important that microscale effects, such as those present in the urban canopy layer (see Chapter 2) are parameterised in the mesoscale model. For this reason the urban canopy scheme BEP has been implemented into the

mesoscale model METRAS for this present study. Results from the combined model for an idealised domain have been described in Chapter 4 and the model has been set up and evaluated for a domain representing the London region in Chapter 5.

The pattern of land use change is important for understanding the dynamics of local climate (He et al. 2007). In this chapter a historical approach was taken to investigate how the impact of the urban area of London has varied with time with different forms of historic urban development of the city. A review of the data available to simulate the urban development of London has been presented in Chapter 2. Due to the limitations in the data, some assumptions have been made when constructing the model simulations.

In order to understand the impact of the principle forms of urban development (i.e. density and spatial extent of the city) it was assumed that the building morphology has remained constant. This limitation may be justified in part by an analysis of the ages of the building stock, for example the London Housing survey in 1992 (London Research Centre 1992) found that 64% of dwellings in London pre-date 1945. Apart from infill following WW2 and new developments contiguous to the urban area, then this assumption would appear to be verified.

Due to the high computational cost of the simulations and the computing resources available, the 48 hour model simulations were performed for one specific case, for which a significant impact of the urban area was expected and for which the model results were evaluated in Chapter 5. This approach has been used in previous studies. For example Krayenhoff et al. (2005) used 48 hour simulations for the city of Toronto, Canada to investigate urban design strategies to reduce the UHI and Klaic et al. (2002) used 48 hour

simulations with two hypothetical scenarios of land cover to investigate the modification of local winds due to urbanisation in the Zagreb surroundings.

In this Chapter differences in near surface temperature, UHI intensity and wind speed between different historic states of urbanisation and a hypothetical state where no urban land cover is present were quantified and analysed.

## 6.1 Description of model runs

In order to analyse the effect of the growth of the urban area on urban climate a series of land cover maps were created to represent different states of past urbanisation for London. There are two main ways in which the urban area could have grown through time. The first represents the spatial expansion of the city, the second consists in increasing the proportion of the built up area within a grid cell relative to the area not covered by buildings and pavements. This second method is referred to in this PhD study as densification, since the density of the urban cover within the grid cell increases, even though the building density within the urban class is kept constant.

### *6.1.1 Urban BASE CASE*

The URB_BASE land cover map was taken from the CEH Land Cover Map 2000 data, as described in Chapter 3. The land cover map corresponding to the URB_BASE case is presented in Figure 5.2 on page 135 in Chapter 5.

### *6.1.2 NOURB CASE*

The NOURB land cover map was created in which all the urban areas were removed and replaced by a combination of rural land cover types, in order to represent the land cover prior to any urbanisation. The distribution of the rural land cover at the sub grid scale was created using combinations of the two rural land cover types ('Meadows' and 'Mixed forest'), so that the land cover map represented a realistic rural state, rather than replacing all of the current urban land use with either of these two rural types. This assumes that in the past the city of London was surrounded by fields and woodlands, as documented in Hunt (2005).

### *6.1.3 COMBINED series*

Land cover maps were created from the current base case urban land cover (URB_BASE) in which the urban surface was removed for all points for which the radial distance from the centre of the domain was more than a critical radius. The current extent of London can be roughly represented as an area characterised by a radius of about 45-50 km. It was necessary to balance the availability of computing resources with the necessity of performing enough simulations to represent the realistic growth of the city from a pre-urban state to the current extent. For this reason eight model simulations were performed with the critical radius of the urban area increasing from 5 km to 40 km in steps of 5 km (COMBINED series – see Table 6.1).

In order to simulate a realistic density distribution within the model domain, the urban land cover fraction P($i,j$) within each grid cell was also reduced and multiplied by a factor

dependent on the r(*i,j*), the radial distance from the centre of the domain and a critical radius R (see Equation 6.1).

$$P(i,j)' = P(i,j) * [1 - \frac{r(i,j)}{R}] \quad \textbf{(Equation 6.1)}$$

The reduced proportion of the urban surface was replaced with the 'Meadows' land use type. This makes the assumption that the land around London was primarily used for agriculture. Whilst it has been stated that the land was mainly fields and woodland (Hunt 2005), treating it purely as 'Meadows' simplified setting up the domains as reproducing realistic woodland areas would be difficult without more detailed data. The sensitivity test in Chapter 4 to the rural surroundings did not show a large variation between these two land cover types, so this is a reasonable assumption.

**Table 6.1: Summary of simulations which form the COMBINED series of runs**

| Series name | Simulation name | Description | R (km) |
|---|---|---|---|
| COMBINED SERIES | combr_40 | The urban land cover fraction for all grid cells outside critical radius R (km) is replaced by the meadows land cover type. For the remaining urban grid cells the urban land cover fraction is reduced by (1-r/R), where r is the distance of the grid cell from the centre of the domain and R is the critical radius. | 40 |
| | combr_35 | | 35 |
| | combr_30 | | 30 |
| | combr_25 | | 25 |
| | combr_20 | | 20 |
| | combr_15 | | 15 |
| | combr_10 | | 10 |
| | combr_5 | | 5 |

The domains constructed in the COMBINED series were considered to reflect the realistic form of past urbanisation, and were similar to the land cover maps presented in the

Literature review in Chapter 2. The simulations are compared to the approximate years from Sinclair (1964) in Table 6.2.

**Table 6.2: Comparison of model simulations and the approximate year of urban development**

| Simulation name | R (km) | Approximate year of urban development |
|---|---|---|
| combr_40 | 40 | ~1958 |
| combr_35 | 35 | 1939 - 1958 |
| combr_30 | 30 | ~1939 |
| combr_25 | 25 | ~1914 |
| combr_20 | 20 | ~1880 |
| combr_15 | 15 | ~1850 |
| combr_10 | 10 | ~1800 |
| combr_5 | 5 | pre 1800 |

The METRAS model resolves sub grid scale land cover. Therefore in setting up these domains an assumption has to be made about the density distribution within the urban area, in order to represent that fact that it was considered likely that in the expansion of the city area, the density of the suburban areas had increased through time due to infill.

### *6.1.4 RADIUS SERIES and DENSITY SERIES*

In order to isolate whether any changes in the near surface temperature were due to the changes in the urban land cover density within the grid cells, or in the radial size of the city, a series of numerical runs were conducted changing one variable at a time, for example by either removing the urban surface from all points for which the radial distance from the

centre of the domain was more than a critical radius (RADIUS series), or by reducing the urban land cover density within each grid cell across the whole domain (DENSITY series).

The RADIUS series consisted of eight simulations (see Table 6.3) with the same critical radii as the COMBINED series, but the percentage of urban land cover in the grid cells within the critical radius was kept at the existing (URB_BASE) level.

**Table 6.3: Summary of simulations which form the RADIUS series of model runs**

| Series name | Simulation name | Description | R (km) |
|---|---|---|---|
| RADIUS SERIES | urb_rad_40 | The urban land cover fraction of all grid cells outside critical radius R (km) are replaced by the meadows land cover type (see R column to the right for values of the Critical Radius). For the remaining urban grid cells the urban land cover fraction is unchanged (same as that for URB_BASE case). | 40 |
| | urb_rad_35 | | 35 |
| | urb_rad_30 | | 30 |
| | urb_rad_25 | | 25 |
| | urb_rad_20 | | 20 |
| | urb_rad_15 | | 15 |
| | urb_rad_10 | | 10 |
| | urb_rad_5 | | 5 |

The DENSITY series consisted of seven simulations (see Table 6.4), for which the urban land cover fraction within all the urbanised grid cells was reduced by a factor varying from 90% to 30%. The size and spatial extent of the urban area remained that of the URB_BASE case. This series represented an investigation into the effect of vegetation within the urban area, since the urban land cover fraction was progressively replaced by green vegetated areas. The presence of vegetation within an urban area has been shown to have a crucial influence on climate (Jonsson 2004).

**Table 6.4: Summary of simulations which form the DENSITY series of model runs**

| Series name | Simulation name | Description | Density factor |
|---|---|---|---|
| DENSITY SERIES | urban90% | For all grid cells the urban land cover fraction is reduced by multiplying it with the density factor (see column to the right for the density factor for each run). | 0.9 |
| | urban80% | | 0.8 |
| | urban70% | | 0.7 |
| | urban60% | | 0.6 |
| | urban50% | | 0.5 |
| | urban40% | | 0.4 |
| | urban30% | | 0.3 |

*6.1.5 Model configuration for the scenarios*

In order to better isolate the effects of the land cover change all model runs were performed with the same model configuration, initial conditions and boundary conditions. As discussed all urban characteristics such as building heights, street widths, surface albedo and emissivity were kept constant. The meteorological conditions used for the series of runs were those for a case study ($6^{th}$-$7^{th}$ August 1998) for which the combined METRAS+BEP model performance was evaluated in Chapter 5. These were summertime anti-cyclonic conditions and part of an extended period of strong UHI conditions, clear skies and low winds.

## 6.2 Effects of the current state of urban land cover on near surface temperature and wind speed

Results are presented in order to understand the effect of the current state of urban land use (as represented by the URB_BASE domain) compared to a domain entirely covered by rural land use (NOURB) on the near surface potential temperature and wind speed.

### *6.2.1 Spatially averaged near surface potential temperature*

It has been observed that the transformation of vegetated land to urban land results in significant differences in near surface temperature (Trusilova 2006). The temperature difference between the urban centre and the rural surroundings is expected to be most significant during night-time (Oke 1982; Karl et al. 1988; Gallo et al. 1996; Kalnay et al. 2003), due to the faster cooling rate of the rural area compared to the urban area. The results of the simulations were analysed at 04:00, since for the city of London it was found that the temperature difference between the rural domain and the urbanised domain is significant at this time. The results were also analysed at 12:00 noon, in order to understand the effect of the land cover conversion during daytime. The second day of simulation was analysed throughout this Chapter to avoid any effect due to model spin-up.

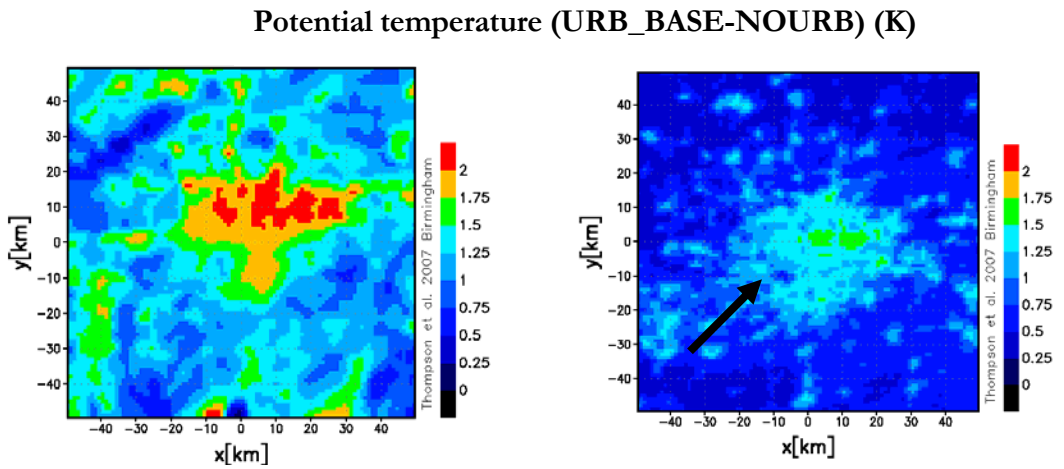


**Figure 6.1: Potential temperature difference (K) between the base case of current urbanised land use (URB_BASE) and a rural case (NOURB) at z = 10 m at 04:00 (left) and 12:00 (right) of the second day of simulation.**

Figure 6.1 shows the potential temperature difference between the urbanised and the rural domains at 04:00 and 12:00 for the entire domain at 10 m, on the second day of simulation. As expected the largest potential temperature differences are observed at night time, whereas at noon the difference between the urbanised domain and the rural one is a lot less intense.

These results can be explained in terms of the urban surface energy balance equation discussed in the literature review in Chapter 2. At noon the incoming solar radiation is stored more efficiently in the urban area when compared with the surrounding rural area (Oke 1982). This is due to the increased thermal heat capacity and differences in albedo of the urban building materials. By contrast, at night the urban surface releases the stored heat and hence is characterised by a reduced rate of cooling. Anthropogenic heat sources might also be expected to be greater during the night in urban areas, although this will be seasonally dependent and affected by increased use of air conditioning during daytime.

During daytime the shape of the area of greatest temperature difference matches that of the urban area very well. In both figures it is possible to distinguish an area of localised cooling representing Richmond Park (see arrow in Figure 6.1), which is a large area in London dominated by rural land use and parkland. This area is visible due to the fact that the park cools more rapidly than the surrounding built up area due to the increased latent heat flux term in the surface energy balance equation and consequent reduced storage (Oke 1989; Upmanis et al. 1998; Dimoudi et al. 2003; Jonsson 2004). These results corroborate those presented in the Greater London Authority report on the London Urban Heat Island (GLA 2006), where differences of up to 1 K are found between Richmond Park and its surroundings. Richmond Park is located upwind of the main urban area, and is the largest park in London, covering 2,469 acres (Chandler 1965). The nearby Wimbledon and Putney Common covers 1,178 acres. By comparison none of the other parks in the urban area cover more than 500 acres. The combination of the size of the park and the upwind location explains why this park is visible in Figure 6.1 whilst smaller parks within the urban area or downwind of it are not.

During night time the shape of the area of greatest temperature difference is slightly shifted compared to the extent of the urban area. This will be further analysed later when calculating the regional impact of the temperature change in Section 6.3.5.

The mean near surface (taken at z = 10 m, i.e. the first grid level) potential temperature for each grid cell (with a horizontal resolution of 1 km) was spatially averaged across the whole domain for both the urbanised and non urbanised model runs. It is found that the increase in near surface potential temperature, spatially averaged across the whole domain,

at 04:00 is (1.29 ± 0.33) K, and at 12:00 it is (0.75 ± 0.29) K. The conversion of rural land cover to urban land cover has caused an increase in the spatially averaged near surface potential temperature across the domain, both during daytime and night time. During night time 82% of the grid cells show a change greater than 1 K with respect to the rural domain, compared with 20% during daytime. These increases can be compared to results for other numerical studies, for example Lee et al. (2008) found an increase of 1.5 K for the rapid urbanisation over 40 years of the Daegu region in Korea, Wang et al. (2007) also found increases for the 2-d averaged temperature of 1.5 K during night time and 0.8 K during daytime due to urbanisation in the Pearl Delta region on China, and Lamptey et al. (2005) found an increase of more than 1 K over urban sites due to urbanisation in the North-Eastern US.

*6.2.2 Diurnal temperature range (DTR)*

Diurnal temperature range is a meteorological indicator which can be associated with climate change and urbanisation (Easterling et al. 1997; Kalnay et al. 2003). Gallo et al. (1996) found that changes in the predominant land use or land cover conditions could significantly affect the climatological DTR.

The DTR was calculated for each grid cell (*i,j*) in the domain by subtracting the minimum diurnal temperature ($T_{min\_diurnal}$) from the maximum diurnal temperature ($T_{max\_diurnal}$), as described in Equation 6.2.

$$DTR(i,j) = T_{max\_diurnal}(i,j) - T_{min\_diurnal}(i,j) \quad \textbf{(Equation 6.2)}$$

The calculation was performed for the base case with current urban land cover (URB_BASE) and the case with no urban surface (NOURB) for the second day of simulation. The difference in the DTR due to the urban effect was calculated by subtracting the DTR for the urbanised run from that of the rural run for each grid cell.

A reduction in the DTR due to the urban area was observed across the entire domain, with an average of (-0.74 ± 0.31) K. The reduction in the DTR is due to changes in both the maximum and minimum diurnal temperatures. In particular an increase in the minimum diurnal temperature was observed across the entire domain, with an average increase of (1.31 ± 0.30) K. The difference in the maximum diurnal temperature showed a smaller variation, with an average increase of (0.57 ± 0.19) K.

The main reason for the increase in the minimum diurnal temperature is the increased heat capacity which leads to increased storage during daytime, which leads to increased release of heat at night time. Other reasons could include the lower albedo of urban surface (where applicable – this might not always be the case, and could be offset by greater reflectivity between buildings), which causes greater energy absorption during the day; less surface water which prevents evaporative cooling; lower latent heat compared to rural areas during the night and higher night time sensible heat fluxes due to anthropogenic heat sources. All these are known to contribute to raising minimum night time temperatures, and to the UHI phenomenon.

The increase in the maximum diurnal temperature in the urban area is primarily due to the effect of the building geometry on the radiation terms of the surface energy balance

equation (Harman et al. 2004). For example it is necessary to consider the importance of the partial shading of urban surfaces due to buildings and the reduced sky view factor.

These values for the increase in maximum and minimum diurnal temperature are broadly consistent with those reported numerical studies. For example Trusilova et al. (2008) found that the DTR was strongly affected by the presence of the urban area and that land use modification resulted in a reduction of the DTR over the total domain representing Western Europe both in summertime and in wintertime, with the largest differences found in areas of urban land cover. The reduction in DTR is also broadly consistent with the investigations of Lamptey et al. (2005) for the North-Eastern United States.

The reduction in DTR due to urbanisation is also widely corroborated by measurements. For example, Gallo et al. (1996) analysed data from weather observation stations from the US Historical Climatology Network and found that a change in the predominant land use class from rural to urban could result in a decrease in the DTR. Kan et al. (2007) observed that 'in most urban regions of the world, DTR has been decreasing because nocturnal minimum temperatures have risen faster than daytime maximum temperatures'. However in some regions such as India, Russia and Northern China an increase has been observed (Kan et al. 2007).

### *6.2.3 Diurnal cycle of the urban heat island intensity*

This section looks at the diurnal cycle and the UHI intensity. For the current urban land cover situation (URB_BASE) the UHI was calculated relative to the rural case (NOURB) and compared with results in the literature for current London. This method was chosen

because finding a rural reference point which was not affected by the urban area in the URB_BASE case was not reliable.

The UHI effect is one of the most rigorously researched examples of human induced climate modification (e.g. Oke 1982). The intensity of the UHI can be assessed in a variety of ways, which include trends in urban measurements at a single station (e.g. Jones et al. 1990; Philandras et al. 1999), the measurement of the urban-rural temperature difference (e.g. Karl et al. 1988; Karaca et al. 1995), transects across an urban area (e.g. Klysik et al. 1999; Unger et al. 2001) and measurements using satellite observations (Roth et al. 1984; Lee 1988). All these methods rely on the availability of adequate meteorological data, and carry certain limitations (Lowry 1977). A further method consists of using an appropriate numerical model to estimate changes in UHI intensity due to land cover changes (e.g. Lamptey et al. 2005; Trusilova 2006; Velazquez-Lozada et al. 2006). A more complete discussion of the UHI is contained within the literature review in Chapter 2.

Figure 6.2 shows the diurnal cycle of the maximum UHI intensity for the domain representing the current state of urban land cover (URB_BASE). The UHI intensity here is defined as:

$$UHI\_intensity = \max_{i,j}\left\{T_{URB\_BASE}(i,j) - T_{NOURB}(i,j)\right\} \qquad \textbf{(Equation 6.3)}$$

This definition has the advantage that the UHI intensity represents a global characteristic of UHI over the whole domain. As shown in Figure 6.2 the UHI intensity is most pronounced during night time, reaching peak values between midnight and 07:00. The intensity decreases after sunrise, reaching a minimum values in the early morning (around 9:00). The

daytime UHI intensity reaches a peak at around 13:00, and then cools reaching a minimum after sunset. After 19:00 the UHI intensity increases.

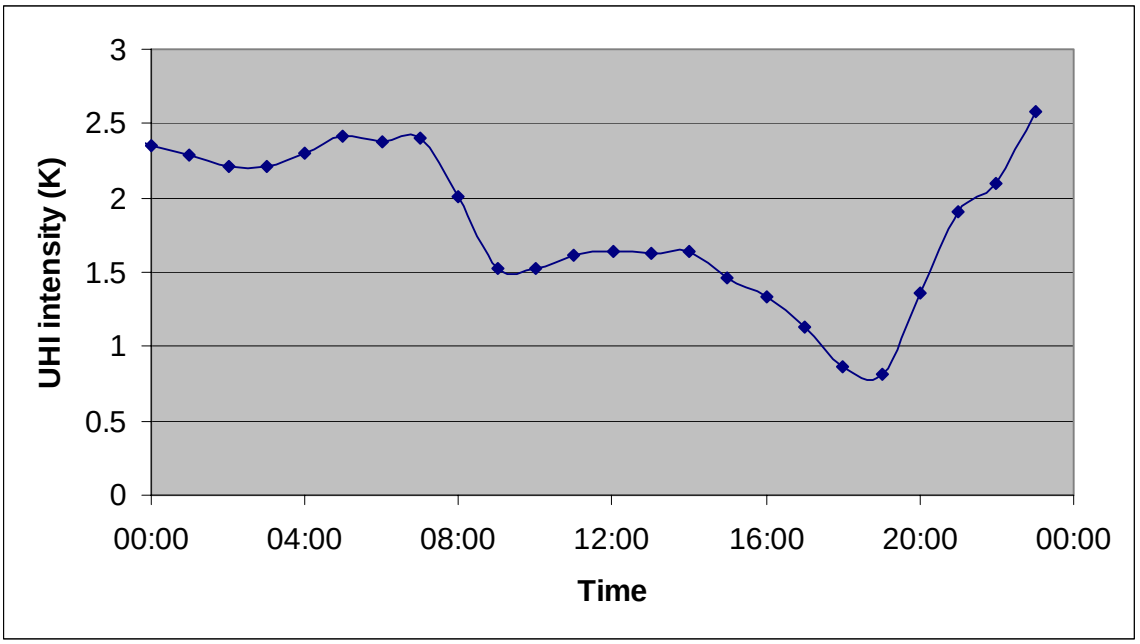


**Figure 6.2: Diurnal cycle of the maximum UHI intensity (K) for the second day of simulation for the URB_BASE case. The UHI intensity is calculated for the current urban land cover case with respect to the rural domain (NOURB).**

The London UHI has been researched since Luke Howard's first contribution in 'The Climate of London' in 1818 (Howard 1833). As reviewed in Chapter 2, recently several studies have investigated the London UHI, and in particular the diurnal cycle and trends in UHI intensity (e.g. Lee 1992; Wilby 2003). A recent report by the Greater London Authority (GLA 2006) analysed the diurnal variation of the Heathrow UHI under ideal conditions (low cloud cover and low wind speeds). The UHI intensity was found to be nearly constant during the day, with a mean of 1 °C. After sunset the UHI intensity rose to reach a maximum, and then decreased following sunrise. The UHI magnitude was also found to vary across London with Richmond Park standing out as a cool spot compared to its surroundings (GLA 2006), highest intensities in the areas classified as continuous urban

development (GLA 2006) and differences in daytime and night time temperatures observed between the measurement sites of Heathrow, London Weather Centre and Kew Gardens (Hacker 2007). These findings are consistent with the some of the results obtained in this PhD modelling study, as can be observed in Figure 6.1, for example the cool spot of Richmond Park and the variation in magnitude of the UHI in the urban area.

The results in Figure 6.2 are broadly consistent with those reported in Wilby (2003) for a central urban location (Westminster) in the city of London as seen in Figure 6.3. Wilby (2003) plotted the diurnal cycle of the UHI for four urban locations with respect to the rural station at Bracknell. For the central urban location of Westminster the heat island is primarily a nocturnal phenomenon, reaching a peak just before 07:00, and the decreasing to reach a minimum at 11:00. The UHI intensity increases directly after sunset. The Westminster location will be most comparable to the results for the maximum UHI intensity in Figure 6.2, since it represents the most highly urbanised of the four locations. The difference is magnitude could be due to the difference in methodology between experimental measurements and numerical modelling. The results presented in Wilby (2003) were taken from six particular days in July and August 1999/2000 whereas the scenario in this PhD study represents one particular case in August 1998. Whilst this case study was selected due to being characterised by anti-cyclonic conditions favourable to UHI development, it was not necessarily a particularly strong case. The UHI intensities presented in Graves et al. (2001), showing a mean intensity between 2 and 3 ºC, are more consistent with the numerical modelling in this chapter.

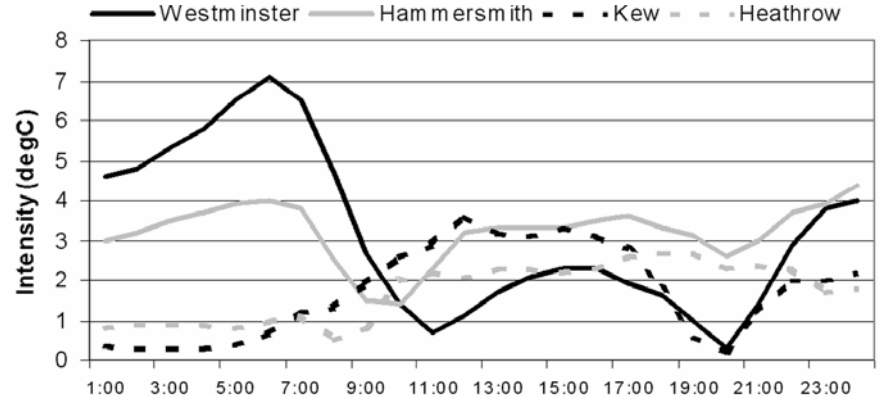


**Figure 6.3: Diurnal variation of the London UHI with respect to Bracknell for six days in July and August 1999/2000. Taken from Wilby (2003).**

It is interesting to note that both the results of this PhD study and Wilby (2003) find the maximum UHI intensity around dawn. This is later than some other studies (e.g. Oke et al. 1975), however the consistency of the modelling with measurement results specific to the city of London suggests this is a real result, rather than an error associated with either the measurement choice or the type of model used in this study. In fact Oleson et al. (2008) discussed the effect of local conditions on the timing of the maximum UHI intensity. It is found that, whilst Oke et al. (1975) found the maximum intensity to occur 3-5 hours after sunset, other studies such as Jauregui (1997) found the intensity to increase throughout the night, reaching a peak just before sunrise, whereas Fortuniak et al. (2005) found the intensity increased until midnight and then remained roughly constant until dawn. Troude et al. (2002) also observed a steady increase in the UHI intensity until about 06:00-07:00 for the city of Paris, with a peak intensity of about 2.5 K. The timing of the maximum heat island intensity depends on the relative cooling rates of the urban and rural surfaces.

*6.2.4 Wind speed and direction*

Klaic et al. (2002) investigated the modification of local winds due to hypothetical urbanisation of the Zagreb surroundings. There are three important aspects in which the present work differs from that of Klaic et al. The first is that this PhD study uses a mesoscale model coupled with the sophisticated urban canopy scheme BEP, whereas Klaic et al. adopted a simplistic approach for modelling the urban surface based on the Monin-Obukhov similarity theory; the second is that METRAS model resolves sub grid scale urban land use whereas Klaic et al. did not; and the third is that Klaic et al. (2002) considered only two future scenarios of urban expansion and did not run their mesoscale model for a non urbanised state, whereas in this PhD a series of states of past and future urbanisation were considered.

Figure 6.4 shows the difference in the horizontal wind speed at 10 m between the urbanised domain (URB_BASE) and the rural domain (NOURB) during night time (04:00) and during daytime (12:00 noon). It is apparent that for both times the horizontal wind speed is reduced over the urbanised area. This reduction is greater during the daytime, and covers a larger area. Such a reduction in wind speed has been documented for the city of London by Bilham (1938) and Wilby (2003).

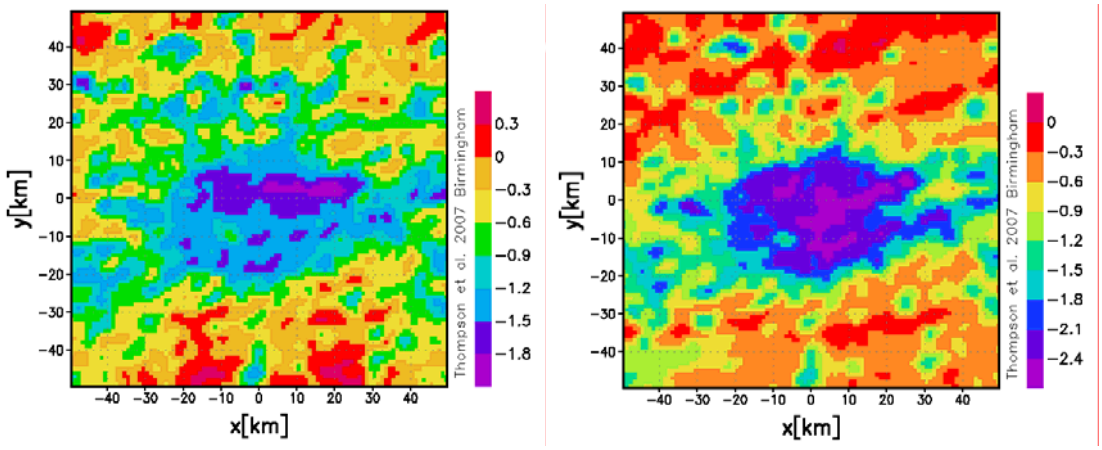


**Figure 6.4: Horizontal wind speed difference ($ms^{-1}$) between the base case of current urbanised land cover (URB_BASE) and rural domain (NOURB) at z = 10 m at 04:00 (left) and 12:00 noon (right) of the second day of simulation.**

The mean wind speed was spatially averaged across the whole domain for the urbanised and rural model runs. The domain averaged change in the mean wind speed is (-0.66 ± 0.49) $ms^{-1}$ at 04:00, and (-0.93 ± 0.64) $ms^{-1}$ at 12:00. At 04:00 56% of the model grid cells are affected by a reduction in mean speed of more than 0.5 $ms^{-1}$, compared to 65% at noon. The maximum reduction is wind speed in the domain is 2.03 $ms^{-1}$ at 04:00, compared to 2.6 $ms^{-1}$ at noon. The largest differences in wind speed were found over the urbanised cells, and in their vicinity, corroborating results in Klaic et al. (2002).

Figure 6.5 shows the wind speed and direction vectors at z = 10 m for the URB_BASE simulation and the NOURB simulation. For the NOURB case no deflection in the wind vectors is observed, whereas in the URB_BASE case there is a small deflection as the flow bends around the urban area (Britter and Hanna 2003). As found in Klaic et al. (2002), urbanisation does not have a significant effect on wind direction.

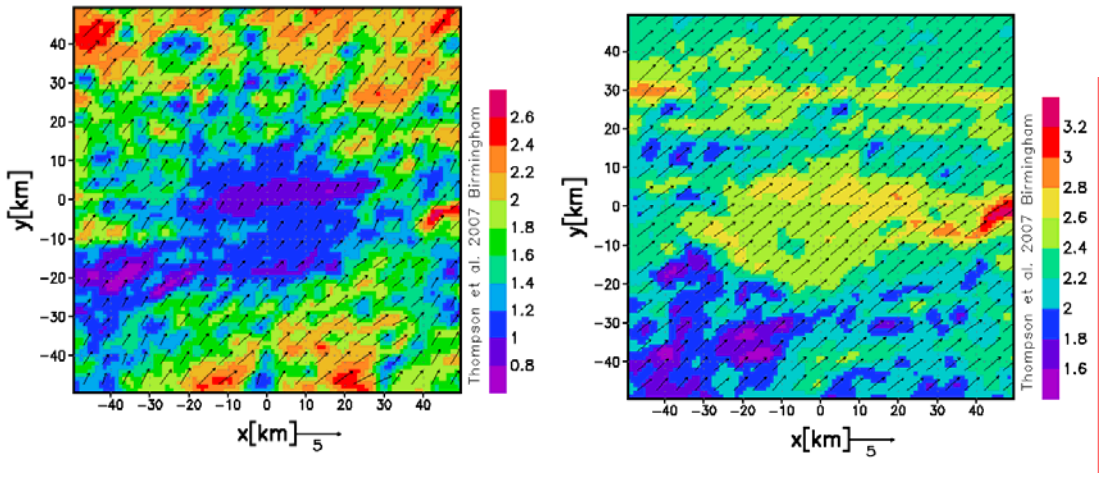


**Figure 6.5: Horizontal wind speed and direction ($ms^{-1}$) for the base case of current urbanised land cover (URB_BASE) (left) and rural domain (NOURB) (right) at z = 10 m at 04:00 of the second day of simulation.**

*6.2.5 Spatial expansion of urban climate anomalies*

Trusilova (2006) defined a Regional Effect Index (REI) in order to analyse the expansion of urban climate anomalies in space, for a study based on a domain representing the whole of Western Europe. This index was defined as the ratio of the total area for which a quantity (e.g. near surface potential temperature) is affected by urbanisation to the total area of urban land (see Equation 6.3). In defining the index Trusilova et al. (2008) assumed that the urban land cover is always affected, and therefore by definition the REI is always greater than 1. A significance threshold of 2.5% (REI > 1.025) was considered to demonstrate a significant regional effect with respect to the variable considered (e.g. maximum diurnal temperature difference). Trusilova et al. (2008) found that during summertime the REI indicated a strong regional impact of the urban area on near surface temperature differences, whereas in wintertime the effects are more local in character.

$$REI(\psi) = \frac{A_{affected\_rural}(\psi) + A_{affected\_urban}(\psi)}{A_{affected\_urban}(\psi)} \quad \textbf{(Equation 6.4)}$$

where $\psi$ is the variable affected by the expansion of the urban land cover e.g. near surface temperature and $A_{affected\_rural}$ and $A_{affected\_urban}$ are the rural and urban areas respectively affected by the change in $\psi$.

One important way in which this work differs from that of Trusilova et al. (2008) is that METRAS+BEP resolves sub grid scale land cover fractions. For this reason the "urban" and "rural" areas in the REI need to be defined. If a grid cell were defined as "urban" by a non zero percentage of urban land cover, then 93% of the domain would be classified as "urban", making it impossible to distinguish a significant regional effect of the anomaly due to the very small percentage of rural cells. It is hypothesised that a grid cell can be defined as "urban" where there is at least 30% urban land cover and the rural area is defined as any grid cell where there is less than 30% urban land cover. This leads to 30.4% of the domain being classified as "urban".

It is also necessary to define the magnitude of the change in the variable $\psi$ which is necessary to consider the grid cell as being 'affected' by the land cover conversion. Again if this were defined as any change greater than zero there would be the danger of the REI being hard to interpret due to a large number of grid cells showing a non zero, but negligible effect. Therefore it is more interesting to define a threshold which demonstrates a more significant effect due to the land cover conversion. This has been defined as the magnitude of change in $\psi$ which is necessary for a number of cells equal to the number of

"urban" cells to be affected by the change. This allows a consistent interpretation of the REI across the differently urbanised domains for the scenarios presented in Section 6.4.

For the base case with the current state of urban land cover the REI is calculated for the meteorological variables of interest and the results are presented in Table 6.5.

**Table 6.5: REI for the URB_BASE-NOURB model comparison, calculated for the second day of simulation.**

| Variable | Threshold | REI |
|---|---|---|
| Near surface potential temperature at 04:00 | 1.43 K | 2.27 |
| Near surface potential temperature at 12:00 | 0.82 K | 1.25 |
| $T_{min\_diurnal}$ | 0.64 K | 1.23 |
| $T_{max\_diurnal}$ | 1.47 K | 2.19 |
| Wind speed at 04:00 | 0.91 $ms^{-1}$ | 1.23 |
| Wind speed at 12:00 | 1.15 $ms^{-1}$ | 1.22 |

The near surface potential temperature at 04:00, 12:00 noon, the maximum and minimum diurnal temperatures and the wind speed at 04:00 and 12:00 noon are all affected by the presence of the urban area, and the change in the variable extends to affect rural cells in and around the urban area.

The regional effect of the change in near surface potential temperature is particularly evident during night time, although the day time effect is also significant and extends to an area about 25% greater than the urban area. Larger temperature differences are expected during night time compared to daytime due to the increased storage in the urban area The regional effect of the wind speed is similar in both daytime and night time, and the effect of reduced wind speed only extends to an area about 22% greater than the urban area.

## 6.3 Effects of the past radial expansion and densification of the city on near surface temperature and wind speed

Many past numerical studies on the effects of urbanisation on weather and climate (e.g. Lamptey et al. 2005; Trusilova 2006) only considered those due to the difference between the current state of urbanisation and a past, entirely rural, state, and did not simulate different forms of increasing urbanisation. Other numerical studies consider a small number of past states of urbanisation, but use a simplified representation of the urban surface (e.g. Ichinose 2001; Lee et al. 2008). No previous numerical studies combine the use of a sophisticated urban canopy scheme like BEP, and a large number of simulations representing urban development.

The dynamics of urban development are harder to study, since precise land cover maps representing the growth of urban areas are not always readily available. However an attempt has been made to simulate the growth of London and its surrounding urban area, based on information available in the literature (see Chapter 2). It is not intended that these simulations should represent an accurate picture of past land cover in the region, but rather that by constructing a series of land cover maps, correlations between the radial growth and the density of the urban grid cells and other parameters such as changes to the near surface temperature might be investigated.

There is limited work of this nature available for the corroboration of model results. For example Ichinose (2001) performed simulations for four land use scenarios to study the effects of land use change in Japan but did not use a model with a detailed representation of

the urban surface. Many other studies (e.g. Klaic et al. 2002; Mölders et al. 2004) have focused on future urbanisation starting from the current state.

Work of this nature has never been attempted for the city of London previously, although Atkinson (2003) did investigate the sensitivity of the urban heat island to various factors including albedo, anthropogenic heat, emissivity, sky view factor and thermal inertia using a simple model and an idealised domain representing a city with the geographical characteristics of London, UK.

There are a number of ways in which the urban area might have grown from its pre-urbanised state to its current extent. For example the radial size of the city might have grown as the city expanded (e.g. Romero et al. 1999), and/or the urban area might have become more compact due to infill and conversion of vegetated areas to built-up surfaces (London Assembly 2005). These two possibilities were represented by the RADIUS and DENSITY series of model runs. Whilst these may represent unrealistic examples of urban land cover, this approach makes it possible to isolate the effect of the different variables. A third series represented a more realistic combination of the effects of radial expansion and densification (COMBINED SERIES).

For each series of model runs an attempt was made to correlate the changes in near surface temperature, DTR, UHI intensity and wind speed with a parameter representing the growth of the city from the pre-urban domain to the current state, i.e. the mean fraction of urban land cover average across the domain. The aim was to investigate whether the change in city size and fraction of urban cover within the grid cells affected the:

- Spatially averaged near surface temperature.
- REI for the near surface temperature and wind speed.
- DTR, the minimum diurnal temperature and the maximum diurnal temperature.
- UHI intensity and diurnal cycle.

*6.3.1 Effect of urban growth on the spatially average near surface potential temperature*

Table 6.6 shows the maximum variation in the near surface (z = 10 m) domain averaged potential temperature for the three series of simulations, for both night time (04:00) and daytime (12:00). This quantity was calculated as the difference in domain averaged near surface potential temperature of the most urbanised compared to the least urbanised simulation. Very little variation was found in the daytime near surface potential temperature for the series where the radial extent of the urban area is varied (RADIUS), whereas a much larger variation was seen for the DENSITY series. For both the RADIUS and DENSITY series a larger variation was seen during night time.

**Table 6.6: Comparison of the maximum variation in near surface potential temperature (%) for daytime and night time for each series of model runs.**

| | Maximum variation in near surface potential temperature (%) at 04:00 | Maximum variation in near surface potential temperature (%) at 12:00 |
|---|---|---|
| RADIUS series | 0.22 | 0.03 |
| DENSITY series | 0.20 | 0.13 |
| COMBINED series | 0.11 | 0.01 |

For the COMBINED series, which represented both changes in radial extent and in urban grid cell density, the maximum change across the series in the mean potential temperature at 12:00 remained very small (0.01%) whereas the maximum change at night time was 0.11%. These results must however be understood in the context of the much smaller variation in the mean urban land cover fractions which was covered by this series. For this

reason the near surface potential temperature was analysed as a function of the mean urban land cover fraction. This variable is calculated as the spatially averaged urban land cover fraction across the whole domain, and therefore can be used as an index to quantify the amount of urban land cover within the domain and enable the comparison of the different series of simulations, both in this Chapter and in Chapter 7.

Figure 6.6 shows the near surface potential temperature averaged across the whole domain for the urbanised domains of the COMBINED, RADIUS and DENSITY series of model runs at 04:00, as a function of the spatially averaged urban land use cover. All series show a linear form of increase in the near surface potential temperature with an $R^2$ value between 0.97 and 0.99. The rate of increase is very similar for the COMBINED and RADIUS series, but larger for the DENSITY series. For all series the total change at 04:00 in mean near surface potential temperature between the least urbanised domain and the most urbanised domain is less than 1 K; however it must be noted that this is the mean change across the entire domain.

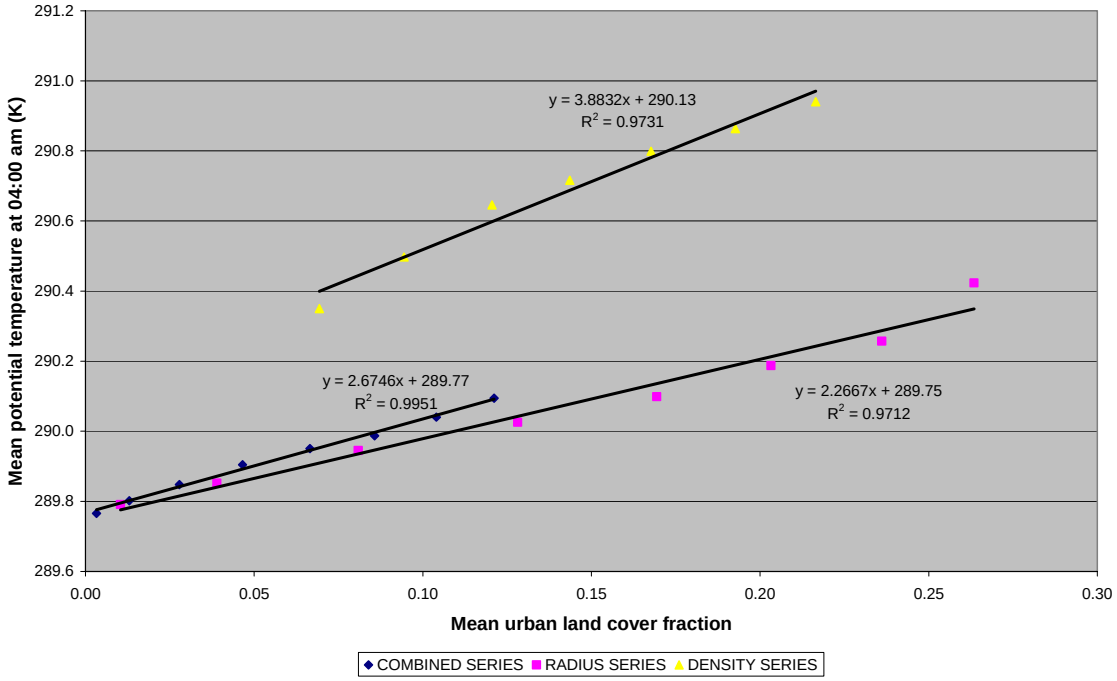


**Figure 6.6: Mean potential temperature (K) as a function of the mean urban land cover fraction for the COMBINED, RADIUS and DENSITY series, at 04:00 of the second day of simulation.**

Figure 6.7 shows the mean potential temperature change at 12:00 as a function of the mean urban land cover fraction for the three series of simulations. It is apparent that both the RADIUS series and the COMBINED series show very little variation in the mean potential temperature at 12:00 and the absolute magnitude of the temperature is very similar in the two sets of simulations. All three series show an almost linear dependency on the mean urban land cover fraction, with $R^2$ values varying from 0.77 for the RADIUS series to 0.97 and 0.94 for the DENSITY and COMBINED series respectively.

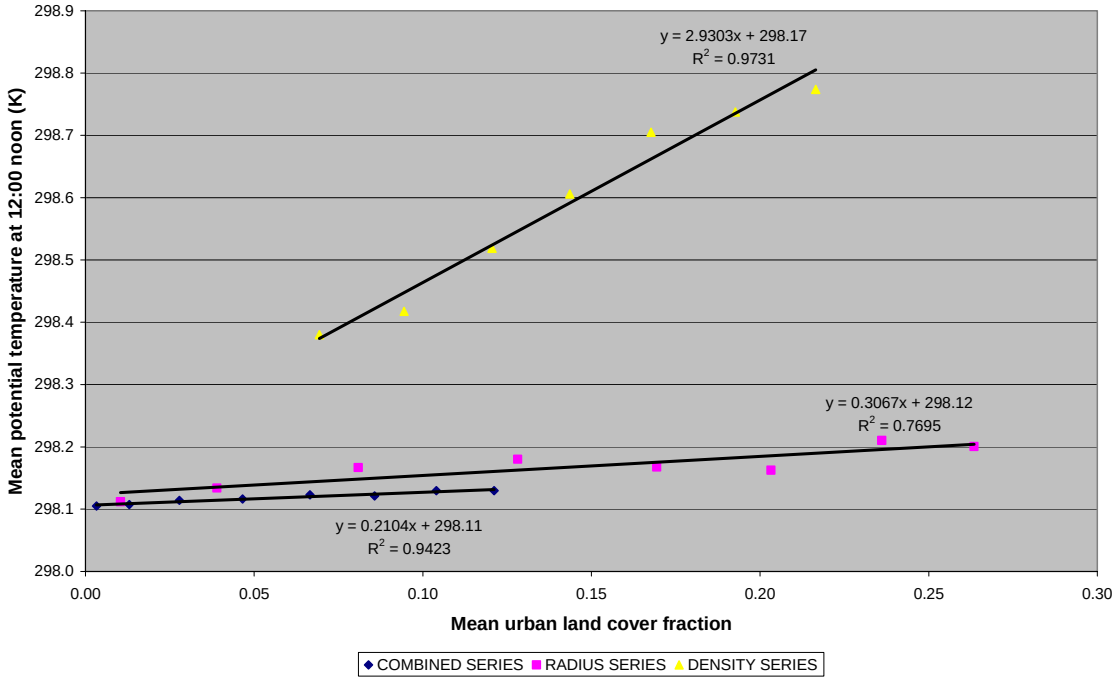


**Figure 6.7: Mean potential temperature (K) as a function of the mean urban land cover fraction for the COMBINED, RADIUS and DENSITY series, at 12:00 of the second day of simulation.**

For the DENSITY series the size of the urban area did not change, and it is the fraction of urban land cover compared to that of the 'Meadows' land cover class within the urban grid cells which drives the change in the spatially averaged potential temperature. As progressively more of the urban land cover is reclassified as 'Meadows', the near surface potential temperature is reduced. This can be compared to the results presented in Civerolo et al. (2000) who found reduced near surface temperatures by 1 ºC or more when 40% of the urban area within New York City metropolitan area was reclassified as deciduous forest. These results confirm the fact that vegetation is a key determinant of near surface temperature (Jenerette et al. 2007).

The DENSITY series shows a much larger starting value and a larger rate of temperature increase, which determines higher daytime (12:00) and night time (04:00) temperatures

compared to the RADIUS series for similar mean urban land cover fractions. The simulations in the DENSITY series have a larger number of less densely urbanised grid cells with an urban land cover fraction compared to the more compact urban area in the RADIUS and COMBINED series. This result suggests that the existence of the extensive suburban areas surrounding the city centre has important implications for determining mean urban temperatures and for the management of cities and their development. For the RADIUS series on the other hand the spatial expansion of the city from 25 $km^2$ to 1600 $km^2$ is the driving factor behind the change in the spatially average near surface potential temperature, but this appears to have a smaller effect compared to the increase in urban land cover fraction in the DENSITY series.

*6.3.2 Effect of urban growth on the REI and effective radius*

It is observed that all the model runs demonstrate an increase in the average value for the near surface potential temperature when compared with the model simulation with rural land use (NOURB). It is however interesting to analyse the area at night time which is affected by a change in the near surface potential temperature greater than a threshold value of 1 K, and to relate this to the area occupied by the city for each domain. After detailed analysis of the horizontal slices at 10 m for each model run, a minimum change of 1 K was considered because all the simulations showed an area affected by this change at 04:00. An effective radius ($R_{eff}$) is calculated for the RADIUS and the COMBINED series of runs using:

$$R_{eff} = \sqrt{A(x)/\pi} \qquad \textbf{(Equation 6.5)}$$

where A(x) is the area affected by the minimum change in near surface temperature of 1 K. The advantage of the effective radius is that it allows a comparison between the urbanised area (as defined by the urban land cover fraction), and the absolute size of the area which is affected by a minimum change in potential temperature compared to the rural domain. It is obvious that the calculation makes the approximation of a circular affected area, which is not necessarily appropriate; however this remains a useful parameter for the intended comparison. This calculation is however not very appropriate for the series of runs in which the urban density is reduced, since the total urban area remains unchanged. The results for the effective radius presented in Table 6.7.

**Table 6.7: Effective radius (km) and the ratio of the effective radius $R_{eff}$ to the actual radius of the urban area $R_{urb}$ for the RADIUS and COMBINED series of model runs. The effective radius is calculated for the second day of simulation at 04:00.**

| | RADIUS SERIES | | COMBINED SERIES | |
|---|---|---|---|---|
| $R_{urb}$ (km) | $R_{eff}$ (km) | $R_{eff}/R_{urb}$ (%) | $R_{eff}$ (km) | $R_{eff}/R_{urb}$ (%) |
| 40 | 27.8 | 70 | 13.5 | 34 |
| 35 | 22.8 | 65 | 12.6 | 36 |
| 30 | 21.1 | 70 | 11.2 | 37 |
| 25 | 18.3 | 73 | 9.6 | 38 |
| 20 | 15.8 | 79 | 6.9 | 35 |
| 15 | 11.8 | 79 | 4.4 | 29 |
| 10 | 7.2 | 72 | 3.3 | 33 |
| 5 | 3.4 | 69 | n/a | n/a |

For the smallest urban area of the COMBINED series it is not applicable to define an effective radius, since the area affected by the threshold change in potential temperature is too small to make the calculation meaningful. These results show that the effective radius, as a % of the radius of the urban area, does not demonstrate any significant increase with the growth of the urban area. For the RADIUS series the effective radius is around 70% of the urban land cover radius, and for the COMBINED series the radius is approximately 35% of the urban land cover radius. The values of the effective radius are much smaller for

the COMBINED series, for which the mean urban land cover fractions for the domains are much smaller than in the RADIUS series. This confirms the results for the spatially averaged temperature in suggesting that the urban land cover density is an important determinant of the area which shows an increase in the night time potential temperature of more than 1 K.

Analysing the model runs using the effective radius does have some limitations. Firstly, it is not possible for example to compare an effective radius with the size of the urban area for the DENSITY series, and secondly, defining a threshold of 1 K is not applicable for the daytime results where the change is much smaller. The split between rural and urban grid cells affected by the 1 K change is also neglected. Therefore a second measure, the REI, is used to understand whether the regional effect of the urban area increases with the radial growth and the increase in urban land cover fraction. This will lead to an understanding of how much of the rural area surrounding the city is affected by the growth of the city.

The REI is calculated for each model run of the three series, for the domain averaged near surface potential temperature at 04:00 and at 12:00. The results are presented in Table 6.8.

**Table 6.8: REI for the RADIUS, DENSITY and COMBINED model series, for night time (04:00) and daytime (12:00), for the second day of simulation.**

| RADIUS series | | |
|---|---|---|
| **RADIUS series (km)** | **REI (04:00)** | **REI (12:00)** |
| 40 | 2.23 | 1.14 |
| 35 | 2.02 | 1.10 |
| 30 | 1.81 | 1.08 |
| 25 | 1.70 | 1.06 |
| 20 | 1.71 | 1.04 |
| 15 | 1.84 | 1.03 |
| 10 | 2.26 | 1.02 |
| 5 | 7.58 | 1.01 |

| DENSITY series | | |
|---|---|---|
| **DENSITY series** | **REI (04:00)** | **REI (12:00)** |
| 90% | 2.36 | 1.12 |
| 80% | 2.53 | 1.12 |
| 70% | 2.81 | 1.13 |
| 60% | 2.77 | 1.15 |
| 50% | 3.14 | 1.20 |
| 40% | 6.28 | 1.34 |
| 30% | n/a | n/a |

| COMBINED series | | |
|---|---|---|
| **COMBINED series (km)** | **REI (04:00)** | **REI (12:00)** |
| 40 | 2.25 | 1.12 |
| 35 | 2.25 | 1.10 |
| 30 | 2.31 | 1.11 |
| 25 | 2.62 | 1.09 |
| 20 | 3.27 | 1.11 |
| 15 | 4.60 | 1.09 |
| 10 | 13.6 | 1.10 |
| 5 | 38.0 | 1.16 |

These results show that at 04:00 there is a significant regional effect with respect to this variable for all the model simulations. The magnitude of the effect appears to grow as the radial size of the city decreases to small values, this however is due to limitations in the definition of the REI, since for very small urban areas there are only a very small number of points which are classified as urban. The RADIUS series shows an increase in the REI for both daytime and night time as the urban area grows from a radius of 25 km to 40 km. For the DENSITY and the COMBINED series the results are less certain, but suggest that the REI does not grow with the city size. The results for the RADIUS series corroborate those of Trusilova (2006) who found an increase in the regional impact with the expansion on the urban area.

*6.3.3 Effect of urban growth on the DTR*

As explained in Section 6.3.2 the DTR is a key meteorological indicator associated with urbanisation and climate change. Figure 6.8 shows the change in the DTR for the urbanised domains as a function of the mean urban land cover change, for all three series of simulations.

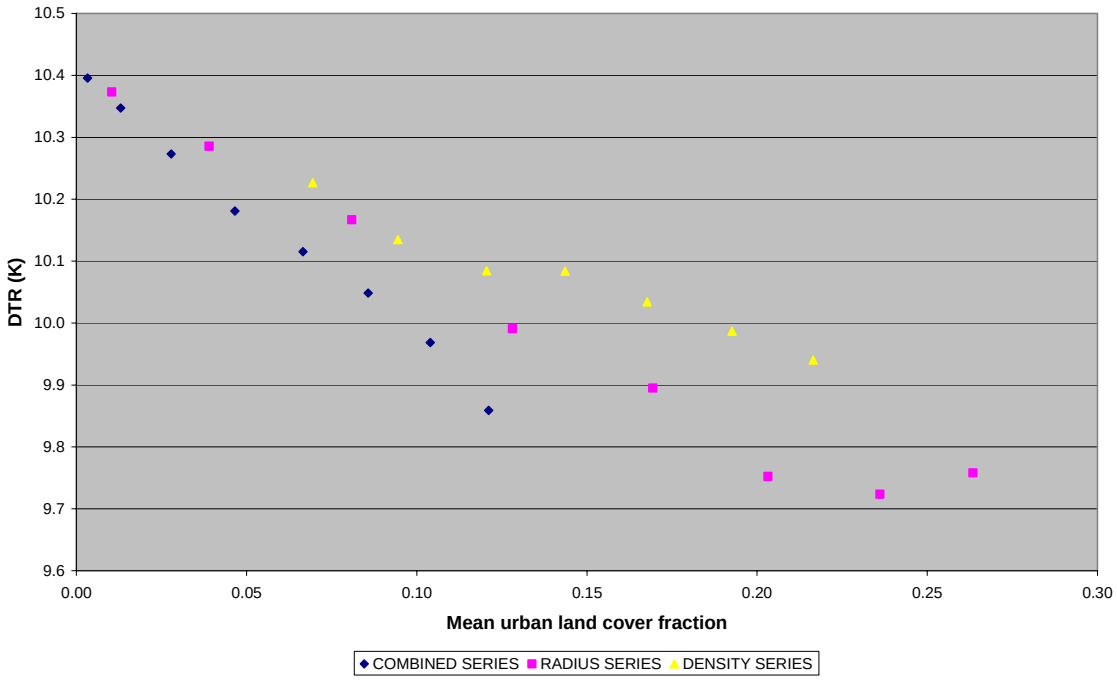


**Figure 6.8: Mean DTR (K) as a function of the mean urban land cover fraction for the COMBINED, RADIUS and DENSITY series, for the second day of simulation.**

These results show that as the mean urban land cover fraction increases the DTR averaged across the whole domain is reduced. For the RADIUS series this reduction in magnitude is linear until a city size corresponding to a radius of 30 km and above is reached, and then the results show a small change. This suggests a threshold for the change might be reached around these values of the mean urban land cover fraction. The DENSITY and

COMBINED series also show a reduction in the DTR, but they do not reach the threshold value of the mean urban land cover.

These results can be analysed in terms of the maximum and minimum diurnal temperature. As seen in Figure 6.9 the DENSITY series shows an increase in the maximum diurnal temperature, compared to the small reduction demonstrated by both the RADIUS and COMBINED series. For the COMBINED series this reduction is linear in nature over the range of the urban land cover which this series spans. The greater uncertainty and differences in the behaviour of the model series as far as the maximum diurnal temperature is concerned are corroborated by Trusilova (2006) who also found lower values in urban areas compared to rural surroundings.

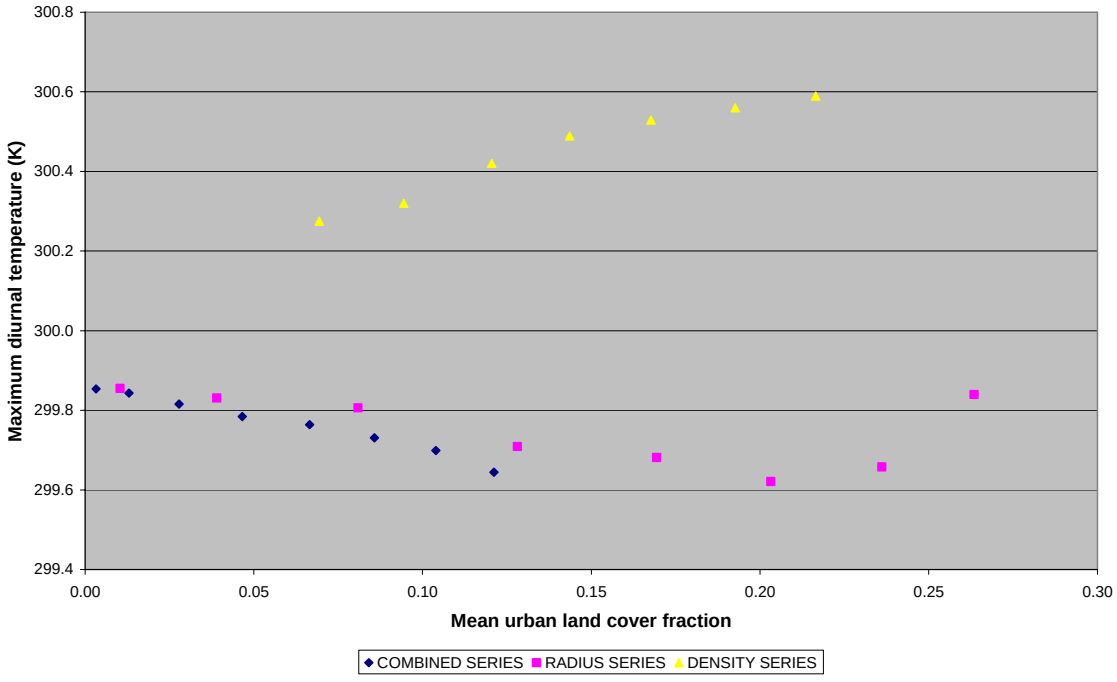


**Figure 6.9: Spatially averaged maximum diurnal temperature (K) as a function of the mean urban land cover fraction for the COMBINED, RADIUS and DENSITY series, for the second day of simulation.**

For the minimum diurnal temperature all the series show a similar functional form of the increase in the minimum temperature with the mean urban land cover fraction, as seen in Figure 6.10. Once again it appears that for similar values of the mean urban land cover fraction the DENSITY series shows larger values for the minimum diurnal temperature compared to the RADIUS and COMBINED series. These results confirm that the total size of the city including the suburban surroundings determines higher values of the minimum diurnal temperature, even if the mean urban land cover fraction within the city is greatly reduced compared to the more compact urban areas represented in the RADIUS series.

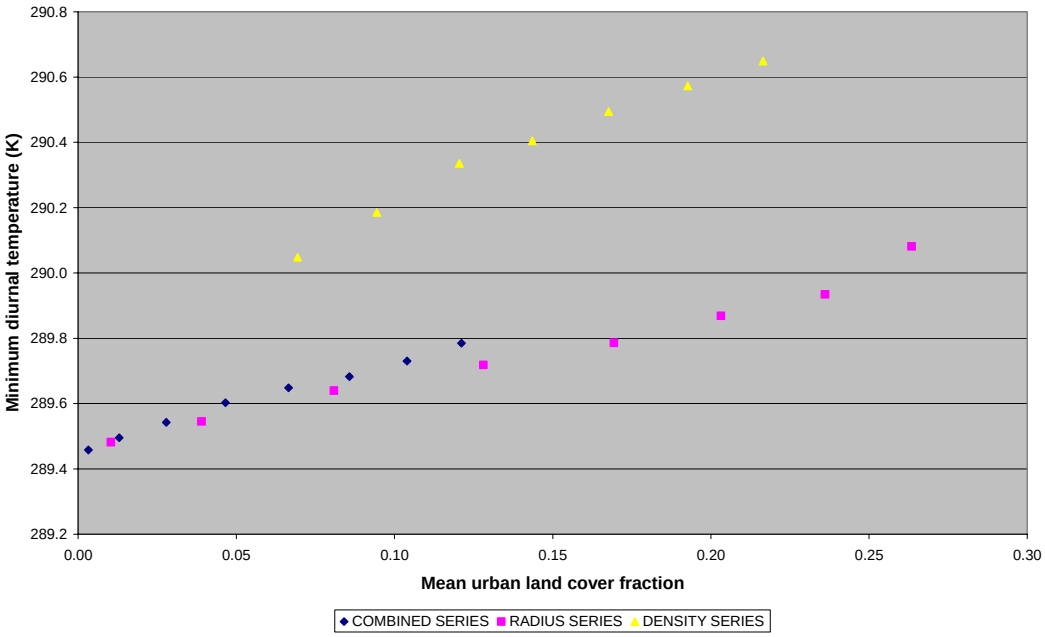


**Figure 6.10: Spatially averaged minimum diurnal temperature (K) as a function of the mean urban land cover fraction for the COMBINED, RADIUS and DENSITY series, for the second day of simulation.**

### *6.3.4 Effect of urban growth on the UHI intensity*

The diurnal cycle of the maximum UHI intensity is analysed for the three series of model runs for the second day of the model simulations and the results are presented in Figure 6.11, Figure 6.12 and Figure 6.13. It is observed that the timing of the cycle is very similar

for all runs in the series, and corroborates that observed in the URB_BASE simulation. For the most highly urbanised runs the greatest maximum heat island intensity is observed at around 02:00 (2.47 K). There is a difference of more than 1 K in the peak UHI intensity between the most highly urbanised domain in the DENSITY series and that with the least urban land use cover in the COMBINED series.

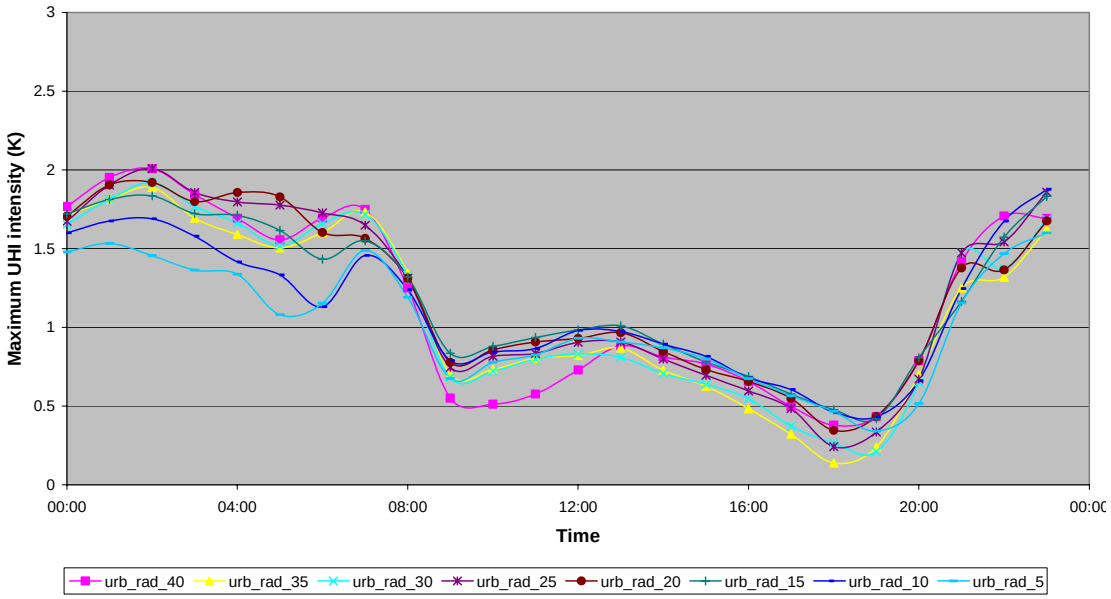


**Figure 6.11: Diurnal cycle of the maximum UHI intensity (K) for the second day of simulation for the RADIUS series**

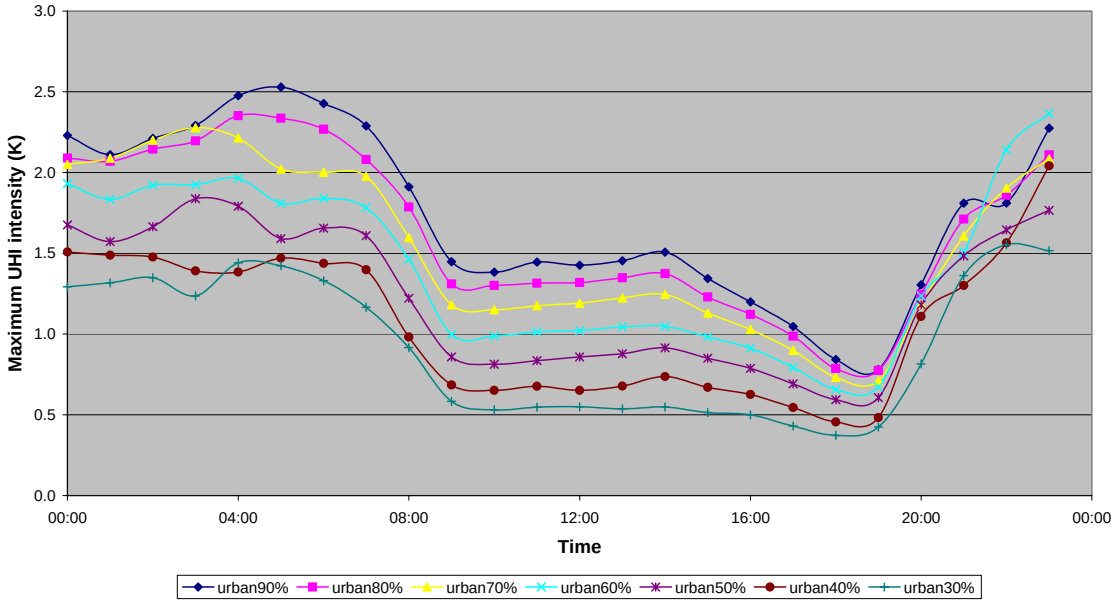


**Figure 6.12: Diurnal cycle of the maximum UHI intensity (K) for the second day of simulation for the DENSITY series**

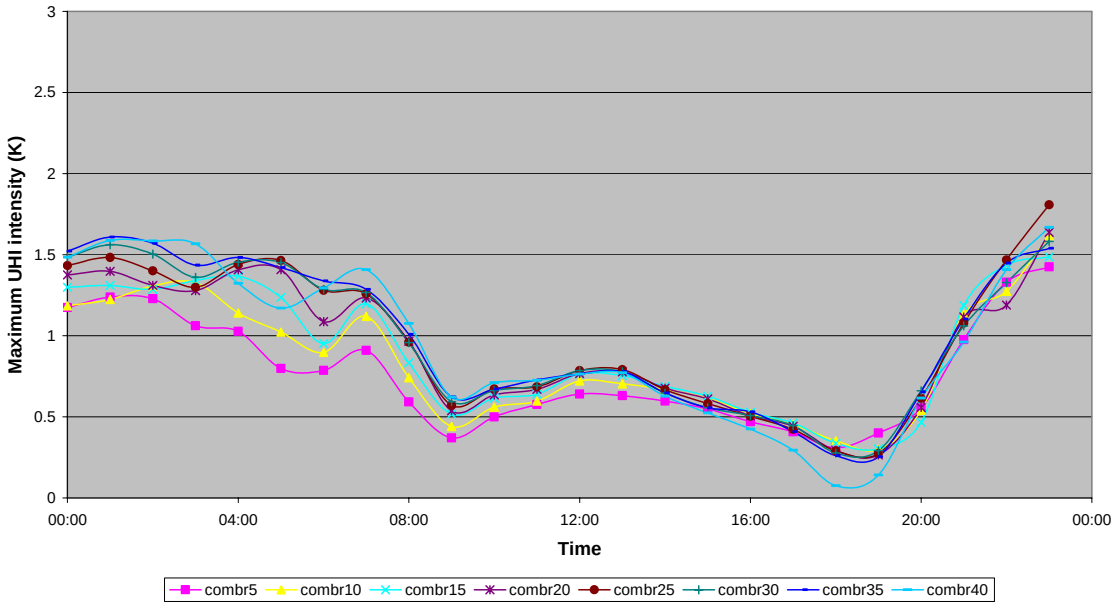


**Figure 6.13: Diurnal cycle of the maximum UHI intensity (K) for the second day of simulation for the COMBINED series**

The runs are then combined into one graph representing the maximum UHI intensity at 02:00 as a function of the mean urban land cover for the domain. These results are presented in Figure 6.14. All three series show an increase in the maximum UHI intensity with the increased in mean urban land cover fraction. The RADIUS series shows a smaller variation in the maximum UHI intensity compared with the DENSITY series. Both the RADIUS and DENSITY series appear to reach a plateau once a mean urban land cover fraction between 0.15 and 0.20 is reached. Within the range of mean urban land cover spanned by the COMBINED series, the results show a linear form of increase and a threshold is not reached.

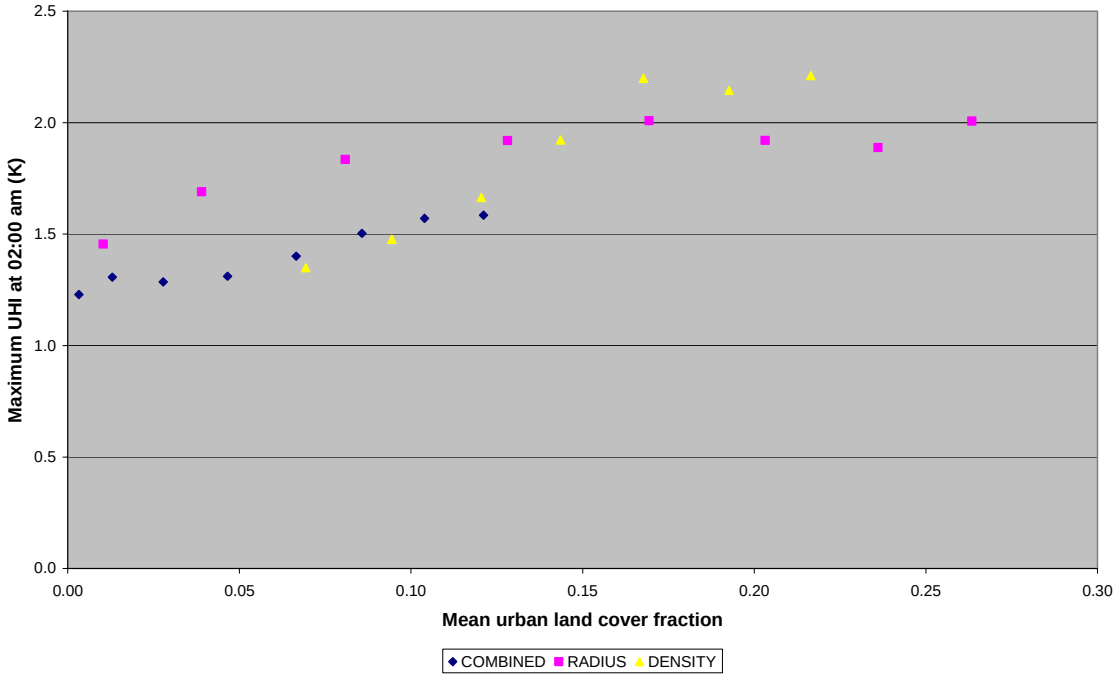


**Figure 6.14: Maximum UHI intensity (K) as a function of mean urban land cover fraction for the RADIUS, DENSITY and COMBINED series of model runs, at 02:00 of the second day of simulation.**

By studying data from meteorological observation stations in and surrounding urban areas, changes in regional land use have been found to be correlated with trends in the UHI intensity (e.g. Brazdil et al. 1999; Brazel et al. 2007; He et al. 2007). The extension of the built up area, and increasing energy consumption are usually correlated with the intensification of the UHI (Brazdil et al. 1999). However, it is also reported in Atkinson (2003) that the UHI intensity did not depend on the size of the urban area, and studies such as Oke (1987) suggested that other factors governing the urban development, such as building heights, albedo, urban density, sky view factor and thermal and radiative characteristics of the city such as the emissivity are more important determinants of the UHI intensity.

These results show that both the spatial expansion (RADIUS) and the reduction in vegetation within the urban area (DENSITY) have an effect on the peak UHI intensity. The reduction in the 'Meadows' class determines a larger increase in UHI intensity when compared to the increase of just over 0.5 K observed for the expansion of the city from an area of 25 $km^2$ to 1600 $km^2$. This is consistent with Oke (1987) in suggesting that other factors, such as density of urban development and presence of vegetation, are more important that city size in determining the UHI, whilst still recognizing that urban expansion has an effect, as observed for the idealised domain and in experimental studies.

Best et al. (2002) found that for Reading and London the ratio of urban to vegetation fraction within the city influenced the surface layer UHI. An increase in urban fraction increased the surface layer UHI in a non linear way, which depended on the change in urban fraction and the size of the urban area. The response for larger urban areas was found

to be more linear than the smaller urban area. This is corroborated by the results from the DENSITY series in which the urban fraction is increased relative to the vegetation fraction.

### *6.3.5 Effect of urban growth on the wind speed*

The RADIUS, DENSITY and COMBINED series of model simulations were analysed in order to investigate the effect of the growth of the city on the mean horizontal near surface wind speed across the whole domain. Figure 6.15 shows the mean wind speed at 12:00 as a function of the mean urban land cover fraction. All three series show a linear reduction in the mean wind speed as the urban land cover fraction increases, and the form of the reduction is similar for all three series. The $R^2$ values range from 0.83 for the RADIUS series to 0.96 and 0.99 for the DENSITY and COMBINED series respectively.

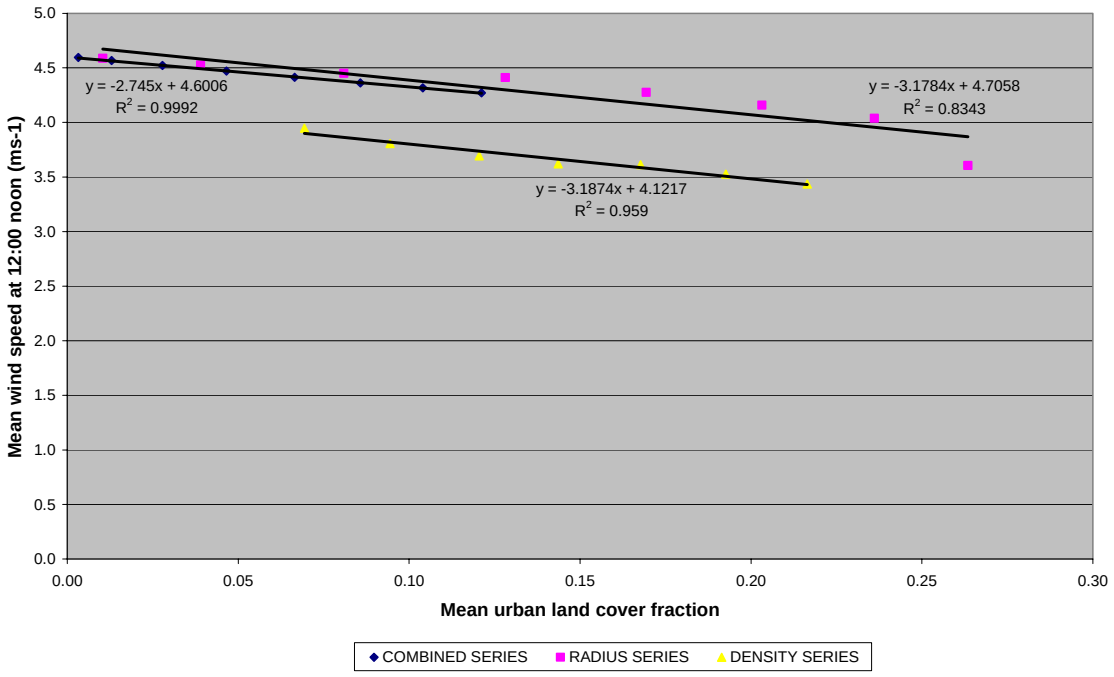


**Figure 6.15: Mean horizontal wind speed at z = 10 m as a function of the mean urban land cover fraction for the RADIUS, DENSITY and COMBINED series of model runs, at 12:00 of the second day of simulation.**

Figure 6.16 shows the same results for 04:00. The COMBINED series again shows a very similar form to the RADIUS series, and all series show a linear reduction in the mean wind speed at 04:00 with the increase in the mean urban land cover. The $R^2$ values range from 0.98 to 0.99.

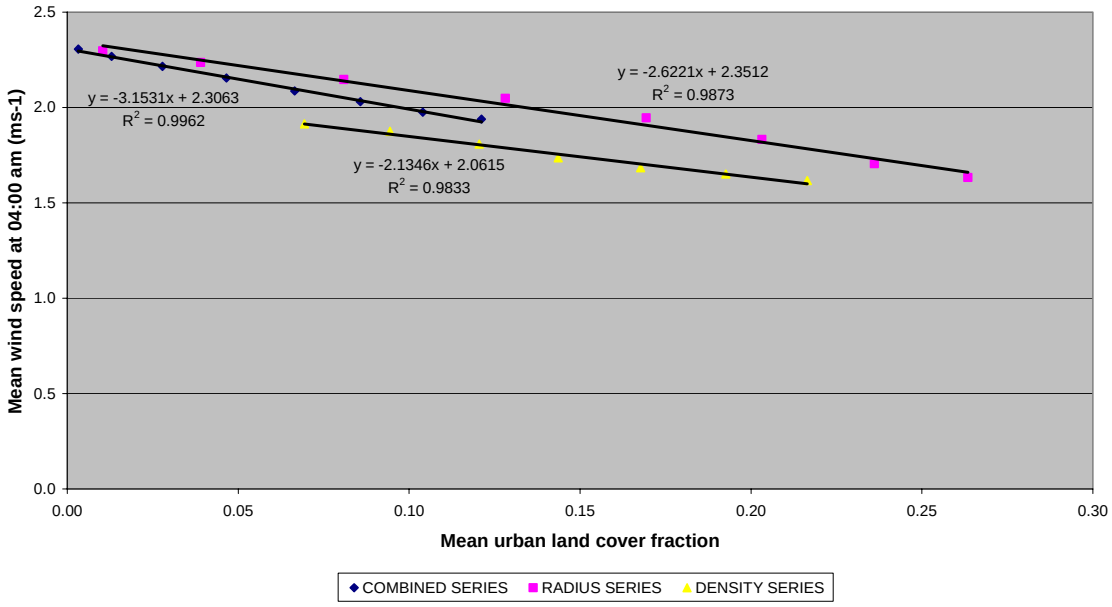


**Figure 6.16: Mean horizontal wind speed at z = 10 m as a function of the mean urban land cover fraction for the RADIUS, DENSITY and COMBINED series of model runs, at 04:00 of the second day of simulation.**

For both daytime and night time, the COMBINED series, whilst spanning a much smaller range of land cover fractions, shows a very similar form to the RADIUS series, which suggests that the change in urban land cover density of the COMBINED series compared to the RADIUS series has a less important effect compared to the increase in the radial size of the city. In general the mean wind speed is smaller for the DENSITY series, which represents a larger city size, compared to simulations from the RADIUS series with a similar mean urban land cover fraction.

The total reduction in mean wind speed in the DENSITY and COMBINED series, at night time, is 16%, which can be compared to the reduction of 29% in the RADIUS series. During daytime the COMBINED series shows a reduction of 7%, compared to a reduction of 12% for the DENSITY series and of 21% for the RADIUS series shows a reduction of 21%. These % reductions are comparable with those in Klaic et al. (2002), who found an average wind speed reduction of 8% and 18% for two simulations which represented small increases in the urban area by 12.5% and 37.5%. They are also comparable with Wang et al. (2007) who simulated a 20% reduction in wind speed due to urbanisation in the Pearl Delta region, China.

## 6.4 Summary and discussion

The aim of this Chapter was to investigate both the effects on near surface potential temperature and wind speed of the current form of urban land cover in the London region, when compared to an idealised rural background simulation, and the effects of the change in radial size and density of the urban area on the same variables.

The comparison of the current state of the urban land cover for London and a rural simulation has shown larger differences in mean near surface potential temperature during night time compared to the daytime, due to the fact the built-up surfaces partition more heat into storage during daytime, limiting the nocturnal cooling of the near surface air. A reduction in the DTR was also observed, and the results corroborate well with other experimental and numerical studies (Gallo et al. 1996; Kalnay et al. 2003; Zhou et al. 2004; Lamptey et al. 2005; Trusilova et al. 2008).

A significant reduction in wind speed over the urban area was also observed during both daytime and night time, which is due to the higher roughness of the city compared to the rural domain which enhances turbulence. Changes in wind speed within urban areas are also well documented in past numerical and experimental studies (Bornstein et al. 1977; Roth 2000; Klaic et al. 2002), and are important because they have been found to reduce sensible heat cooling of the ground (Gaffin et al. 2008).

Two parameters were defined to investigate the effects of the urban area: an effective radius to investigate the fraction of the urban area which is affected by a change in the night time potential temperature above 1 K, and a regional effect index (REI), defined in order to investigate whether the effect of the urban area extends to the rural surroundings of the city.

The REI showed that for all the variables considered there is an effect which extends beyond the area directly classified as urban, and that this extent is much greater during night time than during daytime, when urban effects due to the release of daytime heat stored within the building materials are large.

It is hard to simulate the precise evolution of the urban area, since detailed and comprehensive maps showing the change of urban land cover with time are not readily available in a format which can be assimilated by the METRAS+BEP model. An attempt has therefore made to understand the key determinants of the change in near surface temperature and wind speed by using the mesoscale model as a numerical laboratory, rather than a forecast tool (as suggested in Tjernstorm et al. 2000). The land cover in the scenario domains was constructed from the current London land cover, and assumptions based on the literature and possible forms of urban development.

The results of the scenarios show a higher mean potential temperature for both daytime and night time, and a lower wind speed, for an urban area of the current size of London but with increased vegetation fraction (DENSITY series), when compared to a smaller urban area but with higher urban land cover densities (RADIUS series). The change in the ratio of the effective radius and the urban radius shows only a very small variation as the city size increases. These results show that the extensive urban growth, and in particular the reduction in vegetation within the London urban area, has affected near surface temperature, wind speed and the UHI. The extent of these changes largely coincides with the area of increasing urbanisation, although the REI also shows that the effect is present in the rural areas surrounding the city. The dangers of removing green cover in urban areas

due to the consequent increase in temperatures have been highlighted in previous modelling studies (e.g. Gill et al. 2007).

The UHI is one of the most important effects the urban surface has on climate, and can lead to increased human discomfort (Baker et al. 2002). For the simulation for London with the current urban land cover state, a nocturnal UHI of around 2.5 K is observed. The timing of the UHI peak intensity for the current urban land cover for London shows an excellent agreement with the results of measurements as presented in Graves et al. (2001) and Wilby (2003).

When comparing the maximum UHI intensity for the simulations in which the radial extent and urban land cover density are varied, higher values of the UHI intensity are observed for the scenarios in which the size of the urban area is kept constant, and the land cover fraction is varied. This is consistent with the results for the mean potential temperature and wind speed. However both the DENSITY and RADIUS series appear to reach a plateau as the mean urban land cover increases. These results suggest that further extensive urban growth within the London region might only have a small effect on the UHI intensity; however this will be investigated further in Chapter 7. This would agree with physical and energy budget modelling work in Oke (1981) and Oke et al. (1991) which strongly suggest factors other than size are more important in determining UHI intensity. London has been identified as particularly sensitive to future increases in temperature due to the UHI effect (LCCP 2002), and therefore this investigation could represent an important contribution to understanding future urban climate for London.

Higher temperatures in the urban area, and the reduction in DTR, could have a significant impact on human health and comfort, since the combination of the above represents the worst possible climate scenario for human comfort (Jenerette et al. 2007). Temperature increases in urban areas can also have localised effects such as increases in atmospheric pollutants, as well as effects on energy costs associated with air conditioning, human heat stress and crime (Baker et al. 2002). Urban planning should therefore attempt to mitigate the UHI, by taking into account factors such as construction density and green spaces (Pinho et al. 2000).

The next step is the investigation of the effects of expanding the urban area from its current state. Both urban expansion into the rural surroundings, and the continued reduction of vegetation within the existing urban area, will be explored as these are important determinants of the UHI intensity.

# Chapter 7:

# The effects of future urban expansion and possible mitigation strategies

In Chapter 6 the analysis focused on the effects of past urbanisation on temperature and wind speed, by running simulations in which the urban surface was decreased from the current extent (represented by the CEH Land Cover Map 2000) to a pre-urban situation with no urban land cover. In this Chapter the effects of future urban expansion are considered. The reference case is now the existing urban land cover over the London region, rather than a background entirely rural state as was the case in Chapter 6.

Urban areas are expanding across the globe, in both developing and industrialised countries. In developing countries, urban land areas can be expected to increase, with every new resident converting about 160 $m^2$ of non urban land to urban land by 2030 (Angel et al. 2005). In industrialised countries, urban population is expected to grow by 11% by 2030 (UN 2004), but average densities in large cities are expected to continue to decline at the current rate of 2.2% (Angel et al. 2005), with the expansion of lowly populated suburban areas. Urban expansion puts a strain on natural resources and impacts air pollution and regional climate (Civerolo et al. 2007).

Forms of urban expansion can be very different (Angel et al. 2005). Existing urban areas can be redeveloped at higher densities (e.g. Thomas 1979), infill can occur in open spaces in already built up areas (London Assembly 2005), or new development can occur in areas which were previously non-urbanised through the conversion of land contiguous to the city (or not contiguous) from open green spaces to built-up areas (e.g. Romero et al. 1999).

Over the next ten years the population of London is expected to grow by 800,000 people, causing a challenge to the capital to provide housing and infrastructure in a sustainable manner within its boundary (London Assembly 2005), whilst maintaining existing open green spaces and not encroaching on the Green Belt (Thomas 1970). Between 1989 and 1999 1,000 hectares of green spaces and playing fields were lost to development (London Assembly 2005; London Assembly 2006), and green space is continuing to be lost, although at a slower rate. The development of brown field land (defined as land currently or previously occupied by a structure) is identified as a possible strategy to meet this challenge (London Assembly 2005).

At the same time major urban development is also planned to extend the Greater London area to cover much more of the South-East and it is considered highly likely that this development will impact local weather (Collier 2006). For this reason the consideration of urban effects should be included in the planning of the built environment of the future, to ensure an optimal environment for human well being.

Model domains for the London area were set up in which some of these forms of urbanisation are represented. The forms of urbanisation which can be simulated using the METRAS+BEP model are limited to land cover changes, since it is not possible to directly represent changes in the population in the urban area. Despite current trends showing a decline in the population of London (Lee 1992), on the whole the existing extent of the built up area is unlikely to decline, and the increase in the average built up area per person (defined as the reciprocal of the density) is likely to drive an increase in lower populated suburban areas.

The METRAS+BEP model was run under the same meteorological conditions as those in Chapter 6, in order to analyse the effects of increased urban land cover on near surface temperature and wind speed.

## 7.1 Description of model runs

In order to analyse the effect of the future growth of the urban area on urban climate a series of domains were created to represent different states of future urbanisation for the London area. There are several possible scenarios for increasing the urban land cover within the model domain. These are:

- Increase the urban land cover fraction for all grid cells, independently of whether they are currently urbanised or not.

- Increase the urban land cover fraction only for cells which are already urbanised.

In order to increase the urban land cover fraction within a grid cell, it was necessary that the fraction of other land cover class decreased, since for each cell the land cover types must add up to 100% coverage. It was chosen that the METRAS land cover class representing 'Meadows' should be converted to urban land cover, since this was considered to be more realistic than converting existing forest areas, which were more likely to be protected areas (www.woodlandtrust.org.uk). The increase in urban land cover within the currently urbanised grid cells is possible because METRAS resolves sub grid scale land cover. If this were not the case, it would be possible to urbanise the grid cells contiguous to the urban area only.

### *7.1.1 EXPANSION series*

The first scenario representing future urbanisation consisted in increasing the urban land cover fraction for all cells, independently of whether there was an existing urban land cover fraction or not. This represented the indiscriminate expansion of the urban area into the rural surroundings, as well as the increase in the urban land cover fraction of existing urban grid cells. This series is referred to as the EXPANSION series, although it represents both spatial expansion of the city and densification of the existing urban areas at the expense of green space.

A series of 10 domains was constructed, in which the fraction of the existing 'Meadows' land cover converted to urban land cover was increased from 10% of 'Meadows' to the extreme example in which 100% of the 'Meadows' land cover fraction was converted to urbanised land cover (see Table 7.1). The whole model domain was subjected to the change defined in each of the scenarios.

**Table 7.1: Summary of simulations which form the EXPANSION series of model runs, which represents the urban expansion over all grid cells, independently of whether they are already urbanised or not.**

| Model simulation name | Description |
|---|---|
| urb0.1 | 10% of 'Meadows' converted to 'urban' |
| urb0.2 | 20% of 'Meadows' converted to 'urban' |
| urb0.3 | 30% of 'Meadows' converted to 'urban' |
| urb0.4 | 40% of 'Meadows' converted to 'urban' |
| urb0.5 | 50% of 'Meadows' converted to 'urban' |
| urb0.6 | 60% of 'Meadows' converted to 'urban' |
| urb0.7 | 70% of 'Meadows' converted to 'urban' |
| urb0.8 | 80% of 'Meadows' converted to 'urban' |
| urb0.9 | 90% of 'Meadows' converted to 'urban' |
| urb_all | All of 'Meadows' converted to 'urban' |

Future urban development in grid cells which were not previously urbanised is assumed to be 'suburban' (primarily residential or employment based development away from the urban core) in nature, and therefore the use of the second urban class defined in Chapter 3 is assumed to be a valid. This assumption was also made in Civerolo et al (2007) for future urban growth for the New York City metropolitan area.

### *7.1.2 DENSIFICATION series*

The second scenario used to represent future urban expansion consisted in increasing the urban land cover fraction of grid cells which are already urbanised, i.e. increasing the proportion of the built up area relative to that not covered by buildings and pavements. This represents the well documented loss of green space in the existing city, since the horizontal extent remains constant (London Assembly 2006). Pressure on land use, and planning strategies such as the Green Belt, could drive this form of urban expansion which doesn't greatly alter the extent of the urban area in the model domain. For example future urban planning for Melbourne, Australia aims for a more compact city by increasing housing in urban areas and establishing an urban growth boundary (Coutts et al. 2007).

Another cause of this form of expansion is the continued tendency for partially or wholly covering front gardens with paving, concrete, bricks and other hard surfacing. This has caused two thirds of London's front gardens to become paved, covering an area of 32 $km^2$ (London Assembly 2005).

A percentage of the existing 'Meadows' land cover was converted to urban land cover for all grid cells where the existing urban land cover fraction was greater than 30%, 40% and 50% respectively for three groups of simulations. For each group, six simulations were configured in which the proportions of 'Meadows' converted were 60%, 70%, 80%, 90% and 100% respectively. A series of 18 domains were constructed to form this set of model simulations (see Table 7.2).

**Table 7.2: Summary of simulations which form the DENSIFICATION series of model runs, which represents the urban expansion for existing urban cells (where the urban fraction exceeds a threshold percentage) only**

| Series name and threshold for urban conversion | | | Description |
|---|---|---|---|
| **'30ABCDEF' - 30%** | **40ABCDEF' - 40%** | **50ABCDEF' - 50%** | For all cells where the existing urban land cover % is greater than the threshold: |
| 30A | 40A | 50A | 50% of 'Meadows' converted to 'urban' |
| 30B | 40B | 50B | 60% of 'Meadows' converted to 'urban' |
| 30C | 40C | 50C | 70% of 'Meadows' converted to 'urban' |
| 30D | 40D | 50D | 80% of 'Meadows' converted to 'urban' |
| 30E | 40E | 50E | 90% of 'Meadows' converted to 'urban' |
| 30F | 40F | 50F | All 'Meadows' converted to 'urban' |

Both sets of simulations represent a reduction in the vegetated fraction within the urban area. The fraction of vegetation is a crucial determinant of the urban climate (Jonsson

2004). Both forms of urban expansion assume no change in the basic structure of the building morphology (building size and heights), street width and thermal properties. This means the effect of changing characteristics such as the sky view factor is not represented.

Future urban development in grid cells which were already previously urbanised is assumed to be of the same average characteristics as that already existing within the grid cells. This means the same percentages of the two urban classes defined in Chapter 3 are maintained within the grid cell.

### *7.1.3 Model configuration for the scenarios*

The METRAS+BEP model was run under the same meteorological configuration, initial conditions and boundary conditions as those in Chapter 6, in order to better isolate the effects of the land cover change and to enable a full comparison between the results for future urban expansion and those presented in Chapter 6 for past urbanisation. For the two series all urban characteristics such as building heights, street widths, surface albedo and emissivity were kept constant. The meteorological conditions used for the series of runs were those for a case study ($6^{th}$-$7^{th}$ August 1998) for which the combined METRAS+BEP model performance was evaluated in Chapter 5. These were summertime anti-cyclonic conditions and part of an extended period of strong urban heat island conditions, clear skies and low winds.

## 7.2 Effects of urbanisation for the EXPANSION series

All results are presented for the second day of simulation, in order to avoid any effect due to model spin up. The analysis aims to be consistent with that in Chapter 6, for example model results are compared at the same time, and temperature, DTR and UHI domain averaged values are calculated following the same methods.

### *7.2.1 Spatially averaged near surface temperature*

Both the first two forms of urbanisation were analysed for changes in the domain averaged near surface (z = 10 m) potential temperature at 04:00 and 12:00. It has been seen in Chapter 6 that the increase in urbanisation has the effect of increasing the mean surface potential temperature at 04:00 for all forms of urbanisation, whereas at noon the results show a small or negligible increase.

Figure 7.1 shows an increase in the mean near surface potential temperature at 04:00 as a function of the mean urban land cover fraction for the model simulations of the EXPANSION series described in Table 7.1. The total change in the night time near surface temperature is, however, small. As the number of urbanised grid cells more than doubles, from 3,200 $km^2$ to 7,500 $km^2$, the increase in temperature is less than 1 K. The form of the increase is linear with an $R^2$ of 0.98 and the rate of increase is 3.24 K(mean urban land cover fraction)$^{-1}$. This is smaller than the rate of increase identified for the DENSITY series in Chapter 6 (3.88 K(mean urban land cover fraction)$^{-1}$).

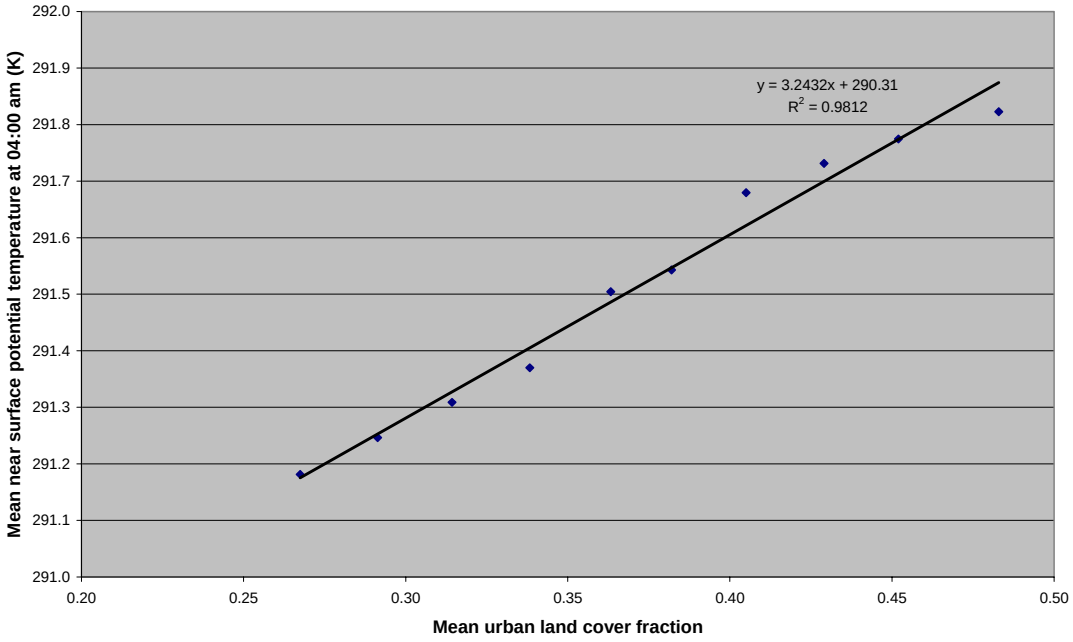


**Figure 7.1: Mean potential temperature (K) as a function of the mean urban land cover fraction as computed by the simulations of the EXPANSION series at 04:00 of the second day of simulation**

Figure 7.2 shows the increase in the mean daytime temperature (at 12:00) as a function of the increasing mean urban land cover fraction for the simulations of the EXPANSION series described in Table 7.1. The domain averaged near surface potential temperature increases more during daytime than during night time. As the number of urban cells more than doubles, the daytime near surface temperature increases by almost 1.4 K. Similarly to the night time results, this result is linear in nature, with an $R^2$ of 0.99 and a rate of increase of 6.25 K(mean urban land cover fraction)$^{-1}$.

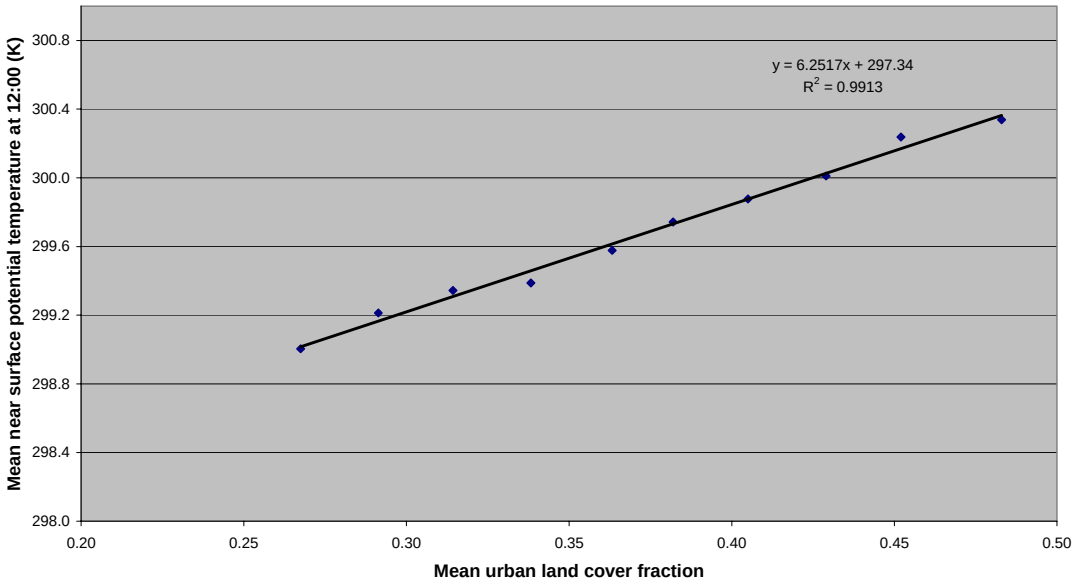


**Figure 7.2: Mean potential temperature (K) as a function of the mean urban land cover fraction as computed by the simulations of the EXPANSION series at 12:00 of the second day of simulation**

At 12:00 the results are significantly different from some of the analysis in Chapter 6, where the maximum rate of increase was 2.93 K(mean urban land cover fraction)$^{-1}$ for the DENSITY series. These results show a change in behaviour when the urban land cover fraction is increased from its current extent. As the urban surface starts to dominate within the domain and the existing urban density within each grid cell is increased at the expense of the rural land use and green space ('Meadows'), there is a sharper, more significant increase in the daytime temperature.

In Chapter 6 it was found that only the DENSITY series showed a significant increase in the domain averaged daytime temperature, whereas the other two series representing past urbanisation showed no significant increase. This result is now confirmed by these model simulations, which represent both the densification and horizontal expansion of the city and which also show an increase in the domain averaged daytime temperature. This result has

important implications for the management of future daytime urban temperatures, as urban expansion and the reduction in green space within cities, coupled with climate change scenarios, could lead to much hotter urban temperatures than currently experienced. This scenario represents the opposite of using vegetation to mitigate urban temperatures, and demonstrates an important reason to preserve green spaces within urban areas.

During night time the increase in the near surface temperature is smaller than during daytime, but nonetheless the urban land cover change represented in this series of simulations causes an increase in the near surface temperature. This is due to the increase in the nocturnal UHI due to the daytime heat storage in the urban building materials and the release of heat during night time.

These results can be compared to Civerolo et al. (2007) who found an average daytime increase of more than 0.6 ºC due to increased urban growth for the New York City metropolitan area.

Figure 7.3 shows the diurnal cycle of the urban heat island intensity for the simulations of the EXPANSION. The scenario described in Chapter 6 representing the current London land use is also included (this simulation is called urban_100) to represent the reference case with respect to which the urban expansion occurs. The urban heat island intensity is calculated in the same way as in Chapter 6, by comparing the simulations to the case of an entirely rural domain (the scenario defined as NOURB in Chapter 6). The second day of simulation is taken to avoid model spin up effects.

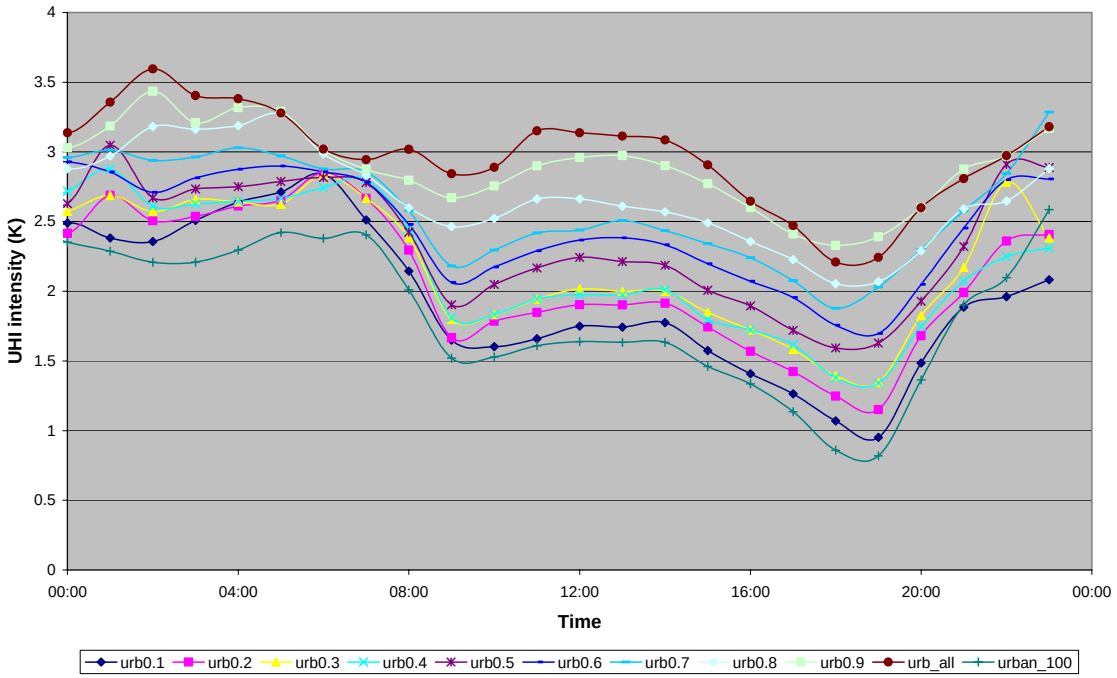


**Figure 7.3: Diurnal cycle of the maximum UHI intensity (K) as computed by the simulations of the EXPANSION series for the second day of simulation**

These results show that as the mean urban land cover within the domain increases, the maximum UHI intensity increases, both during daytime and night time. These results also show how the change in the daytime values dominates over that in the night time values, for example at 19:00 hours the maximum UHI intensity increases from a value of 0.82 K for the current urban situation to around 2.4 K for the most urbanised domain (urb_all), and the difference in UHI between daytime and night time decreases.

Figure 7.4 shows the increase in the maximum UHI intensity at 02:00 as a function the increase in the mean urban land cover fraction. This is consistent with the analysis for the UHI intensity in Chapter 6. The increase in the UHI intensity at 02:00 was also found for the DENSITY series in Chapter 6 and the results suggested that the increase in the suburban land cover was driving the increase in the urban temperature. It appeared in

Chapter 6 that the increase in the nocturnal UHI intensity reached a threshold as the city approached its current extent. The results for the scenarios representing future urbanisation presented in Figure 7.4 show a slow increase for the first six simulations, and then a steeper increase as the urban land cover starts to dominate, covering over 40% of the domain area. A non linearity in the urban effects of expansion and fraction of vegetation within the urban area depending on the size of the urban area has been identified in some previous studies (e.g. Best et al. 2002; Trusilova 2006).

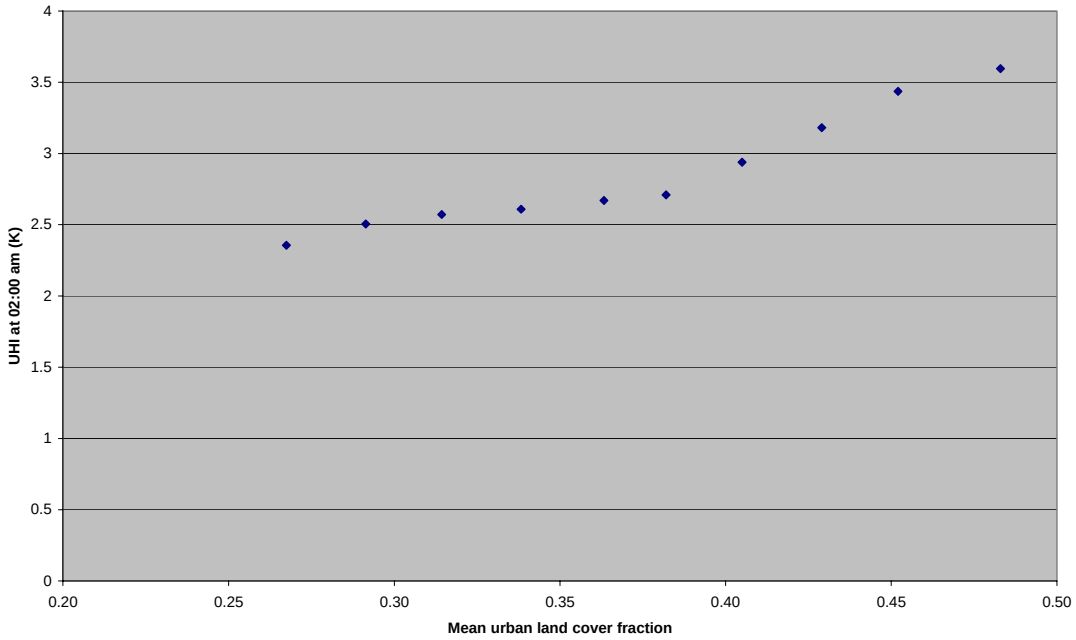


**Figure 7.4: Maximum UHI intensity (K) as a function of mean urban land cover fraction as computed by the simulations in the EXPANSION series at 02:00 of the second day of simulation**

*7.2.2 Diurnal temperature range (DTR)*

The effect of the results presented for the scenarios in the EXPANSION series is that the behaviour of the domain averaged DTR is different from that found in Chapter 6. As a result of the larger increase in the daytime temperature compared to the night time

temperature, an increase in the mean DTR is found (see Figure 7.5). This contradicts both past observational and modelling studies (e.g. Gallo et al. 1996; Easterling et al. 1997; Kalnay et al. 2003), which found a reduction in the DTR with increased urbanisation, due to the fact the daytime temperature increased less rapidly than the night time temperature. Whilst these results appear to contract experimental studies on past urbanisation, an increase in daytime temperatures than exceeds night time temperatures has been observed in a numerical study (Wichansky et al. 2008), although in this case a failure of the model RAMS was identified due to the treatment of anthropogenic heat storage and release.

An increase in the maximum diurnal temperature is also observed in the DENSITY series in Chapter 6, although it was smaller than the increase in the minimum diurnal temperature (night time). The main way in which the DENSITY series differed from the other simulations in Chapter 6 was the fact that the other series removed all of the suburban areas outside of the critical radius which defined the city area. This implies that the more spread out, less dense, suburban areas are critical for determining the increase in the daytime temperature, when compared to a much smaller, more compact city of higher density at the centre of the domain. The series of urban expansion runs presented in this Chapter are also characterised by an increase in the lower density, suburban areas around the city, as well as a densification of the central urban area. The number of urbanised grid cells (defined as having an urban land cover fraction greater than 30%) increases sharply, as well as the mean urban land cover fraction within existing urban cells. This drives a sharper increase in daytime temperatures compared to night time, and the consequent increase in the DTR.

A reason for the sharp increase in daytime temperatures could be the reduction in the water availability within the urbanised grid cells, as the 'Meadows' land cover class is converted to the much drier urban land cover fraction. With less moisture available to absorb the daytime heat, the sensible heat fluxes will increase and consequently raise the daytime temperature. Since the urban areas treated with BEP neglect latent heat fluxes (Martilli 2003), the reduction in 'Meadows' land cover fraction within the domain will cause the urban area to become unrealistically dry because no vegetated surfaces are represented and the lack of cooling through evaporation will raise daytime temperatures (Jonsson 2004). As identified in the sensitivity tests in Chapter 4, changing the fraction of vegetation within an urban area has the highest impact during daytime which explains the larger change in daytime temperatures compared to night time temperatures.

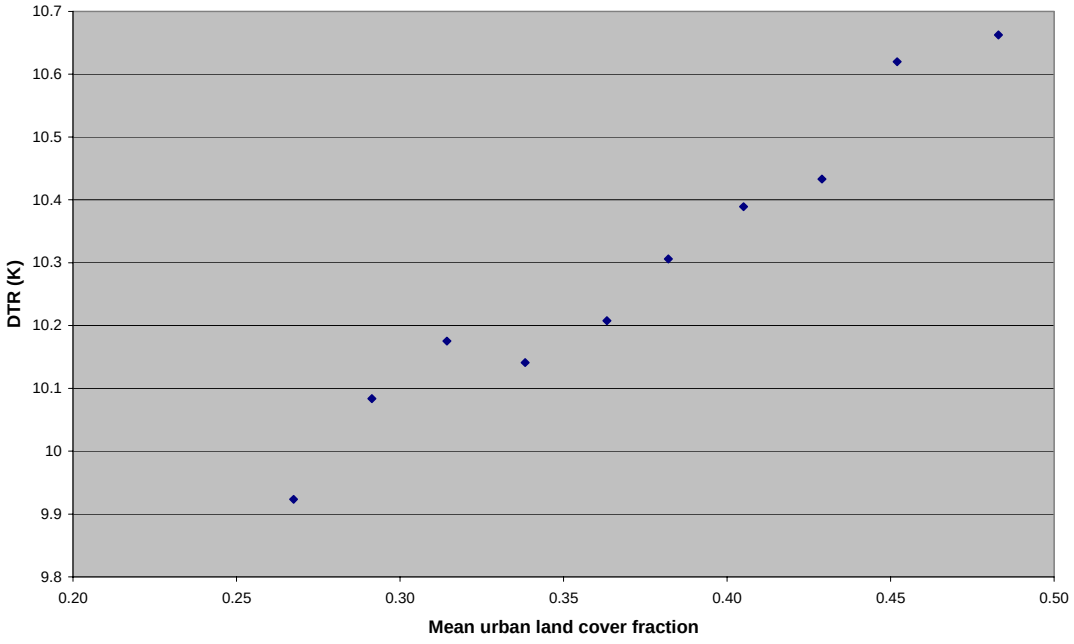


**Figure 7.5: Mean DTR (K) as a function of the mean urban land cover fraction as computed by the simulations in the EXPANSION series for the second day of simulation**

*7.2.3 Wind speed*

The effect of the urban expansion on wind speed is analysed in this section. As seen in Chapter 6, increasing the mean urban land cover fraction has the effect of decreasing the domain averaged wind speed at the first grid level, z = 10 m at both 04:00 and 12:00. Similar results are found here (see Figure 7.6). The total reduction in the mean wind speed is 25% at 04:00, compared to 16% at 12:00.

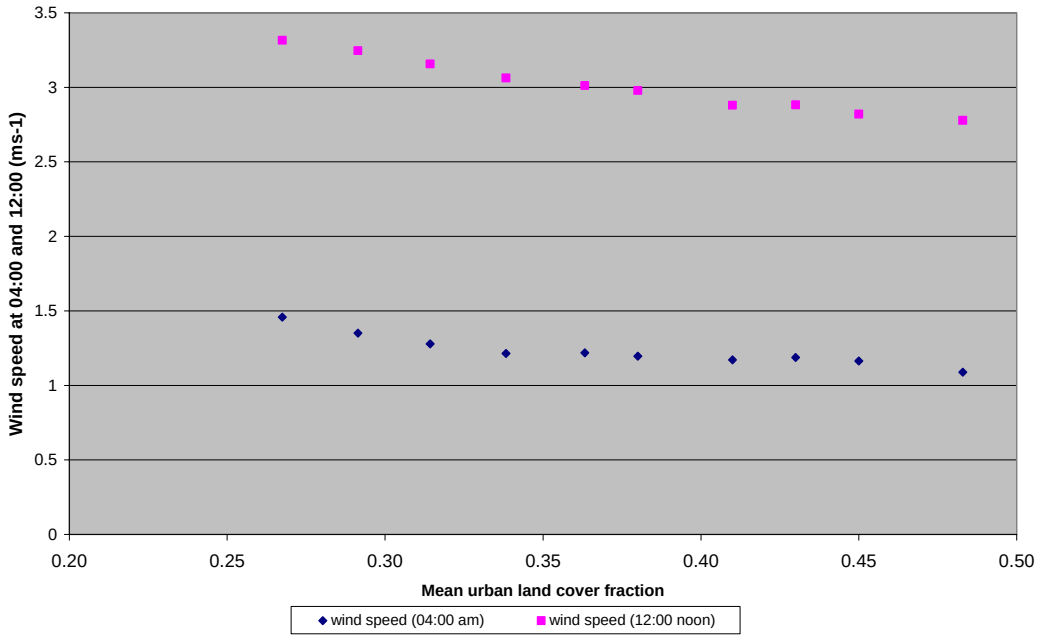


**Figure 7.6: Mean horizontal wind speed ($ms^{-1}$) at z = 10 m as a function of the mean urban land cover fraction as computed by the simulations in the EXPANSION series at 04:00 (blue) and 12:00 (pink) for the second day of simulation**

These % reductions can be compared with those in Klaic et al (2002), who found an average wind speed reductions of 8% and 18% for their two simulations which represented small increases in the urban area of 12.5% and 37.5%. The increase in urban land use is much larger for the simulations in this PhD study, for example the urb_all simulation has an urban area of just under 7,500 $km^2$ compared to the current situation represented by the

URB_BASE case in Chapter 6 of just under 3,200 $km^2$. However it is not directly possible to compare the magnitude of wind speed change with Klaic et al. (2002) due to the differences in the two studies, i.e. the lack of sub grid scale land cover information and the use of a traditional representation of the urban surface in Klaic et al. (2002).

## 7.3 Effects of urbanisation for the DENSIFICATION series

The results of the DENSIFICATION model simulations are analysed in this Section. In this set of runs there was no change in the number of urbanised grid cells. These simulations were based on the domains in which the urban density within a grid cell was increased for existing urban cells (where the urban land cover exceeded a certain threshold i.e. 30%, 40% and 50%) at the cost of green space within the city represented by the 'Meadows' land cover class. The lower density urban cells (below the threshold) remained unchanged. Those cells which are almost 100% urbanised and with zero fractions of "Meadows" land cover also remain unchanged. This lead to a much smaller increase in the mean urban land cover across the whole domain compared to the previous set of simulations. For example in the series '30ABCDEF' (in which all those cells with more than a threshold 30% urban land cover were urbanised) the mean urban land cover fraction of the urban cells increased from 68% to 76%. Therefore any changes in the near surface temperature or wind speed are expected to be smaller, if temperature changes are proportional to the change in the urban land cover.

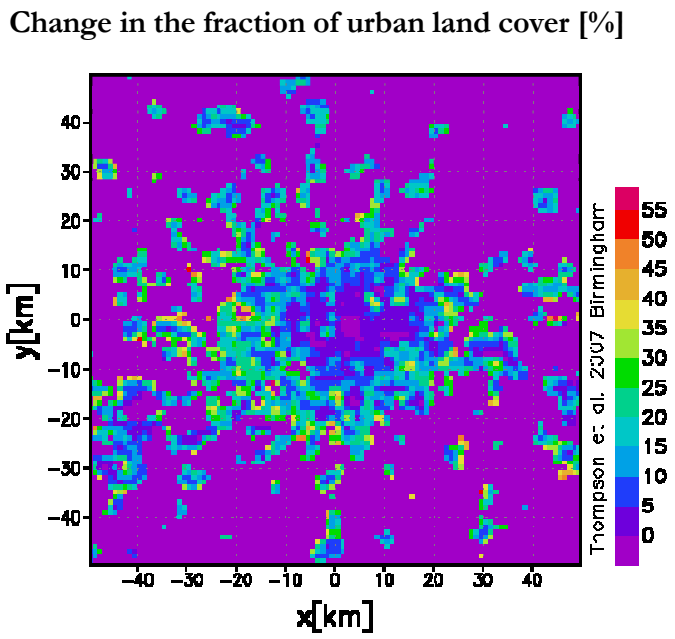


**Figure 7.7: Change in urban land cover for the model simulation '30F' expressed as a percentage change**

Figure 7.7 shows the percentage increase in urban land cover for the '30F' model simulation. This represents the case with the greatest land cover change. For all cells where the existing urban fraction was greater than 30% all of the 'Meadows' land cover was converted to urban land cover. It must be noted that there is very small change in the centre of the London area, since these cells are already almost completely urbanised.

*7.3.1 Spatially averaged near surface temperature*

There were a total of eighteen simulations in this series, as described in Table 7.2. While the total number of urbanised cells did not change, the fraction of urban land cover in the existing number of urbanised cells increased. Changes in the mean near surface potential temperature, when averaged over the whole domain, are very small, with a maximum change of 0.013 K at 04:00 and 0.067 K at 12:00 noon between the least ('30A') and most ('30F') urbanised domains of the '30ABCDEF' series. When compared for example to a

mean near surface potential temperature for simulation '30A' at 04:00 of (291.04 ± 0.39) K and at 12:00 noon of (298.87 ± 0.30) K, then this average change due to the increase urbanisation can be considered negligible. Clearly however the change in temperature during daytime is greater than that at night time, and this is expected as the sensitivity analysis in Chapter 4 showed that vegetation has a greater effect during daytime on temperature.

When considering all three sets of simulations (30ABCDEF, 40ABCDEF and 50ABCDEF), the maximum total change when comparing the most urbanised simulation and the least urbanised simulation is 0.03 K at 04:00 and 0.08 K at 12:00. These changes remain negligible when compared to the variability (standard deviation) in the near surface potential temperature data. The maximum change in the domain averaged DTR between the most urbanised simulation and the least urbanised simulation is 0.13 K, which is also not significant.

Since the change in near surface potential temperature when averaged across the domain is negligible then it is important to investigate whether there is a significant change in the near surface potential temperature for just the cells for which the urban land cover has been changed. Figure 7.8 shows the change in near surface potential temperature for the '30F' simulation when compared with the urban base case of current London land cover, as analysed in Chapter 6.

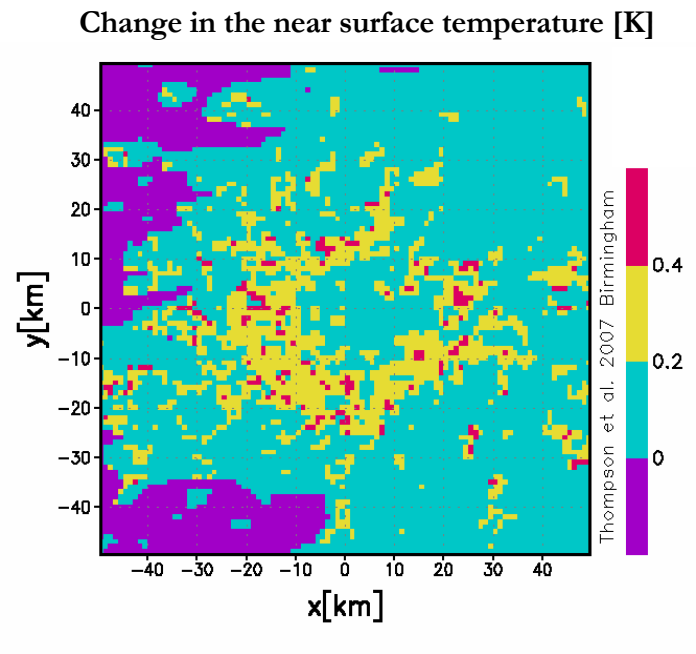


**Figure 7.8: Change in the near surface potential temperature [K] at 12:00 noon for the '30F' simulation compared to the base case of current urban land use for London**

Figure 7.8 shows that the cells for which the land cover is modified do experience a small change in the near surface temperature at 12:00 noon, whereas the unmodified cells experience no change, or a very small change for those situated downwind of the urban area. The average change at 12:00 noon for the modified cells for the '30F' simulation is 0.35 K. This simulation represents the greatest change in land cover amongst all 18 simulations in the DENSIFICATION series, and therefore this could be assumed to represent the maximum effect, averaged across the cells subject to the land cover change.

The change at 12:00 noon is much greater than that observed at night time, in agreement with the results observed for the EXPANSION series in which the day time change is greater than the night time change. From the results of the sensitivity analysis in Chapter 4 it is expected that the effect of vegetation in the urban area will be greatest during daytime.

*7.3.2 Wind speed*

Changes in the mean wind speed are also small in comparison to those which occured when the urban expansion was applied to all grid cells. For example the series '30ABCDEF' shows a total reduction in the mean wind speed of 0.06 $ms^{-1}$ at 04:00 and of 0.04 $ms^{-1}$ at 12:00. This change would also not be considered significant when compared to the variability in the wind speed, for example for simulation '30A' the mean wind speed at 04:00 is (1.48 ± 0.44) $ms^{-1}$.

## 7.4

## Summary and discussion

Future urban expansion has not been extensively studied. Experimental investigations have obviously focused on past temperature and land use records, meaning numerical models are an ideal tool for studying possible future forms of urban expansion. Trusilova (2006) analysed future urbanisation for a large domain representing Europe, but only conducted two scenarios representing the horizontal and vertical expansion of the urban surface. Other studies have focused on the effects of future urbanisation on wind speed (Klaic et al. 2002), surface meteorology and ozone concentrations (Civerolo et al. 2007; Wang et al. 2007), air pollution (Romero et al. 1999) and precipitation (Mölders et al. 2004; Shepherd et al. 2006).

The EXPANSION series of simulations represents the conversion of green space and rural areas both within and surrounding the London urban area to urbanised land cover. The number of urbanised grid cells more than doubles from the current extent to the most urbanised simulation. The urban expansion is found to have a significant effect of near surface temperature, during both daytime and night time. As a result of a larger effect during daytime, the DTR increases as the urban area expands. The conversion of rural cells to urban land cover and the increase in urban land cover fraction for existing urban cells (and consequent reduction in city green space) are the dominant factors in the increase in the temperature in the domain, especially when compared to the results for the DENSIFICATION series in which the number of urban cells doesn't change, but the urban land cover fraction relative to the fraction of green space within the city is increased. This fact could have important implications for urban planning strategies, since it would appear that the urbanisation of rural areas could have a much greater consequence than other urban

expansion strategies such as the reduction in vegetation in existing urban areas. However it must be considered that the change in land cover represented in the DENSIFICATION scenarios is extremely small, and this could have determined the small effect on daytime temperatures and the almost negative effect on night time temperature.

The negligible effect found in the DENSIFICATION series at night time might appear to contradict past studies (e.g. the research by Oke 1987) which suggest that characteristics such as city structure, compactness and sky view factor are more important determinants of the UHI intensity compared to city size. However the DENSIFICATION series does not vary the sky view factor, or compactness of the city – the only thing varied is the relative fraction of urban and 'Meadows' surfaces within the already urbanised grid cells. In the majority of cases the land cover change is extremely small, and it is suggested that this is not sufficient to trigger a change in the near surface temperature at night time. This result could be due to the fact that all the cells which are affected by the land cover change do not become 100% urban land cover but they do maintain a proportion of other land use (e.g. forest, or mixed land use) which will affect the near surface temperature.

The results for the DENSIFICATION series could be investigated further with more targeted model simulations, for example by running simulations for a smaller domain with a higher horizontal resolution in the urbanised cells, or by converting all other land cover types to the urban land cover, not just the "Meadows" (although this might be somewhat unrealistic). Other aspects that should be investigated are the effects of the sky view factor and compactness of the city, as they are considered important determinants of the UHI intensity and have not been investigated in this work (Oke 1987). Representing these in the

BEP urban scheme at the city scale considered in this PhD study is probably not the most appropriate methodology to use.

The increase in the urban fraction in existing urban cells and consequent reduction in green space in the city, represented in the DENSIFICATION series, could simulate the paving of front gardens which currently cover between three and five percent of London's land area (London Assembly 2005). Whilst the results in this Chapter suggest that this conversion would have a small effect on the near surface temperature, with a maximum of 0.35 K during daytime for affected grid cells, other effects which cannot be represented in the METRAS+BEP modelling system are non negligible. For example private gardens are a crucial component of the London ecosystem and wildlife biodiversity. Their covering with hard surfaces affects their ability to absorb rainfall and consequently the vulnerability of the city to flooding and the overburdening of the drainage and sewerage systems (London Assembly 2005).

Currently major urban development is planned to extend the Greater London area to cover much more of the South-East of England (Collier 2006). The results presented in this Chapter suggest that it is highly likely that this urban development will impact local weather, especially if a large amount of rural land cover is converted to built-up areas. Therefore urban effects should be included into the planning of the built environment of the future, to ensure an optimal environment for human well being, for example by protecting the amount of green space within the city (Pinho et al. 2000). This has been recognised for other World cities as a key form of land-use control to break up the UHI phenomenon (Jenerette et al. 2007; Brown et al. 2008). Strategies such as brownfield development

should also be considered to avoid the conversion of extensive rural areas to urban land cover (London Assembly 2005).

Another form of future urban expansion which is not considered here consists in the vertical expansion of the urban area. This represents a situation in which there is considerable pressure on land use and the city is forced to expand in the vertical, by building taller buildings, rather than converting other land covers. It is expected that the development of urban areas with progressively higher buildings will lead to increased temperatures, as seen in the sensitivity studies in Chapter 4. However this is not considered likely to be significant for London, since high rise buildings are generally discouraged except within the central core[3]. For some cities an increase in tall buildings has been documented (e.g. Whitehand et al. 2006; Gaffin et al. 2008), although the vertical expansion is not considered applicable to all urban areas (Grimmond 2007). This form of urban expansion was considered by Trusilova (2006) and found to have an insignificant effect on urban climate.

[3] Changing London: An historic city for a modern world. Report by English Heritage.

# Chapter 8: Conclusions and recommendations for future work

Urban areas represent an extreme form of land cover change, and have well-documented effects on climate at a number of different scales, such as change to local winds, the urban heat island (UHI) effects, changes to precipitation, and increased air pollution. Urban areas have been the subject of many experimental and numerical investigations for a long time. Experimental studies of the urban affect at the regional scale face a number of challenges from obtaining representative measurements at an appropriate scale to identifying methods to classify rural and urban stations. Numerical studies are equally challenging, since it is necessary to parameterise the main thermal and dynamic effects of the heterogeneous and complex urban surface. The correct representation of the urban surface on the atmospheric boundary layer within numerical models has important implications for studying pollutant dispersion and simulating air quality, as well as quantifying urban effects.

The aim of this PhD study was to examine the effects of the urban surface on the major agglomeration of London on local and regional climate by means of the numerical mesoscale model METRAS coupled with the sophisticated urban canopy scheme BEP, developed by Martilli et al. (2002) to represent the dynamic and thermodynamic effects of the urban surface. The implementation of BEP in METRAS has been tested by running the model for an idealised domain and performing a series of sensitivity tests to demonstrate the robustness of the new modelling system. Model results were found to compare favourably with results in the literature for the implementation of BEP into other mesoscale

models, for example Martilli et al. (2002), Martilli (2003), Roulet et al. (2005) and Hamdi (2005). The sensitivity tests have shown that urban characteristics such as the presence of vegetation and the albedo, as well as size of the urban area, can have a significant effect on urban temperatures. This has important implications for the design of cities and the management of urban climate.

A more formal evaluation of the model was performed against meteorological data from UK Met Office London weather stations for a set of case studies and found that the new METRAS+BEP model performed better than the traditional representation of the urban surface; however finding representative measurements for model evaluation was identified as a problem for many cities. This PhD study focused on summertime anti-cyclonic conditions since they are favourable to the development of UHIs. Under climate change scenarios these weather conditions are likely to increase in frequency, which has the effect of increasing the duration and frequency of strong UHI episodes (LCCP 2006).

Having evaluated the model performance, scenarios were run to simulate the effects of past and future land cover changes on near surface temperature and wind fields. These scenarios were constructed based on maps of past land use and assumptions on the future expansion of London. Scenarios were run for 48 hours, allowing a detailed investigation of the effects on near surface meteorological fields (Ichinose 2001; Klaic et al. 2002; Mölders et al. 2004). A full statistical assessment of the urban effects on long term climate was not possible using these short term simulations and therefore this did not fall within the scope of this PhD study. However the investigation of the physical processes involved in the land

cover change and its impact of these meteorological variables is an important step to understanding how the city affects climate at the regional scale.

## 8.1 Conclusions

This work represents a contribution to the development of the METRAS mesoscale model, through the implementation of the urban canopy scheme BEP with its detailed parameterisation of the thermal and dynamic effects of the urban surface. The robustness of the METRAS+BEP system was tested for an idealised domain and it was found to represent key features of the urban surface, such as the UHI effect, better than the original METRAS scheme.

The major contribution of this work is that it represents the development of a tool which can be applied to the London area for detailed investigations of the effects of the urban surface. This work differs from other past investigations into the London climate and UHI, which have focused on the analysis of measurements (Lee 1992), statistical UHI modelling (GLA 2006) and studies on building cooling design (Kolokotroni et al. 2006; Kolokotroni et al. 2007). From a theoretical point of view, the METRAS+BEP modelling system can be used to investigate how changes to the building fabric and form affect the UHI intensity for London, on a variety of different scales. This cannot be done simply via the data analysis or statistical UHI modelling work.

Policy makers are primarily interested in the effects of climate change on people, and where they live (Oleson et al. 2008). This makes the investigation of urban effects a timely issue, since most of the Worlds human population growth over the next years will occur in

cities (Baker et al. 2002). Already more then 80% of the UK population resides in urban areas (DETR 2000). A significant effect of the urban area on regional meteorology and climate has been identified in previous studies for a number of different urban areas (e.g. Dupont et al. 1999; Troude et al. 2002; Trusilova et al. 2008), and has been quantified for London in this PhD study. The urban area, in its current form based on data from the CEH Land Cover Map 2000, is found to affect near surface temperature, the diurnal temperature range (DTR), the UHI, and the near surface wind speed and direction. The effect is shown to have a regional character, with both urban and surrounding rural areas demonstrating a significant impact. Under a given meteorological condition, peak UHI intensities of up to 2.5 K are found during night time hours, with the timing and magnitude of the peak showing good agreement with previous experimental studies for London (Graves et al. 2001).

A large number of studies have investigated the sensitivity of the mesoscale atmospheric models to the presence of vegetation in an urban area, and this was found to have a significant impact on simulated near surface temperatures and air quality (Taha 1996, 1997; Civerolo et al. 2000) and the boundary layer structure (Pielke et al. 1998; Seaman 2000). The results in this PhD study for past urbanisation confirm that the relative fractions of urban land cover and of vegetation within the urban area have important implications for the near surface temperature, DTR, wind speed and UHI intensity. It is suggested that the effect of the relative percentage of urban/vegetation land cover fractions has a more significant effect on these meteorological fields when compared to a more compact urban form. The London Boroughs and Greater London Authority (GLA) have a policy for protecting existing green space from development in order to help offset the UHI effect

(LCCP 2006). It is considered that such policies are vital to avoid urban green spaces being reduced further, with a consequent negative impact on temperatures and human comfort.

Currently, high temperatures are rarely a problem for London (LCCP 2006). However, as average temperatures rise due to climate change, excessive urban temperatures could become a greater problem. Adverse health effects such as increased heat stress and increased mortality have already been observed in extreme cases, such as the heat wave in the summers of 1995 and 2003 (Rooney et al. 1998; Johnson et al. 2005), and higher urban temperatures due to the UHI effect are increasing the installation of air conditioning in homes (LCCP 2006). The results of this PhD study suggest that extensive future growth of the London urban area has the potential to increase temperatures, with significant increases for both daytime and night time. The area of increase coincides generally with the area of increasing urbanisation, although an effect is also identified downwind of the city.

Mitigation strategies, such as reducing the albedo of the urban surface, are also considered for an idealised domain. Changes in albedo are found to have the potential to mitigate daytime urban temperatures by up to 0.4 K for a dense urban area, however retrofitting climate adaptation measures to existing buildings and infrastructure is a costly and challenging task and the benefits must be fully analysed. It is easier to use climate mitigation opportunities in new developments, and therefore their potential must be fully understood so that these might form part of a city-wide planning process for design and construction (LCCP 2006). So far there are no identified systematic policies to implement cool roofs (with lightly coloured coatings to reflect and emit heat, and reduce the UHI effect), however Transport for London have started implementing a similar strategy on

buses, painting the roofs white to reduce absorption of solar radiation (LCCP 2006). However when considering the mitigating potential of high albedo materials it is necessary to also take into account the effect on temperatures during winter months, to ensure the benefit of reducing summertime temperatures is not offset by increased heating demand during winter, and for this reason a modelling approach would require a proper evaluation of METRAS+BEP for winter conditions.

## 8.2 Improvements and recommendations for future work

The work in this PhD study, and in particular the scenarios for past and future urbanisation presented in Chapters 6 and 7, has been limited by the computational demand of the METRAS+BEP model and the resources available at the University of Birmingham. A valuable recommendation for future work would be to devise a faster implementation of the urban module within METRAS and the use of the parallelised version of the model METRAS. Longer simulations would allow a better assessment of the urban effects of climate, for example following some of the methods in Lamptey et al. (2005) and Trusilova et al. (2008) to do a statistical analysis of the effects of the urban surface.

Due to the computational demand of the modelling system, the scope of the analysis has been strictly limited to near surface impacts on temperature and wind speed in and around the urban area. Future work could extend this scope, for example considering the effects of the urbanisation land cover change on the boundary layer structure, surface energy balance. An extension of the model to include air chemistry would permit the model meteorological results to be linked to air quality studies in the urban area.

This PhD study has focussed on the simulation of cloud and rain free days in order to reduce complexity and computational demand. The inclusion of these subroutines could permit an investigation into the effects of the urban area on precipitation. Numerical studies of this sort have been undertaken for many urban areas (Thielen et al. 2000; e.g. Trusilova 2006; Lin et al. 2008) and some experimental studies have observed that the London urban heat island can trigger storms (Atkinson 1968; Hand et al. 2004).

The full influence of different meteorological conditions on the UHI development and intensity has not been part of the scope of this PhD study. The inclusion of the cloud and rain subroutines would permit a full analysis of different weather conditions for the London region, and the impact of meteorological conditions on the UHI. Future work could also investigate the impact of wind speed and direction on the intensity and development of the UHI intensity. These results could be compared with those from experimental studies, for example research for the Greater London Authority observed that heat islands do not occur with wind speeds above 2 $ms^{-1}$ and that there is a shift in the thermal centre of the UHI with wind direction (GLA 2006). Model simulations could be used to attempt to derive a relationship between wind speed and UHI intensity and to confirm if this is a linear relationship.

The evaluation of the METRAS+BEP model for the London region would also benefit from a greater availability of data. For example it was not possible to validate the surface energy fluxes and the turbulent kinetic energy; however these elements of the BEP scheme have been fully validated for other locations, such as Basel (Hamdi 2005; Roulet et al. 2005), Marseille (Hamdi 2005), Athens (Martilli et al. 2003). Future work could also include the incorporation of more precise historical land cover data within the model. As this was not readily available in a digital format it was necessary to infer the distribution of the land cover for the scenarios representing past urbanisation from the literature. Whilst this allows an interesting comparison between different forms of urbanisation, these results could be better related to historic conditions with better land cover information. The definition of the urban parameters for London could also be refined with more detailed building height data.

This work could also be extended by including more scenarios representing mitigation studies. For example the impact of green roofs would make an interesting extension (Bass et al. 2003; Takebayashi et al. 2007). The majority of central London has been identified as able to be retrofitted with green roofs (LCCP 2006), which provide insulation during winter months and reduce overheating during summertime. Changes in albedo could also be considered, as the potential to mitigate daytime temperatures has been identified for the idealised domain. Smaller scale studies could also be performed, for example to investigate local effects of renovation and redevelopment, such as the regeneration of the Docklands area or the 2012 Olympic Games development.

# References


Abercrombie, P. (1945). Greater London Plan 1944. London, HMSO.

Anderson, H. R., A. Ponce de Leon, J. M. Bland, J. S. Bower and D. P. Strachan (1996). "Air pollution and daily mortality in London 1987- 92." British Medical Journal **312**: 665-669.

Angel, S., S. C. Sheppard and D. L. Civco (2005). The Dynamics of Global Urban Expansion. Washington, D.C., Department of Transport and Urban Development, The World Bank.

Angevine, W. M., A. B. White, C. J. Senff, M. Trainer, R. M. Banta and M. A. Ayoub (2003). "Urban-rural contrasts in mixing height and cloudiness over Nashville in 1999." Journal of Geophysical Research-Atmospheres **108**(D3).

Arnfield, A. J. (1998). "Micro-and mesoclimatology." Progress in Physical Geography **22**(1): 403-413.

Arnfield, A. J. (2003). "Two decades of urban climate research: A review of turbulence, exchanges of energy and water, and the urban heat island." International Journal of Climatology **23**: 1-26.

Arnfield, A. J. and C. S. B. Grimmond (1998). "An Urban Canyon Energy Budget Model and its Application to Urban Storage Heat Flux Modelling." Energy Buildings **27**: 61-68.

Atkinson, B. W. (1968). "A preliminary examination of the possible effect of London's urban area on the distribution of thunder rainfall 1951-1960." Transactions of the Institute of British Geographers **44**: 97-118.

Atkinson, B. W. (2003). "Numerical modelling of urban heat-island intensity." Boundary-Layer Meteorology **109**: 285-310.

Avissar, R. (1996). "Potential effects of vegetation on the urban thermal environment." Atmospheric Environment **30**(3): 437-448.

Baker, L. A., A. Brazel, N. Selover, C. Martin, N. McIntyre, F. R. Steiner, A. Nelson and L. Musacchio (2002). "Urbanization and warming of Phoenix (Arizona, USA): Impacts, feedbacks and mitigation." Urban Ecosystems **6**: 183-203.

Baklanov, A., A. G. Mestayer, A. Clappier, S. Zilitinkevich, S. M. Joffe, A. Mahura and N. W. Neilsen (2005). "On the parameterisation of the urban atmospheric sublayer in meteorological models." ACPD: 12119-12176.

Baklanov, A., P. G. Mestayer, A. Clappier, S. Zilitinkevich, S. Joffre, A. Mahura and N. W. Nielsen (2008). "Towards improving the simulation of meteorological fields in urban areas through updated/advanced surface fluxes description." Atmospheric Chemistry and Physics **8**(3): 523-543.

Bass, B., E. S. Krayenhoff, A. Martilli, R. B. Stull and H. Auld (2003). The impact of green roofs on Toronto's urban heat island. First North American Green Roof Conference: Greening Rooftops for Sustainable Communities, Chicago.

Benoit, R., M. Desgagne, P. Pellerin, S. Pellerin, Y. Chartier and S. Desjardins (1997). "The Canadian MC2: A semi-lagrangian, semi-implicit wide band atmospheric model suited for fine scale process studies and simulation." Monthly Weather Review **125**: 2382-2415.

Best, M. J. (2005). "Representing urban areas within operational numerical weather prediction models." Boundary-Layer Meteorology **114**: 91-109.

Best, M. J. (2006). "Progress towards better weather forecasts for city dwellers: from short range to climate change." Theoretical and Applied Climatology **84**(1-3): 47-55.

Best, M. J. and P. R. Clarke (2002). The influence of vegetation on the urban climate. 4th Symposium on the urban environment, Norfolk, Virginia.

Best, M. J., C. S. B. Grimmond and M. G. Villani (2006). "Evaluation of the urban tile in MOSES using surface energy balance observations." Boundary-Layer Meteorology **118**(3): 503-525.

Bilham, E. G. (1938). The climate of the British Isles, London, Macmillan.

Bohnenstengel, S. and K. H. Schlünzen (2008). Performance of different sub-grid-scale surface flux parameterisations for urban areas. COST Action 728. Enhancing mesoscale meteorological modelling capabilities for air pollution and dispersion applications, UK Met Office.

Bonan, G. B. (1997). "Effects of land use on the climate of the United States." Climatic Change **37**: 449-486.

Bornstein, R. D. and K. J. Craig (2001). Urbanisation of numerical mesoscale models. International Symposium on Environmental Hydraulics.

Bornstein, R. D. and D. S. Johnson (1977). "Urban-rural wind velocity differences." Atmospheric Environment **11**(7): 597-604.

Bornstein, R. D. and Q. Lin (2000). "Urban heat islands and summetime convective thunderstorms in Atlanta: three case studies." Atmospheric Environment **34**: 507-516.

Bottema, M. (1997). "Urban Roughness Modelling in Relation to Pollutant Dispersion." Atmospheric Environment **31**: 3059-3075.

Brazdil, R. and M. Budikova (1999). "An urban bias in air temperature fluctuations at the Klementinum, Prague, The Czech Republik." Atmospheric Environment **33**: 4211-4217.

Brazel, A., P. Gober, S.-J. Lee, S. Grossman-Clarke, J. A. Zehnder, B. Hedquist and E. Comparri (2007). "Determinants of changes in regional urban heat island in metropolitan Phoenix (Arizona, USA) between 1990 and 2004." Climate Research **33**: 171-182.

Bretz, S., H. Akbari and A. H. Rosenfeld (1998). "Practical issues for using solar-reflective materials to mitigate urban heat islands." Atmospheric Environment **32**(1): 95-101.

Bretz, S. and A. H. Rosenfeld (1992). Mitigation of Urban Heat Island: Materials and Utility programmes. NIGEC "Supercities", San Francisco, CA.

Britter, R. E. and S. E. Hanna (2003). "Flow and dispersion in urban areas." Annual Review of Fluid Mechanics **35**: 469-496.

Brown, M. (2000). Urban Parameterisations for Mesoscale Meteorological Models. Mesoscale Atmospheric Dispersion. Z. Boybey, Wessex Press**:** 448.

Brown, M. and M. Williams (1998). An Urban Canopy Parameterisation for Mesoscale Meteorological Models. AMS 2nd Urban Environment Symposium, Alberquerque, NM.

Brown, M. A. and F. Southworth (2008). "Mitigating climate change through green buildings and smart growth." Environment and Planning A **40**(3): 653-675.

Burian, S., M. J. Brown and S. P. Velugubantla (2002). Building height characteristics in three U.S. Cities. AMS 4th Symposium on the Urban Environment, Norfolk, VA.

Ca, V. T., T. Asaeda and E. M. Abu (1998). "Reduction in air conditioning energy caused by a nearby park." Journal of Energy and Buildings **29**: 83-92.

Ca, V. T., T. Aseada and Y. Ashie (1999). "Development of a numerical model for the evaluation of the urban thermal environment." Journal of Wind Engineering and Industrial Aerodynamics **81**: 181-191.

Ca, V. T., Y. Ashie and T. Asaeda (2002). "A k-e turbulence closure model for the atmospheric boundary layer including urban canopy." Boundary-Layer Meteorology **102**: 459-490.

Chandler, T. J. (1960). "Wind as a factor of urban temperatures, a survey of North-East London." Weather **15**: 204-213.

Chandler, T. J. (1962). "London's Urban Climate." The Geographical Journal **128**(3): 279-298.

Chandler, T. J. (1965). The climate of London, Hutchinson and Co. Ltd.

Changnon, S. A. (1992). "Inadvertent Weather Modification in Urban Areas: Lessons for Global Climate Change." Bulletin of the American Meteorological Society **73**(5): 619-627.

Changnon, S. A., F. A. Huff and R. G. Semonin (1971). "METROMAX: an investigation of inadvertent weather modification." Bulletin of the American Meteorological Society **52**: 958-967.

Charney, J., W. J. Quirk, S.-H. Chow and J. Kornfeld (1977). "A Comparative Study of the Effects of Albedo Change on Drought in Semi-Arid regions." Journal of Atmospheric Science **34**: 1366-1385.

Christen, A. and R. Vogt (2004). "Energy and radiation balance of a central European city." International Journal of Climatology **24**: 1395-1421.

Civerolo, K. L., C. Hogrefe, B. Lynn, J. Rosenthal, J.-Y. Ku, W. Solecki, J. Cox, C. Small, C. Rosenzweig, R. Goldberg, K. Knowlton and P. Kinney (2007). "Estimating the effects of increased urbanization on surface meteorology and ozone concentrations in the New York City metropolitan region." Atmospheric Environment **41**: 1803-1818.

Civerolo, K. L., G. Sistla, S. T. Rao and D. J. Nowak (2000). "The effects of land use in meteorological modeling: implications for assessment of future air quality scenarios." Atmospheric Environment **34**: 1615-1621.

Clappier, A. and M. W. Rotach (2005). FVM and aLMo models with the BEP module for Basel. FUMAPEX report M4.4, Integrated and validated NWP systems incorporating urban improvements. A. Baklanov**:** 11.

Clark, J. A. (1985). Energy simulation in building design. Bristol, Adam Hilger.

Collier, C. G. (2006). "The impact of urban areas on weather." Quarterly Journal of the Royal Meteorological Society **132**: 1-25.

COMEAP (1998). Quantification of the effects of air pollution on health in Great Britain. T. S. Office, Department of Health Committee on the Medical Effects of Air Pollutants.

Coutts, A. M., J. Beringer and N. J. Tapper (2007). "Impact of increasing urban density on local climate: Spatial and temporal variations in the surface energy balance in Melbourne, Australia." Journal of Applied Meteorology and Climatology **46**(4): 477-493.

Craig, K. J. and R. D. Bornstein (2002). Urbanisation of Numerical Mesoscale Models. Workshop on urban boundary layer parameterisations.

de Jong, B. (1973). Net radiation received by a horizontal surface at the Earth, Delft University Press.

Deardroff, J. W. (1978). "Efficient prediction of ground surface temperature and moisture, with inclusion of a layer of vegetation." Journal of Geophysical Research-Atmospheres **83**: 1889-1903.

DETR (2000). Our towns and cities: the future. CM 4911. London, DETR.

Dhakal, S. and K. Hanaki (2002). "Improvement of urban thermal environment by managing heat discharge sources and surface modification in Tokyo." Energy and Buildings **34**: 13-23.

Dimoudi, A. and M. Nikolopoulou (2003). "Vegetation in the urban environment: microclimatic analysis and benefits." Energy and Buildings **35**: 69-76.

Dupont, E., L. Menut, B. Carissimo, J. Pelon and P. Flamant (1999). "Comparison between the atmospheric boundary layer in Paris and its rural suburbsn during the ECLAP experiment." Atmospheric Environment **33**: 979-994.

Dupont, S., T. L. Otte and J. K. S. Ching (2004). "Simulation of meteorological fields within and above urban and rural canopies with a mesoscale model (MM5)." Boundary-Layer Meteorology **113**: 111-158.

Dyer, A. J. (1974). "A review of flux-profile relationships." Boundary-Layer Meteorology **7**: 362-372.

Easterling, D. R., B. Horton, P. D. Jones, T. C. Peterson, T. R. Karl, D. E. Parker, M. J. Salinger, V. Razuvayev, N. Plummer, P. Jamason and C. K. Folland (1997). "Maximum and minimum Temperature Trends for the Globe." Science **277**: 364-367.

Eliasson, I. (1996). "Urban nocturnal temperatures, street geometry and land use." Atmospheric Environment **30**: 379-392.

Fan, H. L. and D. J. Sailor (2005). "Modeling the impacts of anthropogenic heating on the urban climate of Philadelphia: a comparison of implementations in two PBL schemes." Atmospheric Environment **39**(1): 73-84.

Feigenwinter, C., R. Vogt and E. Parlow (1999). "Vertical structure of Selected Turbulence Characteristics above an Urban Canopy." Theoretical and Applied Climatology **62**: 51-63.

Fenger, J. (1999). "Urban air quality." Atmospheric Environment **33**: 4877-4900.

Figueroa, P. I. and N. A. Mazzeo (1998). "Urban-Rural Temperature Differences in Buenos Aires." International Journal of Climatology **18**: 1709-1723.

Fortuniak, K., K. Klysik and J. Wibig (2005). "Urban-rural contrasts of meteorological parameters in Lodz." Theoretical and Applied Climatology **84**: 91-101.

Fragkou, E., R. Sokhi, E. Batchvarova and N. Kitwiroon (2004). Sensitivity analysis of MM5 to meteorological parameters during an episode period for London. 9th International Conference on Harmonisation within Atmospheric Dispersion Modelling for Regulatory Purposes, Garmish-Partenkirchen.

Gaffin, S. R., C. Rosenzweig, R. Khanbilvardi, L. Parshall, S. Mahani, H. Glickman, R. Goldberg, R. Blake, R. B. Slosberg and D. Hillel (2008). "Variations in New York city's urban heat island strength over time and space." Theoretical and Applied Climatology **In press**.

Gallo, K. P., D. R. Easterling and T. C. Peterson (1996). "The influence of Land-Use/land Cover on Climatological Values of the Diurnal Temperature Range." Journal of Climate **9**(11): 2941-2944.

Gallo, K. P., T. W. Owen, D. R. Easterling and P. Jamason (1999). "Temperature trends of the U.S. Historical Climatology Network Based on Satellite-Designated Land Use/Land Cover." Journal of Climate **12**: 1344-1348.

Gedzelman, S. D., S. Austin, J. E. Cermak, N. Stefano, S. Partridge, S. Quesenberry and D. A. Robinson (2003). "Mesoscale aspects of the urban heat island around New York City." Theoretical and Applied Climatology **75**: 29-42.

Gill, S. E., J. F. Handley, A. R. Ennos and S. Pauleit (2007). "Adapting Cities for Climate Change: The Role of the Green Infrastructure." Built Environment **33**(1): 115-133.

Givati, A. and D. Rosenfeld (2004). "Quantifying precipitation suppression due to air pollution." Journal of Applied Meteorology **43**: 1038-1056.

GLA (2006). London's Urban Heat Island. London, Greater London Authority.

Gomez, F., E. Gaja and A. Reig (1998). "Vegetation and climatic changes in a city." Ecological Engineering **10**: 355-360.

Graves, H. M., R. Watkins, P. Westbury and P. J. Littlefair (2001). Cooling Buildings in London, London CRC Ltd.

Grimmond, C. S. B. (2007). "Urbanization and global environmental change: local effects of urban warming." The Geographical Journal **173**: 83-88.

Grimmond, C. S. B., H. A. Cleugh and T. R. Oke (1991). "An objective urban heat storage model and its comparison with other schemes." Atmospheric Environment **25**: 311-326.

Grimmond, C. S. B. and T. R. Oke (2002). "Turbulent heat fluxes in urban areas: Observations and local scale urban meteorological parameterization scheme (LUMPS)." Journal of Applied Meteorology **41**: 729-810.

Grossman-Clarke, S., J. A. Zehnder, W. L. Stefanov, Y. Liu and M. A. Zoldak (2005). "Urban Modifications in a Mesoscale Meteorological Model and the Effects on Near Surface Variables in an Arid Metropolitan Region." Journal of Applied Meteorology **44**(9): 1281-1297.

Hacker, J., R. Slater, S. E. Belcher, G. McGregor and S. Gosling (2007). Understanding London's Urban Climate. Climate change and the urban heat island: Implications for building design summer weather data. O. A. a. P. Ltd, Greater London Authority.

Hall, P. (1974). "The Containment of Urban England." The Geographical Journal **140**(3): 386-408.

Hamdi, R. (2005). Numerical study of the atmospheric boundary layer over urban areas: Validation for the cities of Basel and Marseilles, Universite Catholique de Louvain.

Hamdi, R. and G. Schayes (2005). "Validation of the Martilli's urban boundary layer scheme with measurements from two mid-latitude European cities." ACPD **5**: 4257-5038.

Hand, W. H., N. I. Fox and C. G. Collier (2004). "A study of twentieth-century extreme rainfall events in the United Kingdom with implications for forecasting." Meteorological Applications **11**(15-31).

Harman, I. N. (2003). The Energy Balance of Urban Areas. Department of Meteorology, University of Reading.

Harman, I. N., J. F. Barlow and S. E. Belcher (2004). "Scalar fluxes from urban street canyons. Part II: Model." Boundary-Layer Meteorology **113**(3): 387-409.

Hawkins, T. W., A. J. Brazel, W. L. Stefanov, W. Bigler and E. M. Saffell (2004). "The role of rural variability in urban heat island determination for Phoenix, Arizona." Journal of Applied Meteorology **43**(3): 476-486.

He, J. F., J. Y. Liu, D. F. Zhuang, W. Zhang and M. L. Liu (2007). "Assessing the effect of land use/land cover change on the change of the urban heat island intensity." Theoretical and Applied Climatology **90**: 217-226.

Henderson-Sellers, A., R. E. Dickinson, T. B. Durbidge, P. J. Kennedy, K. McGuffie and A. J. Pitman (1993). "Tropical Deforestation: Modelling Local to Regional Scale Climate Change." Journal of Geophysical Research **98**: 7289-7315.

Howard, L. (1833). The Climate of London. London, Harvey and Darton.

Hulme, M. and E. Barrow (1997). The Climate of the British Isles. London, Routledge.

Hulme, M., G. J. Jenkins, X. Lu, J. R. Turnpenny, T. D. Mitchell, R. G. Jones, J. Lowe, J. M. Murphy, D. Hassell, P. Boorman, R. McDonald and S. Hill (2002). Climate change scenarios for the UK: The UKCIP02 Scientific Report, Tyndall Centre for Climate Change Research, School of Environmental Sciences, University of East Anglia.

Hunt, J. (2005). London's Environment. Prospects for a Sustainable World City. London, Imperial College Press.

Hunter, L., I. D. Watson and G. T. Johnson (1991). "Modeling air flow regimes in urban canyons." Energy and Buildings **15**: 315-324.

Ichinose, T. (2001). Regional warming related to Land Use Change during the Past 135 Years In Japan. Present and Future Modeling Global Environmental Change:Toward Integrated Modeling. T. Matsumo and H. Kida, TERRAPUB**:** 433-440.

Ichinose, T., K. Shimodozono and K. Hanaki (1999). "Impact of anthropogenic heat on urban climate in Tokyo." Atmospheric Environment **33**: 3897-3909.

Inoue, T. and F. Kimura (2004). "Urban effects on low-level clouds around the Tokyo metropolitan area on clear summer days." Geophysical Research Letters **31**.

IPCC (2001). Climate Change 2001: The Scientific Basis, Cambridge University Press, UK.

Jauregui, E. (1990). "Influence of a large urban park on temperature and convective precipitation in a tropical city." Journal of Energy and Buildings **15-16**: 457-463.

Jauregui, E. (1997). "Heat island development in Mexico City." Atmospheric Environment **31**: 3821-3831.

Jauregui, E. (2005). "Possible impact of urbanization on the thermal climate of some large cities in Mexico." Atmosfera **18**(4): 247-252.

Jauregui, E. and E. Luyando (1999). "Global radiation attenuation by air pollution and its effects on the thermal climate in Mexico City." International Journal of Climatology **19**: 683-694.

Jauregui, E. and E. Romales (1996). "Urban effects on convective precipitation in Mexico City." Atmospheric Environment **30**(20): 3383-3389.

Jenerette, G. D., S. L. Harlan, A. Brazel, N. Jones, L. Larsen and W. L. Stefanov (2007). "Regional relationships between surface temperature, vegetation, and human settlement in a rapidly urbanizing ecosystem." Landscape Ecology **22**: 353-365.

Jin, M. and J. M. Shepherd (2005). "Inclusion of urban landscape in a climate model. How can satellite data help?" Bulletin of the American Meteorological Society **5**: 681-689.

Johnson, H., R. S. Kovats, G. McGregor, J. R. Stedman, M. Gibbs and H. Walton (2005). "The impact of the 2003 heatwave on daily mortality in England and Wales and the use of rapid weekly mortality estimates." Eurosurveillance **10**(7-8): 168-171.

Jones, P. D., P. Y. Groisman, M. Coughlan, N. Plummer, W. C. Wong and T. R. Karl (1990). "Assessment of Urbanization Effects in Time Series of Surface Air Temperature over Land." Nature **347**: 169-177.

Jonsson, P. (2004). "Vegetation as an urban climate control in the subtropical city of Gabarone, Botswana." International Journal of Climatology **24**: 1307-1322.

Kalnay, E. and M. Cai (2003). "Impact of urbanization and land-use change on climate." Nature **423**(6939): 528-531.

Kalnay, E., M. Cai, H. Li and J. Tobin (2006). "Estimation of the impact of land-surface forcings on temperature trends in eastern United States." Journal of Geophysical Research-Atmospheres **111**(D6).

Kan, H., S. J. London, H. Chen, G. Song, G. Chen, L. Jiang, N. Zhao, Y. Zhang and B. Chen (2007). "Diurnal temperature range and daily mortality in Shanghai, China." Environmental Research **103**: 424-431.

Karaca, M., M. Tayanc and H. Toros (1995). "Effects of urbanization on climate of Istanbul and Ankara." Atmospheric Environment **29**(23): 3411-3421.

Karl, T. R., H. F. Diaz and G. Kukla (1988). "Urbanization: Its detection and effect in the United States Climate Record." Journal of Climate **1**: 1099-1123.

Klaic, Z. B., T. Nitis, I. Kos and N. Moussiopoulos (2002). "Modification of the local winds due to hypothetical urbanization of the Zagrep surroundings." Meteorology and Atmospheric Physics **79**(1-2): 1-12.

Klysik, K. and K. Fortuniak (1999). "Temporal and spatial characteristics of the urban heat island of Lodz, Poland." Atmospheric Environment **33**: 3885-3895.

Kolokotroni, M., I. Giannitsaris and R. Watkins (2006). "The effect of the London urban heat island on building summer cooling demand and night ventilation strategies." Solar Energy **80**: 383-392.

Kolokotroni, M., Y. Zhang and R. Watkins (2007). "The London Heat Island and building cooling design." Solar Energy **81**: 102-110.

Kovats, R. S., S. Hajat and P. Wilkinson (2004). "Contrasting patterns of mortality and hospital admissions during hot weather and heat waves in Greater London, UK." Occupational Environmental Medicine **61**: 893-898.

Krayenhoff, E. S., A. Martilli, B. Bass and R. B. Stull (2005). Mesoscale simulation of urban heat island mitigation strategies in Toronto, Canada. ICUC5, Lodz, Poland.

Kusaka, H. and F. Kimura (2004). "Thermal effects of urban canyon structure on the nocturnal heat island: Numerical experiment using a mesoscale model coupled with an urban canopy model." Journal of Applied Meteorology **43**: 1899-1910.

Kusaka, H., H. Kondo, Y. Kikegawa and F. Kimura (2001). "A simple single-layer urban canopy model for atmospheric models: Comparison with multi-layer and slab models." Boundary-Layer Meteorology **101**: 329-358.

Lamptey, B. L., E. J. Barron and D. Pollard (2005). "Impacts of agriculture and urbanizationon the climate of the Northeastern United States." Global and Planetary Change **49**: 203-221.

Landsberg, H. E. (1981). The urban climate, Academic Press.

Laval, K. and L. Picon (1986). "Effect of a Change of the Surface Albedo of the Sahel on Climate." Journal of Atmospheric Science **43**: 2418-2429.

LCCP (2002). London's Warming: The impacts of climate change on London.

LCCP (2006). Adapting to climate change. Lessons for London. London, Greater London Authority.

Lee, D. (1977). "Urban Influence on Wind Directions over London." Weather, 32 (5), 162-170

Lee, D. O. (1979). "Influence of Atmospheric Stability and the Urban Heat Island on Urban-Rural Wind Speed Differences." Atmospheric Environment **13**(8): 1175-1180.

Lee, D. O. (1992). "Urban Warming? An analysis of recent trends in London's heat island." Weather **47**: 50-56.

Lee, D. O. (1993). "Climatic change and air quality in London." Geography **78**: 77-79.

Lee, H. Y. (1988). "An Application of NOAA AVHRR Thermal Data to the Study of the Urban Heat Island." Atmospheric Environment **27B**: 1699-1720.

Lee, S.-H. and H.-D. Kim (2008). "Effects of Regional Warming due to Urbanization on Daytime Local Circulations in a Complex Basin of the Daegu Metropolitan Area, Korea." Journal of Applied Meteorology **47**: 1427-1441.

Lemonsu, A. and V. Masson (2002). "Simulation of a summer urban breeze over Pairs." Boundary-Layer Meteorology **104**: 463-490.

Lin, C.-Y., W.-C. Chen, S. C. Liu, Y. A. Liou, G. R. Liu and T. H. Lin (2008). "Numerical study of the impact of urbanisation on the precipitation over Taiwan." Atmospheric Environment **42**: 2934-2947.

London Assembly. (2005). Crazy Paving. The environmental importance of London's front gardens. London, Greater London Authority.

London Assembly. (2005). Dereliction of Duty? A report on brownfield development for London. London, Greater London Authority.

London Assembly. (2006). Offside. The loss of London's playing fields, Greater London Authority.

London Climate Change Adaptation Strategy. (2008). Greater London Authority.

London Research Centre. (1992). London Housing Survey, London Research Centre.

Longley, P., M. Batty, J. Shepherd and G. Sadler (1992). "Do Green Belts Change the Shape of Urban Areas? A Preliminary Analysis of the Settlement Geography of South East England." Regional Studies **26**: 437-452.

Louis, J. F. (1979). "A Parametric Model of Vertical Eddies Fluxes in the Atmosphere." Boundary-Layer Meteorology **17**: 187-202.

Lowry (1998). "Urban effects on precipitation amount." Progress in Physical Geography **22**(4): 477-520.

Lowry, W. P. (1977). "Empirical estimation of urban effects on climate: a problem analysis." Journal of Applied Meteorology **16**: 129-135.

Lüpkes, C. and K. H. Schlünzen (1996). "Modelling the Arctic convective boundary-layer with different turbulence parameterizations." Boundary-Layer Meteorology **79**(1-2): 107-130.

Mailhot, J., S. Belair, A. Lemonsu, L. Tong, A. Leroux, N. Benbouta and R. Hogue (2007). Urban modelling at the Meteorological Service of Canada. The E.G.U Newsletter.

Martilli, A. (2002). "Numerical study of urban impact on boundary layer structure: Sensitivity to wind speed, urban morphology, and rural soil moisture." Journal of Applied Meteorology **41**(12): 1247-1266.

Martilli, A. (2003). "A two-dimensional numerical study of the impact of a city on atmospheric circulation and pollutant dispersion in a coastal environment." Boundary-Layer Meteorology **108**(1): 91-119.

Martilli, A. (2007). "Current research and future challenges in urban mesoscale modelling." International Journal of Climatology **27**(14): 1909-1918.

Martilli, A., A. Clappier and M. W. Rotach (2002). "An urban surface exchange parameterisation for mesoscale models." Boundary-Layer Meteorology **104**(2): 261-304.

Martilli, A., Y. A. Roulet, M. Junier, F. Kirchner, M. W. Rotach and A. Clappier (2003). "On the impact of urban surface exchange parameterisations on air quality simulations: the Athens case." Atmospheric Environment **37**(30): 4217-4231.

Martilli, A. and R. Schmitz (2007). Implementation of an Urban Canopy Parameterization in WRF-chem. Preliminary results. The Seventh Symposium on the Urban Environment, San Diego, CA.

Masson, V. (2000). "A physically-based scheme for the urban energy budget in atmospheric models." Boundary-Layer Meteorology **94**: 357-397.

Masson, V. (2006). "Urban surface modelling and the meso-scale impact of cities." Theoretical and Applied Climatology **84**: 35-45.

Masson, V., C. S. B. Grimmond and T. R. Oke (2002). "Evaluation of the Town Energy Balance (TEB) scheme with direct measurements from dry districts in two cities." Journal of Applied Meteorology **41**(10): 1011-1026.

Mesinger, F. and A. Arakawa (1976). "Numerical methods used in atmospheric models." Garp Publication series **17**(1).

Mogridge, M. and J. B. Parr (1997). "Metropolis or Region: On the Development and Structure of London." Regional Studies **31**: 97-115.

Mölders, N. and M. A. Olsen (2004). "Impact of urban effects on precipitation in high latitudes." Journal of Hydrometeorology **5**: 409-429.

Moreno, M. C. (1994). "Intensity and Form of the Urban Heat Island in Barcelona." International Journal of Climatology **14**: 705-710.

Morris, C. J. G., I. Simmonds and N. Plummer (2001). "Quantification of the influences of wind and cloud on the nocturnal urban heat island of a large city." Journal of Applied Meteorology **40**: 169-182.

Muller, C. (2007). Improvement of an urban turbulence parameterization for meteorological operational forecast and air quality modeling. Lausanne, EPFL.

Myrup, L. (1969). "A numerical model of the Urban Heat Island." Journal of Applied Meteorology **8**: 908-918.

Nitis, T., Z. B. Klaic and N. Moussiopoulos (2005). Effects of topography on urban heat island. 10th International Conference on Harmonisation within Atmospheric Dispersion Modelling for Regulatory Purposes, Sissi (Malia), Crete, Greece.

Nowak, D. J., K. L. Civerolo, S. T. Rao, G. Sistla, C. J. Luley and D. E. Crane (2000). "A modeling study of the impact of urban trees on ozone." Atmospheric Environment **34**: 1601-1613.

Oestges, C., S. R. Saunders and D. Vanhoenacker-Janvier (1999). Physical statistical modelling of the land mobile satellite channel based on ray tracing. IEE Proceedings - Microwave Antennas Propagation.

Offerle, B., C. S. B. Grimmond and T. R. Oke (2003). "Parameterisation of Net All-Wave Radiation for Urban Areas." Journal of Applied Meteorology **42**: 1157-1173.

Oke, T. R. (1981). "Canyon geometry and the nocturnal heat island. Comparison of scale model and field observations." Journal of Climatology **1**: 237-254.

Oke, T. R. (1982). "The Energetic Basis of the Urban Heat-Island." Quarterly Journal of the Royal Meteorological Society **108**(455): 1-24.

Oke, T. R. (1987). Boundary layer climates.

Oke, T. R. (1988). "The Urban Energy-Balance." Progress in Physical Geography **12**(4): 471-508.

Oke, T. R. (1989). "The Micrometeorology of the Urban Forest." Philosophical Transactions of the Royal Society of London Series B-Biological Sciences **324**(1223): 335-349.

Oke, T. R. (1995). The Heat Island of the Urban Boundary Layer: Characteristics, Causes and Effects. Wind Climate of Cities. J. E. e. a. Cermak. Dordrecht, Boston, Kluwer Academic Publishers**:** 81-107.

Oke, T. R. (1997). Urban Environments. The surface climates of Canada. W. B. Bailey, T. R. Oke and W. R. Rousse. Montreal, McGill-Queen's University Press**:** 303-327.

Oke, T. R., G. T. Johnson, D. G. Steyn and I. D. Watson (1991). "Simulation of surface urban heat islands under "Ideal" conditions at night. Part 2: Diagnosis of causation." Boundary-Layer Meteorology **56**: 339-358.

Oke, T. R., B. D. Kalanda and D. G. Steyn (1981). "Parameterization of Heat-Storage in Urban Areas." Urban Ecology **5**(1): 45-54.

Oke, T. R. and G. B. Maxwell (1975). "Urban Heat Island Dynamics in Montreal and Vancouver." Atmospheric Environment **9**(2): 191-200.

Oleson, K. W., G. B. Bonan, J. Feddema and M. Vertenstein (2008). "An urban parameterization for a global climate model. Part II: Sensitivity to input parameters and the simulated urban heat island in offline Simulations." Journal of Applied Meteorology and Climatology **47**(4): 1061-1076.

Oleson, K. W., G. B. Bonan, J. Feddema, M. Vertenstein and C. S. B. Grimmond (2008). "An urban parameterization for a global climate model. Part I: Formulation and evaluation for two cities." Journal of Applied Meteorology and Climatology **47**(4): 1038-1060.

Otte, T. L., A. Lacser, S. Dupont and J. K. S. Ching (2004). "Implementation of an urban canopy parameterization in a mesoscale meteorological model." Journal of Applied Meteorology.

Palumbo, A. and A. Mazzarella (1980). "Rainfall Statistical Properties in Naples." Monthly Weather Review **108**: 1041-1045.

Parker, D. J. (1995). Hazard in the London megacity, Middlesex University.

Peterson, J. T. (1969). The climate of cities: a survey of recent literature, NAOCA Publications.

Philandras, C. M., D. A. Metaxas and P. T. Nastos (1999). "Climate variability and urbanization in Athens." Theoretical and Applied Climatology **63**: 65-72.

Pielke, R. A. (1984). Mesoscale meteorological modeling. San Diego, Academic Press.

Pielke, R. A., G. Marland, R. A. Betts, T. N. Chase, J. L. Eastman, J. O. Niles, D. S. Niyogi and S. W. Running (2002). "The influence of land-use change and landscape dynamics on the climate system: relevance to climate-change policy beyond the radiative effect of greenhouse gases." Philosophical Transactions of the Royal Society of London. Series A - Mathematical, Physical and Environmental Sciences **360**(1797): 1705-1719.

Pielke, R. A. and M. Uliasz (1998). "Use of meteorological models as input to regional and mesoscale air quality models - limitations and strengths." Atmospheric Environment **32**: 1455-1466.

Pinho, O. S. and M. D. Manso-Orgaz (2000). "The urban heat island in a small city in coastal Portugal." International Journal of Biometeorology **44**: 198-203.

Pino, D., J. Vila-Guerau de Arellano, A. Comeron and F. Rocadenbosch (2004). "The boundary layer growth in au urban area." Science of the Total Environment **334-335**: 207-213.

Piringer, M., C. S. B. Grimmond, S. M. Joffre, P. Mestayer, D. R. Middleton, M. W. Rotach, A. Baklanov, K. De Ridder, J. Ferreira, E. Guilloteau, A. Karppinen, A. Martilli, V. Masson and M. Tombrou (2002). "Investigating the surface energy

balance in urban areas - Recent advances and future needs." Water, Air and Soil Pollution: Focus **2**: 1-16.

Pitman, A. J. (2003). "The evolution of, and revolution in, land surface schemes designed for climate models." International Journal of Climatology **23**: 479-510.

Pujadas, M., J. Plaza, J. Teres, B. Artinano and M. Millan (2000). "Passive remote sensing of nitrogen dioxide as a tool for tracking air pollution in urban areas: the Madrid urban plume, a case of study." Atmospheric Environment **34**(19): 3041-3056.

Rabin, R. M. and D. W. Martin (1996). "Satellite observations of shallow cumulus coverage over the central United States: An exploration of land use impact on cloud cover." Journal of Geophysical Research-Atmospheres **101**(D3): 7149-7155.

Ratti, C., S. Di Sabatino, R. E. Britter, M. Brown, F. Caton and S. Burian (2001). Analysis of 3-D Urban Databases with Respect to Polluttion Dispersion for a Number of European and American Cities. Third International Conference on Urban Air Quality, Loutraki, Greece.

Rigby, M. and R. Toumi (2008). "London air pollution climatology: Indirect evidence for urban boundary layer height and wind speed enhancement." Atmospheric Environment **42**: 4932-4947.

Romero, H., M. I. A. Rivera, P. Zalazar and P. Azocar (1999). "Rapid urban growth, land use changes and air pollution in Santiago, Chile." Atmospheric Environment **33**: 4039-4047.

Rooney, C., A. J. McMichael, R. S. Kovats and M. Coleman (1998). "Excess mortality in England and Wales, and in Greater London, during the 1995 heatwave." Journal of Epidemiology and Community Health **52**: 482-486.

Rosenfeld, A. H., H. Akbari, S. Bretz, B. L. Fishman, D. M. Kurn, D. J. Sailor and H. Taha (1995). "Mitigation of urban heat islands: materials, utility programs, updates." Energy and Buildings **22**: 255-265.

Rosenfeld, A. H., H. Akbari, J. J. Romm and M. Pomerantz (1998). "Cool communities: strategies for heat island mitigation and smog reduction." Energy and Buildings **28**: 51-62.

Rotach, M. W. (1993). "Turbulence Close to a Rough Urban Surface. Part 1: Reynolds Stress." Boundary-Layer Meteorology **65**: 1-28.

Rotach, M. W. (1995). "Profiles of turbulence statistics in and above an urban street canyon." Atmospheric Environment **29**: 1473-1486.

Rotach, M. W. (1999). "On the Influence of the urban roughness sublayer on turbulence and dispersion." Atmospheric Environment **33**: 401-408.

Roth, H., T. R. Oke and W. J. Emery (1984). "Satellite-derived Urban Heat Islands from Three Coastal Cities and the Utilization of Such Data in Urban Climatology." International Journal of Remote Sensing **10**: 1-13.

Roth, M. (2000). "Review of atmospheric turbulence over cities." Quarterly Journal of the Royal Meteorological Society **126**: 1941-1990.

Roth, M. and T. R. Oke (1993). "Turbulent Transfer Relationships over an Urban Surface .1. Spectral Characteristics." Quarterly Journal of the Royal Meteorological Society **119**(513): 1071-1104.

Roulet, Y. A., A. Martilli, M. W. Rotach and A. Clappier (2005). "Validation of an urban surface exchange parameterization for mesoscale models - 1D case in a street canyon." Journal of Applied Meteorology **44**(9): 1484-1498.

Sailor, D. J. (1995). "Simulated urban climate response to modifications in surface albedo and vegetative cover." Journal of Applied Meteorology **34**: 1694-1704.

Sailor, D. J. (1998). "Simulations of annual degree day impacts of urban vegetative augmentation." Atmospheric Environment **32**(1): 43-52.

Sailor, D. J. and H. L. Fan (2004). The importance of including anthropogenic heating in mesoscale modeling of the urban heat island. 84th Annual Meeting of the AMS. Symposium on Planning, Nowcasting and Forecasting in the Urban Zone, Seattle.

Sarrat, C., A. Lemonsu, V. Masson and D. Guedalia (2006). "Impact of urban heat island on regional atmospheric pollution." Atmospheric Environment **40**: 1743-1758.

Schlünzen, K. H. (1988). "Das mesoskalige Transport- und Stromungsmodell 'METRAS' - Grundlagen, Validierung, Anwendung." Hamb. Geophys. Einzelschriften **A 88**: 139.

Schlünzen, K. H. (1990). "Numerical studies on the inland penetration of sea fronts at a coastline with tidally flooded mudflats." Beitr. Phys. Atmosph. **63**: 243-256.

Schlünzen, K. H., K. Bigalke, C.-L. Lenz, C. Lüpkes, U. Niemeier and K. von Salzen (1996). Concept and realisation of the mesoscale transport and fluid model 'METRAS'. METRAS Technical Report 5, Meteorologisches Institut der Universitat Hamburg.

Schlünzen, K. H. and J. J. Katzfey (2003). "Relevance of sub-grid-scale land-use effects for mesoscale models." Tellus Series a-Dynamic Meteorology and Oceanography **55**(3): 232-246.

Schultz, P. and T. Warner (1982). "Characteristics of summertime circulations and pollutant ventilation in the Los Angeles basin." Journal of Applied Meteorology **21**: 672-683.

Seaman, N. L. (2000). "Meteorological modelling for air quality assessments." Atmospheric Environment **34**: 2231-2259.

Seaman, N. L., F. L. Ludwig, E. G. Donall, T. T. Warner and C. M. Bhumralkar (1989). "Numerical studies of urban planetary boundary layer structure under realistic synoptic conditions." Journal of Applied Meteorology **28**: 760-781.

Shashua-Bar, L. and M. E. Hoffman (2000). "Vegetation as a climatic component in the design of an urban street. An empirical model for predicting the cooling effect of urban green areas with trees." Energy and Buildings **31**: 221-235.

Shea, D. and A. Auer (1978). "Thermodynamic Properties and Aerosol Patterns in the Plume Downwind St. Louis." Journal of Applied Meteorology **17**: 689-698.

Shepherd, J. (2005). "A review of current investigations of urban-induced rainfall and recommendations for the future." Earth Interactions **9**: 1-27.

Shepherd, J., M. Manyin and D. Messen (2006). Projected Regional Climate Changes in 2025 Due to Urban Growth. AGU Joint Assembly, Baltimore, Maryland.

Shepherd, J. M., H. Pierce and A. J. Negri (2002). "Rainfall modification by major urban areas: Observations from spaceborne rain radar on the TRMM satellite." Journal of Applied Meteorology **41**(7): 689-701.

Shudo, H., J. Sugiyama, T. Yokoo and T. Oka (1997). "A study on temperature distribution influenced by various land uses." Energy and Buildings **26**: 199-205.

Sinclair, D. J. (1964). The Growth of London since 1800. A Guide to London Excursions, Supplement to the International Geographical Union Congress. K. Clayton. London, International Geographical Union**:** 12-19.

Spangler, T. C. and R. A. Dirks (1974). "Meso-scale variations of the urban mixing height." Boundary-Layer Meteorology **6**(3): 423-441.

Spanton, A. M. and M. L. Williams (1988). "A comparison of the structure of the atmospheric boundary layers in Central London and a rural/suburban site using acoustic sounding." Atmospheric Environment **22**: 211-223.

Spronken-Smith, R. A., T. R. Oke and W. P. Lowry (2000). "Advection and the surface energy balance across an irrigated urban park." International Journal of Climatology **20**(9): 1033-1047.

Stanhill, G. and J. D. Kalma (1995). "Solar dimming and urban heating at Hong Kong." International Journal of Climatology **15**: 933-941.

Stedman, J. R. (2004). "The predicted number of air pollution related deaths in the UK during the August 2003 heatwave." Atmospheric Environment **38**: 1087-1090.

Stewart, I. D. (2007). "Landscape representation and the Urban-Rural Dichotomy in Empirical Urban Heat Island Literature 1950-2006." Acta climatologica et chronologica **40-41**: 111-121.

Stohlgren, T. J., T. N. Chase, R. A. Pielke, T. G. F. Kittels and J. S. Baron (1998). "Evidence that local land use practices influence regional climate, vegetation, and stream flow patterns in adjacent natural areas." Global Change Biology **4**: 495-504.

Stull, R. B. (1988). An introduction to Boundary Layer Meteorology, Kluwer Academic Publishers.

Svirejeva-Hopkins, A., H. J. Schellnhuber and V. L. Pomaz (2004). "Urbanised territories as a specific component of the global carbon cycle." Ecological Modelling **173**: 295-312.

Taha, H. (1996). "Modeling impacts of increased urban vegetation on ozone air quality in the South Coast Air Basin." Atmospheric Environment **30**(20): 3423-3430.

Taha, H. (1997). "Modeling the impacts of large-scale albedo changes on ozone air quality in the South Coast Air Basin." Atmospheric Environment **31**(11): 1667-1676.

Taha, H. (1997). "Urban climates and heat islands: albedo, evapotranspiration, and anthropogenic heat." Energy and Buildings **25**: 99-103.

Taha, H. (1999). "Modifying a mesoscale meteorological model to better incorporate urban heat storage: a bulk parameterisation approach." Journal of Applied Meteorology **38**: 466-473.

Taha, H., H. Akbari and A. H. Rosenfeld (1988). "Residential Cooling Loads and the Urban Heat Island: The effects of Albedo." Building and Environment **23**(4): 271-183.

Taha, H., D. J. Sailor and H. Akbari (1992). High albedo materials for reducing cooling energy use. Lawrence Berkeley Laboratory Reports 31721. Berkeley, California.

Takebayashi, H. and M. Moriyama (2007). "Surface heat budget on green roof and high reflection roof for mitigation of urban heat island." Building and Environment **42**(8): 2971-2979.

Tapper, N. J., P. D. Tyson, I. F. Owens and W. J. Hastie (1981). "Modelling the winter urban heat island over Christchurch, New Zealand." Journal of Applied Meteorology **20**(4): 365-376.

Tayanc, M. and H. Toros (1997). "Urbanization effects on regional climate change in the case of four large cities of Turkey." Climatic Change **35**: 501-524.

Therry, G. and P. Lacarrere (1983). "Improving the Eddy Kinetic-Energy Model for Planetary Boundary-Layer Description." Boundary-Layer Meteorology **25**(1): 63-88.

Thielen, J., W. Wobrock, A. Gadian, P. G. Mestayer and J.-D. Creutin (2000). "The possible influence of urban surfaces on rainfall development: a sensitivity study in 2D in the meso-gamma-scale." Atmospheric Research **54**: 15-39.

Thomas, D. (1970). London's Green Belt, London: Faber.

Threlfall (2001). A study of urban-rural temperature and humidity differences between Beaufort Park, Bracknell and London, Heathrow, Reading University.

Tiedke, M. and J. F. Geleyn (1975). "The DWD general circulation model - description of its main features." Beitr. Phys. Atmosph. **48**: 255-277.

Tjernstorm, M. and B. Grisogono (2000). "Simulations of supercritical flow around points and gapes in a coastal atmosphere." Journal of Atmospheric Sciences **57**(1): 108-135.

Troude, F., E. Dupont, B. Carissimo and A. I. Flossmann (2002). "Relative influence of urban and orographic effects for low flow conditions in the Paris area." Boundary-Layer Meteorology **103**: 493-505.

Trukenmüller, A., D. Grawe and K. H. Schlunzen (2004). "A model system for the assessment of ambient air quality conforming to EC directives." Meteorologische Zeitschrift **13**(5): 387-394.

Trusilova, K. (2006). Urbanisation impacts on the Climate in Europe. Technical Reports 9. Hamburg, Max-Planck Institut fur Biogeochemie**:** 82.

Trusilova, K., M. Jung, G. Churkina, U. Karstens, M. Heimann and M. Claussen (2008). "Urbanization impacts on the climate in Europe: Numerical experiments by the PSU-NCAR Mesoscale Model (MM5)." Journal of Applied Meteorology and Climatology **47**(5): 1442-1455.

Tumanov, S., A. Stan-Sion, A. Lupu, C. Soci and C. Oprea (1999). "Influences of the city of Bucharest on weather and climate parameters." Atmospheric Environment **33**(24-25): 4173-4183.

UN (2004). World urbanization prospects: The 2003 revision. United Nations Population Division. New York, USA, Department of Economic and Social Affairs, United Nations Secretariat**:** 335.

Unger, J., Z. Sumeghy and J. Zoboki (2001). "Temperature cross-section features in an urban area." Atmospheric Research **58**(2): 117-127.

Uno, I., H. Ueda and S. Wakamatsu (1989). "Numerical modelling of the Nocturnal Urban Boundary Layer." Boundary-Layer Meteorology **49**: 77-98.

Upmanis, H., I. Eliasson and S. Lindqvist (1998). "The influence of green areas on nocturnal temperatures in a high latitude city (Goteborg, Sweden)." International Journal of Biometeorology **18**: 681-700.

Velazquez-Lozada, A., J. E. Gonzalez and A. Winter (2006). "Urban heat island analysis for San Juan, Puerto Rico." Atmospheric Environment **40**: 1731-1741.

Wang, X. M., W. S. Lin, L. M. Yang, R. R. Deng and H. Lin (2007). "A numerical study of influences of urban land-use change on ozone distribution over the Pearl River Delta region, China." Tellus B **59**(3): 633-641.

West, C. C. and M. J. Gawith (2005). Measuring Progress: Preparing for climate change through the UK Climate Impacts Programme. UKCIP Technical Report. Oxford, UKCIP.

Whitehand, J. W. R. and K. Gu (2006). "Research on Chinese urban form: retrospect and prospect." Progress in Physical Geography **30**(3): 337-355.

Wichansky, P. S., L. T. Steyaert, R. L. Walko and C. P. Weaver (2008). "Evaluating the effects of historical land cover change on summertime weather and climate in New Jersey: Land cover and surface energy budget changes." Journal of Geophysical Research-Atmospheres **113**(D10).

Wilby, R. L. (2003). "Past and projected trends in London's urban heat island." Weather **58**: 251-260.

Wilby, R. L. and G. L. W. Perry (2006). "Climate change, biodiversity and the urban environment: a critical review based on London, UK." Progress in Physical Geography **30**(1): 73-98.

WMO (1996). Guide to Meteorological Instruments and Methods of Observation. Geneva.

WMO (2006). Initial Guidance to Obtain Representative Meteorological Observations at Urban Sites.

Wong, K. and R. Dirks (1978). "Mesoscale perturbations on Airflow in the Urban Mixing Layer." Journal of Applied Meteorology **17**: 677-688.

Wosik, G., K. Bigalke and K. H. Schlunzen (1994). GRITOP - Preprozessor zur Initialisierung von Topographiedaten fur das Modell METRAS. METRAS Technical Report 3, Meteorologisches Institut, Universitat Hamburg**:** 24.

Xue, Y. and J. Shukla (1993). "The Influence of Land Surface Properties on Sahel Climate. Part 1: Desertification." Journal of Climate **6**: 2232-2245.

Yague, C., E. Zurita and A. Martinez (1996). "Statistical Analysis of the Urban Heat Island." Atmospheric Environment **30**: 429-435.

Zhang, Y.P., Y.L. He, G.Y. Ren (2006). "Characteristics of urban heat island intensity in Kunming, China." IAUC Newsletter, Issue No. 16.

Zhou, L. M., R. E. Dickinson, Y. Tian, J. Fang, Q. Li, R. K. Kaufmann, C. J. Tucker and R. B. Myneni (2004). "Evidence for a significant urbanization effect on climate in China." PNAS **101**(26): 9540-9544.